POLITECNICO DI TORINO

SCUOLA INTERPOLITECNICA DI DOTTORATO

Doctoral Program in Innovation Management and Product Development

Final Dissertation

Effective Product Lifecycle Management: the role of uncertainties in addressing design, manufacturing and verification processes

Francesco Ricci

Tutor
prof. Paolo Chiabert

Co-ordinator of the Research Doctorate Course
prof. Luca Settineri

1st March 2012

Index

Abstract

The aim of this thesis is to use the concept of uncertainty to improve the effectiveness of Product Lifecycle Management (PLM) systems. Uncertainty is a rather new concept in PLM that has been introduced with the new technical language, drawn by ISO, to manage Geometrical Product Specification and Verification (GPS) in the challenging environment of modern manufacturing. GPS standards regard in particular design and verification environments, and want to guarantee consistence of information through a technical language which define both specification and verification on sound logical and mathematical bases. In this context, uncertainty is introduced as the instrument that measures consistency: between the designer intentions (specifications) and the manufactured artefact (as it is observed through measurement) as well as between the measurand definition provided by designers (the specification again) and that used by metrologists.

The implications of such an approach have been analyzed through a case study dealing with flatness tolerance and paying particular attention to the verification processes based on Coordinate Measuring Machines (CMM). A Design of Experiment (DoE) has been used and results have been analyzed and used to build a regression model that allows generalization in the experiment validity domain.

Then, using Category Theory, a categorical data model has been defined which represents the operation based structure of GPS language and uses the flatness research results in order to design a software able to concretize the GPS vision of geometrical product specifications management. This software is able to translate specification requirements into verification instructions, estimate the uncertainty introduced by simplified verification operations and evaluate costs and risks of verification operations. It provides an important tool for designers, as it allows a responsible definition of specifications (designer can simulate the interpretation of specifications and have an idea of the costs related with their verification), and for metrologist, as it can be a guide for designing GPS compliant verification missions or handling the usual verification procedures according to the GPS standards.

However, during the study, it has been matured the consciousness that this approach, even if correct and valuable, was not the most suitable to fully exploit the real potential of CMM. Then, aside the GPS oriented work, an adaptive sampling strategy, based on Kriging modelization, has been proposed with very encouraging results.

Introduction

The main aim of this thesis is to understand the role of uncertainties in the management of product information, thus in the Product Lifecycle Management (PLM).

Uncertainty is a rather new concept in PLM that has been introduced with the new technical standards drawn by ISO in order to cope with the new challenges of modern manufacturing [1, 2]. Globalization, with the delocalization of manufacturing facilities with respect to the design or assembly centres as well as the cooperation of several manufacturing companies to the realization of high precision products, has stressed the need for a technical language able to manage the aspects related with the geometry control and to grant information consistency throughout the whole product lifecycle [3].

ISO/TC 213 is drawing the new technical language entrusted to bridge the actual gap between design, manufacturing and verification through a corpus of standards going under the name of Geometrical Product Specification and Verification (GPS) standards [3]. The main aim of these standards is to guarantee the information consistency through a new technical language based on mathematical sound definitions. This kind of approach overcomes the traditional expert-based system of Geometrical Dimensioning and Tolerancing (GD&T), which has characterized the industrial world since soon after the post World War II. GD&T is a technical language consisting of a series of rules and symbols which have been improved through the last century to face the evolution of industry requirements and to answer the specific problems of interchangeability of components and rapid verification of mass productions. Nowadays, very complex shapes characterize components and the tendency is towards customization and flexibility rather than mass production, pushing verification processes far from the hard gauges, evolved in symbiosis with the GD&T language, toward three dimensional metrology and instruments such as coordinate measuring machines (CMM).

This change in the complexity of geometries to be described and in the potential of measuring instruments forces the new language to be used for describing products geometry and verification operations to evolve towards greater generality [4]. GPS language is born with the aim to describe geometry in the most accurate way (there is not a symbiosis with a particular instrument as for GD&T) and not simply to guarantee interchangeability inside assemblies. For this reason geometry is completely described, from the mathematical point of view, through sets of elementary operations that are combined inside operators. The background idea is that the workpiece geometry can be fully expressed, as a continuous or discrete signal, with Fourier transforms. This approach inspired by signal processing theory has been endorsed by the availability of instruments that are able to measure dense clouds of

points in a very short time. Moreover, it allows the definition of geometrical specifications (measurands) regardless the equipment that should be used for verification.

The quality of verification processes is assessed by means of uncertainties, which are the instrument used to quantify the distance of actual verification operations from their perfect counterparts fully compliant with standards. Several types of uncertainty are defined and the concept of uncertainty is elected as the currency for business management. Uncertainty becomes the discriminant element of decision rules and it is used to decide the allocation of resources for both design and verification.

This thesis deals with the use of uncertainty in managing product lifecycle and try to address most of the problems related with uncertainty estimation in case of verification processes non-compliant with GPS standards. In Chapter 1 an introduction to GPS language with the definition of operations, operators and uncertainties is provided in order to lay the foundations of the whole work. Chapter 1 in particular highlights the main differences between the GPS approach and the already consolidated GD&T.

The problem of uncertainty estimation for CMM-based verification of form errors is then afforded according to the new GPS standards. First of all, the state of the art in CMM sampling is assessed, in Chapter 2, looking for all the aspects responsible of generating uncertainty.

In Chapter 3 a case study is selected which becomes the test bench for the GPS based verification approach with respect to flatness tolerance. In particular, the perfect specification operator is defined, which is different from the GD&T geometrical tolerances, and the standard verification process is derived from it. This verification process is implemented with a CMM (Dea Iota 0101) for the case study's workpiece and simplified verification operators (which represent the actual industrial practice) are obtained from it as subsamples. Actual verification operators have been defined, according to a Design of Experiment (DoE), in order to simulate the range of most common practices as the use of different cut-off wavelengths, different sampling grids, different association criteria or simply reduction of sampling density. Flatness estimation algorithms have been applied, together with different methods for uncertainty estimation and the results have been analyzed in order to understand the effect of different factors on the performance of verification operators. Particularly, in order to clarify the effect of sampling accuracy (the measurement uncertainty associated with the sampling of each point) on the performance of verification operations, the same study performed on the case study's flatness feature has been reproduced on a virtual surface (Chapter 4).

Then all the results obtained for the flatness case study and the knowledge of GPS standards supporting specification and verification operations have been structured into a data model, in Chapter 5. This data model, defined according to Category Theory (the top method in this field, at the state of the art) has been used to build a software able to assist metrologists allowing them to perform GPS-based verification operations and to manage them reasoning on uncertainties to which costs can be associated as GPS standards suggest. A further novelty

for this approach is represented by the ability to exploit the valuable know-how of companies in order to develop, from experimental results, predictive capabilities that can be used for improving design of verification processes as well as allowing a responsible definition of geometrical specifications.

However, dealing with CMMs it was evident that GPS standards result in verification requirements too much time demanding for the most widely spread trigger-contact-probe CMMs. This evidence has been the motivation for a research on adaptive sampling strategies that, even if working differently from standards suggestions (blind sampling strategies based only on the measurand definition: specification), allow to detect the main component of form deviation with few sampling points. Chapter 6 develops an adaptive sampling strategy, based on Kriging modelization, that uses the information contained in the points already sampled in order to infer about the surface geometry and search for the feature peaks and valleys: the relevant areas for the correct estimation of form error.

References

[1] Srinivasan V. (2001) *An Integrated View of Geometrical Product Specification and Verification*. in proc. of 7th CIRP Seminar on Computer-Aided Tolerancing.

[2] Nielsen H.S. (2006) *New concepts in specifications, operators and uncertainties and their impact on measurement and instrumentation.* Measurement Science and Technology, **17** (3) 541.

[3] ISO/TR 14638 (1995) *Geometrical product specifications (GPS) - Masterplan*. ISO, Geneve.

[4] Srinivasan V. (2008) *Standardizing the specification, verification, and exchange of product geometry: Research, status and trends.* Comput. Aided Des., **40** (7) 738-749.

1 The ISO-GPS standards

1.1 Introduction

Globalization, with the delocalization of manufacturing facilities with respect to the design or assembly centres, as well as the cooperation of several manufacturing companies to the realization of high precision products, has stressed the need for a technical language able to manage the aspects related with geometry control and to grant information consistency throughout the whole product lifecycle. Many examples can be found to understand the complexity level and the precision requirements that have to be guaranteed by technical standards. Good ones are offered by the aeronautic industry with Boeing 787 and Airbus 380, the new long range and high capacity airliners which have the last assembly phase in one single facility but whose subassemblies are prepared in different countries (often continents) and have to fit with incredibly low error margins. A so complex manufacturing system requires the use of a common technical language able to carry all the information necessary to describe the workpiece geometry that is meant to guarantee the functional requirements.

ISO/TC 213 is drawing the new technical language entrusted to bridge the gap between design, manufacturing and verification through a corpus of standards going under the name of Geometrical Product Specification and Verification (GPS) standards. The main aim of these standards is to guarantee the information consistency through a new technical language based on mathematical sound definitions. This kind of approach overcomes the traditional expert-based system of Geometrical Dimensioning and Tolerancing (GD&T) which has characterized the industrial world since soon after the post World War II.

Vijay [1] underlines the latest efforts and the achievements of ISO TC/213 from the point of view of Product Lifecycle Management. As a matter of fact, the GPS program is the industry response to the beginning of the new information age; to the revolution brought by new possibilities of communication and movement on a global scale.

1.2 The traditional GD&T approach

GD&T is a technical language consisting of a series of rules and symbols that have been improved through the last century to face the evolution of industry requirements and to answer to specific problems. In Figure 1.1 there is the example of a part drawing: it carries all the information necessary to define the workpiece intended geometry and the allowed deviations.

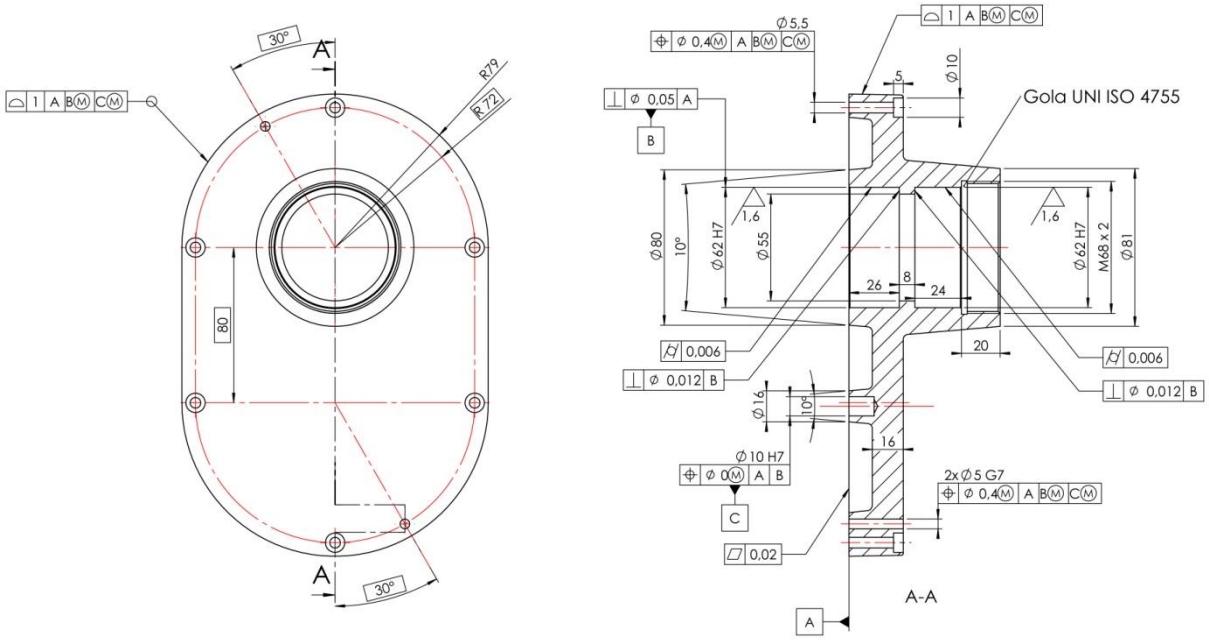

Figure 1.1 - Part drawing according to GD&T standards (ISO approach).

Drawings consist of two-dimensional projected views of the part nominal geometry where all indicated dimensions are to be intended as nominal dimensions. But the nominal geometry could not be obtained in practice and the allowed deviation must be stated, for each feature, through notes and symbols accompanying the two-dimensional projected views. The overall look is of suggestive "engineering hieroglyphics" (see Figure 1.1) which can be interpreted only with a deep knowledge of the standards lying behind. Standards define both the language syntax and semantics [2], the former being two-dimensional (as reported on projected views) while the latter three-dimensional. An example of syntax and semantics for the flatness tolerance symbol is reported in Figure 1.2.

Syntax	▱ | *toll*
Semantics	The extracted (actual) surface shall be contained between two parallel planes a distance "toll" apart. 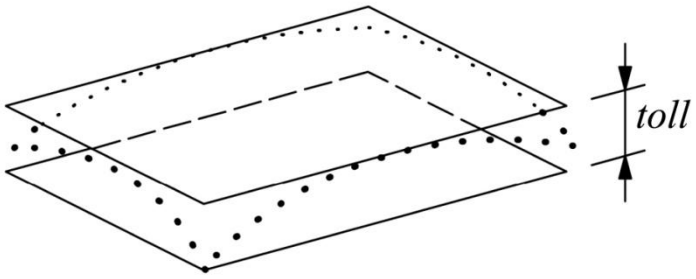

Figure 1.2 - Syntax and semantics of flatness tolerance according to ISO 1101.

GD&T is an expert-based system, as it needs a deep knowledge of rules and familiarity with all the possible cases and examples. Every time it is not possible to specify some characteristic according to the current standards, the pool of experts responsible for its

definition and maintenance has to be consulted and the solution becomes part of the knowledge that will be embodied in the next standard amendment. This has been the leitmotif of the GD&T approach. It led to a complex structure of symbols, definitions and cases that, anyway, are no longer suitable to express many new product requirements.

The main drawbacks of GD&T will be briefly presented in the next section, with a comparison of the ISO and ASME standards, their main divergences and some examples of specifications they are no longer suitable to deal with.

1.3 GD&T: ISO (ante GPS) versus ASME

GD&T can be based on both European (ISO) and American (ASME) standards with slightly different approaches that will be briefly analyzed in order to underline the origins of the need for a new technical language with wider and stronger foundations.

According to ASME, GD&T is based only on standard Y14.5 [3] which provides respectively the syntax and semantics of symbols (together with many examples and empiric rules about their application). The mathematic definition of the dimensioning and tolerancing principles is provided by the standard Y 14.5.1M [4]. On the other hand, the GD&T ISO fundaments (ante GPS) consisted of nearly 20 standards that had been object of several reviews in different periods. A huge effort was required to keep the consistency of definitions throughout the numerous non-simultaneous reviews that easily led to ambiguities.

Analysing the fundaments, we find an opposite approach between ASME and ISO standards. ASME's "Rule# 1" establishes a deep correlation between size and form prescribing the explicit definition of the dimensional limits and defining the Envelope Principle. This principle states: "no variation in form is permitted if the regular feature of size is produced at its Maximum Material Conditions (MMC) limit of size unless a straightness or flatness tolerance is associated with the size dimension or the Independency symbol is applied". Thus, according to the default set by Rule #1, the feature shape can vary only between the dimensional limits, resulting in a perfect shape in MMC and in the maximum permissible form error in Least Material Conditions (LMC). Designers can choose to avoid the use of Envelope Principle on a feature by specifying a form tolerance or appealing to Independency principle. In the latter case, they need to state their will explicitly in the drawing title box.

On the opposite ISO 8015 [5] bases GD&T on the "Independency Principle" meaning that dimensional and geometric tolerances have to be considered as independent. Geometric tolerances apply regardless of parts dimensions. Designers can eventually use the envelop principle but they need to state it clearly, beside the tolerance it applies to, using the symbol Ⓔ. Otherwise, they can state it in the drawing title block if its use is intended for all features.

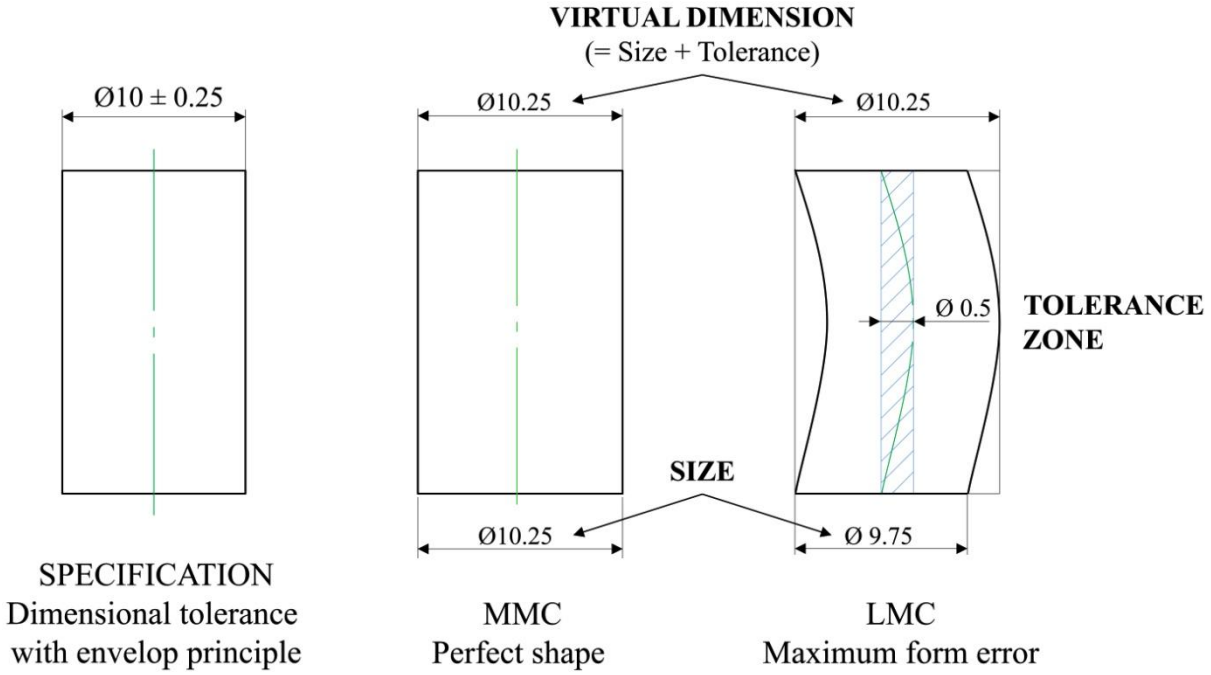

Figure 1.3 - Interpretation of the envelop principle for a cylindrical feature (shaft). Form error is allowed provided that the local size respects dimensional tolerance and the actual mating envelop does not exceed the MMC dimension.

ISO differs from ASME also for the opportunity of stating dimensional tolerances of mating parts through standardized codes [6]. For example (see Figure 1.4) H7/f6 represents the couple of tolerances to be applied on the couple Hole/shaft to get a fitting with clearance. In particular the letter identifies the position of the tolerance zone with respect to the nominal feature while the number identifies the extent of the tolerance zone (the higher the number the larger the tolerance). The letter used to identify the tolerance zone position is capitalized for the hole and lower-case for the shaft. ISO/R 1938 [7] defines the characteristics of plug gauges for the verification of this kind of specification.

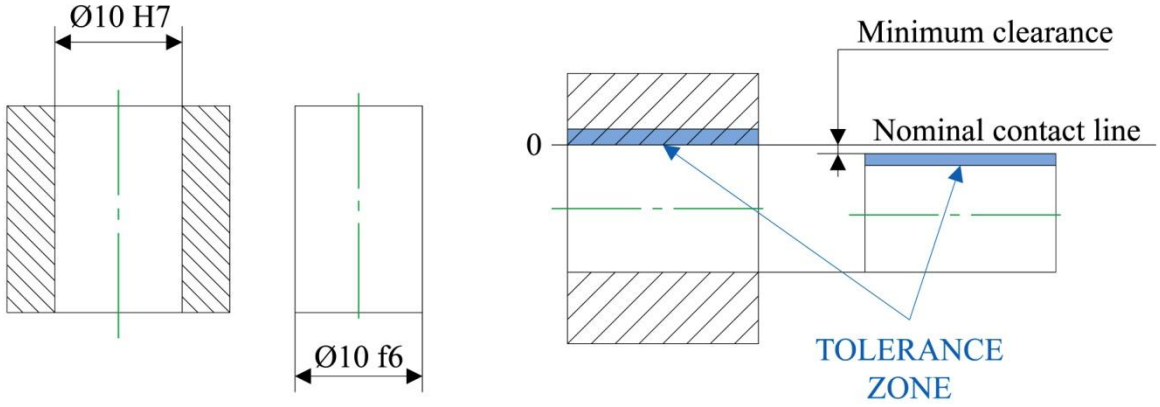

Figure 1.4 - Example of geometrical specification for a hole/shaft clearance fitting according to ISO 286-1.

Another difference between ISO and ASME GD&T concerns the definition of datum reference frames. In particular the difference is about the management of the orientation problem when the datum feature is convex. According to ISO [8] if a datum feature is convex

and results in an unstable orientation of the part, the part should be stabilized with adequate supports (wedges) in an "average" orientation (Figure 1.5) and all the features should be verified with respect to this orientation. Obviously this approach lacks of repeatability as ISO standards do not propose any rule to orient the workpiece. The ASME approach is completely different and solves the orientation problem stating that tolerances should be verified according to each possible orientation (candidate reference frame) and that the workpiece can be considered compliant if all specifications are satisfied at least in one orientation.

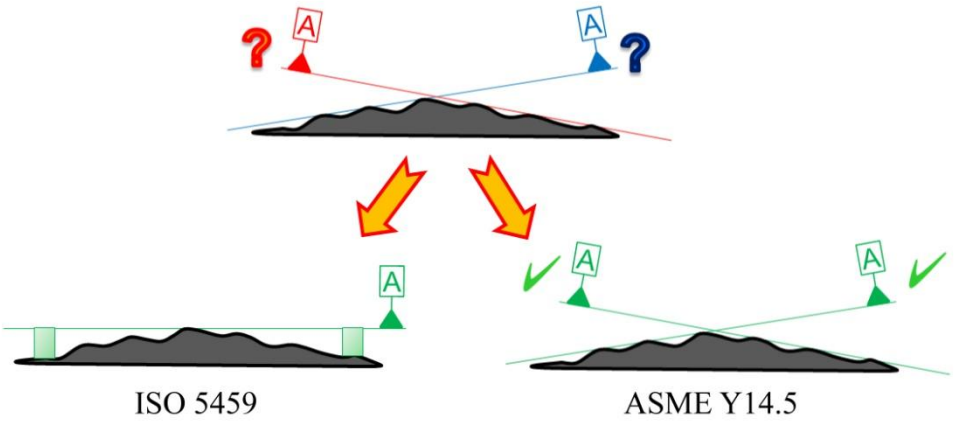

Figure 1.5 - ISO (left) and ASME (right) approaches to solve the orientation problem when a convex datum feature leads to instability.

The last important difference is about the nature of surfaces and how to deal with surface texture when assessing form errors. According to ASME, the actual feature surface consists of two different elements, respectively form and texture, which should be separated by a filtration operation. ANSI B46.1 [9] provides the smoothing functions to separate roughness from form when performing compliance verifications. On the opposite ISO (ante GPS) does not address the issue of surface texture in form error assessments, thus allowing possible ambiguous situations to arise.

Even if with some drawbacks, the GD&T language has been able to deal with the problems of geometry characterization for a long time and still represents a good base for many mechanical applications. However, its deficiencies are increasing with respect to the needs of the modern high precision industry.

GD&T evolved in a context where form errors and surface texture were two completely different domains separated by several orders of magnitude. Nowadays, thanks to breakthrough developments in tribology and in manufacturing capabilities, many precision products require form tolerances of a magnitude that until few decades ago was intended for surface texture only. In some cases surface texture presents a magnitude similar or even greater to that of the form error stressing the need for a new paradigm able to separate the different surface deviations. The distinction between form and surface texture is no longer based only on deviations magnitude but also on frequency.

1.4 The structure of GPS standards

Since 1996, ISO Technical Committee 213 (ISO/TC 213) has been working for the harmonization of the previously standardized practices in tolerancing and related metrology. The reasons behind such an effort have been partially explained in the previous section, with respect to the specification ambiguities. The first important step toward the birth of GPS project comes from Bennich in 1994 [10] with the identification of the gaps and contradictions affecting the standards that dealt with the specification and verification of geometrical tolerances. The stimulus coming from the awareness of these drawbacks was enforced by the demand of a continuously spreading and evolving CAD/CAM/CAQ marketplace asking for a clear mathematical formalism. This was necessary to enable the construction of compact and reliable softwares in order to support computerized applications [11].

The first effort aimed at harmonising the existing ISO standards is described by the "GPS matrix", presented in the ISO Masterplane in 1995 [12]. Standards are classified in 4 different classes, and collected in as many tables, according to their validity domain:

- **Fundamental GPS standards** establish the fundamental rules and procedures for dimensioning and tolerancing of workpieces and products. For example, the Principle of Independency [13] belongs to this class.
- **General GPS standards** are the main body of GPS standards establishing the rules for drawing indications, definitions and verification principles for the different types of geometrical characteristics. General standards are organized in the GPS matrix (see Figure 2 of the GPS Masterplan [12]). Each row of the matrix represents the chain of standards necessary to describe a certain geometrical characteristic from specification to verification, thus there is one row for each geometrical characteristic. Rows take the name of chains because the order of columns represents a progression through the product lifecycle and reflects the natural sequence of users reading, understating and deploying the concepts contained in standards.
- **Global GPS standards** cover or influence several or all chains of *General GPS standards* and *Complementary GPS standards*.
- **Complementary GPS standards** establish complementary rules for drawing indication, definitions and verification principles for a specialized category of features or elements. These rules depend on the type of manufacturing process and/or the type of machine element itself and can be arranged in chains of standards in the same fashion of General GPS standards matrix.

1.5 Three different domains

The GPS language wants to guarantee the information consistency along the whole product manufacturing cycle. It recognizes three different domains for products representation on which to base its structure (Figure 1.6) [14]:

- **Nominal model** embodies the designer idea and is characterized by nominal dimensions. It defines a workpiece of perfect form with shape and dimensions that perfectly fit the functions of the mechanism. This representation is far from reality, as manufacturing and measuring processes are characterized by their own variability or uncertainty, but is the base for technical representation in drawings and CAD models.
- **Non-ideal surface model (Skin model)** corresponds to the designer imagination of the variations that could affect the real geometry of the workpiece. This model is used by designers to figure out the possible effects of workpiece geometry deviations in order to set the limits necessary to guarantee the part functional requirements. These limits are the geometrical specifications and are expressed in the form of dimensional and geometrical tolerances to complete the nominal geometry on drawings and CAD models.
- **Real workpiece** geometry is the result of the workpiece manufacturing process. It is different from the nominal model because of the intrinsic variability of all the aspect concerning a real product (material, ambient conditions, manufacturing process, etc.). However deviations from the nominal model geometry should be within the geometrical specifications set by designers. Measurement is the unique way to know the real workpiece geometry but introduces further distortions and uncertainties intrinsic of the instrument and measurement procedure.

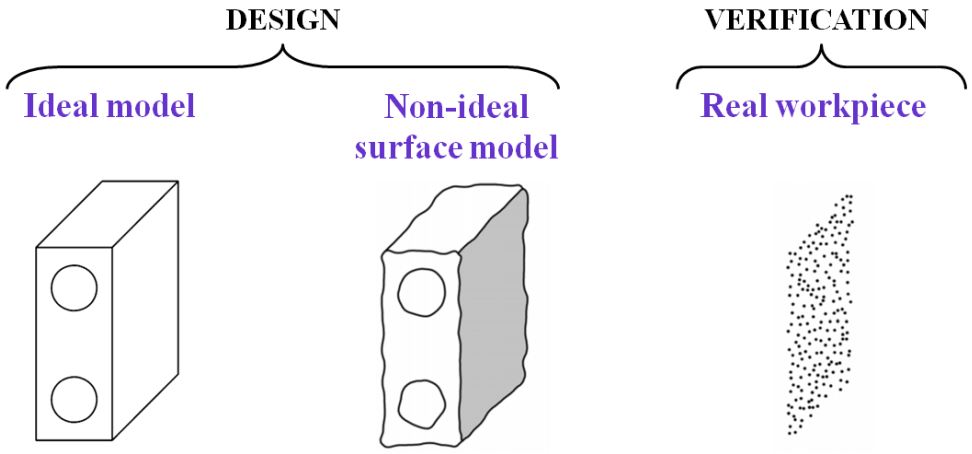

Figure 1.6 - Three domains of product representation for ISO GPS standards [14].

Then, compliance verification for a geometrical characteristic consists of comparing the real surface geometry against the limits set on the skin model. Obviously, this comparison must take into account the uncertainty of the measurement process through which we know

the real feature, according to the classical concept of measurement uncertainty provided by GUM [15].

But the skin model is not merely used by designers to set the limits for the variation of features geometry. According to the operation based approach that will be presented in next sections, it represents also the base on which the verification process is defined as the dual of specification. Thus the skin model is a representation used also by metrologists to understand specifications and figure out the proper measurement strategy.

1.6 Features and characteristics

The definition of feature is that of point, line or surface entities. Features can be classified as ideal or non ideal with respect to the context they are in. Ideal features refer to the nominal model while non-ideal features refer to the skin model and real workpiece. Features are the simplest elements necessary to completely define whatever workpiece geometry and are named after the type they belong to. Feature type corresponds to the invariance class the feature belongs to: one among the seven possible that are summarized in Table 1.1 according to ISO/TS 17450-1.

Invariance class	Type	Examples of situation features
complex	elliptic curve hyperbolic paraboloid ...	ellipse plane, symmetry planes symmetry planes, tangent point ...
prismatic	prism with an elliptic basis ...	symmetry planes, axis
revolute	circle cone torus ...	the plane containing the circle, the circle centre the symmetry axis, apex the plane perpendicular to the torus axis, the torus centre ...
helical	helical line helical surface with a basis of involute to a circle ...	helix helix ...
cylindrical	straight line cylinder	the straight line [a] the symmetry axis [a]
planar	plane	the plane
spherical	point sphere	the point [a] the centre [a]
[a] No alternative situation feature can be chosen, because the result would be a different invariance class for the considered feature.		

Table 1.1 - Geometrical features classification according to their invariance class [14].

Features can be defined also as associated, integral or derived according to ISO 14660-1 [16].

- **Associated features** are nominal features related to non-ideal features according to particular association criteria.
- **Integral features** represent parts (line or surface) actually belonging to a surface whatever its nature is (nominal, non-ideal, real).

- **Derived features** are entities obtained with the application of mathematical operations to a certain feature. Examples of derived features are cylinders axes, circles or spheres centres and symmetry planes (Figure 1.7).

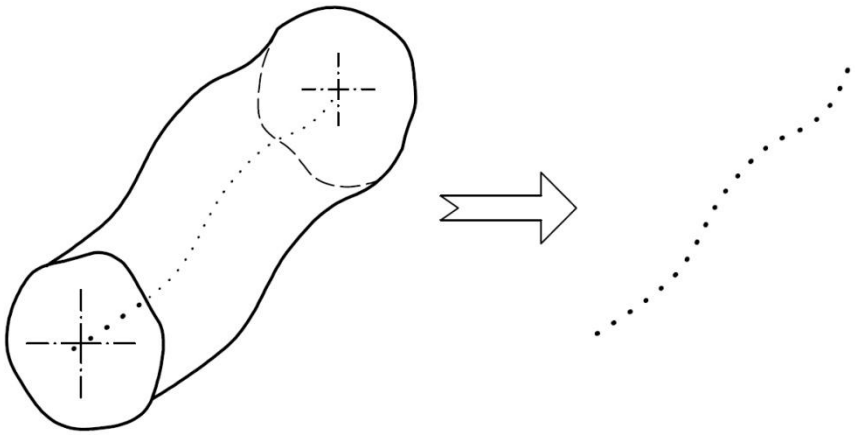

Figure 1.7 - Axis of a non-ideal cylinder: example of derived feature [14].

The representation of the workpiece geometry through features is nothing else than a mathematical representation. The classification introduced by invariance classes allows a univocal identification of the nature of geometry, but it is not enough to completely define a feature. Invariance classes represent only the surface degrees of freedom with respect to rigid motions; they are not able to represent dimensions and completely grasp the nature of bounded features.

A bounded feature is a feature with a finite dimension, which can then be encircled within the virtual boundary of a finite radius sphere. To complete features representation ISO 17450-1 introduces the concepts of intrinsic and situation characteristics.

- **Intrinsic characteristics** are defined on ideal features and are responsible for the identification of the feature size.
- **Situation characteristics** are defined either between couples of ideal features or between ideal and non-ideal features. They are responsible for the definition of distances, thus for the feature location in the space.

1.7 Operations and operators

At this point, a clear structure for the GPS language has been outlined. The product data management system has been structured in three different domains and a univocal representation of geometry has been introduced through the concepts of features and characteristics. The building of a language based on mathematics proceeds with the definition of seven operations entrusted to define specification and verification operators (Figure 1.8).

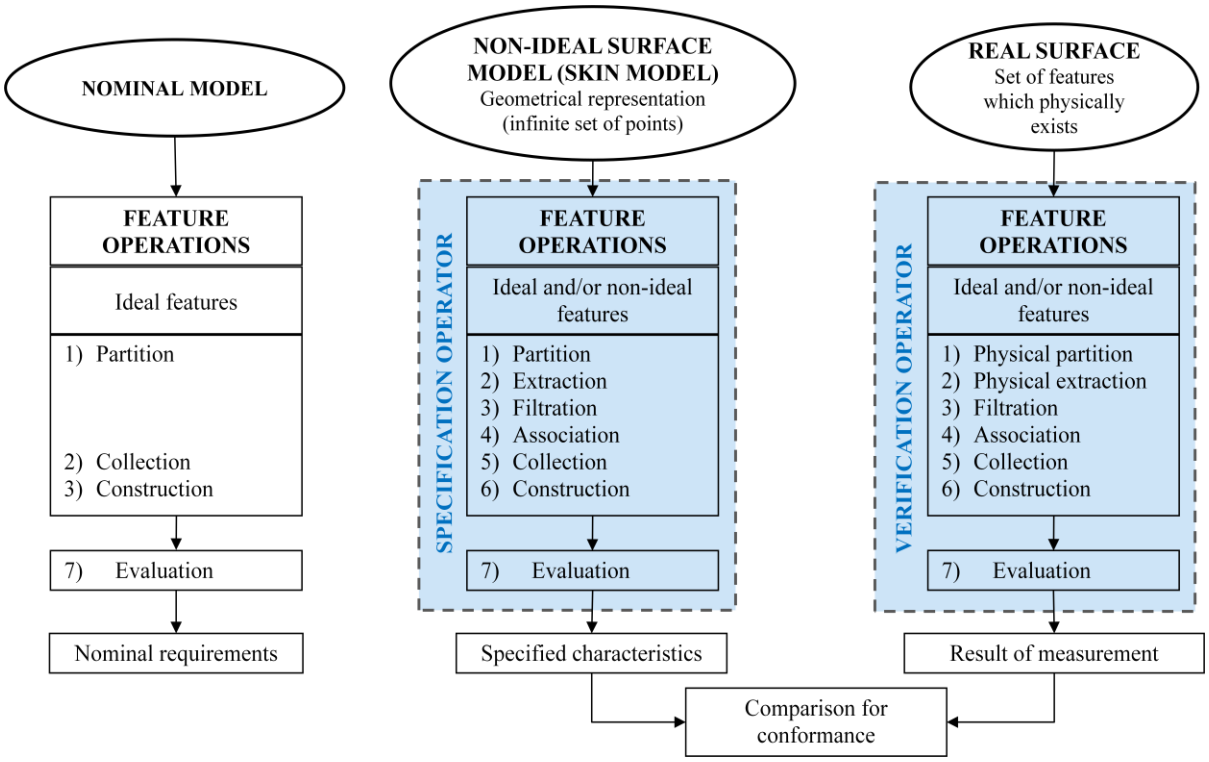

Figure 1.8 - Operations defining specification and verification operators.

An operator, by definition [17], is an ordered set of operations that apply on any feature. As we can see in Figure 1.8 some operations are not reported for the nominal model as they are not necessary. As a matter of fact, extraction, filtration and association are defined for non-ideal features only, with the aim of identifying the counterparts of the nominal model. The seven operations are briefly introduced according to the ISO/TS 17450-2 definitions.

1.7.1 Partition

The feature operation called partition is used to identify bounded features. From a computational point of view, it is straightforward if used on nominal models but becomes trickier when dealing with non-ideal surface models or real surfaces.

In nominal models features are described by equations, thus the partition is intrinsic to the definition of each feature domain: the equation domain corresponds to the feature boundaries (contour lines in Figure 1.9).

In non-ideal surface models and real surfaces, features are affected by several deviations such that it is not possible to describe them by means of equations, unless introducing approximations (see section 1.7.4). In this case partition is used to identify which portion of the non-ideal surface model, or of the real surface, corresponds to a nominal feature on the nominal model. The number of non-ideal (or real) features identified on a surface must be equal to the number of features on the relative nominal model.

Figure 1.10 shows one of the main problems presented by partition in the attempt of performing the operation without the reference of a nominal model. The shown surface is the skin model corresponding to Figure 1.9 with the sphere north pole lowered by a

manufacturing defect. The lowered area presents an almost constant curvature that, together with its centre location, is slightly different from that of the remaining spherical feature. At a first glance, the surface resembles a sphere and, if we try to fit a sphere, we can see that it matches quite well. But we can still improve the fitting performance, due to the flattened geometry of the sphere pole, trying to fit two independent spheres. The result is that the fitting performance improves, Figure 1.10, but the partition obtained is no longer correct.

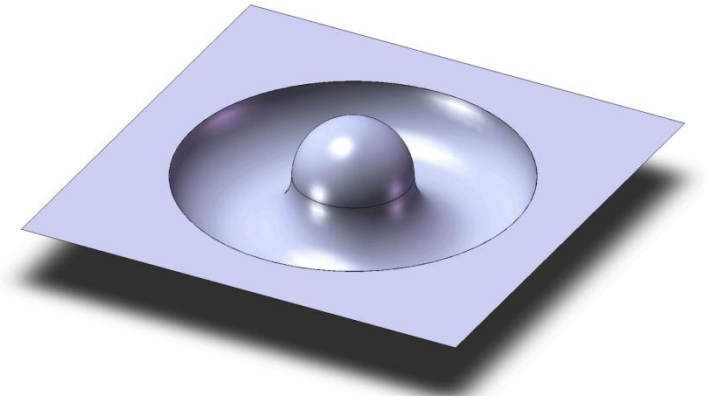

Figure 1.9 - Example of nominal model with the features boundaries corresponding to the domains of the respective equations.

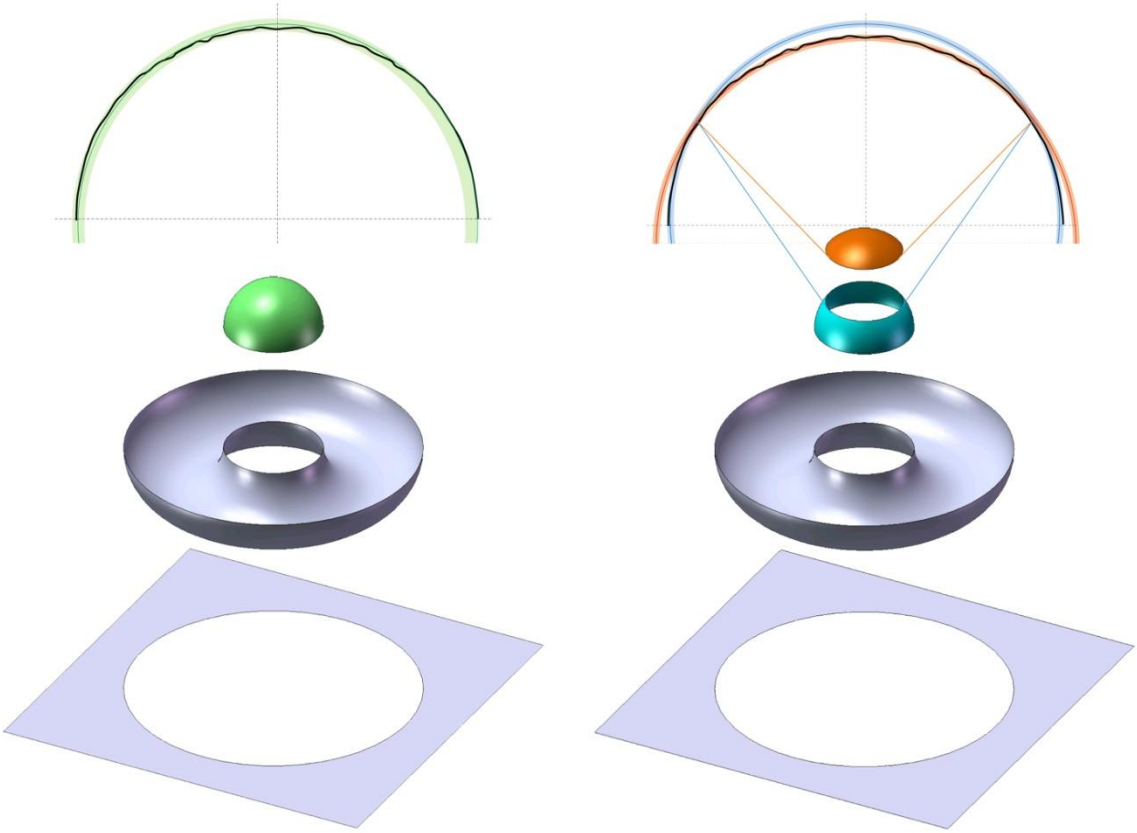

Figure 1.10 - Partition of a non-ideal surface. On the left only one sphere is used, resulting in a poor fitting performance but in a correct partition. On the right fitting performances are improved, using two different spheres, while the partition operation identifies features not corresponding to the nominal model.

In this case we can say that it is not correct because we know the nominal model, but without this information we would have not been able to figure out which of the two partitions was the right one. That with the best fitting performance? Clearly not.

Other important issues when partitioning non-ideal or real surfaces come from the definition of the features boundaries. For these reasons, at the state of the art, partition operation cannot be defined univocally with a mathematical formulation and is not yet implemented in any software.

Before closing this section we have to consider that ISO/TS 17450-1 defines as partition also the operation used to identify limited portions of an ideal or non-ideal feature (e.g. a segment of a straight line or a section of a non-ideal surface). But this operation presents none of the problems highlighted above.

1.7.2 Extraction

Extraction is the feature operation used to identify a finite number of points from a feature, according to specific rules (see Figure 1.11).

If we are dealing with a real surface, extraction represents the contact between metrologist and measurand (the process of acquiring knowledge about the surface geometry) and corresponds to the measurement process. Hence, the importance of adequate extraction operations in order to be able to collect the information that effectively allows us to assess the compliance of features with their specifications.

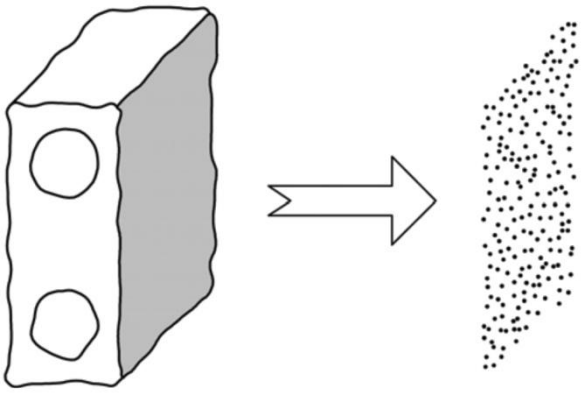

Figure 1.11 - Example of extraction operation according to ISO 17450-1.

1.7.3 Filtration

Filtration is the feature operation used to distinguish between roughness, waviness, structure and form. It permits the separation and identification of different scale characteristics from non-ideal features (see Figure 1.12) allowing to define different specifications for each of these characteristics.

Figure 1.12 - Example of filtration operation used to separate the form error components of a straightness profile [14].

1.7.4 Association

The association operation is used to fit ideal features to non ideal features according to specific rules called criteria. Association criteria give an objective for a characteristic and can possibly set constraints to fix the value of the characteristic or to set limits to it. Constraints can apply either to intrinsic or situation characteristics (where situation characteristics can be both between ideal features and between ideal and non-ideal features).

An example of association operation is visible in Figure 1.13 where an ideal cylinder is associated to a non ideal feature according to the criterion that asks to maximize the diameter of the inscribed cylinder. However, several different association criteria are available for each kind of feature. They are characterized by different objective functions and constraints and, therefore, they end up in the association of ideal features with different characteristics.

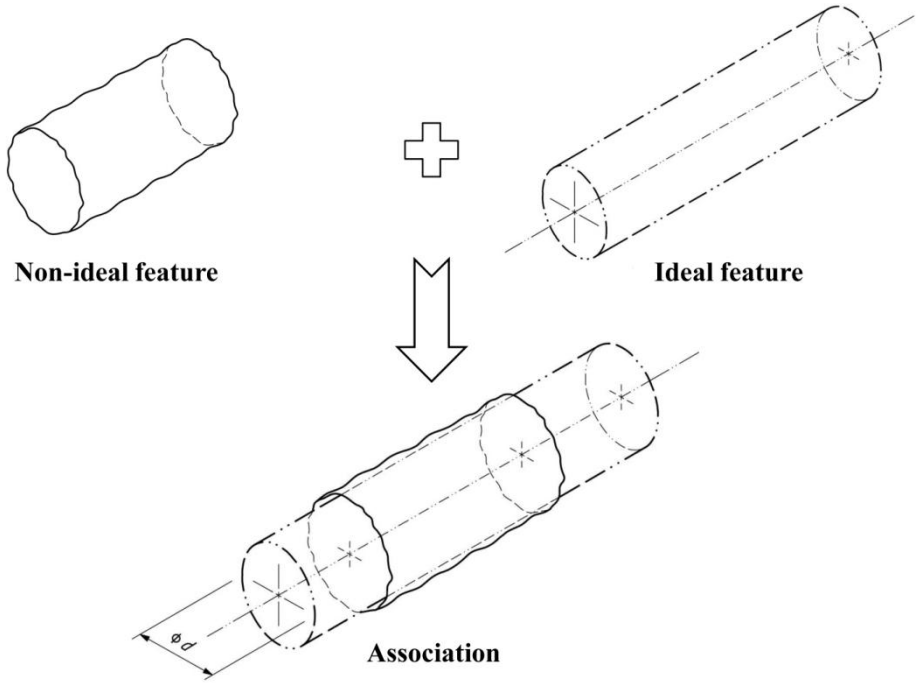

Figure 1.13 - Association of an ideal cylinder to a non-ideal feature [14].

The associated feature is usually the base of the verification process for assessing the compliance with tolerances. Thus, for the variability it may potentially introduce, the association criterion to be used for defining a certain geometrical feature (both in specification and verification) must be chosen by the designer and clearly stated along with the feature specification.

Association criteria can be classified according to the nature of the algorithm they are based on:

- *Statistical association criterion*: if the algorithm is such that all the measurement points coordinates participate to the definition of the nominal feature equation.
- *Extreme-fit association criterion*: if the algorithm is such that the nominal feature equation is defined according to coordinates of extreme points only.

1.7.5 Collection

The feature operation called collection is used to identify and consider together some features which together play a functional role. Collection operation can be performed equally with ideal or non-ideal features. Features built with collection operations can be of a type and degree of invariance different from those of the simple features composing the collection. Moreover, if two features are related by a situation characteristic, after the composition operation, the situation characteristic will be an intrinsic characteristic of the collection feature.

An example of collection operation is visible in Figure 1.14 where two parallel cylinders are considered together to build a common datum. The axes of both cylinders lie parallel in the same plane and once they are considered as a single feature the distance "L" between them becomes an intrinsic characteristic of the collection feature. In this case the collection feature has only a translational degree of freedom (in the direction identified by the two axes) and belongs to the prismatic invariance class while the two simple features belong to the cylindrical invariance class.

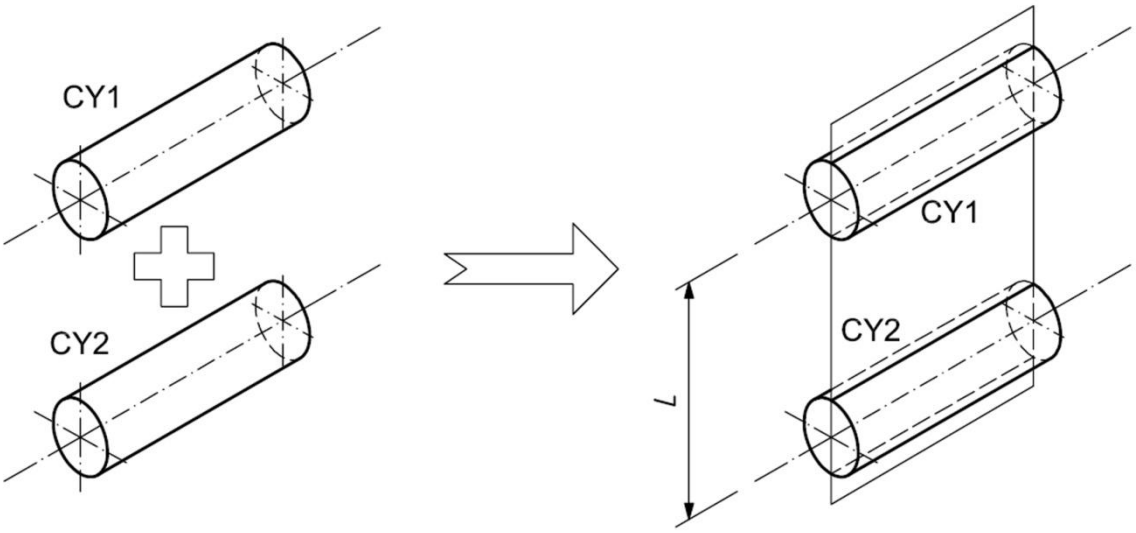

Figure 1.14 - Example of collection of two ideal cylinders [14].

1.7.6 Construction

Construction is the feature operation used to build ideal features starting from other ideal features. This operation requires the definition of constraints. A simple example, from ISO 17450-1, is reported in Figure 1.15 and shows the construction of a straight line defined as the intersection of two ideal planes.

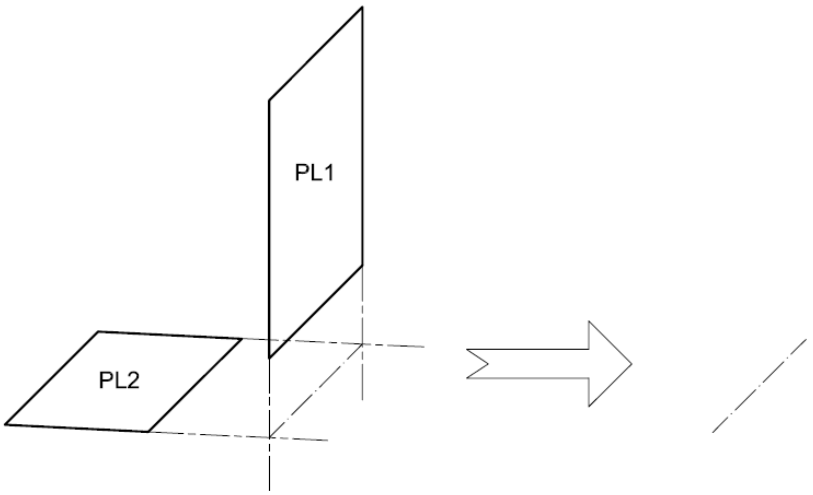

Figure 1.15 - Construction of a straight line by intersection of two planes [14].

1.7.7 Evaluation

Evaluation is the operation entrusted to identify the value of characteristics. If it is applied to a non-ideal feature it returns the characteristic nominal value and the limit (or limits) of its deviation. Both in specification and verification it can be applied only after the complete definition of the specification or verification operator respectively, thus after any other possible operation (see Figure 1.8).

1.8 Uncertainty contributions

The seven operations defined in previous sections allow a consistent definition of specification and verification operators. The operation and operator based approach allows a substantial improvement of the workpiece data management, thus the minimization of the uncertainty related to the possible interpretations of geometrical specifications. Differently from GD&T, the GPS system is based on mathematics (not on experts) and, rather than interpreting symbols, metrologists shall simply apply procedures: the ordered sets of operations called operators. From this point of view the GPS aim is to unable the univocal interpretation of specifications, if these are defined according to the new language.

However, in the fundaments of GPS approach there is the awareness that such a kind of language will require ages before becoming common practice. Many compromises are required when dealing with the actual facilities of metrology laboratories and the majority of instruments actually used is not suitable to implement a perfect verification operator.

Nevertheless, the compromises are not only related with the interpretation of specifications and the verification of workpieces' compliance. GPS language looks at products on a broader perspective as the final aim of a workpiece is to perform a function (on its own or in the assembly of a more complex machine). This means that geometrical specifications have to be adequate to guarantee the workpiece functionalities (named also 'functional needs' and 'functional requirements') and that they represent a possible source of uncertainty with respect to the correct workpiece functioning. The GPS language, as a matter

of fact, is able of describing products along their whole lifecycle and evaluating the consistency of the actual workpieces with the functional needs they are demanded to satisfy. This is the breakthrough with respect to GD&T, which enabled only the representation of geometrical specifications without taking into account the overall workpiece functional requirements.

To guarantee the best workpiece description and the evaluation of its correspondence to functional requirements, GPS language introduces the definition of new uncertainty contributions that are able to characterize products at different stages of their lifecycle. These uncertainty contributions are presented in ISO/TS 17450-2 [17] and participate in the definitions of the workpiece *total uncertainty* according to the scheme presented in Figure 1.16. Each uncertainty contribution will be briefly presented in the following sections in an order that respects the levels of the composition scheme. Note that these are not hierarchical levels, as the uncertainty contributions are defined independently from each other.

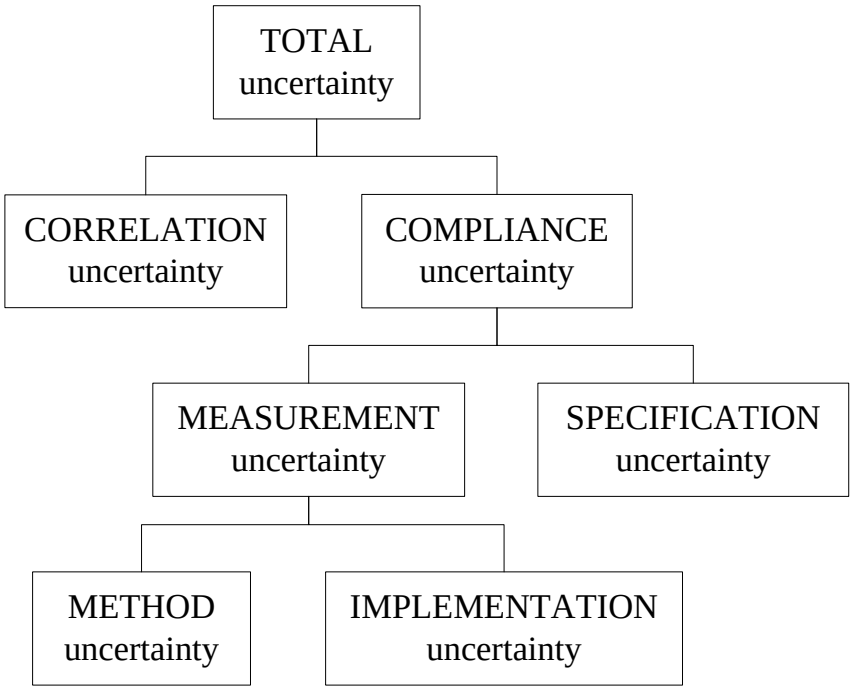

Figure 1.16 – Composition scheme for the GPS uncertainty contributions.

1.8.1 Total uncertainty

Total uncertainty represents the deviation of the actual verification operator from the functional operator, namely the functional requirements the workpiece is demanded to satisfy. It is intended to measure the attitude of a certain workpiece, measured through a certain verification operator, to:

- satisfy the functional requirements when measured as being compliant with geometrical specifications;
- do not satisfy the functional requirements when measured as being non compliant with geometrical specifications.

For this reason total uncertainty takes into account the uncertainty related with the verification process (*measurement uncertainty*), the possible interpretations of the geometrical specification (whenever this is not complete *specification uncertainty* arises) and the suitability of the geometrical specification to match the functional requirements it is intended for (*correlation uncertainty*). Total uncertainty is defined as the sum (in the sense of the word according to GUM) of *correlation uncertainty*, *specification uncertainty* and *measurement uncertainty* [17].

1.8.2 Correlation uncertainty

Correlation uncertainty is defined as "the uncertainty arising from the difference between the actual specification operator and the functional operator, which defines the intended function of the workpiece, expressed in the terms and units of the actual specification operator" [17]. In other words, it measures the suitability of the geometrical specification to guarantee the functional requirements it has been intended for.

Different features, or different specifications on the same feature, can be involved in the same functional requirement. In these circumstances, all features and/or specifications involved have to be taken into account together with their mutual relationships.

Correlation uncertainty is aimed at assessing if a workpiece compliant with geometrical specifications is able to satisfy the functional requirements it was intended for, and vice versa. The difference with respect to total uncertainty is that correlation uncertainty does not care about the way the workpiece compliance has been assessed with. On the contrary, total uncertainty does. Thus the remaining part of total uncertainty, the one related with the compliance assessment, is defined by compliance uncertainty, which is presented in the next section.

1.8.3 Compliance uncertainty

Compliance uncertainty collects all the uncertainties related with the compliance of the workpiece geometry with respect to specification requirements. It quantifies the uncertainty with which it can be proved that a workpiece complies with every possible interpretation of a specification [17]. Compliance uncertainty covers both the practical aspects of measurement processes (actual verification operator and its measurement uncertainty) and the quality of specification (if specification has not a univocal interpretation, specification uncertainty arises). It consists of the sum (with the meaning of the word according to GUM) of measurement uncertainty and specification uncertainty.

1.8.4 Specification uncertainty

Specification uncertainty has the role of quantifying the ambiguity in specification operators [17]. Actually, if the actual specification operator is not complete, metrologists have to reconstruct the complete specification operator from which, according to the duality principle, the perfect verification operator is derived. The reconstruction of the complete

specification operator is obtained by adding operations, or parts of operations, missing in the incomplete specification and consistent with it. But this reconstruction cannot be univocal, as there may be several operations equally suitable to complete an incomplete specification operator. Specification uncertainty can be easily eliminated using complete specification operators.

1.8.5 Measurement uncertainty

Measurement uncertainty collects all the uncertainties generated by the use of an actual verification operator. It corresponds to the classical concept of measurement uncertainty and consists of the sum (in the sense of the word intended by GUM) of method uncertainty and implementation uncertainty [17]. It takes into account the non-idealities of the instrumentation as well as the intentional deviations from the perfect verification operator introduced to facilitate its practical use.

1.8.6 Method uncertainty

Method uncertainty "arises from the differences between the actual specification operator and the actual verification operator, disregarding the metrological characteristic deviations of the actual verification operator" [17]. Method uncertainty collects the effects of verification operations different from those required by the actual verification operator, which is derived from the actual specification according to duality principle.

1.8.7 Implementation uncertainty

Implementation uncertainty arises from the divergence of the metrological characteristic of the actual verification operator from the ideal metrological characteristic defined by the perfect verification operator [17]. It collects the effects of the non-idealities (deviations) of actual verification operators from the perfect verification operator.

The magnitude of the part of implementation uncertainty introduced by measuring instrument can be estimated through calibration. Other components due to environmental effects, not directly related to the measuring equipment, have to be taken into account and, if possible, compensated [18, 19].

1.9 Decision rules for workpieces acceptance

As presented in last sections ISO GPS standards provide a new language for the definition of products characteristics along the product lifecycle together with the definition of uncertainty components suitable for describing every possible deviation from the perfect verification operator.

Calculation of measurement uncertainty is of primary importance in assessing the compliance of workpiece geometry with respect to the geometrical specifications. This uncertainty contains all the deviations of the actual verification operator with respect to the

perfect verification operator, thus expresses the goodness of the verification operator used for the measurement mission. GPS standards provide also a decision rule to guide the acceptance/rejection of workpieces according to the results of measurement processes and their uncertainties.

The aim of ISO/TS 14253, a standard made of five parts up to now, is to provide an acceptance rule to be used to avoid or resolve disputes between suppliers (manufacturers or metrology laboratories) and customers on the conformance of manufactured or traded parts. The first part of ISO/TS 14253 [20] provides the rule for proving conformance or non-conformance. It states that a workpiece can be defined compliant or non-compliant with specification only if the interval that completely expresses the measurement result is, respectively, completely inside or completely outside the specification interval (Figure 1.17). The interval that completely expresses the measurement result is defined as the measured value together with its expanded uncertainty: interval *y'* in Figure 1.17. In case the interval *y'* includes one of the specification limits neither conformance nor non-conformance can be proved.

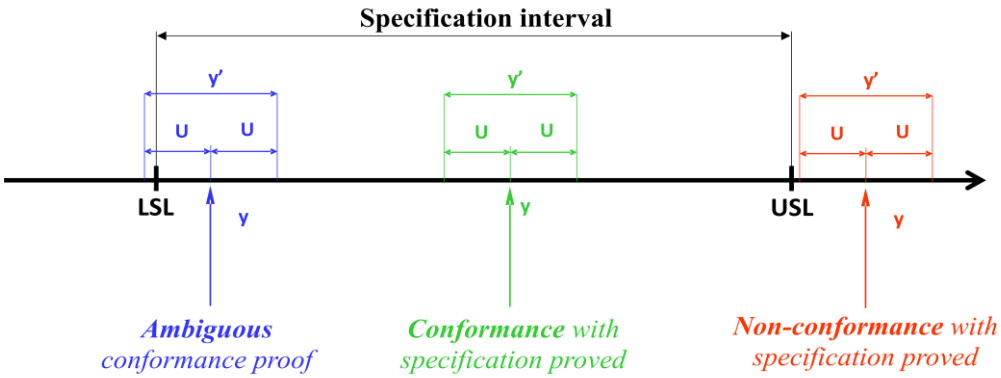

LSL: Lower Specification Limit
USL: Upper Specification Limit
y: measurement result
U: expanded measurement uncertainty
y': interval which completely express the measurement result

Figure 1.17 - Rule for proving conformance or non-conformance with specifications according to ISO/TS 14253-1.

The principle behind this decision rule is that measurement uncertainty always counts against the party who makes the measurement in order to provide the proof of conformance or non-conformance. In this way, the party who makes measurements is incentivized to reduce measurement uncertainty as much as possible.

The second part of ISO/TS 14253 [18] wants to guide the implementation of concepts introduced by the "Guide to the estimation of uncertainty in measurement" (GUM) [15] to foster their application in industry for the design of verification processes, calibration of verification instruments and measurement of workpiece GPS characteristics. The aim is to improve communication between purchasers and suppliers providing full information on how

to achieve uncertainty statements and the basis for international comparison of measurement results and their uncertainties.

It is becoming always more common for suppliers to provide customers with a detailed perspective on their quality system in order to give them a satisfactory insurance that the workpiece they are receiving conforms with specifications. This practice avoids costly duplicate inspections and can benefit from ISO/TS 14253-2 that, basically, provides instructions for preparing budgets of measurement uncertainty as defined in the GUM. However, there is still the possibility that customers and suppliers can disagree on the measurement uncertainty estimation. If this happens, and if the uncertainty estimation has been performed in accordance with ISO/TS 14253-1, the third part of ISO/TS 14253 provides guidelines and procedures to help customer and supplier to reach amicable agreements and avoid costly and time-consuming disputes [21].

The fourth part of ISO/TS 14253 outlines the main assumptions behind the decision rules established in ISO/TS 14253-1. It discusses why these rules have to be the default rules and the considerations that should be taken into account before applying different decision rules [22]. ISO/TS 14253-4 defines the meaning of specification limits and provides definitions and guidelines to transform functional limits in specification limits. Functional limits are defined, on the functional level degradation curve of the workpiece characteristic, in order to guarantee a certain level of functionality. This standard identifies different shapes of functional level degradation-curves and defines the rules to set functional limits and choose the adequate specification limits even in the complex circumstance where different characteristics combine in the same performance.

1.10 Conclusions

Geometrical Product Specification and Verification (GPS) is an international standard system covering all the issues related with products manufacturing, ranging from the first design phase to the metrological principles and practices for their verification [12].

The aim of GPS standards framework is to grant coherence to all the data generated along product lifecycle in order to enable the information age industry to be more cost effective [1]. This aim is pursued through the definition of a new rigorous language, based on mathematics, that relying on the concepts of operations, operators and uncertainties enables the harmonization of information throughout a global scale manufacturing industry [23]. Such a language, completely based on mathematics, enables information consistency but still needs to be encapsulated into an integrated information system to spread into industrial practice, as it often turns out to be too complicated to be used directly. GPS language allows the development of next generation PLM softwares that are intended to fully exploit the potential provided by improvements in the field of measuring instruments and informatics for management of production [24].

In this context, the ISO/TC 213 (which has the aim of standardization in the field of Geometrical Product Specifications and Verification) focuses on the improvement of specification and verification phases and tries to match them postulating the "principle of duality" [25, 26]. This principle establishes that the sets of operations used in the specification phase to address variability limits are in biunivocal relationship with the same sets of operations used in the verification phase to identify the element subject to the specification and to evaluate its conformity.

According to duality principle specifications and their verification are defined on the skin model: the designers' or metrologists' mental representation of the possible workpiece geometrical deviations. For its nature, skin model is continuous and its continuity deeply characterizes the whole GPS framework. In order to define the domain of different tolerances (to distinguish among errors of form, undulation, roughness or lay) geometry is considered and treated as a continuous signal to be decomposed and analyzed into its different wavelengths.

This approach based on continuity of information is justified by the direction in the evolution of measuring instruments, which tends towards three-dimensional surface acquisition by means of optical devices. These instruments provide good or excellent accuracy together with contained measurement times and, the most important, enable the achievement of a knowledge level of the actual surface geometry that is very similar to a continuous model. Optical instruments allow the measurement of dense clouds of points and the reconstruction of the actual surface geometry with a mesh so fine to enable also the reconstruction of the smaller wavelength form errors. A case study [27] shows that a specification over a flatness error characterized by a wavelength greater than 2.5 mm requires, for the correct reconstruction of the actual surface geometry, a sampling of the surface with a distance lower or equal than 0.35 mm. Such a sampling distance implies a massive amount of points to be measured but does not represent a problem for optical instruments.

The main problem in the application of GPS standards is represented by the traditional measuring instruments that populate most of metrology laboratories around the world. Thanks to their accuracy and flexibility Coordinate Measuring Machines (CMM) are the most popular measuring instrument, preferred every time there is the need to measure few points with high accuracy. CMMs are not competitive when specification requires the measurement of thousands of points but, many times, they are the only available instrument and are used anyway, introducing important deviations with respect to the perfect verification operator.

The flexibility and widespread of CMMs means that these instruments will continue to dominate in the field of metrology for a long time to come. The aim of this thesis is to investigate the issues related with inspection of workpieces performed by means of CMMs and compliant with GPS standards. The main drawbacks will be pointed out and an operative strategy will be proposed to assess the uncertainty generated during their use by deviations from the perfect verification operator.

A data model is proposed to deal with the management of information during the inspection phase and is implemented into a category-based software enabling the assessment of uncertainty according to GPS standards and cost of measurement missions. Further, the problem of form error assessment is afforded, from a perspective that is not considered by ISO standards yet, presenting an adaptive inspection strategy able to maximize the efficiency of CMM measurements by taking into account the information about the actual surface that has been collected during the measurement mission already performed.

1.11 References

[1] Srinivasan V. (2008) *Standardizing the specification, verification, and exchange of product geometry: Research, status and trends.* Comput. Aided Des., **40** (7) 738-749.

[2] ISO 1101 (2004) *Geometrical product specifications (GPS) - Geometrical tolerancing - Tolerances of form, orientation, location and run-out*. ISO, Geneve.

[3] ASME Y 14.5 (2009) *Dimensioning and Tolerancing – Engineering Drawing and Related Documentation Practices*.

[4] ASME Y 14.5.1.M (1994) *Mathematical Definition of Dimensioning and Tolerancing Principles*.

[5] ISO 8015 (1985) *Technical drawings - Fundamental tolerancing principles*. ISO, Geneve.

[6] ISO 286-1 (1988) *ISO system of limits and fits - Part 1: Bases of tolerances, deviations and fits*. ISO, Geneve.

[7] ISO/R 1938 (1971) *ISO system of limits and fits - Part 2 : Inspection of plain workpieces*. ISO, Geneve.

[8] ISO 5459 (1981) *Technical drawings - Geometrical tolerancing - Datums and datum-systems for geometrical tolerances*. ISO, Geneve.

[9] ANSI B46.1 (1985) *Surface Texture (Surface Roughness, Waviness and Lay)*. ASME, New York.

[10] Bennich P. (1994) *Chains of Standards - A new Concept in GPS Standards.* Manufacturing Review, The American Society of Mechanical Engineers, **7** (1) 29-38.

[11] Srinivasan V. (2001) *An Integrated View of Geometrical Product Specification and Verification*. in proc. of 7th CIRP Seminar on Computer-Aided Tolerancing.

[12] ISO/TR 14638 (1995) *Geometrical product specifications (GPS) - Masterplan*. ISO, Geneve.

[13] ISO 8015 (2011) *Geometrical product specifications (GPS) - Fundamentals - Concepts, principles and rules*. ISO, Geneve.

[14] ISO/TS 17450-1 (2005) *Geometrical product specifications (GPS) - General concepts - Part 1: Model for geometrical specification and verification*. ISO, Geneve.

[15] ISO/IEC (2008) *Guide to the Expression of Uncertainty in Measurement (GUM: 1995)*. BIPM, IEC, IFCC, ISO, IUPAP, IUPAC, OIML.

[16] ISO 14660-1 (1999) *Geometrical product specifications (GPS) - Geometrical features - Part 1: General terms and definitions*. ISO, Geneve.

[17] ISO/TS 17450-2 (2002) *Geometrical product specifications (GPS) - General concepts - Part 2: Basic tenets, specifications, operators and Uncertainties*. ISO, Geneve.

[18] ISO 14253-2 (2011) *Geometrical product specifications (GPS) - Inspection by measurement of workpieces and measuring equipment - Part 2: Guidance for the estimation of uncertainty in GPS measurement, in calibration of measuring equipment and in product verification*. ISO, Geneve.

[19] ISO/IEC (2007) *International vocabulary of metrology - Basic and general concepts and associated terms (VIM).*
[20] ISO 14253-1 (1999) *Geometrical product specifications (GPS) – Inspection by measurement of workpieces and measuring equipment – Part 1: Decision rules for proving conformance or non-conformance with specifications*. ISO, Geneve.
[21] ISO 14253-3 (2011) *Geometrical product specifications (GPS) - Inspection by measurement of workpieces and measuring equipment - Part 3: Guidelines for achieving agreements on measurement uncertainty statements*. ISO, Geneve.
[22] ISO 14253-4 (2010) *Geometrical product specifications (GPS) – Inspection by measurement of workpieces and measuring equipment – Part 4: Background on functional limits and specification limits in decision rules*. ISO, Geneve.
[23] ISO/TS 12781-1 (2006) *Geometrical product specifications (GPS) - Flatness - Part 1: Vocabulary and parameters of flatness*. ISO, Geneve.
[24] ISO/TS 12781-2 (2011) *Geometrical product specifications (GPS) - Flatness - Part 2: Specification operators*. ISO, Geneve.
[25] Kruth J.-P., Van Gestel N., Bleys P. and Welkenhuyzen F. (2009) *Uncertainty determination for CMMs by Monte Carlo simulation integrating feature form deviations.* CIRP Annals - Manufacturing Technology, **58** (1) 463-466.
[26] Dowling M.M., Griffin P.M., Tsui K.-L. and Zhou C. (1997) *Statistical Issues in Geometric Feature Inspection Using Coordinate Measuring Machines.* Technometrics, **39** (1) 3-17.
[27] Chiabert P., De Maddis M., Ricci F. and Ruffa S. (2011) *Uncertainty management in flatness verification operations within the GPS framework.* in proc. of AITeM, Naples.

2 Uncertainty estimation in CMM verification operations

2.1 Introduction

Three-dimensional metrology has brought a significant change in dimensional measurement if compared to the traditional two point distance measurements. Instead of measuring dimensions, it returns the coordinates of points sampled from the measurand surface, providing more comprehensive information about the measurand geometry. The output of the measurement process is a collection of coordinates of surface points, whose analysis allows the observation of surface shape details, the evaluation of feature characteristics (sizes and distances) and their deviations from nominal values. Usually data analysis is completely independent from the data acquisition process. The former is a software procedure while the latter a hardware procedure traditionally based on the contact of a probing stylus with the measurand (CMMs). More recently, probing styli are often substituted with optical (non-contact) measurement devices that, when deployable, avoid the morphological filtration introduced by stylus tip geometry.

Most of literature deals with traditional CMM verification processes where data analysis is performed, after the extraction phase (measurement), through the LS association criterion. This is the most widespread measurement approach and is also coherent with the direction of ISO standards development. If there is no transversal knowledge about the workpiece history, there is no reason to expect geometrical defects in particular locations and a blind approach is necessary to explore the whole feature with the same level of accuracy. However, if the manufacturing process is characterized by a known signature (geometry presents systematic errors) the sampling strategy can be designed ad hoc in order to identify the signature characteristics (magnitude of defects) by sampling the lowest possible number of points.

Measurement data analysis can be performed by means of several different numerical algorithms. In terms of GPS language [1] the algorithm used to analyze the measurement data, to infer about the real feature characteristics, is named “association criterion” and must be defined by the specification on the part drawing. Many association criteria are already implemented in CMMs software in order to provide measurement outputs consistent with the characteristic to be measured and avoid off-line data analysis. Association algorithms can be classified, according to their nature, in:

- **Statistical algorithms**, such as Least Squares, that are able to associate to the coordinates of all measurement points the maximum likelihood nominal feature.
- **Extreme fit algorithms** (such as Minimum Zone, Maximum Inscribed, Minimum Circumscribed etc.) that, according to the envelop of all measurement points, define an ideal feature on the basis of extreme points only.

For both kinds of association criteria, the uncertainty assessment can be either analytic or experimental. The analytic formulation is more suitable for statistical algorithms, as it is a natural derivation of the statistical formulation of maximum likelihood algorithms, while experimental approach is the best solution to deal with extreme fit association criteria.

Regardless the association criterion used to fit the nominal feature and evaluate real feature deviations, CMM verification operations are strongly affected by sampling strategy: the number of sampling points and their distribution over the measurand surface.

This chapter investigates the main issues related with CMM-based verification and the assessment of the uncertainty deriving from the selected association criterion. Particularly, the investigation is focused on flatness tolerance, as it is one of the most popular tolerances both in industrial practice and in literature studies. However, despite the simple formulation that makes it so suitable for research purposes, findings can be easily extended to most of geometrical form tolerances.

2.2 State of the art in CMM sampling strategies

Parameters of sampling strategy have been extensively studied in CMM literature in the last decades. However, the majority of studies are characterized for being oriented at statistical evaluation due to the widespread implementation of LS association criterion in CMM softwares. Two different branches of research can be identified: one aimed at optimizing sample size and another dealing with the optimization of measurement points location.

The definition of sample size depends on factors such as the feature size, the transmission band of tolerance specification, the machining process capability and the measurement uncertainty [2-4]. The state of the art for defining sample size is reviewed in §2.2.1.

The situation is even more complex from the point of view of location of measurement points on the measurand surface. The literature dealing with this issue is analyzed in §2.2.2 with a particular highlight on the main advances in sampling strategies aimed at reducing verification costs by improving sampling performance.

2.2.1 Sample size

CMM inspection is characterized by a discrete measurement which essentially results in an approximation process: if the sample size is infinite the approximation error is zero while, in any real case with a finite sample size, it is non-zero [5]. The sample size directly affects measurement time (they are directly proportional), thus the whole cost of verification processes that should be always minimized [6]. The great economic impact of sample size has justified an intense research aimed at getting the best reports of form deviation with the lowest possible number of points. Yau and Menq were among the first to work in this direction and proposed to relate the sample size to process capability through a statistical approach [7].

Weckenmann et al. [8] recognized the influence of verification operations (sampling strategy, fitting algorithm and evaluation of deviations from the nominal fitted feature) on the correct verification of the geometrical specifications that are intended to guarantee the functional requirements. They recommended the use of functionality-oriented verification strategies, anticipating the evolution of ISO standards that actually ask for the complete definition of verification operations in design phase; particularly through the complete definition of the specification operator and the application of duality principle. They also showed that, as the number of measurement points increases, the estimated values converge to the "true" value of form error and the sampling strategy dispersion converges to zero.

Lin and Chen [9] noticed that sample size was a function of the pattern elements in a feature based solid model. Later on, Fan and Leu [10] studied how sample size should be selected according to the shape of the planar surface and the ratio between the length and width of the actually sampled area.

Hurt [11], comparing different plane fit algorithms, noticed that the accuracy of the LS estimate improves by increasing the number of measurement points. He recommended the sampling of at least 20 measurement points in order to have an accurate report of flatness. Hocken et al. [12] suggest a larger number of points to obtain the convergence of form error evaluation. Working on a straightness line 1000 mm long and on a flatness feature 500 x 500 mm wide, they described that, in both cases, at least 50 points are needed to obtain the convergence of parameters describing the fitted line and plane. A similar conclusion, for the case of plane fit, was made by Caskey et al. too [13].

All these studies about sample size have been performed without taking into account the uncertainty arising in the different verification scenarios. At this point, it is clear that sample size is affected by the measuring equipment at hand, the type of feature to be checked, and the details of the tolerance definition. In other words, it is not possible to define a sample size suitable for every kind of feature a-priori. Often the same feature presents different shapes (defects) even for workpieces manufactured on the same machine, in different moments, just for the variability of the machining process itself (e.g. different tool wear). Therefore, tailored samplings should be used in order to correctly detect the actual surface geometry [9].

The first study on sample size that tries to address the problem of uncertainty evaluation is provided by Zhang et al. [4]. They propose a neural network approach to bypass the complexity of relationships between sampling size and all the variables of manufacturing and inspection processes. An adequate training set allows the neural network to build an effective model able to estimate the uncertainty of the form error evaluation, for the feature on which the network has been trained. The main advantage of neural networks is that they are able to build models according to the training sets provided, without requiring users to deeply understand all problem details. Obviously, users need to have an overall perspective of the problem in order to provide adequate training sets.

The intricate bundle of factors and variables affecting the determination of proper sample size for the evaluation of form errors has been afforded by Hwang et al. [14] with a hybrid neuro-fuzzy approach where the tolerance and feature geometry are considered as factors.

Raghunandan and Venkateswara Rao [15] classify the effects of manufacturing processes for the purpose of sample size definition using the information carried by roughness tests. Roughness specifications are usually combined with form tolerances. They require very fine, small-scale, measurements and are particularly suitable to identify the technological signature of the manufacturing process; a precious information for the design of the best sampling strategy. As a small-scale local characteristic, roughness is particularly suitable to detect the surface variations at different locations and identify those more critical for the correct form error evaluation. The study established that surface finish plays an important role and shall be considered one of the parameters for sample size definition. Poor quality surfaces, with high R_a values, require a sample size greater than well-finished surfaces to obtain the same accuracy of error evaluation.

2.2.2 Position of measurement points

Concerning the location of measurement points on the feature to be inspected, the CMM literature offers several studies on the application of statistical methods like uniform, random or stratified sampling [10], rather than grid extraction strategies compliant with GPS standards [16], particular sequences for low density extractions [5, 17, 18] or adaptive strategies [19-21].

The most popular extraction strategies are random sampling, uniform sampling and stratified sampling. Particularly, the last one is necessary whenever the surface consists of multiple features forming strata [10].

Other sampling strategies have been presented, mainly for flatness features, aimed at reducing the number of sampling points necessary to reach a predefined accuracy level. Woo and Liang [5], introducing the application of Hammersley sequence, achieved a nearly quadratic reduction of the sample size with respect to the sample size necessary to guarantee the same accuracy with random sampling or uniform sampling. They further compared Hammersley sequence with Halton-Zembra sequence on simulated surfaces but they did not find significant differences of performance. The choice is a matter of convenience mainly, as the Halton-Zembra sequence suffers from the limitation that sample size has to be a power of 2. The efficiency of Hammersley sequence has been proven also by Lee et al. [18]. They integrated the Hammersley sequence together with stratified sampling to obtain an improved feature-based inspection technique. This was tested and compared with random and uniform samplings on a set of stratified features obtained with numerical simulations. It was proved also that Hammersley sequence is more accurate than random sampling and that, when dealing with stratified features, stratified Hammersley sequence is more robust than stratified random or stratified uniform sampling [18].

Scattering measurement points over a feature in order to cover the whole surface is very useful but does not guarantee to detect the peaks and valleys of form deviation. Form error evaluation completely relies on the identification of these points, thus modelling approaches are necessary in order to guess the location of these points and reduce the sample size the most possible. Different studies in literature proposed adaptive sampling strategies based on the knowledge of manufacturing processes and their technological signature.

The first work in this direction was made by Badar et al. [19]. They presented an adaptive sampling that uses manufacturing error patterns (technological signature) and optimization search techniques to check straightness and flatness tolerances with LS association criterion. This adaptive sampling requires the inspection of some arbitrary located points in order to be started.

In a further work, Badar et al. identified the location of sample points relying on the surface error pattern left by the manufacturing process [22]. Then, they proposed to decide the initial inspection locations according to the form error profile (the signature of manufacturing process) and the workpiece geometry [20]. Surface profile guides the inspection of the initial points only; the additional ones are measured according to the search heuristics. This adaptive sampling was tested on a set of face-milled and end-milled plates, made respectively of cast-iron and 7075-T6 aluminium alloy [20]. It was compared with other non adaptive samplings and resulted to be the most reliable and effective [20]. This approach requires the availability of models for surface error patterns, which may be not available for every manufacturing process. In this case important information about the manufacturing process may be obtained from the analysis of surface roughness [15].

This thesis presents, in Chapter 6, a Kriging-based adaptive sampling that relies almost exclusively on the information collected through measurement points. Particularly the Kriging model (that is an interpolatory model) improves with the sampling of each measurement point (as the actual knowledge of the measurand does) and is used to focus the sampling in areas that are likely to be more significant for the form error evaluation: namely where peaks or valleys are expected [21, 23].

The approach of ISO-GPS standards is quite different from those previously mentioned. In order to enable the correct implementation of verification operators, sampling (that in terms of GPS language is an extraction operation) has to be defined directly from specifications. Number and position of sampling points are defined according to the tolerance specification band (upper and lower cut-off wavelengths). The form of features profiles is regarded as a signal. In this sense the lower cut-off wavelength represents a limit on the signal bandwidth that, according to Nyquist criterion, poses a constraint for correct signal reconstruction. Nyquist theorem states:

"*If it is known that an infinitely long signal contains no wavelengths shorter than a specified wavelength, then the signal can be reconstructed from the values of the signal at*

regularly spaced intervals provided that the interval is smaller than half of the specified wavelength".

Then, in order to avoid aliasing, sampling distance must be shorter than one seventh of the smallest wavelength to be reconstructed: namely the lower cut-off wavelength [24].

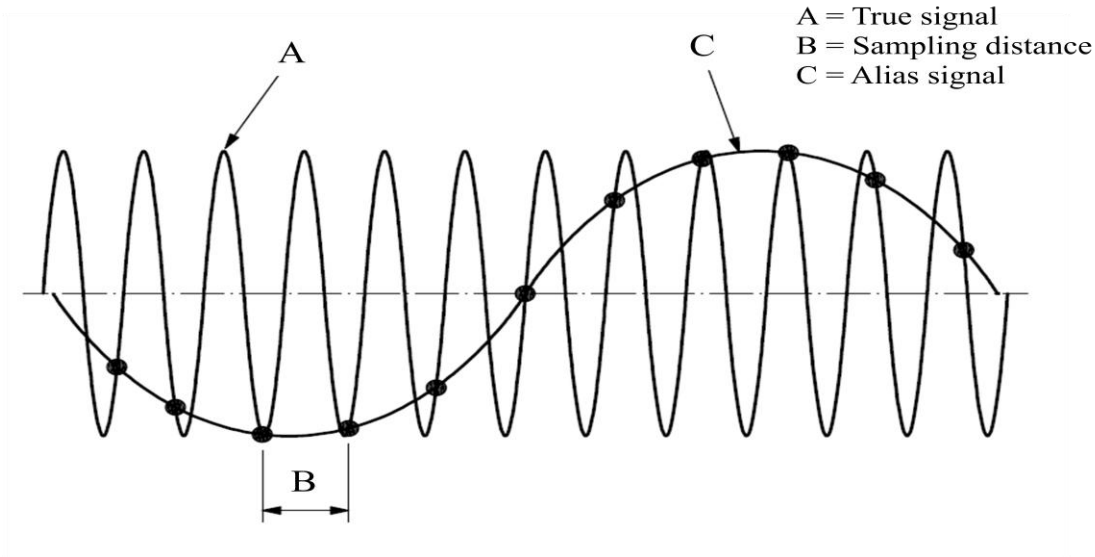

Figure 2.1 - Aliasing example: sampling distance is too large to define the true shape of the signal [24].

The ISO-GPS approach requires a massive amount of points to be measured. It can be easily implemented with new generation measuring instruments, mainly those based on optical acquisition of three-dimensional surfaces, that are able to acquire the coordinates of thousands of points pour second. However, these instruments are not currently available in most of metrology laboratories where the dominant instrument is represented by CMM that, usually, is recommended for measuring few points only. ISO-GPS standards recognize that sample size could be a critical aspect for the correct implementation of perfect verification operators, and suggest the use of grid extraction strategies based on the measurement of profiles (checked according to perfect verification operator) arranged in grids in order to properly cover the whole surface [16]. Besides different grid extraction strategies, ISO standards recognize also the random sampling. Anyway, GPS standards do not allow the specification of the parameters necessary to completely define grids, and this possibility is neither considered in future amendments. Therefore grids cannot be defined univocally in design phase and, unless dedicate notes are used, their use will always generate method uncertainty.

2.3 Algorithms for form error assessment

2.3.1 Statistical algorithms

Thanks to its analytical formulation and the possibility to be implemented with fast algorithms, Least Squares (LS) is the association criterion most widely embedded in CMM

softwares. Usually, when a CMM does not offer the possibility to choose among different association criteria, LS is the one implemented by default.

LS is the most traditional among the direct best fitting methods. As the name says, these methods try to best fit a nominal feature to a set of measurement points. LS, in particular, is based on the minimization of the sum of squared distances of measurement points from the fitting nominal feature.

With respect to flatness tolerance, the definition of the LS problem is the following. Given a dataset of sampling points $(x_i, y_i, z_i)\ _{i=1}^{n}$ where x_i and y_i are independent variables and z_i is a dependent variable whose value is found by observation (the height of sampling points). The model function has the form $f(x, y, \boldsymbol{\beta})$, where the m adjustable parameters are held in the vector $\boldsymbol{\beta}$. The goal is to find the parameter values for the model which "best" fits the data. The least squares method finds its optimum when the sum, S, of squared residuals (2.1) is minimized.

$$S = \sum_{i=1}^{n} r_i^2 \qquad \textbf{(2.1)}$$

A residual is defined as the difference between the actual value of the dependent variable and the value predicted by the model: $r_i = z_i - f(x_i, y_i, \boldsymbol{\beta})$. Particularly for the solution of a flatness problem, the equation of a nominal plane has to be fitted to the set of measurement points. Denoting the intercept as β_0 and the slope with respect to x and y direction as β_1 and β_2 respectively, the model function is given by: $f(x, y, \boldsymbol{\beta}) = \beta_0 + \beta_1 x + \beta_2 y$.

LS method does not comply with the mathematical definition of tolerance zone. It is able to define an envelop volume that contains all measurement points, but this envelop is not of minimal size. Therefore it generally overestimates form errors [25] and can lead to rejection of good parts that would be in specification under a Minimum Zone (MZ) evaluation.

However, LS association criterion is often preferred to MZ because of its easier and faster implementation, because it allows the analytic estimation of evaluation uncertainty and because the form error overestimation can be regarded as an additional safety with respect to the real compliance with functional requirements. On the other hand it introduces a restriction on the error actually allowed by specification, restricting manufacturability.

An alternative to the traditional LS algorithm has been proposed by Zhu et al. [26]. The method relies on an ‘Iterative Reweighted Least Squares’ (IRLS) algorithm that allows the approximate estimation of form deviation through the iterative solution of a series of weighted least squares problems. The weight parameters are updated, for each iteration, to minimize the squared maximum deviation. Anyway, the form error is usually overestimated if the measurement points are not well aligned.

2.3.2 Extreme fit algorithms

Extreme fit association criteria are more consistent with the geometrical definition of tolerance zones (see for example the definition of flatness tolerance zone [27] or roundness tolerance zone [28]) thus more suitable for functional verification. On the other hand extreme fit algorithms are more sensitive to sampling and do not allow a straightforward assessment of the uncertainty associated with the form error estimation.

The most popular extreme fit association criterion is doubtless Minimum Zone. It naturally descends from the definition of tolerance zone (according to both ISO [29] and ASME [30] standards) and several algorithms are available for its computation on most of features. Other feature-dedicated extreme fit association criteria are available for features presenting revolute symmetry. E.g. maximum inscribed and minimum circumscribed association criteria can be used on circular [28], cylindrical [31] and spherical features; their use should be related with the feature functional requirements.

The algorithms developed for MZ error evaluation can be classified in two different families according to the nature of the method used to solve the MZ problem. On one hand there are numerical methods (§2.3.2.1) based on Monte Carlo, simplex and spiral search, Chebyshev approximations, non-linear optimization and conversion from non-linear to linear optimization. On the other hand there are computational-geometry-based techniques (§2.3.2.2) that rely on the computation of a convex hull for the given finite set of measurement points.

2.3.2.1 Numerical methods

In the initial works by Murthy and Abdin [32] the MZ evaluation problem has been afforded through methods based on Monte Carlo, simplex and spiral search. These methods formulate the problem as an optimization model to minimize the maximum distance from an ideal reference feature or the difference between the maximum and minimum distance from a given reference. Different approaches have been followed to solve these optimization models and will be briefly analysed in this section. The first possible approach consists of direct solution of optimization problems. Shunmugam [33] tested the simplex search to minimize an average deviation, then he proposed a simple approach, called the Median technique, which obtains the minimum value of errors [34]. A different approach was followed by Kanada and Suzuki [35], and Hossein et al [36], who used non-linear optimization techniques to calculate the exact values of straightness and flatness errors.

Instead of directly solving the optimization problem, several approximated ways have been searched to enhance the computational efficiency and easiness of implementation. Obviously, the introduction of approximations is paid with a reduction of the evaluation accuracy. Chetwynd [37] has been the first to propose linear programming techniques for approximating the simplex search in flatness error assessment. The linear programming approach was then standardized by Portman et al. [38] for the evaluation of straightness,

flatness, cylindricity and sphericity form errors. Other approximation methods were presented by Fakuda and Shimakohbe [39] who used a minimax approximation method. However, the minimum zone values were reached by Shunmugam and Danish with the use of discrete Chebyshev approximations [40]. On the other hand Carr and Ferreira [41] converted the non-linear problem of MZ solution into a linear optimization problem through a combination of coordinate and scaling transformations. Anyway, search-based numerical methods require long computational times as they need a large number of trials in order to satisfy the convergence criteria [25].

Another family of numerical methods is based on exchange techniques. These methods sequentially exchange some points from the current set of interested points with other from the remaining set according to precise criteria [39, 42]. Huang et al. developed an algorithm for the evaluation of straightness [43] and flatness [44] errors called the Control Plane Rotation Scheme. The algorithm is based on the criteria for MZ solution and strict rules for data exchange.

The last family of methods for solving MZ problems relies on the use of meta-heuristics such as tabu search, simulated annealing and genetic algorithms (GAs). A genetic algorithm had been proposed by Sharma et al. [45] to solve generalized minimax problems that can be applied for the assessment of various form errors. Then, a generalized but simplified version of Sharma et al.'s GA has been presented by Cui et al. [46]. On the other hand Liu et al. proposed the hybridization of GA with the geometric characterization method used for the rapid convergence of solution [47]. GA-based techniques have several drawbacks represented by the possibility of non-convergence to an exact optimal solution (due to their nature of probabilistic processes) and the computational burden associated with large datasets.

2.3.2.2 Computational-geometry-based techniques

After the first efforts to solve the MZ problem with numerical methods, researchers started exploring more promising techniques based on computational geometry [48, 49]. These techniques are based on the analysis of the convex-hull containing the whole set of measurement points. The convex-hull of a set of points in the Euclidean space is the boundary of the smallest convex domain containing all the points of the set. A domain is said to be convex if the segment connecting any pair of points is entirely contained in the domain. In a three dimensional space, the convex-hull takes the shape of an elastic wrap tightened to close all points inside [50].

Traband et al. [48] performed the MZ evaluation of straightness and flatness tolerance using, for the first time, the concept of the convex-hull applied on measurement datasets. Lee [51] proposed a new method called the "convex-hull edge method", a comprehensive search algorithm that is able to find the MZ form error working with the edges of the convex-hull.

Samuel and Shunmugam [25] noticed that MZ evaluation criteria are often applied regardless the origin of measurement data and the feature functional requirements. Literature

had shown the importance of function-oriented verification strategies [8, 52] as the contact between engineering parts occurs at their extreme functional boundaries [53]. Moreover, the measurement data analysis cannot neglect the bias introduced by measurement processes, as the data obtained by using form measuring instrument/setups are affected by orientation issues that are easily avoidable with CMM measurements. Data from different measuring instruments need different types of analysis. These have been studied in detail for the case of form error evaluations based on computational geometric techniques [25].

The convex-hull edge method has been recently enhanced by Lee [54] with the decomposition of the three-dimensional flatness problem in a set of two-dimensional straightness evaluations. A straightness analysis is associated to every face of the convex-hull and the face presenting the lowest straightness deviation defines the orientation of the MZ envelop. This approach allows hundreds of points to be analyzed in a negligible time even with a normal personal computer [54]. Particularly, this method will be used every time a MZ flatness deviation is assessed in this thesis.

2.4 Uncertainty evaluation for statistical association criteria

Several researches have been investigating the aspects related with CMM sampling and the assessment of the uncertainty associated with the whole verification process (sampling of measurement points together with their analysis by means of an association criterion). Most of literature deals with the traditional CMM verification process where the data analysis is performed at the end of the extraction phase (measurement) through the LS association criterion.

LS is the most popular association criterion and, being a statistical method, it allows the analytic determination of the uncertainty associated with the form error evaluation. It determines the fitting geometry using a maximum likelihood method on all the measured points: every point participates into the equation that defines the reference plane. Therefore, it is possible to determine the uncertainty of the evaluation starting from the reference plane equation, the definition of flatness deviation and the instrument measurement uncertainty (see §2.4.1).

The situation is more complex if the uncertainty to be assessed is that of the whole verification process. Many variables affecting measurement results cannot be taken into account in analytic form. For example uncertainty contributions can be generated by: the measuring equipment [55, 56], the evaluation criterion [57, 58], the density and location of sampling points with respect to the actual form deviation, and form error patterns [8, 59]. Usually the verification process cannot be completely expressed with a function (because the influence of many input variables is unknown) and the analytic approach is limited to the effect of the association criterion [60]. In this case, approaches based on experimental models and Monte Carlo simulations are adopted [60, 61]. These are briefly presented in §2.4.2

2.4.1 Analytic evaluation

Yau [58], dealing with best fit algorithms, proposed the analytical determination of the evaluation uncertainty due to the fit algorithm. He defined the measurand Y as the output of a function f depending on a number of input quantities X_i (i = 1, 2, …, m):

$$Y = f(X_1, X_2, ..., X_m)$$

Usually the exact values of quantities X_i are not known and are substituted by the estimated values x_i. Under the hypothesis of uncorrelated input variables, the uncertainty on the estimation of value Y can be expressed as:

$$s_y^2 = \sum_{i=1}^{m} \left(\frac{\partial f}{\partial x_i} \right)^2 s_{x_i}^2 \qquad \textbf{(2.2)}$$

The partial derivatives $\partial f / \partial x_i$ describe the sensitivity of the algorithm output (Y) with respect to each input variable. They are the weights for the sum of all *input uncertainties*: the uncertainties on the measurement of sampling points coordinates and the uncertainties on the coefficients describing the orientation of the LS tolerance zone (see §3.5.1 for an example and further details).

According to this idea, Cui, Fu and Huang [57] perform a systematic analysis of uncertainty estimation in measurements involving LS association criterion. Starting from the nominal feature equation, under the hypothesis of sampling points normally distributed with respect to the fitting plane, they develop equations for estimating the uncertainty of LS algorithm applied for the main form tolerances. The nominal feature equation is used, together with the definition of the tolerance zone, to determine the partial derivatives that give the sensitivity coefficients of model variables.

This uncertainty evaluation approach has been validated through the use in several works and researches [62-64]. Usually flatness tolerance is the most analyzed due to its popularity and to the fact that every surface to be used as a datum feature needs to be qualified at least with a form tolerance (flatness for instance).

2.4.2 Experimental evaluation

The analytic approach for estimating the uncertainty of a certain association criterion is quite straightforward, especially if this is a statistical criterion. It becomes trickier when dealing with the estimation of the uncertainty of the whole verification process. The equation relating all the verification process variables to the measurement output is never known. For example the influence of sampling strategy can be negligible or important according to the shape and magnitude of form deviation, that is unknown when the workpiece first enter the measurement process [61].

Balsamo et al. [65] proposed Monte Carlo simulation to evaluate the combined effect of all the task specific uncertainties related with CMM verification processes. This kind of simulation is based on the generation of a population of output variables given the probability

density function of input parameters. The output variable can then be characterized according to the population of simulated output variables. Schwenke et al. [66] translated this approach into a modular and visual software to be used in combination with CMM verification operations to assess the different contributions to measurements uncertainty. Wübbeler et al. [60] proposed a numerical method to evaluate the measurement uncertainty based on Monte Carlo simulation. Kruth et al. [61] improved the performance of Monte Carlo simulation approach by taking into account the technological signature that strongly characterizes the feature shape and affects the performance of sampling strategy (density and location of sampling points).

Gao [67] suggests a different method for uncertainty estimation that has been further developed by Qin et al. [68]. They discuss the estimation of non statistical uncertainty in precision measurements using grey system theory [69]. Particularly they deal with the problem of uncertainty assessment when the sample size is small and the distribution of the data is unknown. They use a cumulated true size vector and a cumulated measurement data vector in order to reduce the effects of errors occurring in measurement and numerical calculation. The uncertainty assessment is based on the l_∞ norm of the difference between the two vectors.

Another approach, based on Bootstrap methodology [70, 71], estimates the uncertainty due to the sampling and the use of a certain association criterion through the construction of a set of simulated samples extracted from the nominal measurement dataset [64]. As it is based on an operation of extraction with reintroduction, this system has the drawback of a poor performance if applied on too small datasets. This approach will be further described from a theoretical point of view in §2.6 and will be applied on a flatness error assessment in Chapter 3. Its performance will be analyzed with respect to statistical and extreme fit association criteria.

2.5 Uncertainty evaluation for extreme fit association criteria

The problem of uncertainty estimation for verification processes involving extreme fit association criteria is quite new and few researches deal with it. The main efforts in the last decades have been addressed to the improvement of extreme fit association criteria and at researching efficient algorithms for an effective implementation. Due to the non linearity of the numerical methods traditionally used to solve the extreme fit problem, it is not possible to estimate uncertainty in analytic way (§2.5.1). The analytical estimation is neither allowed by the computational-geometry-based techniques. Despite the unavailability of analytic approaches, a semi-analytic approach has been proposed, with different nuances, that is presented in §2.5.2.

2.5.1 Semi-analytic evaluation

Wen et al. [72] propose to estimate the uncertainty of MZ evaluation starting from the equation of the MZ reference plane and applying equation (2.2) to extract the uncertainty model. The approach is the same of the one used for the LS method (see theory in §2.4.1 and the flatness example in §3.5.1). However, the big difference with respect to statistical methods is that there are no statistics for the MZ reference plane. The equation of the reference plane is deterministic (determined on the extreme points of the convex-hull only) and there is no estimation of the uncertainties of the reference plane coefficients: fundamental elements among the uncertainty model inputs. While for the LS method the statistics of the reference plane are an intrinsic characteristic of the method itself, for extreme fit association criteria, such as MZ, they can be estimated only by replicating the verification operator. Therefore, the approach suggested by Wen et al. is classified as semi-analytic because it partially relies on experiments.

In order to have an uncertainty assessment that does not require any further measurement, an alternative approach is presented in this thesis that relies on bootstrap method for estimating the statistics of the MZ reference plane. The method is detailed in §3.6.1 for the case of a flatness tolerance verification.

2.5.2 Experimental evaluation

Choi et al. [73] investigated the relationship between form error evaluation and the number of sampling points. They recognize that the uncertainty of the evaluation is largely affected by the shape of the feature surface and the ability of measurement points (those on which the form error evaluation is based) to detect the extreme points: peaks and valleys. For better describing the probability of detecting those points on engineering surfaces with non-random error patterns, they use beta density probability functions (Figure 2.2). These kinds of probability density functions are quite common as the normal one is suitable to describe small-magnitude random errors only.

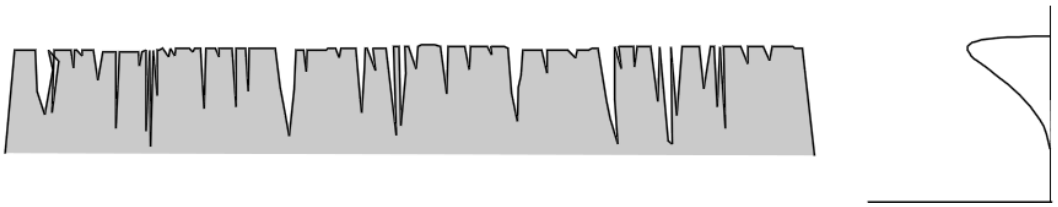

Figure 2.2 - Example of non-normal form error (left) and of the beta probability density function (right) which describes it [73].

They explore an analytical approximation method based on the use of order statistics to model the flatness evaluation and obtain statistical properties of ranked elements, included the maximum and minimum points. However, the analytic derivation of the uncertainty function is too complex, so they propose an experimental approach based on the use of neural networks. In this way, the phase of interpreting the variables affecting the uncertainty model

can be avoided. They find that, if points are sampled uniformly on the feature surface, the evaluation uncertainty does not depend on their density but on their number only. The neural network approach is the method proposed for practical implementation. However it is not suitable for everyday measurements because its performance heavily relies on the goodness of the training sets.

As suggested for the experimental estimation of the uncertainty of statistical-algorithms-based verification processes (§2.4.2), other experimental methods can be applied. Particularly Monte Carlo simulations, grey system theory and bootstrap methodology are suitable also for extreme fit association criteria. In this thesis, bootstrap method is preferred and will be applied on both the LS and MZ evaluation of a case study flatness deviation (see §3.5.2 and §3.6.2 respectively).

2.6 Bootstrap

Bootstrap methodology has been introduced by Efron [70] as a more primitive representation of Quenouille-Tukey jackknife. Jackknife is a nonparametric method for the estimation of the bias and variance of a statistic of interest, and for testing the null hypothesis that the distribution of a statistic is centered at a certain point [74]. Being more general, bootstrap is able to clarify the theoretical basis of jackknife, which can be thought as a linear expansion method for approximating the bootstrap. The bootstrap method will be briefly presented, according to Efron formulation [70], for the one-sample situation dealing with a sample of size *n* from a completely unspecified probability distribution *F*.

Let's denote the random sample and its observation as $\mathbf{X} = X_1, X_2, \cdots, X_n$ and $\mathbf{x} = x_1, x_2, \cdots, x_n$ respectively. Given a specified random variable $R(\mathbf{X}, F)$, the problem solved by bootstrap is the estimation of the sampling distribution of R on the basis of the observed data **x**. Traditional jackknife theory focuses on two particular choices of R:

$$R(\mathbf{X}, F) = t(\mathbf{X}) - \theta(F) \tag{2.3}$$

$$R(\mathbf{X}, F) = \frac{t(\mathbf{X}) - \mathrm{Bias}(t) - \theta(F)}{\mathrm{Var}(t)^{\frac{1}{2}}} \tag{2.4}$$

where $\theta(F)$ is the parameter of interest, e.g. the mean or correlation of F, and $t(\mathbf{X})$ is an estimator of $\theta(F)$, respectively the sample mean or sample correlation. The sampling distribution of $R(\boldsymbol{X}, F)$ from equation (2.3), or more exactly its mean (the bias of t) and variance, is estimated using the standard jackknife theory. The estimates of bias and variance, $\mathrm{Bias}(t)$ and $\mathrm{Var}(t)$, are functions of **X** obtained by recomputing $t(\cdot)$ n times, each time removing one component of **X** from consideration.

Equation (2.4) is the second traditional choice of *R*. According to Tukey's original suggestion [74] it should be treated as having a standard Student's *t* distribution with *n*-1 degrees of freedom.

The bootstrap method for the one-sample problem consists of three main steps:

1. The sample probability distribution F is constructed putting mass $1/n$ at each point $x_1, x_2, \cdots, x_n$.

2. With F fixed, a sample of size *n* has to be drawn from F.

$$X_i^* = x_i^*, X_i^* \sim_{ind} F \qquad i = 1, 2, \cdots, n \tag{2.5}$$

   Then $\mathbf{X}^* = (X_1^*, X_2^*, \cdots, X_n^*)$ and $\mathbf{x}^* = (x_1^*, x_2^*, \cdots, x_n^*)$ are called the bootstrap samples. These samples are not permutations of the original distribution F since the values are selected with replacement from the set $\{x_1, x_2, \cdots, x_n\}$. The ordinary jackknife corresponds to the extraction without replacement of samples of size *n*-1.

3. The sampling distribution of $R(\mathbf{X}, F)$ is approximated by the bootstrap distribution of $R^*(\mathbf{X}^*, F)$. An example is represented by the distribution of R^* induced by the random mechanism (2.5), with F fixed at his observed value. The distribution of R^* equals the desired distribution of R if $F = F$. The goodness of approximation of R^* depends on the form of *R*.

Three different methods are available for calculating the bootstrap distribution.

- **Method 1:** direct theoretical calculation, that is available for the two random variables *R* traditionally chosen by jackknife.
- **Method 2:** Monte Carlo simulation, to approximate the bootstrap distribution, through repeated realizations of $\mathbf{X}^*$ generated by taking random samples of size *n* from F. If x^{*1}, x^{*2}, $\cdots$, x^{*N} are the random samples, the histogram of the corresponding values $R(x^{*1}, F)$, $R(x^{*2}, F)$, $\cdots$, $R(x^{*N}, F)$ is taken as an approximation of the actual bootstrap distribution.
- **Method 3:** Taylor series expansion methods used to obtain the approximate mean and variance of the bootstrap distribution of R^*. This method goes under the name of *delta method* also and is the same of the usual jackknife theory.

Bootstrap is then a general computer-based methodology able to substitute theoretical analysis with intense computation. One of the main problems in applied statistics is the estimation of unknown parameters: it is necessary to choose the adequate estimator θ and, once it has been chosen, it is necessary to evaluate its accuracy. Bootstrap is particularly useful for the estimation of estimators accuracy and can routinely answer questions that are too complicated for traditional statistical analysis.

Bootstrap will be used in this work using the Monte Carlo based evaluation of the bootstrap distribution. This approach requires only minor modifications of the problem formulation as it reiterates the original algorithm used for computing *R*. The amount of time required is just about *N* times the time necessary for the original computation [71].

2.7 Conclusions

This chapter presented a systematic review for the evaluation of form deviations in CMM-based verification operations. The evolution of the algorithms for evaluating geometric characteristics and for assessing the uncertainty of these evaluations has been analyzed. Particularly the systematic review allowed pointing out a gap between statistical and extreme fit association criteria, about the estimation of implementation uncertainty. For extreme fit criteria there is no way to assess the implementation uncertainty with a fully analytic approach. One method has been found in literature, but it requires measurements replication and does not allow a definition of the uncertainty based on the dataset at hand only.

With respects to the assessment of geometric characteristics (form errors), two families of algorithms have been identified: statistical (e.g. LS) and extreme fit (e.g. MZ) association criteria. On the other hand, also the approaches for uncertainty estimation have been classified in two different families: analytic or experimental. Particularly, analytic approaches are preferable with statistical association criteria while the experimental ones with extreme fit. None of these methods can be preferred a-priori and pros and cons have to be carefully analyzed. Both the association criteria and the approaches for uncertainty estimation (both for each association criterion) will be tested and compared on a flatness case study in Chapter 3. Particularly, among all the experimental methods for uncertainty estimation the bootstrap method will be preferred.

A further novelty is provided by the semi-analytic approach proposed for the assessment of MZ implementation uncertainty. This approach bridges the gap with the LS method providing a method, suitable to cope with extreme fit algorithms, which carries all the benefits of the analytic approach.

2.8 References

[1] ISO/TS 17450-1 (2005) *Geometrical product specifications (GPS) - General concepts - Part 1: Model for geometrical specification and verification*. ISO, Geneve.

[2] Yau H.-T. and Menq C.-H. (1996) *A unified least-squares approach to the evaluation of geometric errors using discrete measurement data.* Int. J. Mach. Tools Manufact., **36** (11) 1269-1290.

[3] Menq C.-H., Yau H.-T., Lai G.-Y. and Miller R.A. (1990) *Statistical Evaluation of Form Tolerances Using Discrete Measurement Data.* ASME Advances in Integrated Product Design and Manufacturing, **47** 135-149.

[4] Zhang Y.F., Nee A.Y.C., Fuh J.Y.H., Neo K.S. and Loy H.K. (1996) *A Neural Network Approach to Determining Optimal Inspection Sampling Size for CMM.* Computer-Int. Manufa. Syst, **9** (3) 161-169.

[5] Woo T.C. and Liang R. (1993) *Dimensional measurement of surfaces and their sampling.* Comput. Aided Des., **25** (4) 233-239.

[6] Kim W.-S. and Raman S. (2000) *On the selection of flatness measurement points in coordinate measuring machine inspection.* Int. J. Mach. Tools Manufact., **40** (3) 427-443.

[7] Yau H.-T. and Menq C.H. (1992) *An automated dimensional inspection environment for manufactured parts using coordinate measuring machines.* Int. J. Prod. Res., **30** (7) 1517-1536.

[8] Weckenmann A., Eitzert H., Garmer M. and Webert H. (1995) *Functionality-oriented evaluation and sampling strategy in coordinate metrology.* Precision Engineering, **17** 244-252.

[9] Lin Z.C. and Chen C.C. (1997) *Study of the automatic planning of measurement points with basic element features.* Int. J. Prod. Res., **35** (11) 3157-3178.

[10] Fan K.C. and Leu M.C. (1998) *Intelligent planning of CAD-directed inspection for coordinate measuring machines.* Comput. Integr. Manuf. Syst., **11** (1-2) 43-51.

[11] Hurt J.J. (1980) *A Comparison of Several Plane Fit Algorithms.* CIRP Annals, **29** (1) 381-384.

[12] Hocken R.J., Raja J. and Babu U. (1993) *Sampling Issues in Coordinate Metrology.* ASME Manuf. Rev., **6** (4) 282-294.

[13] Caskey G., et al. (1992) *Sampling Techniques for Coordinate Measuring Machines*. in proc. of 1992 NSF Design and Manufacturing Systems Conf., Atlanta, GA, pp 983-988.

[14] Hwang I., Lee H. and Ha S. (2002) *Hybrid neuro-fuzzy approach of measuring points for knowledge based inspection planning.* Int. J. Prod. Res., **40** (11) 2507-2520.

[15] Raghunandan R. and Rao P.V. (2008) *Selection of sampling points for accurate evaluation of flatness error using coordinate measuring machine.* J. Mater. Process. Technol., **202** 240-245.

[16] ISO/TS 12781-2 (2011) *Geometrical product specifications (GPS) - Flatness - Part 2: Specification operators*. ISO, Geneve.

[17] Woo T.C., Liang R., Hsieh C.C. and Lee N.K. (1995) *Efficient Sampling for Surface Measurements.* J. Manuf. Syst., **14** (5) 345-354.

[18] Lee G., Mou J. and Shen Y. (1997) *Sampling strategy design for dimensional measurement of geometric features using Coordinate Measuring Machine.* Int. J. Mach. Tools Manufact., **37** (7) 917-934.

[19] Badar M.A., Raman S. and Pulat P.S. (2003) *Intelligent Search-Based Selection of Sample Points for Straightness and Flatness Estimation.* ASME J. Manuf. Sci. Eng., **125** (2) 263-271.

[20] Badar M.A., Raman S., Pulat P.S. and Shehab R.L. (2005) *Experimental Analysis of Search-Based Selection of Sample Points for Straightness and Flatness Estimation.* Journal of Manufacturing Science and Engineering, **127**.

[21] Barbato G., Panciani G.D., Ricci F., Ruffa S. and Vicario G. (2011) *Form tolerance verification using the Kriging method*. in proc. of ENBIS-DEINDE, Turin.

[22] Badar M.A., Raman S. and Pulat P.S. (2005) *Experimental Verification of Manufacturing Error Pattern and its Utilization in Form Tolerance Sampling.* Int. J. Mach. Tools Manuf., **45** (1) 63-73.

[23] Vicario G., Barbato G., Ruffa S., Panciani G.D. and Ricci F. (2011) *Form tolerance verification: a sequential approach of the inspected design*. in proc. of AMCTM 2011 Conference, Gothenburg (Sweden).

[24] ISO/TS 12780-2 (2006) *Geometrical product specifications (GPS) - Straightness - Part 2: Specification operators*. ISO, Geneve.

[25] Samuel G.L. and Shunmugam M.S. (1999) *Evaluation of straightness and flatness error using computational geometric techniques.* Comput. Aided Des., **31** 829-843.
[26] Zhu X., Ding H. and Wang M.Y. (2004) *Form error evaluation: An iterative reweighted least squares algorithm.* Journal of Manufacturing Science and Engineering, **126** 535-41.
[27] ISO/TS 12781-1 (2006) *Geometrical product specifications (GPS) - Flatness - Part 1: Vocabulary and parameters of flatness*. ISO, Geneve.
[28] ISO/TS 12181-1 (2006) *Geometrical product specifications (GPS) - Roundness - Part 1: Vocabulary and parameters of roundness*. ISO, Geneve.
[29] ISO 1101 (2004) *Geometrical product specifications (GPS) - Geometrical tolerancing - Tolerances of form, orientation, location and run-out*. ISO, Geneve.
[30] ASME Y 14.5 (2009) *Dimensioning and Tolerancing – Engineering Drawing and Related Documentation Practices*.
[31] ISO/TS 12180-1 (2006) *Geometrical product specifications (GPS) - Cylindricity - Part 1: Vocabulary and parameters of cylindrical form*. ISO, Geneve.
[32] Murthy T.S.R. and Abdin S.Z. (1980) *Minimum zone evaluation of surfaces.* International Journal of Machine tool Design and Research, **20** 123-36.
[33] Shunmugam M.S. (1987) *New approach for evaluating form errors of engineering surfaces.* Comput. Aided Des., **19** (7) 368-74.
[34] Shunmugam M.S. (1986) *On assessment of geometric errors.* International Journal of Production Research, **24** (2) 413-25.
[35] Kanada T. and Suzuki S. (1993) *Evaluation of minimum zone flatness by means of nonlinear optimization techniques and its verification.* Precision Engineering, **15** (2) 93-99.
[36] Hossein S.C., Huay S.L. and Saied M. (1996) *Straightness and flatness tolerance evaluation: an optimization approach.* Precision Engineering, **18** (1) 30-37.
[37] Chetwynd D.G. (1985) *Applications of linear programming to engineering metrology.* Proceedings of the Institute of Mechanical Engineers, **199** (B2) 93-100.
[38] Portman V.T., Weill R.D., Shuster V.G. and Rubenchik Y.L. (2003) *Linear-programming-based assessments of geometrical accuracy: Standard presentation and application area.* International Journal of Machine Tools & Manufacture, **43** 1023-33.
[39] Fakuda M. and Shimokohbe A. (1984) *Algorithms for form error evaluation - methods of minimum zone and the least squares*. in proc. of International Symposium on metrology and Quality Control in Production, Tokyo, pp 197-202.
[40] Danish P.B. and Shunmugam M.S. (1991) *An algorithm for form error evaluation using the theory of discrete and linear Chebyshev approximations.* Computer Methods in Applied Mechanics and Engineering, **92** 309-24.
[41] Carr K. and Ferreira P. (1995) *Verification of form tolerances, part I: basic issues, flatness and straightness.* Precision Engineering, **17** (2) 131-43.
[42] Burdekin M. and Pahk H.J. (1989) *The application of a microcomputer to the on-line calibration of the flatness of engineering surfaces.* Proceedings of the Institute of Mechanical Engineers, **203** 127-37.
[43] Huang S.T., Fan K.C. and Wu J.H. (1993) *A new minimum zone method for evaluating straightness errors.* Precision Engineering, **15** (3) 158-65.
[44] Huang S.T., Fan K.C. and Wu J.H. (1993) *A new minimum zone method for evaluating flatness errors.* Precision Engineering, **15** (1) 25-32.
[45] Sharma R., Rajagopal K. and Anand S. (2000) *A genetic algorithm based approach for robust evaluation of form tolerances.* Journal of Manufacturing Systems, **19** (1) 46-57.
[46] Cui C., Li B., Huang F. and Zhang R. (2007) *Genetic algorithm-based form error evaluation.* Meas. Sci. Technol, **18** 1818-1822.

[47] Liu C.-H., Chen C.-K. and Jywe W.-Y. (1989) *Evaluation of straightness and flatness using a hybrid approach - Genetic algorithms and the geometric characterization method.* Proceedings of the Institute of Mechanical Engineers, **215** (Part B) 377-82.

[48] Traband M.T., Joshi S., Wysk R.A. and Tom M. (1989) *Evaluation of straightness and flatness tolerances using the minimum zone.* Manufacturing Review, **2** (3) 189-95.

[49] Barber C.B., Dobkin D.P. and Huhdanpaa H.T. (1996) *The Quickhull algorithm for convex Hulls.* ACM Trans. Math. Software, **22** (4) 469-483.

[50] Preparata F.P. and Shamos M.I. (1985) *Computational geometry: an introduction*, Berlin.

[51] Lee M.-K. (1997) *A new convex hull based approach to evaluating flatness tolerance.* Comput. Aided Des., **29** (12) 861-8.

[52] Weill R. (1988) *Tolerancing for function.* Annals of the CIRP, **37** (2) 603-10.

[53] Namboothiri V.N.N. and Shunmugam M.S. (1998) *Function-oriented form evaluation of engineering surfaces.* Precision Engineering, **22** (3) 98-109.

[54] Lee M.-K. (2009) *An enhanced convex-hull edge method for flatness tolerance evaluation.* Comput. Aided Des., **41** 930-41.

[55] ISO/IEC (2008) *Guide to the Expression of Uncertainty in Measurement (GUM: 1995)*. BIPM, IEC, IFCC, ISO, IUPAP, IUPAC, OIML.

[56] Canning J.C., Ziegert J.C. and Schmitz T.L. (2007) *Coordinate metrology uncertainty using parallel kinematic techniques.* Int. J. Mach. Tools Manuf., **47** (3-4) 658-65.

[57] Cui C., Fu S. and Huang F. (2009) *Research on the uncertainties from different form error evaluation methods by CMM sampling.* The International Journal of Advanced Manufacturing Technology, **43** (1) 136-145.

[58] Yau H.-T. (1998) *Uncertainty analysis in geometric best fit.* Int. J. Mach. Tools Manufact., **38** 1323-1342.

[59] Weckenmann A., Knauer M. and Kunzmann H. (1998) *The Influence of Measurement Strategy on the Uncertainty of CMM-Measurements.* Annals of the CIRP, **47** (1) 451-54.

[60] Wübbeler G., Krystek M. and Elster C. (2007) *Numerical evaluation of measurement uncertainty by a Monte Carlo method*. in proc. of (ISMTII) International Symposium on Measurement Technology and Intelligent Instruments, Sendai, pp 1-4.

[61] Kruth J.-P., Van Gestel N., Bleys P. and Welkenhuyzen F. (2009) *Uncertainty determination for CMMs by Monte Carlo simulation integrating feature form deviations.* CIRP Annals - Manufacturing Technology, **58** (1) 463-466.

[62] Lu W.L., Jiang X., Liu X.J. and Xu Z.G. (2008) *Compliance uncertainty of diameter characteristic in the next-generation geometrical product specifications and verification.* Meas. Sci. Technol, **19**.

[63] Wang J.X., Jiang X., Ma L.M., Xu Z.G. and Li Z. (2006) *Decision rules for workpieces based on total uncertainty.* Int. J. Adv. Manuf. Technol., **28** 1169-1174.

[64] Chiabert P., De Maddis M., Ricci F. and Ruffa S. (2011) *Uncertainty management in flatness verification operations within the GPS framework*. in proc. of AITeM, Naples.

[65] Balsamo A D.C.M., Mugno R, Rebaglia B, Ricci E, Grella R (1999) *Evaluation of CMM Uncertainty through Monte Carlo Simulations.* Annals of the CIRP, **48** (1) 425-28.

[66] Schwenke H S.B., Wäldele F, Kunzmann H (2000) *Assessment of Uncertainties in Dimensional Metrology by Monte Carlo Simulation: Proposal of a Modular and Visual Software.* Annals of the CIRP, **49** (1) 395-98.

[67] Gao Y., Wang Z., Tao Z. and Lo C. (2003) *Estimation of non-statistical uncertainty in precision measurement using grey system theory.* Int. J. Adv. Manuf. Technol., **22** (3-4) 271-77.

[68] Qin P., Shen Y. and Wang Z.Y. (2006) *Grey evaluation of non-statistical uncertainty in multidimensional precision measurement.* Int. J. Adv. Manuf. Technol., **31** (5-6) 539-45.
[69] Deng J.L. (1989) *Introduction to Grey system theory.* J. Grey Syst., **1** (1) 1-24.
[70] Efron B. (1979) *Bootstrap Methods: Another look at the jackknife.* The Annals of Statistics, **7** (1) 1-26.
[71] Efron B. and Tibshirani R. (1986) *Bootstrap Methods for Standard Errors, Confidence Intervals, and Other Measures of Statistical Accuracy.* Statistical Science, **1** (1) 54-77.
[72] Wen X.-L., Zhu X.-C., Zhao Y.-B., Wang D.-X. and Wang F.-L. (2012) *Flatness error evaluation and verification based on new generation geometrical product specification (GPS).* Precision Engineering, **36** (1) 70-76.
[73] Choi W., Kurfess T.R. and Cagan J. (1998) *Sampling uncertainty in coordinate measurement data analysis.* Precision Engineering, **22** 153-163.
[74] Miller R.G. (1974) *The jackknife-a review.* Biometrika, **61** 1-15.

3 Flatness verification case study

3.1 Introduction

The main aspects of form error verification by means of CMM are analyzed in this chapter through a case study based on flatness verification. The analyzed flatness tolerance is used to control the form error of the primary datum feature of a clamp that is used to close the extremities of an air cushion guide and position it (Figure 3.1).

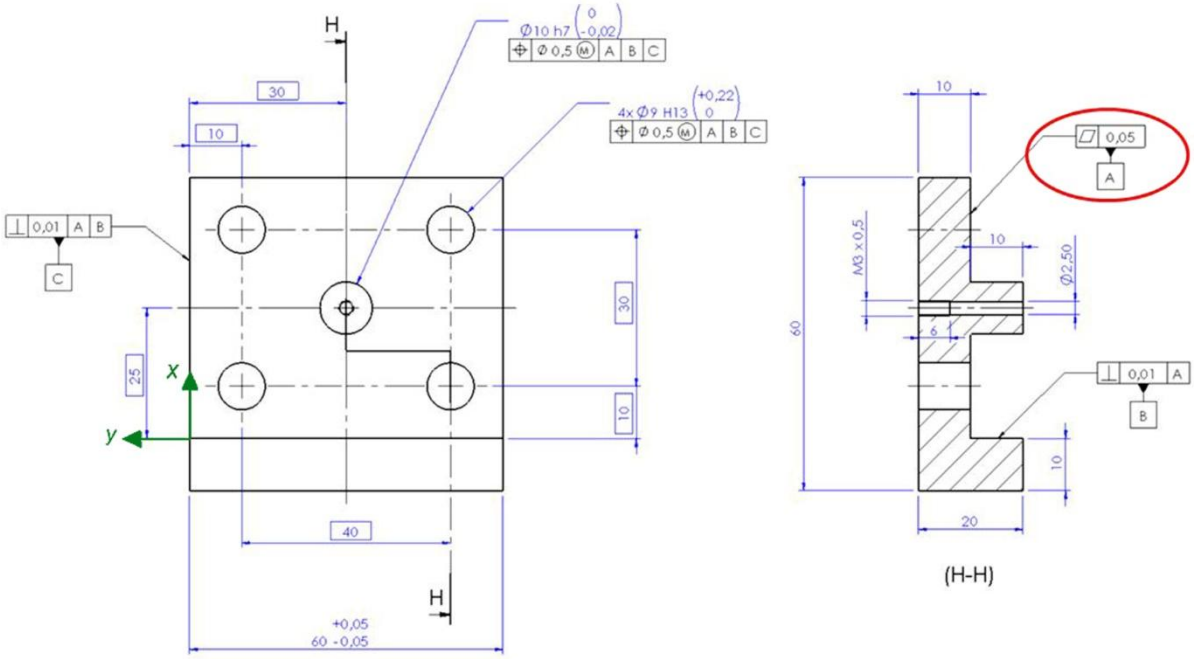

Figure 3.1 - Flatness case study: clamp drawing according to ISO (ante GPS) GD&T standards [1]. The primary datum feature A is controlled by the highlighted flatness tolerance.

Among the different form tolerances, the analysis has been focused on flatness because it is one of the most popular specifications: it is able to satisfy many industrial requirements such as orientation of mating parts, sealing, sliding and in some cases even positioning. Even if the shape of flatness tolerance zone is very simple, conclusions are quite general and apply for most of the form error evaluations, mainly with regards of the aspects associated with the assessment of the evaluation uncertainty.

The traditional best practice for flatness tolerance evaluation relies on the control of several straightness profiles by means of dial gauges. Both the verification method and the technical language evolved in symbiosis in the old GD&T standards [1, 2]. The dial-gauge-based method is still correct and valid, however it is not the most effective as the dial gauge needs to be perfectly positioned with respect to the flatness surface in order to measure the form error while disregarding the error of its orientation. On the other hand, CMMs offer a

more flexible and versatile control, so there is the tendency to use them for the verification of every characteristic. Moreover CMM measurement output is completely different from that of dial gauge. While the latter bases the measurement on the orientation of the instrument with respect to the feature to be inspected, the former offers the possibility to obtain measurement data which are independent from the measurand orientation. Adequate data analysis must be performed according to the different circumstances [3].

When a dial gauge is used, its reference plane, supposed to be perfectly flat, matches the feature to be inspected by touching the peaks of form deviation: it is oriented by the feature to be inspected. In this way it simulates the outmost plane of the flatness tolerance zone and the measurements of the actual surface are interpreted as the form deviations, which have to be minor than the tolerance value. In GPS words, most of traditional equipment for form error verification embeds an association criterion. On the contrary, the assessment of form deviation based on CMM measurement does not embed any association operation: measurement point coordinates are expressed with respect to a reference frame which can be completely independent from the orientation of the measured feature. Thus the full GPS operator shall be employed to guide the measurement process as well as the measurement data interpretation.

The aim of this chapter is to investigate the industrial procedures used to specify and verify flatness tolerance and to highlight the improvements achievable using the mathematical concepts introduced by ISO GPS standards.

3.2 Perfect specification operator

The flatness tolerance highlighted in Figure 3.1 is compliant with GD&T standards (ASME 14.5 or ISO 1101 ante GPS) but does not contain enough information to comply with GPS standards too. As a matter of fact it does not contain any information about the bandwidth limitations (upper and lower cut-off wavelengths), the filter and the association criterion to be used.

The design of a verification process, according to GPS standards, requires the definition of the complete specification operator as a first step. Then the corresponding verification operator is derived from it according to the duality principle [4, 5].

When the specification reported in product documentation is not complete, metrologist has to complete the specification operator according to his experience, the eventual knowledge of the workpiece functional requirements or the manufacturing process that has been used. This operation is necessary because the definition of the complete verification operator relies entirely on the definition of a complete specification operator, according to duality principle [4]. Obviously, when the specification reported on the drawing is not complete, the complete specification operator reconstructed by metrologists can introduce deviations from the original designer intent. All the possible interpretations allowed by the

incompleteness of specification are synonymous of specification uncertainty. To be unambiguous, the specification operator must be complete.

However, all the information necessary to define the complete specification operator cannot be expressed through the GD&T syntax, with the tolerance cartouches defined by ISO and ASME standards [6, 7]. TC 213 is going to introduce a new larger tolerance cartouche in the amendments to the new version of ISO 1101. The new cartouche presents dedicate fields for containing all the information necessary to define each operation of the specification operator; an example is shown in Figure 3.2. This is not the most general and complete cartouche as it presents the fields necessary to define flatness tolerance only.

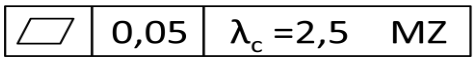

Figure 3.2 - Complete specification for flatness tolerance. The position of different elements does not respect the proposal of ISO 1101 AMD2.

For this case study, the complete specification operator has been defined during the design phase, by designers. This allows the best protection of functional requirements through the choice of the most adequate specification, then the minimization of *correlation uncertainty*. In particular the datum feature A is demanded to guarantee the sealing of the air cushion guide by means of a rubber gasket and participates to the orientation of the whole assembly when it is mounted on the machine/laboratory bench.

The bandwidth limitation on flatness tolerance is set according to the elastic behaviour of the rubber gasket which the surface has to mate with. As a matter of fact the elastic deformation of the gasket is not able to compensate form deviations shorter than 2.5 mm and deeper than the acceptable form error (the flatness tolerance). Thus the lower cut-off wavelength is set equal to 2.5 mm while the upper cut-off wavelength is infinite, because of the definition of form error: all the harmonics of the form deviation with a wavelength higher than a given threshold (the lower cut-off wavelength) [8].

According to the association criterion, MZ has been chosen in order to enlarge the effective compliance range and improve manufacturability [9, 10]. As a matter of fact, if applied on the same measurement dataset, the MZ evaluation ends up in the lowest form error estimation. MZ does not overestimate the form error as it exactly corresponds to the mathematical definition of flatness tolerance zone. The difference between the value of flatness error estimated with MZ and those estimated with other association criteria represents the possible increase in manufacturing errors (form deviation) that would not result in an out-of-specification workpiece. From the point of view of manufacturing, it represents an increase in manufacturability (and an obvious saving of money).

In Figure 3.2 it is shown the complete specification operator for the case study's flatness tolerance. This cartouche resembles the one proposed for the amendment 2 of ISO 1101, which is the GD&T standard actually designated to define the drawing syntax and semantics [6]. The part regarding filtration is not considered in this work in order to contain the number

of variables to be analyzed. Moreover, CMM measurement is performed using the minimum number of points compliant with the tolerance bandwidth limitation, therefore filtration would not be very effective for the lower wavelengths, as there is very few information from which to filter. Particularly, filtration can hardly be used when CMMs are used in the touch trigger inspection mode: in this case they are usually deployed to measure only few points.

3.3 Perfect verification operator

According to the duality principle, the definition of the complete specification operator implies the definition of the perfect verification operator. This passage is natural and straightforward from a theoretical point of view but it may present several issues when the actual feature cannot be known with the same level of detail that can be associated to the skin model. As a matter of fact the skin model is continuous and allows the easy definition of verification operations through mathematical functions based on signal processing theory (this is true for extraction and filtration operations mainly).

However, when dealing with the verification of actual features, the whole performance of the verification operator is strongly conditioned by the measuring instrument at hand. Every measurement process relies on the sampling of a certain number of points from the measurand surface and can be classified as *continuous* or *discrete* according to the type of output data.

- *Continuous measurements*: they are those measurements whose output consists of a continuous or nearly-continuous dataset. Continuous datasets are generated by continuous scanning devices (which can be contact or non-contact devices) while nearly-continuous datasets are usually obtained with optical instruments able to acquire dense clouds of points at each measurement. A measurement dataset can be considered nearly-continuous if the density of sampling points is higher than the requirement set by the lower cut-off wavelength of the tolerance.
- *Discrete measurements*: they are characterized by the measurement (extraction) of single points, then by a cost function directly related to the number of sampled points. In order to contain costs, there is the need to extract from the workpiece the minimal information only. Nevertheless, for the correct implementation of verification operators, we should be able to oversample and extract the information about the harmonics of the form error we are interest in, by means of filtration. The main problem in case of downsampling is represented by aliasing, which can be avoided by sampling at least the minimum number of points required by the Nyquist criterion for the specified lower cut-off wavelength [8].

In this work only discrete measurements will be considered, as they introduce important issues for the implementation of verification operators and represent the most common practice in metrology laboratories. One of the aims of this work is to allow the definition of a measurement process, based on CMM, compliant with GPS standards.

When dealing with the classical CMM-based measurement, which relies on the exploration of measurand by means of a touch probe (a stylus), particular care has to be dedicated to the choice of the probe tip dimension. According to ISO 3274 the theoretically exact stylus tip geometry is a sphere whose radius has to be carefully chosen according to the bandwidth limitations on the feature to be inspected [11]. As a matter of fact this kind of measurement introduces a morphological filtration [12] through the contact of the stylus tip with the feature surface asperities. The form profile actually measured by the stylus is that produced by a *discrete closing filter*, with the same geometrical characteristics of the stylus tip, applied on the actual feature surface (see example in Figure 3.3).

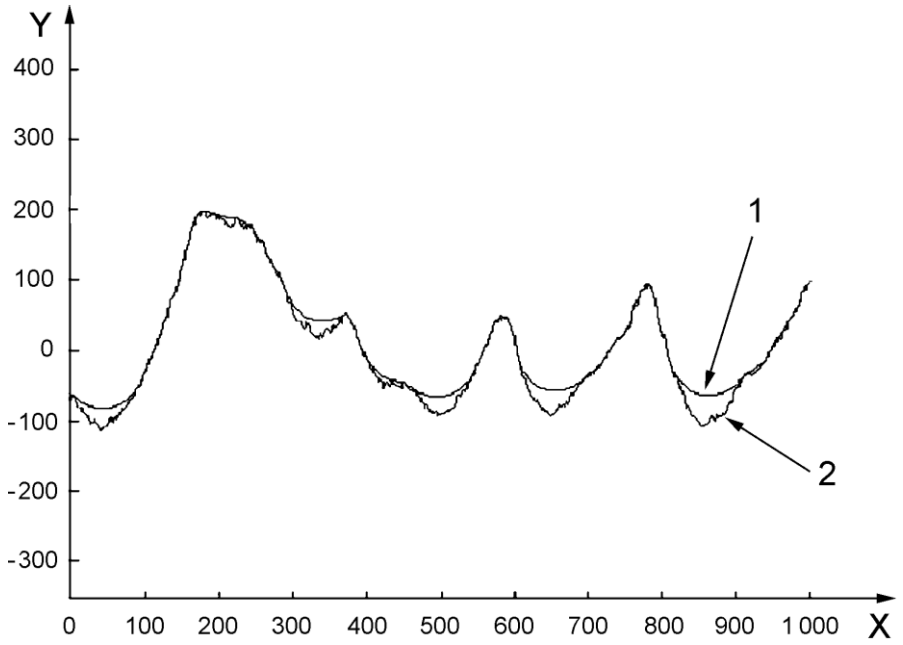

Figure 3.3 - Example of discrete closing filter with the filtered result (1) reported above the input function (2). The input function is sampled at 0,5 μm intervals with a circular disk of 50 μm radius [13].

As previously mentioned, ISO standards offer the possibility to use limited extraction strategies (simplified verification operators) in order to save on verification cost. For flatness verification, these limited extraction strategies consist of dense straightness profiles arranged in different typologies of grids [8]. Considering that there is no recommendation about the spacing of straightness profiles but only about their arrangement in grids, the best surface inspection can be achieved by spacing profiles of the same distance used to space sampling points along each profile.

For the flatness tolerance analyzed in this work, the lower cut-off wavelength of 2.5 mm implies that the stylus tip radius has to be smaller than 1.5 mm [14]; then a stylus with 1mm tip radius has been chosen. According to sampling density ISO/TS 12780-2, in accordance with Nyquist criterion, requires the sampling distance to be minor than 0.357 mm. The constraints on maximum stylus tip radius and maximum sampling distance induced by the choice of the tolerance lower cut-off wavelength are reported in Table 3.1. This table is

referred to straightness tolerance, and not to flatness, because flatness verification can be regarded as the simultaneous verification of straightness profiles [8].

Thus, chosen a probe with 1 mm tip radius, and taking into account the maximum spacing between sampling points recommended by ISO/TS 12780-2, the complete specification operator consists of a uniform sampling with points spaced 0.35 mm and arranged in straightness profiles which are 0.35 mm apart and parallel to the surface external edges. Such a perfect verification operator requires the measurement of 17575 points, an inspection time that cannot be justified in industrial practice.

Longwave-pass filters

Filter transmitting from infinite wavelength down to*	Maximum sample point spacing*	Maximum stylus tip radius*
8	1,14	5
2,5	0,357	1,5
0,8	0,114	0,5
0,25	0,0357	0,15
0,08	0,0114	0,05

*Measures in millimeters

Table 3.1 – Verification constraints induced by the tolerance cut-off wavelength [14].

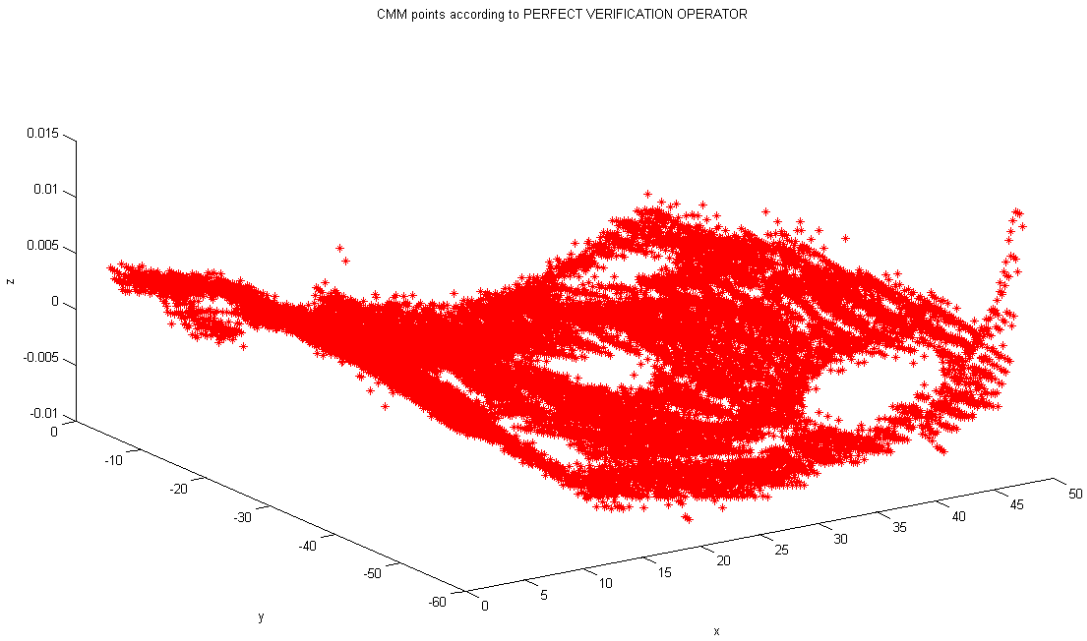

Figure 3.4 - Feature extraction with the perfect verification operator (dataset of 17575 points).

After sampling (Figure 3.4), the assessment of form error deviation with the MZ association criterion ends up in the estimation of a flatness error of 0.01897 mm (Table A.2) against a specification of 0.05 mm. Considering that two different methods have been used for assessing the implementation uncertainty of the verification operator, in the worst case, the standard deviation of the form error evaluation is 0.00097 mm (see Table A.3) thus, according to the acceptance rule suggested by GPS standards [15], the workpiece complies with specification for any reasonable coverage factor.

3.4 Simulation of simplified verification operators

Designers, at specification level, cannot define the limited extraction strategies suggested by ISO/TS 12781-2 so their use can generate different verification operators according to the choices made by metrologists. As one of the main drivers in industry is the reduction of costs, in metrology the number of sampling points is kept the lowest possible and many times more than possible.

Different sampling densities have been tested, starting from the 17575 points compliant with the GPS perfect verification operator and going down to the about ten used in most of metrology laboratories. The different sampling densities have been simulated by varying the parameters used to characterize the GPS grids (see Figure 3.5) according to the Design of Experiment (DoE) summarized in Table 3.2. In particular all the grid extraction strategies but the polar one (suitable only for flatness features with revolute symmetry [8]) have been explored (see Figure 3.6). Grids have been generated only when $D \geq d$, for a total of 60 different grids, and on each grid all the association criteria have been applied, for a total of 300 verification operators (1 perfect verification operator + 299 simplified verification operators).

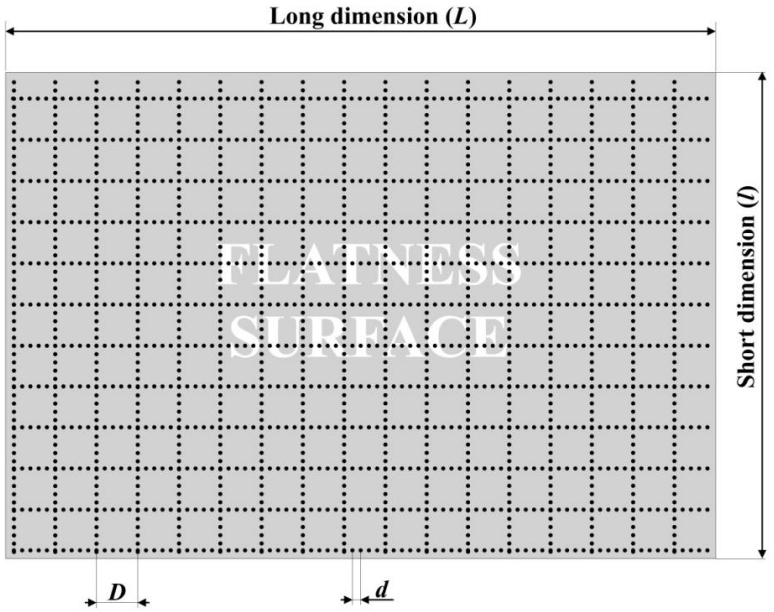

Figure 3.5 – Example of rectangular grid for flatness verification. Parameters defining the grid are the distance between straightness profiles (D) and the sampling distance along profiles (d).

FACTORS	**LEVELS**				
	1	**2**	**3**	**4**	**5**
Grid	Rectangular (Rec)	Parallel to x (Px)	Parallel to y (Py)	Union Jack (UJ)	
***D* [mm]**	0.35	0.7	3.5	7	14
***d* [mm]**	0.35	0.7	3.5	7	14
Method	LS (*FLT*t)	MZ (*FLT*t)	FLTp	*FLT*v	*FLT*q

Table 3.2 - Design of Experiment for analysis of simplified verification operators.

The main characteristic of GPS extraction grids, the density, can be easily represented through the combination of parameters *D* and *d*. As shown in Figure 3.5, *D* and *d* represent the distance between straightness profiles and the sampling distance along them, respectively.

In order to make the definition of each point of the grid univocal, other aspects should be completely defined such as the origin from which the grid generates and the safety distance allowed from the feature edges. All these aspects are strongly related with the measuring equipment at hand and cannot be defined at specification level. Anyway, for the purpose of this work, the origin of every grid is shifted from the origin visible in Figure 3.1 of a distance equal to the safety distance allowed from the feature edges (see Figure 3.6). The safety distance from feature edges has to take into account the stylus tip radius (1 mm) and possible misalignments (0.5 mm have been allowed for this purpose), thus amounting to a total of 1.5 mm. With these boundary conditions and a sampling distance of 0.35 mm, the perfect verification operator consists of 17575 measurement points.

Simplified verification operators have been obtained as subsamples of the 17575 points dataset measured for the perfect verification operator. In order to allow this operation, the distances *D* and *d* explored with the experiment have been chosen as exact multiples of 0.35 mm, as reported in the briefing scheme of Table 3.2. This kind of approach forces an approximation for the Union Jack grid: the sampling of diagonal straightness profiles with a sampling distance slightly larger than 0.35mm (exactly $\sqrt{2} * 0.35 \simeq 0.495$ mm). Anyway, this approximation does not affect the form error assessment as the main component of form deviation has a wavelength much larger than the lower cut-off wavelength and, according to the manufacturing process undergone, there is no reason to expect particular form deviations along the diagonals directions.

Moreover, the approach of extracting the grids of simplified verification operators from the 17575 points dataset does not introduce any bias in the evaluation of the performance of verification operators. As a matter of fact this work is aimed at understanding the goodness of form error evaluation (then the quality of the knowledge of the actual surface geometry achieved through measurement) when intentional deviations from the perfect verification operator are introduced. We are not interested in the possible error that could be detected reiterating measurements but in the error that is introduced if some point is not measured at all, if some piece of information is missing. The aspects related with the accuracy of measuring instrument and repeatability of measurement process will be dealt with by considering the instrument Maximum Permissible Error (MPE) and supposing that the measurement process is performed under a six-sigma quality control.

The last aspect to be considered in order to simulate all the possible deviations from the perfect verification operator is the form-fitting criterion (association criterion) used for the form error evaluation. The substitution of MZ with the more popular LS criterion is not unlikely, as the latter is embedded in most of CMMs. Moreover, LS criterion introduces a form error overestimation that may not be negligible. According to the 17575 points dataset,

for example, if the form error assessment is based on LS, the resulting flatness error is 0.02410 mm against the 0.01897 mm of the MZ evaluation required by specification (see Table A.1 and Table A.2). This difference in form error evaluation depends on the different orientation of the tolerance reference plane: for MZ it is conditioned by the extreme points only, while for LS it reflects the actual position of all measurement points (see Figure 3.7).

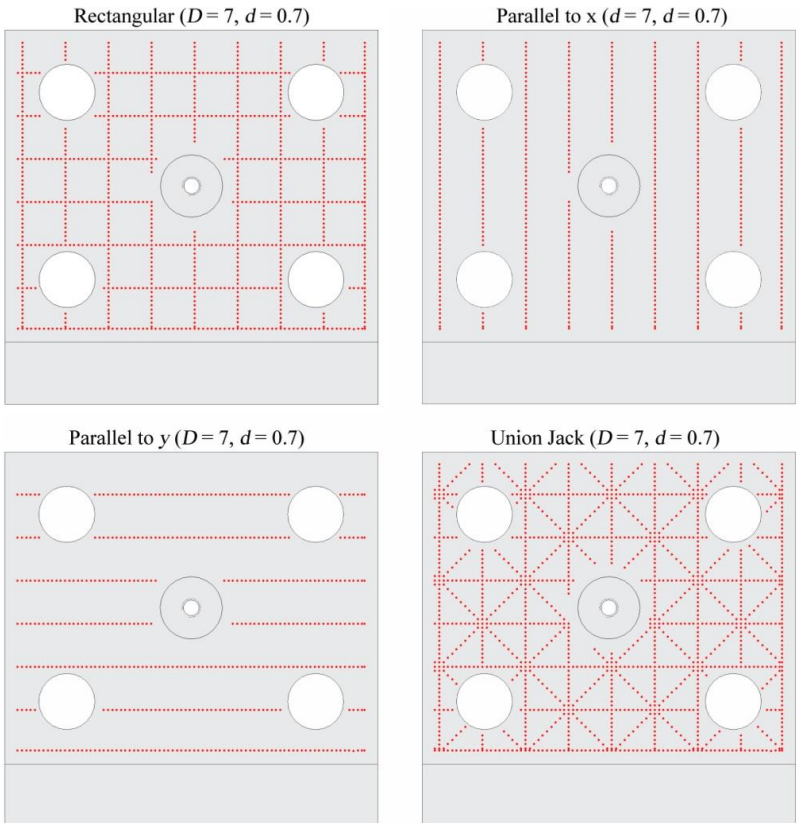

Figure 3.6 - Examples of simplified sampling grids on the flatness feature of the case study. Sampling grids do not cover the whole feature surface but keep a safety distance from the edges to avoid collisions of the touch probe.

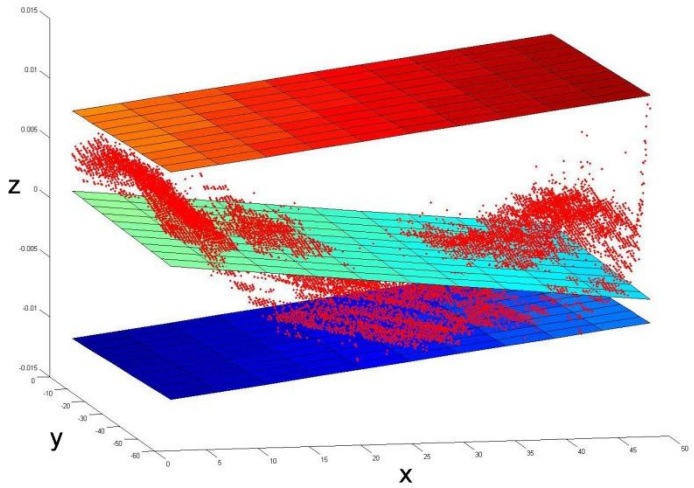

Figure 3.7 - Different orientations of the flatness feature according to LS (plane in the middle) and MZ (symmetry plane of the two outmost planes) association criteria.

Note that, according to ISO/TS 12781-1, the flatness specification could be tightened in some particular area of the tolerance zone by setting restrictions on particular parameters:

- ***FLT*t: peak-to-valley** flatness deviation. It can be defined for both MZ and LS association criteria and corresponds to the whole tolerance zone.
- ***FLT*p: peak-to-reference** flatness deviation. For LS only, it restricts the control to the volume above the LS reference plane. It is recommended for controlling the entity of peaks and guaranteeing a uniform contact surface.
- ***FLT*v**: **peak-to-valley** flatness deviation. For LS only, it restricts the control to the volume below the LS reference plane and is particularly suitable to control the entity of grooves and valleys.
- ***FLT*q**: **root mean square** flatness deviation. It is defined for LS only according to equation (3.1), where *LFD* is the Local Flatness Deviation and *A* is the surface area of the flatness feature.

$$FLTq = \sqrt{\frac{1}{A}\int_A LFD^2 dA} = \frac{1}{N}\sum_{N}^{i=1} LFD_i^2 \qquad \textbf{(3.1)}$$

The three parameters *FLT*p, *FLT*v and *FLT*q, which are associated only with LS association criterion, should be regarded and studied as independent association criteria. These parameters do not represent any tolerance zone, but are used only to set restrictions on some particular area of the tolerance zone. When they are used, they always follow a flatness specification in order to characterize the shape of form deviation inside the boundary already fixed by the flatness tolerance. Anyway, even if they are not suitable candidates to substitute the flatness LS or MZ evaluation (that represented by parameter *FLT*t) they will be analyzed aside in order to cover all possible verification scenarios. They are beyond the possible simplifications that could affect the verification operator, as their semantic is quite different from the definition of flatness tolerance zone. However, their semantic is not different enough to avoid that they are erroneously replaced by the *FLT*t parameter or used to replace it as well. Therefore, the analysis of their performance is necessary in order to be able to cope with these situations too.

In this chapter, only the results related to the *FLT*t parameter, evaluated with both the LS and MZ method, will be discussed. This because all the LS evaluated parameters are defined with respect to the same LS reference plane which, moreover, is the main player in the estimation of the implementation uncertainty related with the evaluation operations (see Annex B for further remarks). Thus, *FLT*t represents very well the other parameters too and each consideration on its performance similarly applies for the others.

3.5 *FLT*t with LS association criterion

For each of the 60 sampling grids generated by the experiment, the LS flatness deviation and its uncertainty have been evaluated and the computational time has been registered in

order to compare the performance of analytic and experimental approaches for uncertainty estimation (see Table A.1). The results are here analyzed as a function of sample size and with a particular highlight on the typology of extraction grid they are related to.

Figure 3.8 shows the trend of flatness error evaluation according to sample size. In particular, the true flatness error for LS association criterion is that associated with the 17575 points dataset (the circled point where the points of all grids correspond). Almost all sampling grids show a good evaluation performance even with relatively small samples: a horizontal line can be distinguished that corresponds to the true LS flatness value and obviously increases its width when approaching the vertical axis, as the uncertainty increases when the sample size reduces (see Figure 3.11 or Figure 3.14).

Actually, another cluster of points, quite far from the true form deviation, can be identified in the left bottom of Figure 3.8. In general, this cluster corresponds to particularly poor verification operators that are not able to detect the peaks and valleys of form deviation. These operators easily occur when the sample is too small; however, the grids with straightness profiles parallel to y-axes show a poor performance for sampling size of up to 5000 points. The reason of this poor performance is not related with the sample size itself but with D parameter as, for $D \geq 0.7$ mm, the Py grid is not able to detect a form defect located on a corner of the workpiece. Figure 3.9 shows evidence of that.

From the point of view of computational performance, Figure 3.10 shows that the computation time increases linearly with respect to sample size and goes up to 0.015 seconds about for the 17575 points dataset; an acceptable time for industrial applications. Few points slightly detach from the main linear trend, but they simply correspond to fluctuations in the computer performance during the experiment simulation.

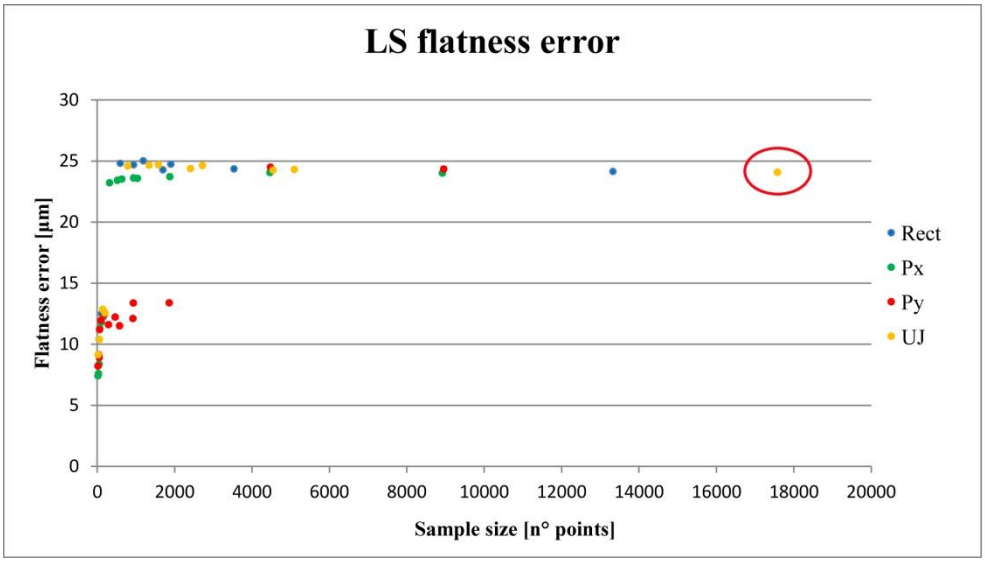

Figure 3.8 - Flatness error as a function of sample size. All grids but Py are able to maintain a good evaluation performance even with low sample size. The circled point can be considered the true LS flatness deviation, as it corresponds to the more detailed sampling compliant with the lower cut-off wavelength of specification.

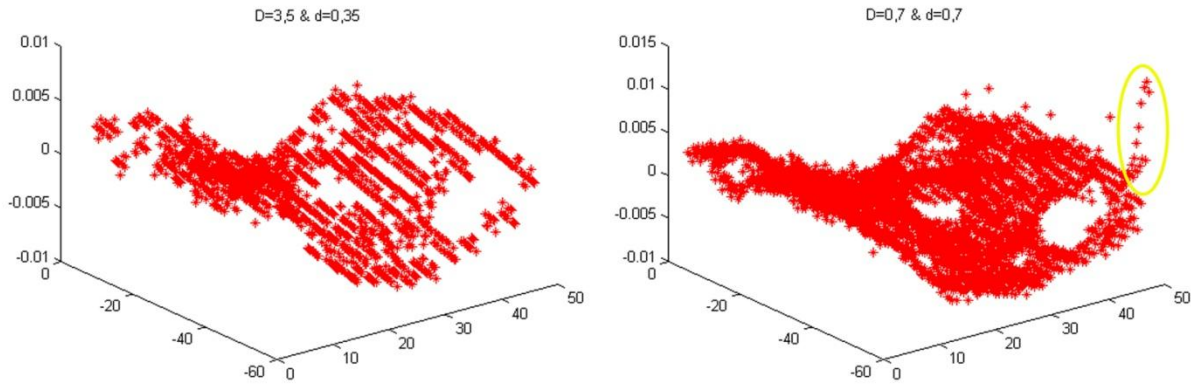

Figure 3.9 - Py grid is not able to detect the defect (corresponding to the mill exit) highlighted in the right picture when $D \geq 0.7$ mm, leading to poor inspection performances.

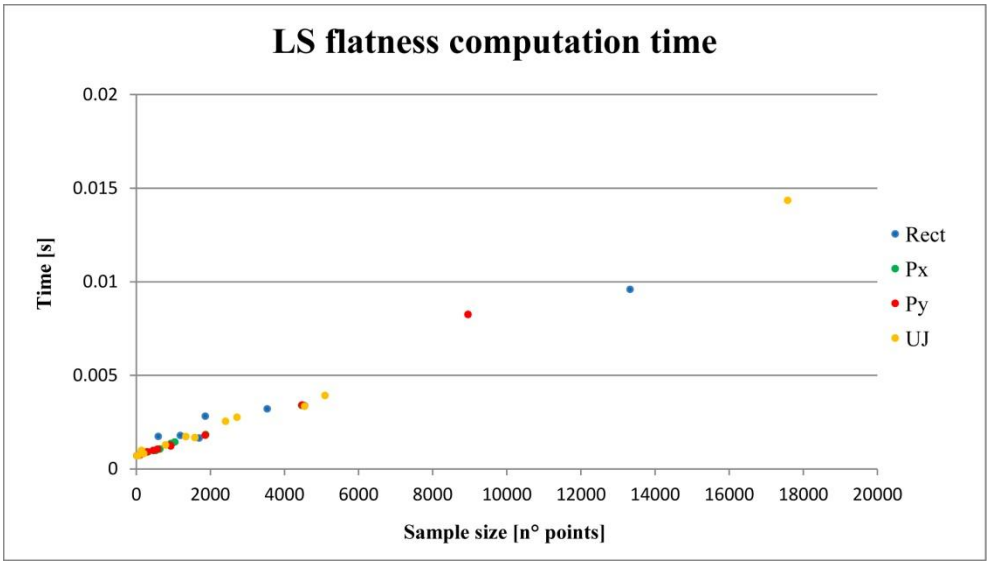

Figure 3.10 - The computation time for LS flatness evaluation increases linearly with the increase of sample size.

As it has been introduced in §1.9 the form error assessment, as every measurement result, has to be accompanied by the measurement uncertainty in order to allow decisions about compliance with specifications. In next subsections the aspects related with the use of LS association criterion will be analyzed in order to evaluate what, according to GPS standards, is classified as implementation uncertainty [4].

The uncertainty due to the algorithm used for error evaluation depends on the distribution of the points used for error evaluation (the algorithm input) and on the performance of the algorithm itself. Different approaches are available to cope with the different association criteria and user requirements (§2.4, §2.5, §2.6). Let us explore those actually available from the state of the art and commonly used by practitioners.

3.5.1 LS implementation uncertainty with analytic approach

LS based association criteria (all but *FLT*q parameter) allow the definitions of the form error with a linear equation based on the orientation of the LS reference plane and on the position of the farthest points. These LS based criteria allow the determination of the partial

derivatives of the measurand with respect to every measured point, thus enabling the use of the transparent box model for uncertainty estimation [16].

Writing the LS reference plane in the form "$z = ax + by + c$", the distance of a given sampling point (x_i, y_i, z_i) from it (usually called residual) can be expressed as:

$$d_i = \frac{z_i - ax_i - by_i - c}{\sqrt{1 + a^2 + b^2}} \tag{3.2}$$

The LS flatness is then defined as the difference between the maximum and minimum of residuals and can be written as: $\delta = \max(d_i) - \min(d_i)$. If the maximum and minimum residuals occur at the point (x_1, y_1, z_1) and (x_2, y_2, z_2) respectively, the flatness error can be also written as follows:

$$\delta = \frac{(z_1 - z_2) - a(x_1 - x_2) - b(y_1 - y_2)}{\sqrt{1 + a^2 + b^2}} \tag{3.3}$$

According to the propagation formula given by ISO 14253-2 to calculate the uncertainty of δ, it is necessary to determine the uncertainty and propagation coefficients of each of the elements x_1, y_1, z_1, x_2, y_2, z_2, a, b. Therefore the implementation uncertainty of flatness error δ can be expressed as in equation (3.4) where: u_{x_i}, u_{y_i} and u_{z_i} represent the instrument accuracy (uncertainties due to the instrument and to the effects of environmental conditions on instrument and measurand) while u_a, u_b and ρ_{ab} represent the goodness of the association criterion. In particular, supposing that the verification process is managed under a six-sigma quality control, the uncertainty on the measurement of each point can be assumed as the sixth part of the instrument Maximum Permissible Error (MPE). Parameters u_a, u_b and ρ_{ab}, on the other hand, are extracted from the statistics of LS solution, particularly from the covariance matrix.

$$\begin{aligned} u_{Im}^2 = u_e^2 = &\left(\frac{\partial \delta}{\partial x_1} u_{x_1}\right)^2 + \left(\frac{\partial \delta}{\partial x_2} u_{x_2}\right)^2 + \left(\frac{\partial \delta}{\partial y_1} u_{y_1}\right)^2 + \left(\frac{\partial \delta}{\partial y_2} u_{y_2}\right)^2 + \left(\frac{\partial \delta}{\partial z_1} u_{z_1}\right)^2 \\ &+ \left(\frac{\partial \delta}{\partial z_2} u_{z_2}\right)^2 + \left(\frac{\partial \delta}{\partial a} u_a\right)^2 + \left(\frac{\partial \delta}{\partial b} u_b\right)^2 + 2 \frac{\partial \delta}{\partial a} \frac{\partial \delta}{\partial b} \rho_{ab} u_a u_b \end{aligned} \tag{3.4}$$

This formulation of the implementation uncertainty mixes the effects of the association criterion (how the measurement points are considered as a whole dataset) together with the effect of the accuracy of measuring instrument (possibility of variation for the coordinates of each measuring point). Looking at equation (3.4) it is easy to notice that most of the terms of implementation uncertainty come from the accuracy of the measuring instrument (all the terms containing u_{x_i}, u_{y_i} and u_{z_i}) while only the last three addendums are related to the performance of the association criterion.

Then, for every LS verification operation used in each of the 60 sampling grids generated by the experiment, the implementation uncertainty has been evaluated and the computation time has been registered in order to compare the performance of analytic and experimental approaches (Table A.1). The results are here analyzed as a function of the sample size and with a particular highlight on the typology of extraction grid they are related to.

Figure 3.11 shows that the implementation uncertainty decreases hyperbolically as the sample size increases. In particular, for a sample size slightly larger than 100 points, implementation uncertainty almost reaches the lower asymptote of 1 µm about and further increases in sampling density do not provide significant improvements. Looking at Figure 3.11, no particular difference can be noticed in the performance of different grids even if we know that Py grids, particularly, are responsible of very poor error assessments when $D \geq 0.7$ mm. Due to this inconvenience, a separate cluster of points could be expected, similarly to that noticed in Figure 3.8, but nothing can be seen. The reason has to be searched in the analytic formulation of LS implementation uncertainty, as it reflects the stability of the orientation of the LS reference plane mainly (see Annex B). This stability can be regarded as the inertia of the LS reference plane with respect to the addition of a new measurement point. Then, provided that all grids guarantee a uniform coverage of the flatness feature and that the increase of sample size is based on the increase of sampling density (and not on an increase of the extension of the inspected area) the inertia of some hundreds of points, on a feature of this size, is already very near to the asymptote. On the other hand, the asymptote value is strictly related with the instrument MPE (see Annex B).

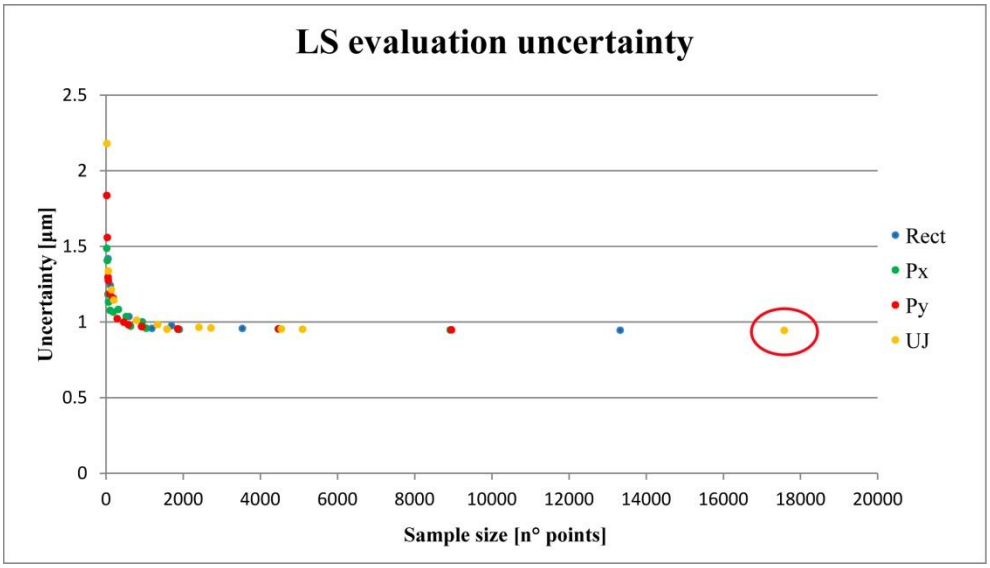

Figure 3.11 - The implementation uncertainty of LS error evaluation decreases hyperbolically as the sample size increases. The minimum uncertainty corresponds to the four grids sampled with the maximum density (circled point).

From the computational point of view, the analytic approach for the estimation of implementation uncertainty is almost independent from sample size (see Figure 3.12). The parameters used to estimate uncertainty are calculated during the solution of the LS problem,

thus their computation time is not considered when assessing the computational performance of uncertainty evaluation. Computation time is half a second about.

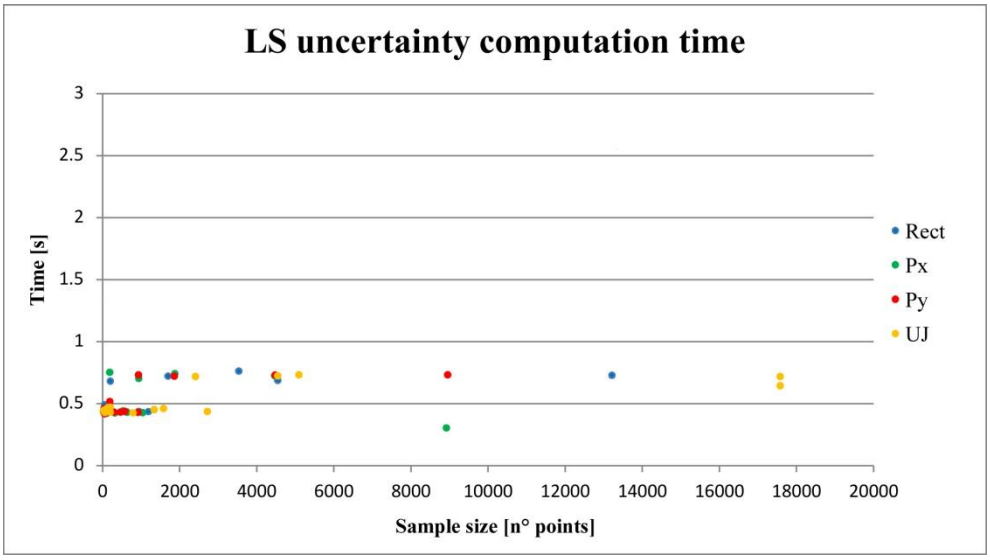

Figure 3.12 - The computation time for the estimation of implementation uncertainty is almost independent from sample size.

3.5.2 LS implementation uncertainty with experimental approach

Apart the analytical approach (§3.5.1), the uncertainty of LS form fitting can be estimated by means of experimental methods too. In particular, it will be estimated with bootstrap method, whose use is unavoidable for the MZ evaluation, and the different performances will be compared in order to choose the most effective (§3.5.3).

The implementation uncertainty has been evaluated through the combination of bootstrap method with Monte Carlo simulation. 100 bootstrap samples have been generated and analyzed with the LS method; then the bootstrap implementation uncertainty has been calculated as the standard deviation of the 100 evaluations (for the details of bootstrap samples generation see §2.6). This leads to the immediate consideration that the time necessary to estimate the uncertainty is expected to be 100 times the time necessary to perform a single evaluation of the LS flatness deviation (Figure 3.13 confirms).

Figure 3.14 shows a hyperbolical decrease of implementation uncertainty with respect to sample size. In particular, two trend functions can be distinguished. The first trend function, located near the origin, corresponds to the cluster of points, identified in Figure 3.8, that are not able to detect the main form defect (as shown in Figure 3.9). The second one collects the results of all the verification operators that are able to detect most of the form deviation even with small samplings. Both trend functions widen when the sample size reduces because the smaller is the sample size and the more probable is that some important point is lost during the extraction of bootstrap samples (more variability affects the results). This is also the reason that explains why the group of poor verification operators, which are unable to detect the main part of form defect, apparently has a lower estimation uncertainty: for these samples

most of the form error is missed systematically, thus bootstrapping from the measurement dataset cannot generate much variability in results.

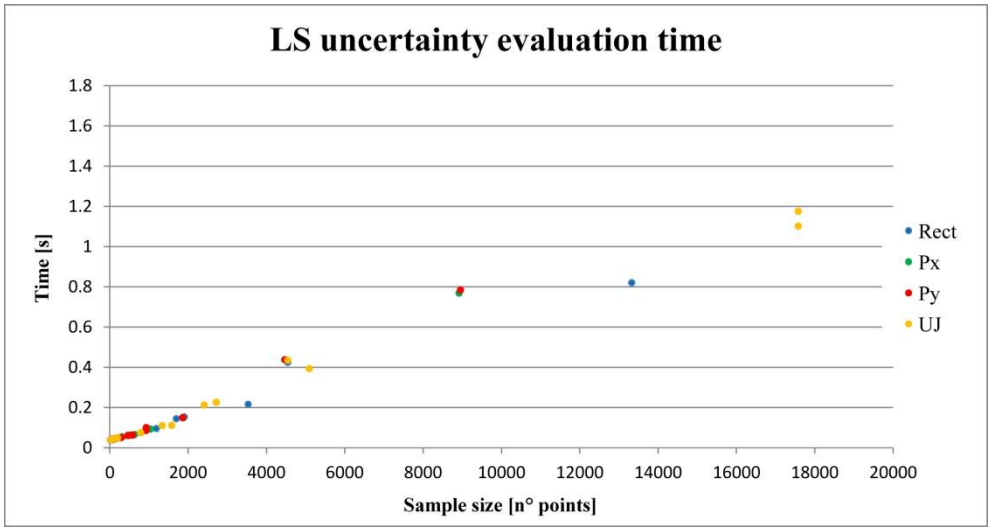

Figure 3.13 - The computation time increases linearly with sample size. Due to the number of bootstrap samples analyzed it is about 100 times the time necessary for one LS error evaluation.

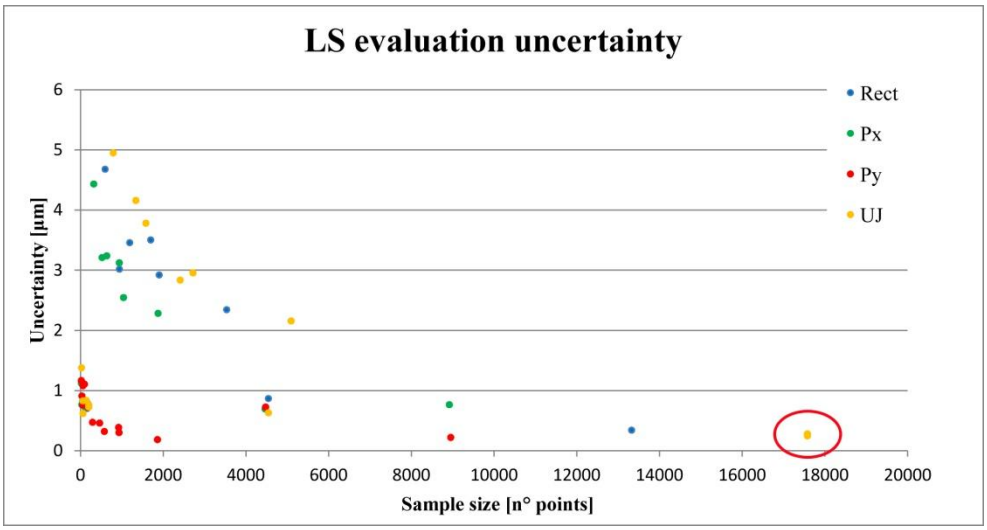

Figure 3.14 - The implementation uncertainty of LS evaluation decreases hyperbolically as sample size increases. The minimum uncertainty corresponds to the perfect verification operator (circled point).

3.5.3 Analytic VS experimental uncertainty estimation

The choice of the analytic or experimental approach for assessing the LS implementation uncertainty can now be performed on the basis of the different observed performances.

A first consideration is about the direct cost of verification: the time spent to analyze results is almost constant and independent from sample size for the analytic method, while it increases linearly for the experimental approach (Figure 3.15). Thus, the analytic approach should be preferred if large samples are expected or if the number of bootstrap samples is too

large. For very small samples the bootstrap results to be much faster but, on the other hand, the uncertainty estimated is more variable.

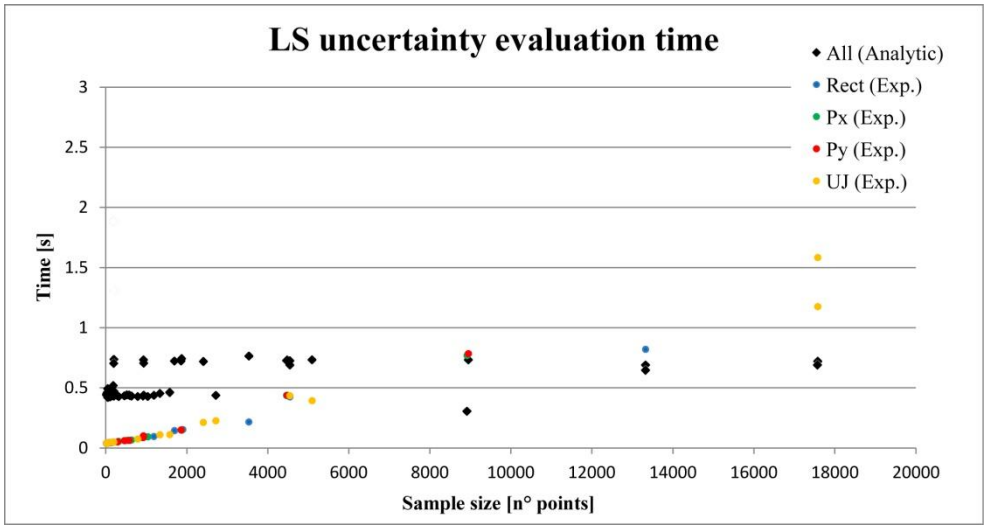

Figure 3.15 - Comparison of the computation time necessary for the evaluation of LS implementation uncertainty with the analytic and experimental approach.

If the main concern is the best estimation of uncertainty, then Figure 3.16 has to be taken into larger consideration. For small samples the bootstrap method seems to favour safety, as it estimates an uncertainty larger than the analytic method. However, this is true only when the verification operator is able to detect the real form deviation, as shown in Figure 3.16. The same figure shows also that the uncertainty of error evaluation may result to be lower than the analytic one if the shape of the actual flatness feature is not measured properly.

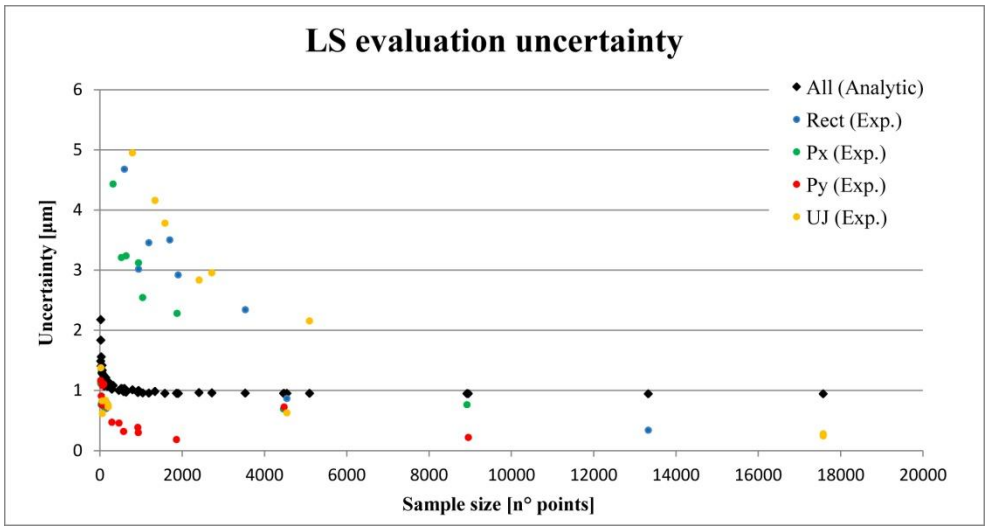

Figure 3.16 - Comparison of the implementation uncertainties calculated with the analytic and experimental approach.

As a matter of fact, it seems that the experimental evaluation of uncertainty is mainly affected by the magnitude of the form deviation that is actually detected by a certain sampling grid. It is clearly unable to understand if the sampling grid at hand is suitable to correctly explore the flatness feature. The uncertainty decreases when the sampling size increases, but

this process is faster when the defect actually measured is smaller. Thus, the lower is the defect detected by a certain grid and the lower will be the uncertainty of the error evaluation. Uncertainty seems to be a function of the sample size, but also of the magnitude of the error actually sampled.

On the other hand, the uncertainty of the analytic evaluation is a function of the sample size only (or better of the sample density once the sampling area has been fixed). The value of analytic uncertainty is affected more by the position of sampling points and the uncertainty in their measurement (see Annex B), than by the values of deviation actually sampled.

Then, to resume, bootstrap method is limited by the actual sample it is applied to, but is particularly sensitive to the form error contained on that sample. On the other hand, the analytic evaluation is less sensitive to the form error contained in each sample, but provides an evaluation of the verification operator that goes beyond the information contained in the sample at hand, by taking into account the geometrical characteristics of measurand. Thus the former seems to suite more data analysis requirements while the latter measurement planning: the decision about the sample size necessary for estimating the LS reference plane with a given robustness (uncertainty). Moreover, the experimental approach has an uncertainty asymptote that approaches 0.3 μm, while that of the analytic approach is 1 μm about (Figure 3.16). The reasons of such a difference will be investigated by simulating measurement on a virtual surface (§4) and analyzing in details the different terms of equation (3.4) for the different verification operators (Annex B).

3.6 *FLT*t with MZ association criterion

The MZ flatness error has been calculated with the computational geometry based technique of convex-hull. For each measurement dataset, the convex-hull of all measurement points has been calculated and its edges have been analyzed according to the method introduced by Lee in [17]. Then, the 60 flatness errors, one for each of the 60 grids generated by the design of experiment, have been registered in Table A.2 together with the estimated uncertainties and the time necessary for their computation.

The results of form error evaluation are very similar to those obtained with the LS association criterion and two different groups of data can be identified (see Figure 3.17). The first group is disposed along a horizontal line corresponding to the true value of MZ flatness deviation, 19 μm about, and lumps together all the sampling grids which are able to detect the main component of form deviation that is concentrated in one corner of the flatness feature (see Figure 3.9). This horizontal line widen as the sample size decreases because the uncertainty of the error evaluation increases (see Figure 3.19 and Figure 3.21). The second group of points corresponds to the cluster in the left bottom of Figure 3.17. This cluster, similarly to that of Figure 3.8, represents the extraction grids (mainly Py grids) that are not able to detect the main form defect because they do not cover the surface densely enough ($D \geq$ 0.7 mm).

Differently from the LS association criterion, the computation time increases, with the increase of sample size, according to a logarithmic trend (see Figure 3.18). For the perfect verification operator, which consists of 17575 points, it takes almost 2 seconds: a time much larger than that required by LS method but that could be still suitable for many industrial applications.

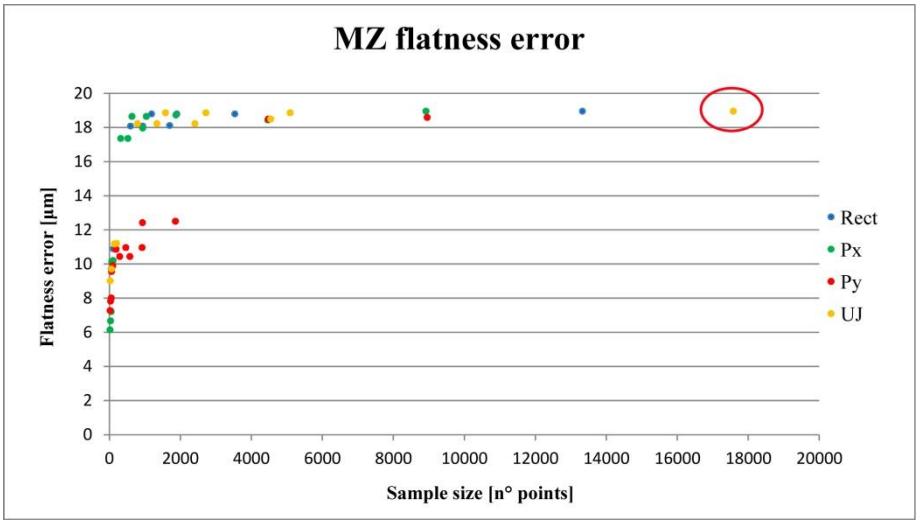

Figure 3.17 - Flatness error as a function of sample size. All the grids but Py achieve good evaluation performances even with small samples. The circled point can be regarded as the true MZ flatness deviation, as it corresponds to the result of the perfect verification operator.

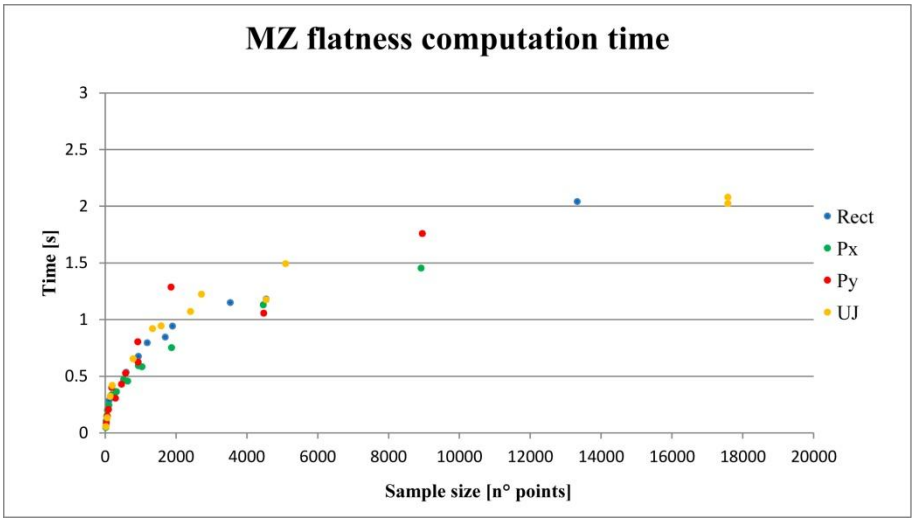

Figure 3.18 – The computation time required by the convex-hull edge method, for the evaluation of MZ flatness deviation, increases logarithmically with respect to sample size.

One of the main problems for the MZ association criterion is that, at the state of the art, there is no analytic method suitable for evaluating the uncertainty that has to quantify the quality of the form error assessment. Some attempts have been tried, by using neural networks [18], but the proposed approach relies too much on the quality of the training dataset to achieve reasonable performances and is not suitable for use in everyday measurements. Another approach, which can be only partially considered analytic, has been proposed more recently by Wen et al. [19]. This approach relies on the same analytic model that has been

presented for the LS method, but proposes to replicate measurements (and then the application of the evaluation criterion) in order to find the statistics that for the LS method are associated with the regression model.

However, in this work an attempt to use analytic uncertainty evaluation has been done on the line of the considerations that are valid for statistical association criteria (§3.5.1) and that have been used by Wen et al. The result is a semi-analytic method that, differently from the one proposed by Wen et al., can be defined for each verification operator, without demanding for measurement replications, as relies on bootstrap methodology for estimating the statistics of the MZ reference plane. The details and results of this method will be presented (§3.6.1) and compared with the experimental evaluation approach (§3.6.3).

3.6.1 MZ implementation uncertainty with semi-analytic approach

According to the MZ association criterion, at the state of the art there is not a purely analytic approach allowing the assessment of implementation uncertainty. An analytic approach has been proposed by Wen et al. [19], but it relies on the same formulation presented for the LS method, with the only difference that the statistics of the reference plane, which are not available for extreme fit association criteria, should be determined by replicating measurements. In order to have robust statistics, the verification operator should be replicated several times, requiring a verification effort that cannot be easily afforded. If the measurement cannot be replicated, bootstrapping is the best alternative. In this section a semi-analytic approach is proposed which relies on bootstrap for the estimation of the MZ reference plane statistics.

Once the MZ reference plane has been identified and written in the form "$z = ax + by + c$", the distance of a point (x_i, y_i, z_i) from it can be calculated according to equation (3.2). If points (x_1, y_1, z_1) and (x_2, y_2, z_2) are two points belonging to the two planes which define the MZ tolerance zone (they represent one of the peak points and one of the valley points respectively) the MZ flatness deviation "δ" can be written as the sum of the distances of these two points from the MZ reference plane; then according to equation (3.3). Under the same considerations valid for the LS method (§3.5.1), the uncertainty of δ can be assessed according to equation (3.4) where u_{x_i}, u_{y_i} and u_{z_i} represent the instrument accuracy (uncertainties due to the instrument and to the effects of environmental conditions on instrument and measurand) while u_a, u_b and ρ_{ab} represent the stability of the MZ reference plane. Under the hypothesis that the verification process is managed within a six-sigma quality control, the uncertainty on the measurement of each point can be assumed as the sixth part of the instrument Maximum Permissible Error (MPE). In order to estimate parameters u_a, u_b and ρ_{ab}, for each verification operator the MZ flatness plane has been estimated for 100 bootstrap samples. Then, the 100 values of the MZ plane coefficients (a, b and c) have been used to estimate the uncertainties u_a, and u_b as the standard deviation of the coefficients a and

b respectively. On the other hand, the correlation ρ_{ab} is estimated as the correlation between the two vectors of parameters *a* and *b*.

For every MZ verification operation used in each of the 60 sampling grids generated by the experiment, the implementation uncertainty has been assessed and the computation time has been registered in order to compare the performance of analytic and experimental approaches (Table A.2). The results are here analyzed as a function of sample size and with a particular highlight on the typology of extraction grid they are related to.

Figure 3.19 shows the implementation uncertainty of MZ-based verification operators. A lower sill can be noticed at 1 µm about, which corresponds to the asymptote observed for the analytic assessment of LS implementation uncertainty (Figure 3.11). Moreover, two different clusters of points can be distinguished in proximity of the vertical axis, which correspond to the two clusters of points identified in Figure 3.17 respectively. The uncertainty is then a function of the instrument MPE (which is responsible for the lower sill) but also of the actual form deviation that is detected by the sampling strategy. The latter is the typical effect of the bootstrap method: it could be misleading as it estimates a lower uncertainty for sampling grids (such as Py when $D \geq 0.7$ mm) that measure only a small part of the form deviation.

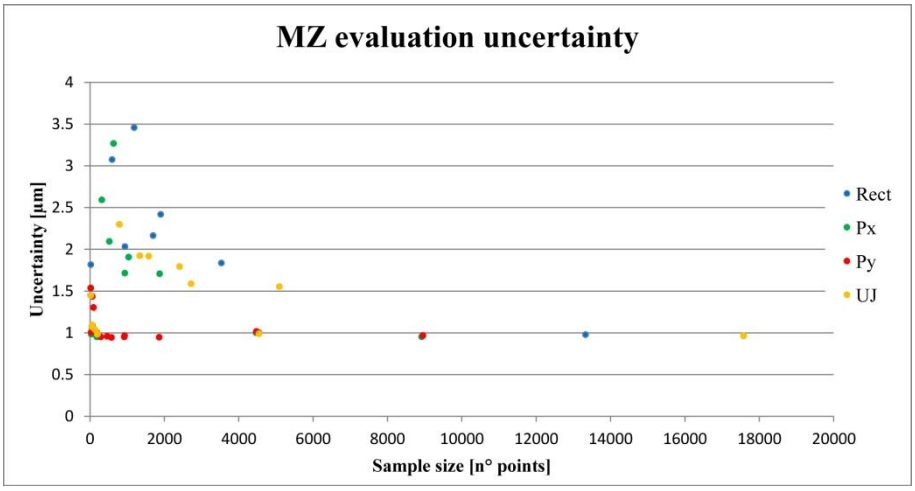

Figure 3.19 – The implementation uncertainty of MZ flatness evaluation decreases hyperbolically with respect to sample size. The lower sill of 1µm about corresponds to the asymptote of analytic estimation of LS uncertainty (Figure 3.11), thus to the effect of the instrument MPE.

With regard to the time necessary for the analytic evaluation of uncertainty, Figure 3.20 shows the same trend that can be noticed, in Figure 3.18, for the solution of the convex-hull problem and calculation of MZ flatness error. However, the magnitude is magnified by the number of bootstrap samples for which the MZ problem has to be solved: 100 times.

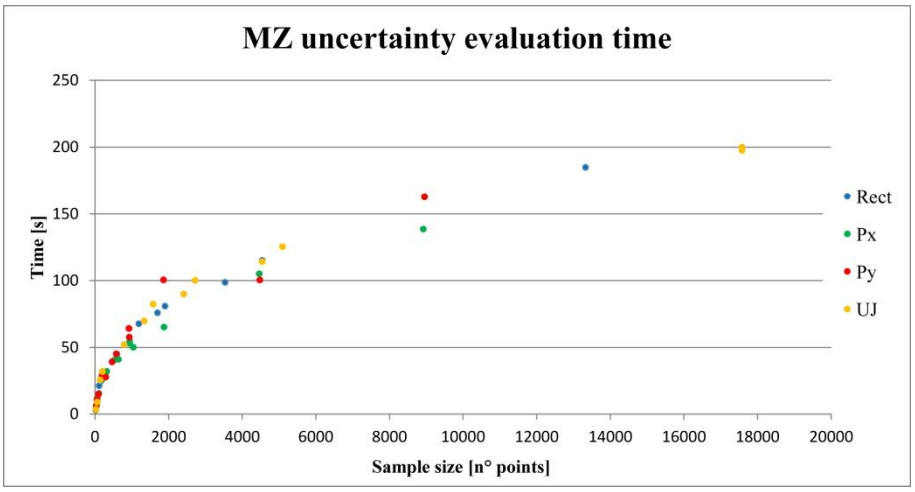

Figure 3.20 - The computational time for the analytic assessment of MZ evaluation uncertainty increases logarithmically as it mainly consists of the time necessary to solve the MZ problem for each of the bootstrap samples.

3.6.2 MZ implementation uncertainty with experimental approach

The experimental evaluation of MZ implementation uncertainty relies on the bootstrap method combined with the Monte Carlo simulation. As for the LS association criterion (§3.5.2), 100 bootstrap samples have been generated, the MZ flatness error has been assessed for each of them and the uncertainty of the evaluation operation has been defined as the standard deviation of the results obtained from the 100 bootstrap samples. The results for the perfect verification operator and for each of the simplified verification operators are reported in Table A.2.

Figure 3.21 shows that MZ evaluation uncertainty estimated by means of bootstrap has a behaviour very similar to that obtained for the LS association criterion. The uncertainty decreases when sample size increases but the rapidity of this decrease strongly depends on the entity of the form error that has been actually sampled by each verification operator. Thus, two main groups of points can be identified; one for each of the two clusters of points that can be distinguished in Figure 3.17. This sharp distinction is due to the fall in the ability of some grids to detect most of the form error when their straightness profiles are too loose. This is particularly true for the Py grids with $D \geq 0.7$ mm.

The main drawback of bootstrap method for the assessment of MZ evaluation uncertainty is represented by the computation time. MZ algorithm requires non negligible computation times and, if the operation has to be repeated for each bootstrap sample, the time required may become unacceptable. The perfect verification operator requires 2 seconds about for the assessment of flatness deviation and almost 3 minutes for the evaluation of uncertainty (Figure 3.22). Faster computers should be used in industrial practice even if, very large datasets, such as those generated by verification processes based on optical instruments, could be too demanding for this approach and actually limit its use.

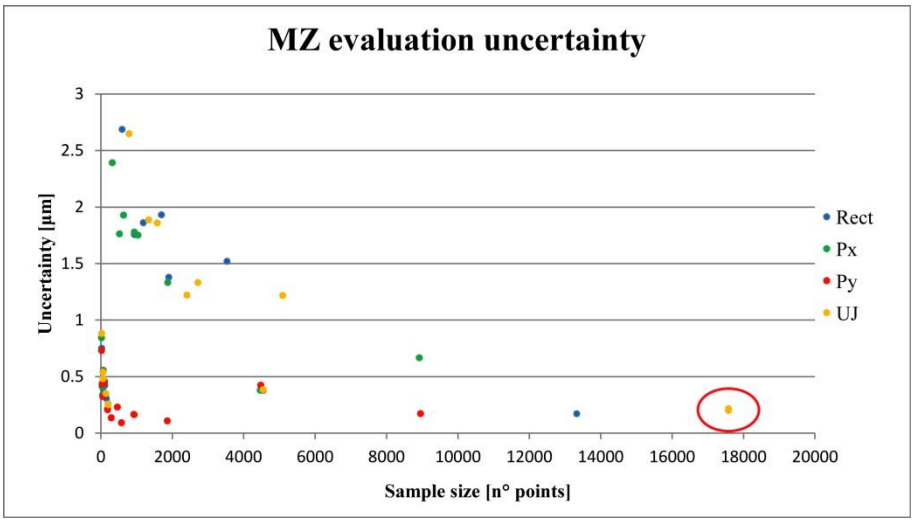

Figure 3.21 - The MZ evaluation uncertainty is inversely proportional to the sample size and to the entity of form error actually detected by the verification operator.

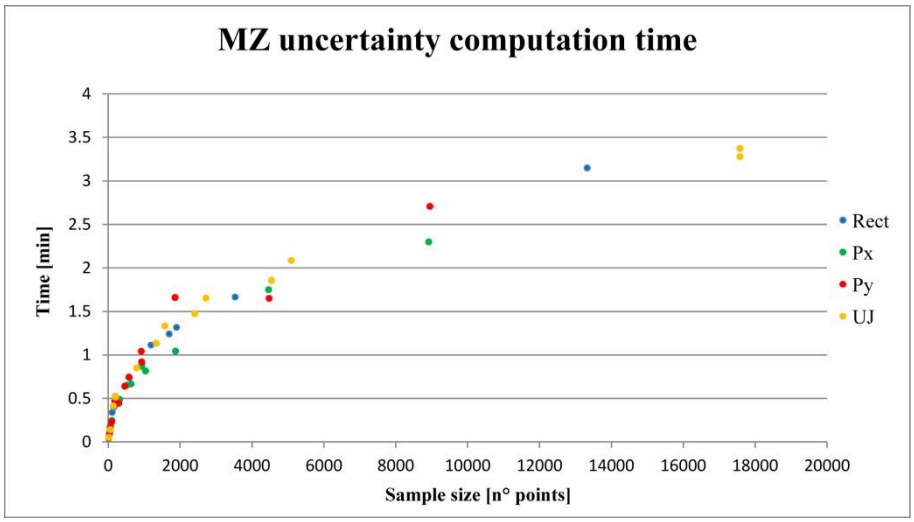

Figure 3.22 - The time required by bootstrap evaluation of MZ uncertainty increases logarithmically with sample size, in the same way that the time necessary for error evaluation does but magnified by the number of bootstrap samples generated (100 times).

3.6.3 Semi-analytic VS experimental uncertainty estimation

Comparing the results of analytic and experimental estimation of the uncertainty of MZ-based verification operators, an interesting behaviour can be noticed for the semi-analytic approach (see Figure 3.23). From the point of view of safety, the semi-analytic approach seems preferable as it systematically overestimates uncertainty introducing a lower sill, at 1µm about, that is representative of the measurement uncertainty introduced during the sampling of each measuring point. This sill is the effect of the first six terms of equation (3.4), which are almost independent from sample size and particularly representative of the instrument MPE only (see Annex B). However, apart the lower sill, the semi-analytic method shows a hyperbolical decrease with a trend very similar to the experimental method. This trend is due to the last three terms of equation (3.4) and particularly to their bootstrap-based evaluation.

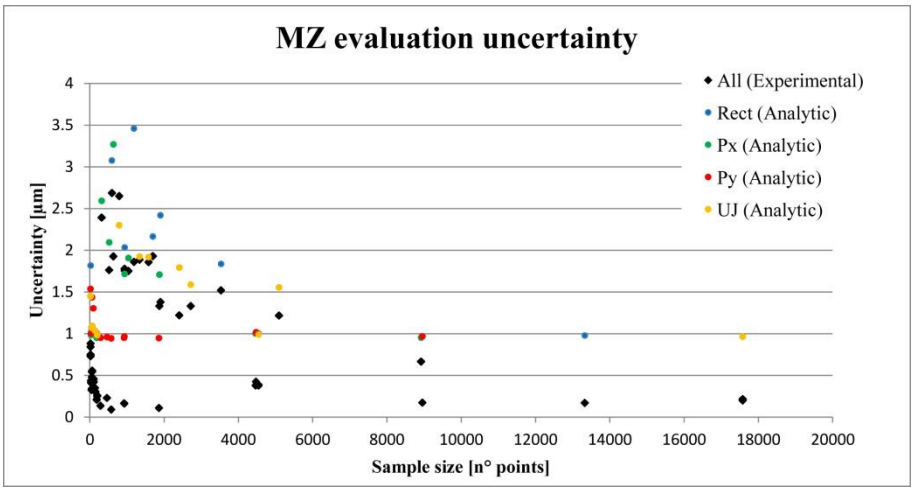

Figure 3.23 - Comparison of semi-analytic and experimental assessment of the uncertainty of MZ error estimation. The semi-analytic approach favours safety as it estimates a larger uncertainty. Both methods are biased by the effectiveness of sampling grids in detecting the form error.

As well as the fully experimental approach, the semi-analytic method is biased by the ability of sampling grids to properly detect all the form error. This is one of the main drawbacks of bootstrapping: it is limited to the sample actually available and cannot simulate other measurements and the occurring of different errors. It is particularly effective in considering the stability of fitted reference planes with respect to the spatial distribution of sampling points on the measurand (if the sampling is uniform), but not equally effective in estimating the effect of measurement errors (in this sense it is limited by the measurement errors contained in the sample at hand). For a deeper analysis, see Chapter 4.

If the semi-analytic approach can be preferred from the point of view of safety, no different advice can be provided from considerations on the computation time required by the two approaches. Figure 3.24 shows the same computation time for both approaches because also the semi-analytic one requires a bootstrap simulation for the estimation of the MZ reference plane statistics. The time required for the calculation of statistics is negligible with respect to the one required by the replications of convex-hull calculation and solution of the MZ problem. Therefore, if both the approaches use the same number of bootstraps, the computation time is the same.

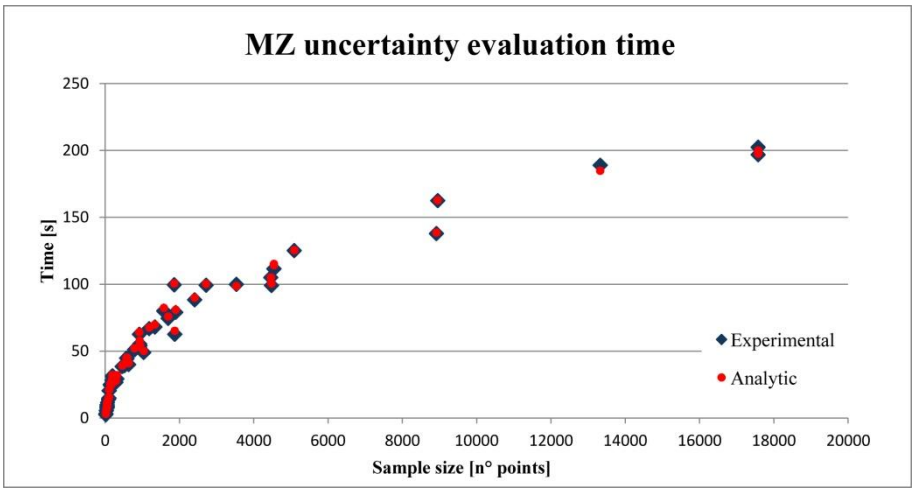

Figure 3.24 - Comparison of computation time for the semi-analytic and experimental approach. Times are undistinguishable as the main effort required by the semi-analytic approach is for the bootstrap estimation of the MZ reference plane statistics.

3.7 The method uncertainty of simplified verification operators

In order to be able to assess the measurement uncertainty, we still need to determine the method uncertainty. While implementation uncertainty is the expression of the uncertainty contained in the actual verification operator, method uncertainty evaluates the effects of using actual verification operators that are different from the perfect one. Intentional deviations from the perfect verification operator are the main responsible of method uncertainty. These deviations can affect the sampling strategy (density of sampling and number of measurement points), as well as the choice of filters or association criteria different form specification requirements. Anyway they are usually aimed at reducing costs or enforced by the measuring instruments actually available in metrology laboratories.

GPS standards define the method uncertainty as the difference between the flatness error assessed with the perfect verification operator (δ^*) and the value given by each simplified verification operator (δ_i) [4]. This definition is expressed by equation (3.5); where δ^* is the *FLT*t parameter evaluated with the perfect verification operator and δ_i is the result of the actual verification operator for which the uncertainty is estimated. The method uncertainty of each verification operator is reported in Table A.3.

$$u_{Mt_i} = \left|\delta^* - \delta_i\right| \tag{3.5}$$

Figure 3.25 shows the plot of method uncertainty against sample size and with the distinction of the association criterion that has been used. For the MZ method it can be noticed a marked discontinuity between the grids that are able to detect all the form deviation and those that are not. For large samples, the use of LS instead of MZ is responsible of the largest method uncertainty (by definition, for the perfect verification operator, that uses MZ, there is no method uncertainty). However, for very small samples, the method uncertainty of MZ overcomes that of LS. This is an effect of LS always overestimating the flatness error:

this behaviour reduces the error with respect to the perfect verification operator when the sampling grid is not able to detect all the form deviation (compare Figure 3.8 and Figure 3.17 for further remarks).

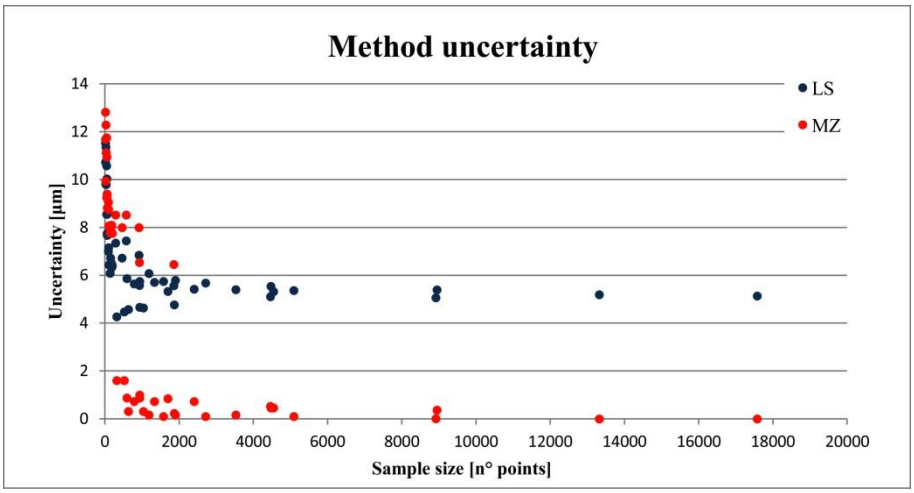

Figure 3.25 - Method uncertainty for all the verification operators. For the MZ method there is a marked discontinuity between the sampling grids that are able to detect all the form deviation and those that are not.

3.8 The measurement uncertainty and compliance uncertainty

Once the implementation uncertainty and method uncertainty have been estimated, measurement uncertainty can be calculated as their sum (with the meaning of the word according to GUM):

$$u_M = \sqrt{u_{Mt}^2 + u_I^2} \tag{3.6}$$

On the other hand, the compliance uncertainty is defined as the composition of measurement uncertainty and specification uncertainty [4]:

$$u_C = \sqrt{u_{Sp}^2 + u_M^2} = \sqrt{u_{Sp}^2 + u_{Mt}^2 + u_{Im}^2} \tag{3.7}$$

This case study deals with a complete specification operator so, by definition, there is no specification uncertainty. In these conditions *compliance uncertainty* (u_C) is equal to *measurement uncertainty* (u_M). Moreover, if specification is the most adequate in order to guarantee the functional needs, *correlation uncertainty* is equal to zero and *compliance uncertainty* (thus *measurement uncertainty* also) becomes synonymous of *total uncertainty*.

However, for the purpose of this work, only measurement uncertainty will be considered. Measurement uncertainty completes the results of flatness error verification (the value δ) and enables assessing the compliance of the form of the actual feature with the specification requirements; through the ISO-GPS acceptance rule [15]. Figure 3.26 shows the trend of measurement uncertainty with respect to sample size for verification operators based on both MZ and LS, and with an experimental assessment of the implementation uncertainty.

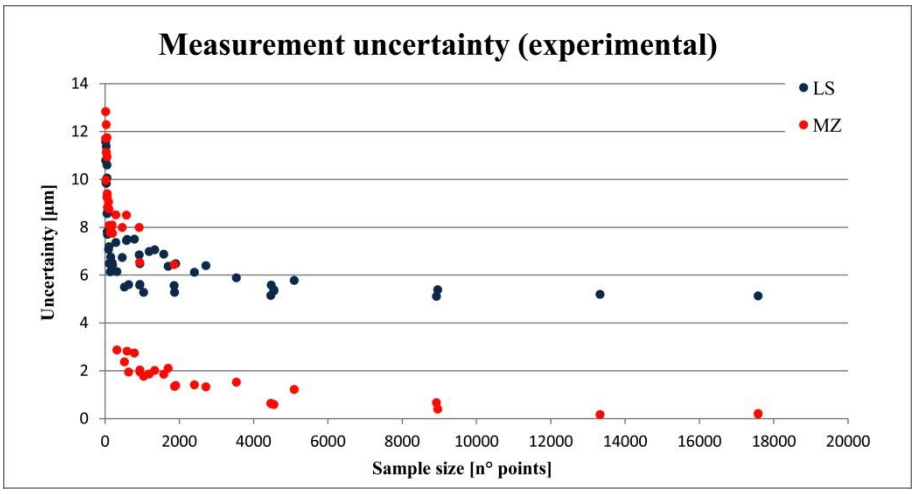

Figure 3.26 - Measurement uncertainty for verification operators based on LS and MZ association criteria, both with an experimental assessment of the implementation uncertainty.

Compliance uncertainty will be no longer mentioned although, in this particular case, it can be considered equivalent to measurement uncertainty and there is no contraindication for its use.

Specification uncertain has not been analyzed in this work, even if from a theoretical point of view it can be studied through a design of experiment similar to the one developed here. In such a case the confrontation should be between the actual (incomplete) specification operator and all the possible actual (simplified and not) verification operators. In case of incomplete specification operator the metrologist is asked to complete the specification, adding operations in order to obtain a complete specification operator from which to derive the perfect verification operator [8]. This means that, according to the scheme reported in Figure 3.27, for each incomplete verification operator, *m* possible complete specification operators could be reconstructed (according to the experience and knowledge of metrologists) and for each of them a DoE with *n* actual verification operators should be performed. Considering that the incomplete specification operator is not unique, *l* possibilities may occur and the study could hardly be handled. Thus it has been limited to the case of complete specification; in different cases (incomplete specifications) the analysis should be started from the complete specification operator generated by the metrologist.

For the total uncertainty the question is more complex as there is no way to estimate it, at the state of the art, and there is no way to detect it until the actual specification does not show any drawback. The only system available to try to contain it, is an accurate rationale design combined with the simulation of the best design solutions.

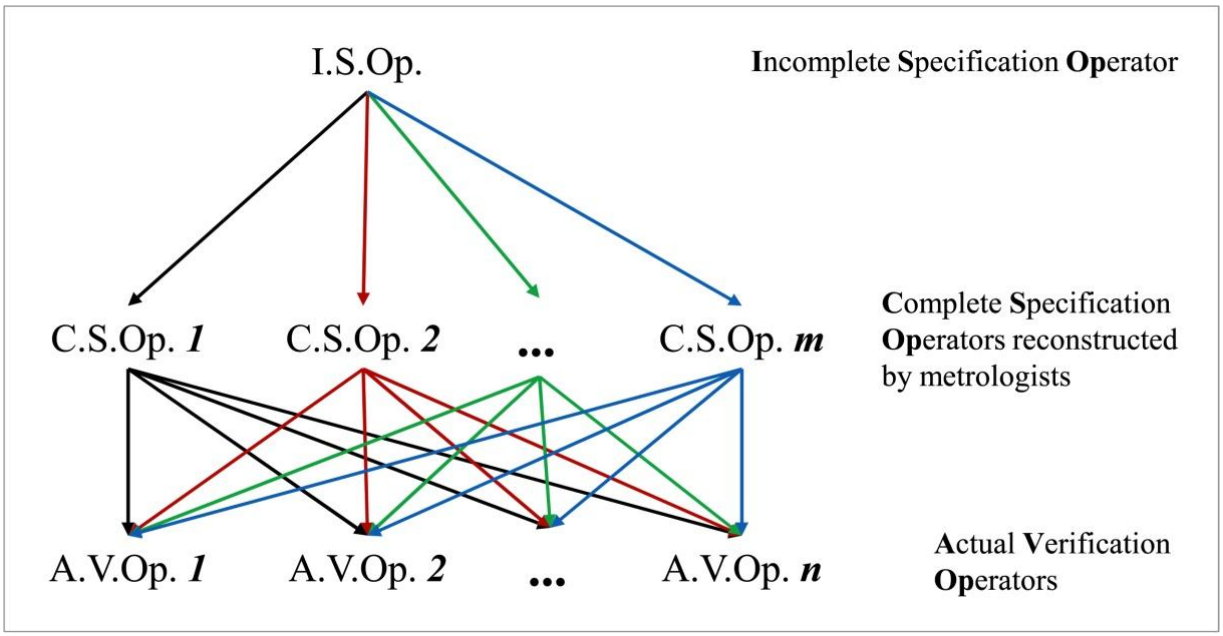

Figure 3.27 - Scheme of the DoE necessary to analyze the specification uncertainty of an incomplete specification operator.

3.9 Compliance test

In order to assess the compliance of the flatness feature with geometrical specifications on the part drawing, the acceptance rule presented in §1.9 has been used. Particularly, for an easier representation, the measurement uncertainty has been added to the value of form deviation assessed through each verification operator, instead of being represented as a grey zone around the specification limit. This is just a convention to allow the comparison of different verification operators at the same time, as each of them is characterized by its own measurement uncertainty. Particularly each point in Figure 3.28 and Figure 3.29 consists of: $FLT\mathrm{t} + U_M = FLT\mathrm{t} + k \cdot u_M$.

Figure 3.28 shows the acceptance test with a coverage factor k = 2. This is the value most widely used in metrology and usually adopted when not explicitly stated. The flatness feature is compliant with specification according to all verification operators. It is easy to notice how the MZ based verification operators allow a higher manufacturability, as they do not overestimates flatness deviation as the LS method does. Moreover the measurement result is not very sensitive to sample size, as the increase in measured flatness error is almost balanced by a reduction of measurement uncertainty.

Also for a coverage factor k = 3, the flatness feature is compliant for all verification operators (Figure 3.29). However, mainly for rather small samples, the measurement result is particularly near to the specification limit. It means that both the acceptable limits of flatness deviation and uncertainty of the measurement process have been completely exploited: no further error can be accepted (it is neither a manufacturing nor a measuring error). Particularly when the sample is very large, MZ maintains a larger margin and the difference with respect

to LS depends mainly on method uncertainty. This is a further remark of the importance of using the perfect verification operator before using simplified ones. Obviously it would not make sense to apply simplified verification operators after a perfect one but, it could be very useful to apply the perfect verification operator on a sample from a mass production and use simplified verification operators to verify the remaining (provided that both manufacturing and verification process are kept under control).

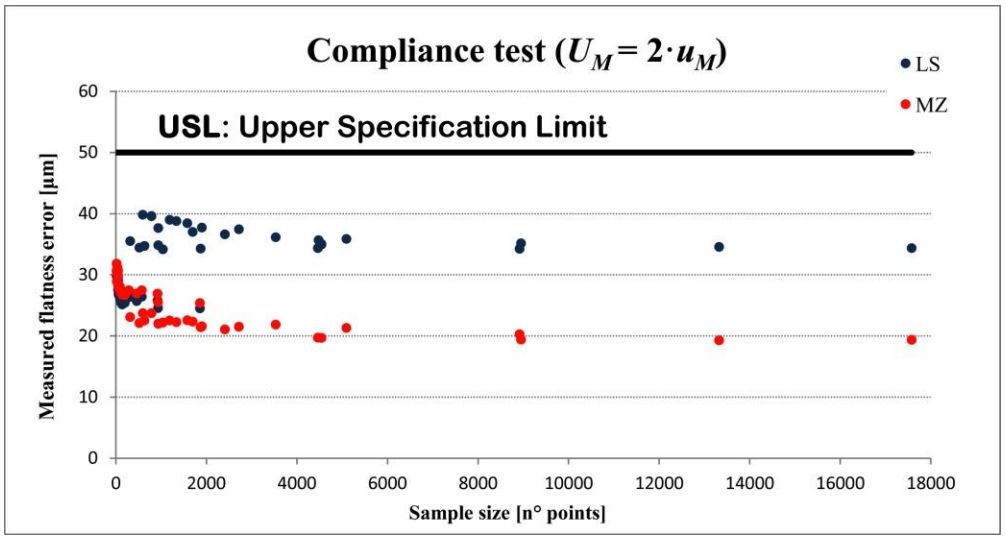

Figure 3.28 - Compliance test using coverage factor k = 2. Each dot represents the complete result of a verification operator: flatness deviation plus the expanded measurement uncertainty. Measurement uncertainty contains u_{Im} estimated experimentally.

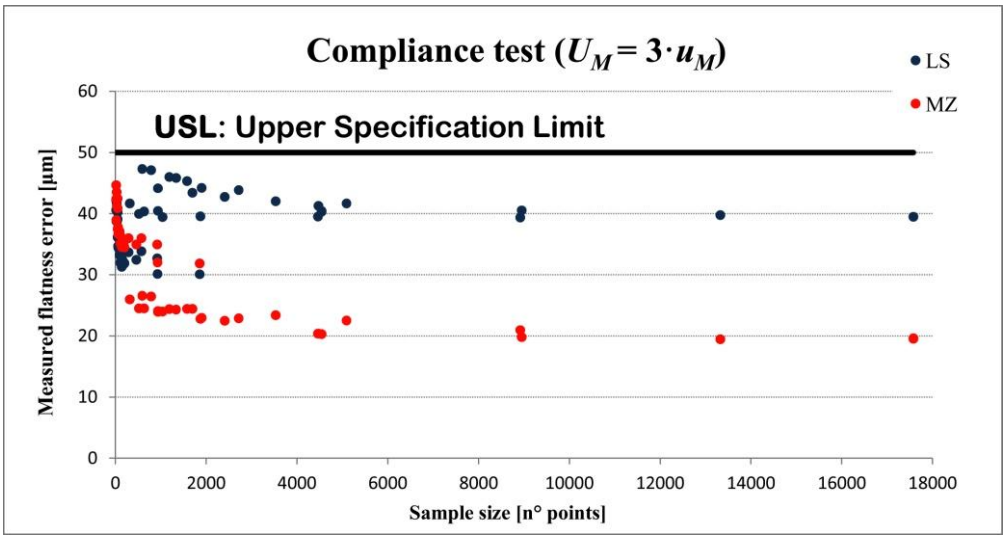

Figure 3.29 - Compliance test using coverage factor k = 3. Each dot represents the complete result of a verification operator: flatness deviation plus the expanded measurement uncertainty. Measurement uncertainty contains u_{Im} estimated experimentally.

The results presented in Figure 3.28 and Figure 3.29 report estimations of the measurement uncertainty in which implementation uncertainty has been assessed experimentally. The results for verification operators based on the analytic assessment of

implementation uncertainty are not much different and, for the sake of brevity, their plots are omitted; numerical values, however, are available in Table A.3.

3.10 Surface response regressions

The effects of single factors and their interactions have been assessed using a response surface method. Particularly, a Quadratic Response Surface has been used to analyze the different terms of uncertainty (measurement uncertainty, method uncertainty and implementation uncertainty) versus factors *D*, *d*, *Grid* and *Association* method.

Given that the implementation uncertainty can be estimated both analytically and experimentally, the analysis has been performed twice: one time for verification operators based on the analytic approach (§3.10.1) and another time for those based on the experimental one (§3.10.2). Method uncertainty is completely independent from the approach used for assessing the implementation uncertainty, therefore it has been analyzed only once (§3.10.3). All the results have been compared in §3.10.4. As a rule, useful for the interpretation of results, the observation order corresponds to the row index of the results table on which the surface response is built.

3.10.1 Verification operators based on analytic uncertainty estimation

3.10.1.1 Measurement uncertainty

The Quadratic Response Surface of measurement uncertainty shows that the most significant factors are the sampling *Grid* together with the *Association* criterion and the interaction effect of sampling *Grid* and *d*. The interaction of factors *D* and *Association* criterion (sampling grids that are inadequate to detect all the form deviation) is secondary because in measurement uncertainty (see Figure 3.28 or Figure 3.29) there is not the split trend noticed for the implementation uncertainty every time an experimental method is used for its assessment (see Figure 3.14 and Figure 3.21).

Term	Coef	SE Coef	T	P
Constant	27.8353	8.08529	3.443	0.001***
D	-1.9311	0.78688	-2.454	0.016**
Grid	2.9965	1.11016	2.699	0.008***
ASS	-17.2385	3.14426	-5.483	0.000***
d*d	0.0594	0.03049	1.947	0.054*
Grid*Grid	-0.2440	0.06046	-4.035	0.000***
D*ASS	0.6405	0.25189	2.543	0.012**
d*ASS	0.9966	0.25189	3.956	0.000***

S = 1.49021
R-Sq = 79.69% R-Sq(pred) = 74.18% R-Sq(adj) = 77.20%

Table 3.3 - Significant terms in Quadratic Response Surface Regression of measurement uncertainty versus *D*, *d*, *Grid* and *Association* method. P-values less than 0.10 are marked with *, less than 0.05 with **, less than 0.01 with ***.

3.10.1.2 Implementation uncertainty

With respect to the analytically assessed implementation uncertainty, the Quadratic Response Surface (Table 3.4) shows that all the factors reported are very significant (0.01 level). The Grid factor only is significant at the 0.05 level (particularly in the form of the squared interaction with itself) because implementation uncertainty varies almost uniformly with respect to all the other parameters and has a particular interaction with sampling grid only in few cases (see Figure 3.9). Even if the response surface is able to explain only the 46.48% (R-sq value) of the variability contained in the data, the most significant factors seem to be *d* (which influence the most the sample size) and the interaction of the association criterion with both *d* and *D* (namely the density of the sampling). However, given the low reliability of the model, any of the previous comments has to be considered carefully and accepted only if supported by the previous analysis (§3.5 and §3.6).

Term	Coef	SE Coef	T	P
D	-0.46988	0.17096	-2.749	0.007***
d	0.66995	0.17412	3.848	0.000***
ASS	1.93489	0.69578	2.781	0.006***
d*d	0.02042	0.00675	3.026	0.003***
Grid*Grid	0.02861	0.01338	2.138	0.035**
D*Grid	-0.02192	0.00831	-2.639	0.010**
D*ASS	0.30267	0.05574	5.430	0.000***
d*Grid	0.02338	0.00831	2.813	0.006***
d*ASS	-0.44198	0.05574	-7.929	0.000***
Grid*ASS	-0.17803	0.07180	-2.480	0.015**

S = 0.859684

R-Sq = 46.48% R-Sq(pred) = 32.97% R-Sq(adj) = 39.91%

Table 3.4 - Significant terms in Quadratic Response Surface Regression of implementation uncertainty versus *D*, *d*, *Grid* and *Association* method. P-values less than 0.05 are marked with **, less than 0.01 are marked with ***.

3.10.2 Verification operators based on experimental uncertainty estimation

3.10.2.1 Measurement uncertainty

The strategy used for the assessment of implementation uncertainty (experimental rather than analytic) does not seem to affect the Quadratic Response Surface of measurement uncertainty too much (compare Table 3.3 and Table 3.5). Therefore, the same comments apply.

Particularly, the experimental assessment of implementation uncertainty leads to a higher significance of factors *d*, and a lower significance of factor *Grid* and interaction *D*Association* method. These differences can be interpreted as an actual divergence between the two approaches for the assessment of implementation uncertainty, and not as an error of the analysis, because both models are quite reliable (R-sq ~ 80%).

Term	Coef	SE Coef	T	P
Constant	32.9487	8.24942	3.994	0.000***
d	-2.5471	0.80286	-3.173	0.002***
Grid	2.5460	1.13270	2.248	0.027**
ASS	-20.0389	3.20809	-6.246	0.000***
Grid*Grid	-0.2349	0.06169	-3.807	0.000***
D*ASS	0.4601	0.25701	1.790	0.076*
d*ASS	1.3714	0.25701	5.336	0.000***

S = 1.52046
R-Sq = 80.71% R-Sq(pred) = 75.37% R-Sq(adj) = 78.34%

Table 3.5 - Significant terms in Quadratic Response Surface Regression of measurement uncertainty versus *D*, *d*, *Grid* and *Association* method. P-values less than 0.10 are marked with *, less than 0.05 with **, less than 0.01 with ***.

3.10.2.2 Implementation uncertainty

The Quadratic Response Surface of implementation uncertainty versus the factors varied in the experiment (Table 3.6) is rather different from that obtained when the implementation uncertainty is estimated with the analytic (or semi-analytic) approach: see §3.10.1.2. The most significant factors are *D* and *Grid*, because pure experimental assessment of implementation uncertainty is strongly affected by the ability of the grid to detect all the form deviation (see the comparison with the semi-analytic method in Figure 3.23). No further consideration can be done on this response surface, given the scarce validity of the model that is able to explain only the 46.5% of the process variability.

Term	Coef	SE Coef	T	P
D	1.31731	0.44569	2.956	0.004***
D	-0.82061	0.45394	-1.808	0.073*
Grid	-1.43616	0.64044	-2.242	0.027**
Grid*Grid	0.10274	0.03488	2.946	0.004***
D*ASS	-0.30541	0.14531	-2.102	0.038**
d*ASS	0.26051	0.14531	1.793	0.076*

S = 0.859684
R-Sq = 46.48% R-Sq(pred) = 32.97% R-Sq(adj) = 39.91%

Table 3.6 - Significant terms in Quadratic Response Surface Regression of implementation uncertainty versus *D*, *d*, *Grid* and *Association* method. P-values less than 0.10 are marked with *, less than 0.05 with **, less than 0.01 with ***.

3.10.3 Method uncertainty

Method uncertainty does not depend on the approach used to evaluate the implementation uncertainty (analytic rather than experimental), as it is defined as the difference between the flatness error estimated with the current verification operator and the result that would have been obtained with a perfect verification operator: see equation (3.5).

The Quadratic Response Surface of method uncertainty versus factors *D*, *d*, *Grid* and *Association* method (Table 3.7) shows that factors *d*, *Grid* and *Association* criterion are significant at 0.01 level. The factor *D* is not significant here because the poor performance of some sampling grids (the Py grids highlighted in Figure 3.9) is interpreted as an effect of the

sampling grid more than an effect of the distance between straightness profiles. Other grids with the same *D* work perfectly. Notice that the most important factor is represented by the association criterion that introduces a systematic error in flatness evaluation: thus it is the first source of method uncertainty in order of relevance.

Term	Coef	SE Coef	T	P
Constant	33.9932	9.63817	3.527	0.001***
d	-2.7373	0.93801	-2.918	0.004***
Grid	3.1800	1.32338	2.403	0.018**
ASS	-21.3423	3.74816	-5.694	0.000***
Grid*Grid	-0.2891	0.07207	-4.011	0.001***
d*ASS	1.5146	0.30027	5.044	0.000***

S = 1.77643
R-Sq = 77.89% R-Sq(pred) = 71.81% R-Sq(adj) = 75.18%

Table 3.7 - Significant terms in Quadratic Response Surface Regression of method uncertainty versus *D*, *d*, *Grid* and *Association* method. P-values less than 0.05 are marked with **, less than 0.01 with ***.

Residuals analysis (Figure 3.30) shows some phenomenon that is not completely explained by model factors. There is a linear behaviour of residuals versus fitted values particularly for very small flatness errors. It means that the model has a poor performance mainly in the asymptote area. In the plot of residuals versus observation order, the visible patterns are the effect of progressive order in factors variation given that the runs were not randomized.

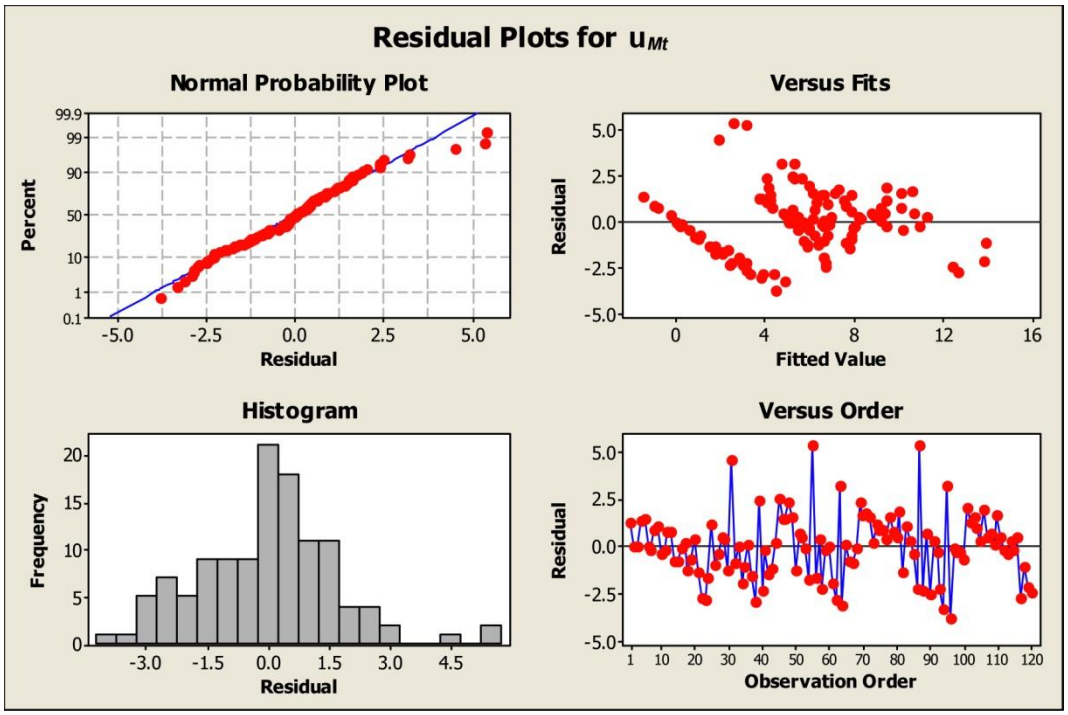

Figure 3.30 - Residuals analysis for the Quadratic Response Surface of method uncertainty.

3.10.4 Comparison

According to the factors that are significant in each response surface there is no consideration that add information with respect to the analysis previously performed on each factor (§3.5 to §3.8). The only difference with Quadratic Response Surfaces is that the factors are considered all together into a numerical model, interactions are quantified, and a model is drawn, which allow to infer about the results of experiments that have not been actually performed (it is a regression model).

The significant factors of the Quadratic Response Surfaces presented above, and the R-sq value of each model have been collected in Table 3.8. If we think to use these regression models for doing predictions within the domain explored by the experiments, the first thing to be considered is the model reliability: its R-sq value. The Quadratic Response Surface for method uncertainty is able to explain almost 80% of the variability contained in the experiment results, therefore the regression model obtained is quite robust. The model is quite reliable also for the measurement uncertainty (R-sq ~ 80%), which in most cases is made up by method uncertainty mainly. On the contrary, for implementation uncertainty the model is less reliable (R-sq < 50%). A consequence of the scarce reliability can be observed in the important differences in the significant factors of the two models built for implementation uncertainty. The two models look completely different, much more than the data they are made from.

		R-sq	const	D	d	Grid	ASS	d*d	Grid*Grid	D*Grid	D*ASS	d*Grid	d*ASS	Grid*ASS
u_{Mt}		77,9%	3		3	3	3		3				3	
u_M	**Analytic**	79,7%	3		2	3	3	1	3		2		3	
	Experim	80,7%	3		3	2	3		3		1		3	
u_{Im}	**Analytic**	46,5%		3	3		3	3	2	2	3	3	3	2
	Experim	46,5%		3	1	2			3		2		1	

Table 3.8 - Comparison of the significant factors of the Quadratic Response Surfaces. The number of stars used to classify the P-value, in each table of results, has been reported explicitly here (3 for ***, 2 for ** and 1 for *).

The particular shape of the feature analyzed could explain the poor performance of the regression models for implementation uncertainty. The analysis presented in §3.5 and §3.6 showed that for a value $D > 0.7$ mm some sampling grids are no longer able to detect all the form deviation. Py grid becomes particularly unsuitable and a group of verification operators affected by the same fault can be identified: their results are clustered and strongly separated from the others. These results are so far from the others that they could be considered as outliers and, as they are rather numerous, the model quality is very poor. Quadratic Response

Surfaces have been generated also for a smoother feature in order to prove this explanation (see §4.6).

3.11 Conclusions

This Chapter presents a comprehensive critical investigation of the measurement practices (the actual verification operators with different densities of sampling) used every day in most of metrology laboratories. The novelty here is in the method used to perform this investigation. For the first time the factors affecting the output of a measurement process have been investigated according to the new concepts introduced by the GPS framework. The main association criteria and methods for the assessment of uncertainty (of each single term of measurement uncertainty) have been systematically analyzed, tested on a real case study, and compared. Furthermore, a novel approach for the semi-analytic assessment of MZ implementation uncertainty has been detailed, in §3.6.1, and compared with the others available in literature.

A further content of novelty in this chapter is represented by the use of the analysis results. These have been used to build regression models that, in their turn, can be used to extend the findings of this analysis to similar cases. As a matter of fact, the surface responses presented in this chapter give inspiration to half of the categorical data model that is presented in Chapter 5. Particularly they provide the predictive capabilities necessary to cope with the flexibility requirements of many small metrology laboratories.

With respect to the Quadratic Response Surfaces presented in §3.10 and with respect to the possibility to use them for predictive purposes, some strategic considerations are necessary. Among the different models, those defined for the implementation uncertainty are the worst (R-sq < 50%),therefore they should be avoided. However, this consideration is not discouraging at all, as the implementation uncertainty can be calculated, for each verification operator, without any need for regression models (see §3.5 and §3.6 for a thoroughly presentation). On the other hand, a regression model particularly important is that for method uncertainty, as in practice the perfect verification operator is rarely used and it is not possible to assess the method uncertainty according to equation (3.5). Luckily, this model is quite reliable (R-sq ~ 80%) and can be used to obtain valuable estimations. Finally there are the models for measurement uncertainty that are quite reliable too (R-sq ~ 80%). However, considering that measurement uncertainty is the composition of method uncertainty and implementation uncertainty, the regression model for measurement uncertainty is not necessary and its use should be avoided in favour of the more transparent composition of its two components.

The optimal strategy for handling simplified verification operators and assessing the GPS measurement uncertainty (or compliance uncertainty too if the specification is complete) is therefore provided by the following steps:

- estimate *FLT*t from the measurement dataset, using the association criterion required by the verification operator;
- assess u_{Im}, for the association criterion used at the previous step, using the measurement dataset at hand and one of the approaches presented in §3.5 or §3.6;
- assess u_{Mt} with the regression model available for the feature in object;
- calculate the measurement uncertainty $u_M = \sqrt{u_{Im}^2 + u_{Mt}^2}$.

This strategy is the foundation for the branch of the categorical data model designed to deal with the scenario of small flexible metrology laboratories (§5.3.2). It allows to exploit the valuable know-how of many metrology laboratories (the experiments and derived surface responses should be organized into a knowledge database) in order to improve the value of their uncertainty statements.

3.12 References

[1] ISO 1101 (1983) *Technical drawings - Geometrical tolerancing - Tolerancing of form, orientation, location and run-out - Generalities, definitions, symbols, indications on drawings*. ISO, Geneve.

[2] ASME Y 14.5M (1994) *Dimensioning and Tolerancing*.

[3] Samuel G.L. and Shunmugam M.S. (1999) *Evaluation of straightness and flatness error using computational geometric techniques.* Comput. Aided Des., **31** 829-843.

[4] ISO/TS 17450-2 (2002) *Geometrical product specifications (GPS) - General concepts - Part 2: Basic tenets, specifications, operators and Uncertainties*. ISO, Geneve.

[5] ISO/DIS 14659.2 (2009) *Geometrical product specification (GPS) – Fundamentals – Concepts, principles and rules* ISO, Geneve.

[6] ISO 1101 (2004) *Geometrical product specifications (GPS) - Geometrical tolerancing - Tolerances of form, orientation, location and run-out*. ISO, Geneve.

[7] ASME Y 14.5 (2009) *Dimensioning and Tolerancing – Engineering Drawing and Related Documentation Practices*.

[8] ISO/TS 12781-2 (2011) *Geometrical product specifications (GPS) - Flatness - Part 2: Specification operators*. ISO, Geneve.

[9] Lu W.L., Jiang X., Liu X.J. and Xu Z.G. (2008) *Compliance uncertainty of diameter characteristic in the next-generation geometrical product specifications and verification.* Meas. Sci. Technol, **19**.

[10] ISO/TR 14638 (1995) *Geometrical product specifications (GPS) - Masterplan*. ISO, Geneve.

[11] ISO 3274 (1996) *Geometrical product specifications (GPS) - Surface texture: Profile method - Nominal characteristics of contact (stylus) instruments*. ISO, Geneve.

[12] ISO/TS 16610-40 (2006) *Geometrical product specifications (GPS) - Filtration - Part 40: Morphological profile filters: Basic concepts*. ISO, Geneve.

[13] ISO/TS 16610-41 (2006) *Geometrical product specifications (GPS) - Filtration - Part 41: Morphological profile filters: Disk and horizontal line-segment filters*. ISO, Geneve.

[14] ISO/TS 12780-2 (2003) *Geometrical product specifications (GPS) - Straightness - Part 2: Specification operators*. ISO, Geneve.

[15] ISO 14253-1 (1999) *Geometrical product specifications (GPS) - Inspection by measurement of workpieces and measuring equipment – Part 1: Decision rules for proving conformance or non-conformance with specifications*. ISO, Geneve.

[16] Cui C., Fu S. and Huang F. (2009) *Research on the uncertainties from different form error evaluation methods by CMM sampling.* The International Journal of Advanced Manufacturing Technology, **43** (1) 136-145.

[17] Lee M.-K. (2009) *An enhanced convex-hull edge method for flatness tolerance evaluation.* Comput. Aided Des., **41** 930-41.

[18] Choi W., Kurfess T.R. and Cagan J. (1998) *Sampling uncertainty in coordinate measurement data analysis.* Precision Engineering, **22** 153-163.

[19] Wen X.-L., Zhu X.-C., Zhao Y.-B., Wang D.-X. and Wang F.-L. (2012) *Flatness error evaluation and verification based on new generation geometrical product specification (GPS).* Precision Engineering, **36** (1) 70-76.

4 Verification operators on simulated surfaces

4.1 Introduction

The analysis and comparison of the different methods available for estimating the uncertainty of verification processes has shown that there are two main sources of uncertainty represented by: the ability of the sampling strategy in detecting all the form deviation and the accuracy of the measuring instrument (the measurement uncertainty affecting the sampling of each measuring point). Some method shows more sensitivity to the former, some to the latter but, until both are present together, it is not possible to discern their effects. For this reason the same Design of Experiment used in Chapter 3 has been deployed also for the simulation of measurements on a virtual surface. Particularly, verification operations have been simulated in two different conditions:

- ***Ideal measuring instrument,*** which is able to measure without introducing any error (§4.3).
- ***Real measuring instrument,*** which introduces a measurement error whose probability density function is supposed to be normal (§4.4). It generates measurement uncertainty.

Among the stimuli of this investigation there is the difference among the results produced by different association criteria, for the evaluation of flatness deviation, and among the approaches used for assessing the uncertainty of the evaluation.

The different methods for the assessment of implementation uncertainty that have been used in Chapter 3 do not use the classical concept of measurement replications [1]. Bootstrap is the approach that more resembles the classical one, but the bootstrap samples are all generated from the same dataset (sampling); thus the possibility to obtain a different measurement of the same sampling point (because of measurement errors) is not considered. It is a valid method if there is not the possibility to replicate measurements and its validity increases in parallel with sample size.

As the simulation of verification operators is inexpensive with respect to a real measurement (it is just a short computation time), the approach based on the replication of verification operators [1] has been explored in this chapter (§4.6.2). In this case, uncertainty is defined as the variability (standard deviation) of the output of the verification process over the number of replications.

Particularly, each of the measurement simulations presented in this chapter is aimed at addressing one of the issues that are not explained by the case study:

- **The simulation of an ideal measurement (§4.3 and §4.5)**, based on an ideal measuring instrument, is aimed at highlighting the effect of sampling accuracy (the

measurement uncertainty on the sampling of each measurement point) on the performance of the verification operator (the measurement points considered as a whole). The results of this simulation shall be compared with a real measurement on the same feature and with the same verification operators.

- **The simulation of a real measurement (§4.4 and §4.6)**, based on the simulation of a real measuring instrument, is aimed at providing the benchmark for the ideal measurement required at the previous point.
- **100 replications of each verification operator (§4.6.2),** based on a real measuring instrument, in order to assess the performance of the association criteria regardless the sample size

The results, summarized and compared in §4.8, allow the conclusion that the analytic assessment of implementation uncertainty overestimates the effect of the measurement uncertainty which affects measurement points. Notwithstanding this behaviour, the analytical estimation of LS implementation uncertainty is a powerful tool to understand how much the selected sample size is suitable to get a robust estimation of the LS reference plane and, if the sampling is uniform, a robust coverage of the measurand (§4.9). Therefore, analytic and experimental approaches should be used consciously and, when possible, compared in order to exploit the best of each one (§4.9).

4.2 Virtual surface

In order to have a virtual surface the most useful to make comparisons with the DoE performed on the real flatness feature, the virtual surface used in this chapter has been defined as an approximation of the case study's flatness feature. The real geometry of the case study's flatness feature is known at the best only through the perfect verification operator, thus with all the uncertainty introduced by the measuring instrument. Therefore, the virtual surface can be defined as a regression of the measurement points dataset.

The problem of surface reconstruction form unorganized points has been widely afforded in literature. In particular, within the family of surface fitting problems, Hoppe et. al. [2] distinguish two different approaches: the function reconstruction and the surface reconstruction. The function reconstruction methods can be used in simple, special cases, where the surface to be reconstructed can be regarded as the graph of a function over a known domain surface (usually a plane or a sphere [2]). On the other hand, the surface reconstruction methods can be further classified, according to the way they represent the reconstructed surface, as parametric or implicit methods. Parametric reconstruction techniques represent the reconstructed surface as a topological embedding of a two-dimensional parameter domain into $\mathbb{R}^3$, but they have been developed only for very simple shapes [3, 4].

The family of implicit reconstruction methods is aimed at interpolating the points $\{(x_i, y_i, z_i)\}_{i=1}^{n}$ with an implicitly formulated surface $f(x, y, z)$. In fields nearer to CAD

systems, Constructive Solid Geometry (CSG) represents the leading approach and the implicit model is defined by primitive functions through a combination of Boolean operations and blending functions [5]. The implicitly reconstructed surfaces have been defined also by means of piecewise low-order algebraic surfaces, also known as implicit patches or semi-algebraic sets [6]. However, all these representations lead to a surface that is continuous and differentiable piecewise only.

In order to avoid the disadvantages related with piecewise defined surfaces, Carr et. al. [5] propose an implicit representation based on Radial Basis Functions (RBF), which allow the complete definition of tree-dimensional surfaces with a single continuous and differentiable implicit function. The advantages of modelling surfaces with RBFs had been already recognized by Turk & O'Brien [7, 8] and Carr et. al. [9]. In particular, Turk & O'Brien tried to model laser scan data with RBFs but they were constrained to work with small datasets in order to keep them computationally manageable. Carr et al. used RBFs to reconstruct cranial bone surfaces from 3D-CT scans. The areas surrounding large irregular holes were represented with thin-plate spline RBFs and the surface of prosthesis was defined from these. This approach is restricted to the surfaces that can be expressed explicitly as a function of two variables, and could be suitable to deal with the case study's flatness feature, which also presents several holes. Later on, the same authors use RBFs to reconstruct and represent three-dimensional objects starting from point-cloud data acquired with optical scanners [5]. In this work they introduce also RBF approximation for noisy data. The interpolatory behaviour is damped in order to do not exactly interpolate the measurement points, which do not exactly belong to the real surface but are just near it (displaced of an unknown random measurement error: namely the noise), and obtain a smoother function which is more representative of the feature shape.

RBFs have excellent interpolatory/reconstruction performance, but require a computational effort that is not justified by the purpose of the virtual surface we need to define. For this reason, and considering that the main content of flatness deviation has the shape of a horse saddle, a polynomial function has been chosen which minimizes the quadratic distance from measured points. The best performance (Figure 4.1) has been obtained with the following type of regression function:

$$z = \left(ax^3 + bx^2 + cx + d\right) * \left(ly^3 + my^2 + ny + p\right)$$

Figure 4.2 proves the goodness of the regression surface with a projection of Figure 4.1 on the X-Y plane. Only the measurement points above the regression surface are visible in this view and they draw some patterns that, to use the GPS language, are lower wavelength defects. These patterns have been clearly produced by the interaction of tool (end mill) trajectories.

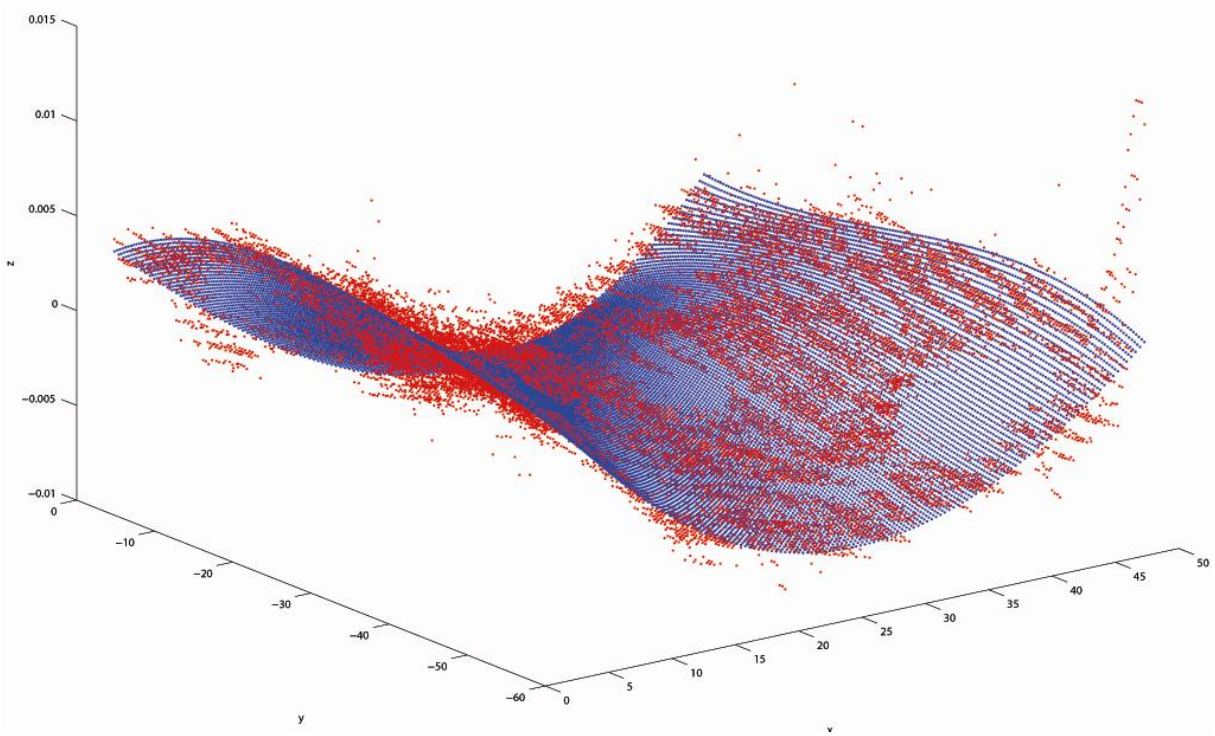

Figure 4.1 - Polynomial regression function (blue) interpolating the cloud-data points (red) of perfect verification operator. The regression function is able to grasp the main content of form deviation but the defect in the right corner and lower wavelength form defects highlighted in Figure 4.2.

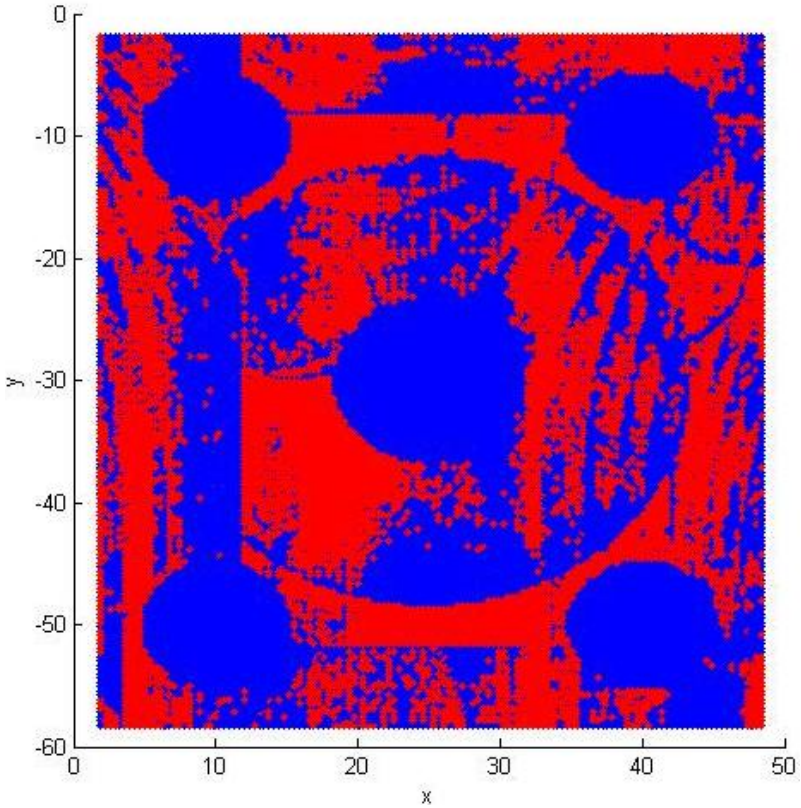

Figure 4.2 - (X-Y) projection of Figure 4.1. The pattern of red points (measurement points above regression function) shows the lower wavelenth defects produced by the overlapping of tool trajectories.

4.3 Simulation of ideal measuring instrument

A measuring instrument is defined ideal if it is able to measure the exact coordinates of any point on the measurand surface. Obviously such an instrument cannot exist in practice but represents the ideal, utopian, target aiming the evolution of measuring instruments. An ideal measurement does not introduce any error and is perfectly repeatable. Measured coordinates and nominal coordinates are the same thing, therefore the measurement dataset corresponding to a certain extraction grid can be easily obtained by evaluating the function of the surface geometry (that in our case is known, as we are dealing with a virtual surface) over the extraction grid.

As a matter of fact, for flatness features, an extraction grid is defined as a set of points identified by their (x, y) coordinates, with the identification of the z coordinate being the purpose of the measurement process. Provided that the geometry of a three-dimensional surface can be expressed in the form $z=f(x, y)$, the measurement of a generic point $P_i(x_i, y_i, z_i)$ can be regarded as the evaluation of $z_i=f(x_i, y_i)$.

The ideal measuring instrument allows us to perform verification operators that are not affected by sampling induced errors. Comparing verification operators based on ideal instruments with those based on real (simulated) instruments, we should be able to discern the amount of flatness deviation that is actually due to the feature shape (result of ideal measurement) from the one due to the accuracy of real (simulated) samplings.

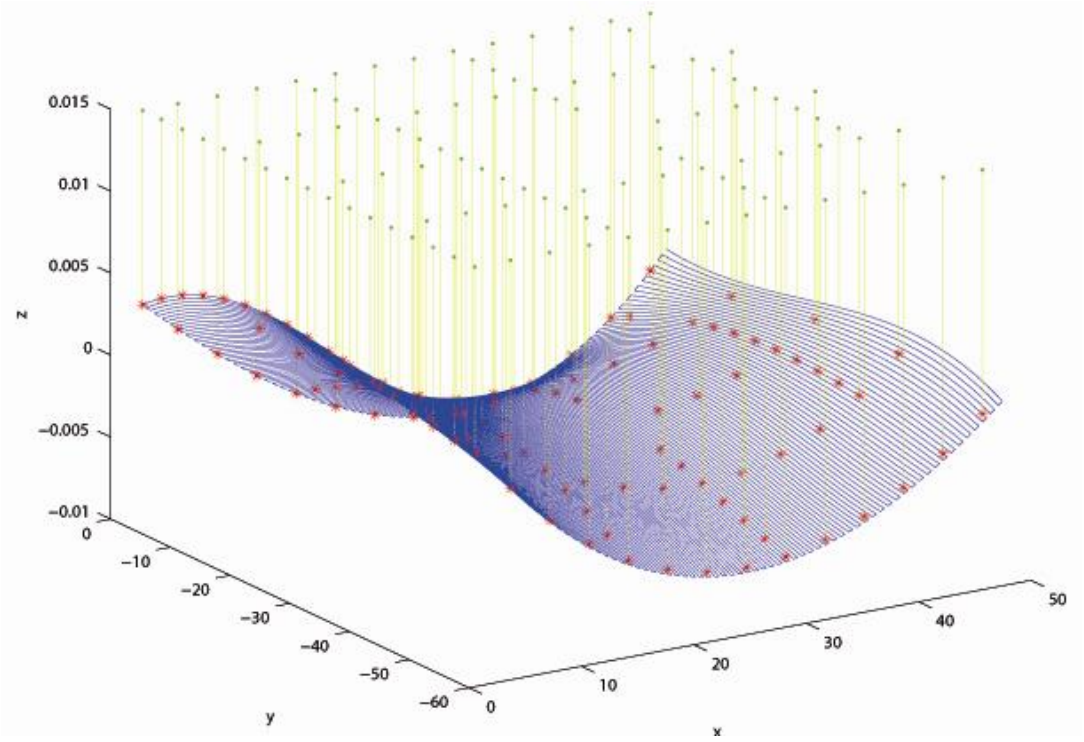

Figure 4.3 - Sampling with an ideal instrument can be easily simulated by projecting the sampling grid (green points) onto the feature surface along the touch probe approach direction (yellow lines). Sampling grid presents some discontinuities in correspondence to the position of holes or pin of the real feature.

4.4 Simulation of real measuring instrument

For a general virtual surface we are able to simulate ideal verification operations according to §4.3, thus to extract the nominal coordinates of sampling points from the virtual flatness surface. From these nominal sampling datasets, measurement by means of CMMs can be easily simulated under the hypothesis that the measurement errors introduced by the instrument are randomly distributed within a Gaussian probability density function. In particular the standard deviation of this Gaussian distribution is assumed to be one sixth of the instrument maximum permissible error (MPE). This assumption can be supported by a 6 sigma quality management [10].

The measurement simulation is then obtained by adding to the nominal coordinates of sampling points an error randomly extracted from a Gaussian population with σ = MPE/6. An example of the MATLAB® code performing the measurement simulation is the following:

```
%% Instrument accuracy
MPE=0.004;  % CMM Maximum Permissible Error
sX=MPE/6;   % Standard deviation of sampling error along x, y and z
sY=MPE/6;   % directions (under the hypothesis of 6 SIGMA quality control)
sZ=MPE/6;

%% Vectors with nominal coordinates of sampling points (X_nom)
x=P_nom(:,1); y=P_nom(:,2); z=P_nom(:,3);

%% Simulation of measurement adding Gaussian error on nominal coordinates
x_sim=normrnd(x,sX);  % Simulation of measurement process realized by
y_sim=normrnd(y,sY);  % adding to the nominal coordinates an error normally
z_sim=normrnd(z,sZ);  % distributed and with standard deviation = MPE/6
P_sim=[x_sim y_sim z_sim]; % Simulated measurement dataset
```

4.5 Analysis of ideal measurements

The purpose of these experiments is to understand the actual capability of sampling grids in detecting flatness deviations and the effects of the measurement uncertainty affecting sampling points. The same experimental campaign performed for the case study's flatness feature (§3.4) has been repeated for a virtual surface sampled with an ideal instrument. This allows reasoning on grids performance regardless the uncertainties that, in the real practice, are introduced by measurement errors. The results are reported in Annex C with the same criterion used to organize the case study's results: Table C.1 contains the flatness values and implementation uncertainties calculated with LS criterion, Table C.2 those obtained with MZ criterion, and Table C.3 the method and measurement uncertainties.

Figure 4.4 compares the estimation of flatness deviation with LS and MZ association criteria. In particular LS association criterion systematically ends up with a higher estimation (this is expected by definition) and several sampling grids, even with samples of several hundreds of points, estimate a flatness deviation particularly large (about 2 or 3 µm more than the true value estimated by MZ).

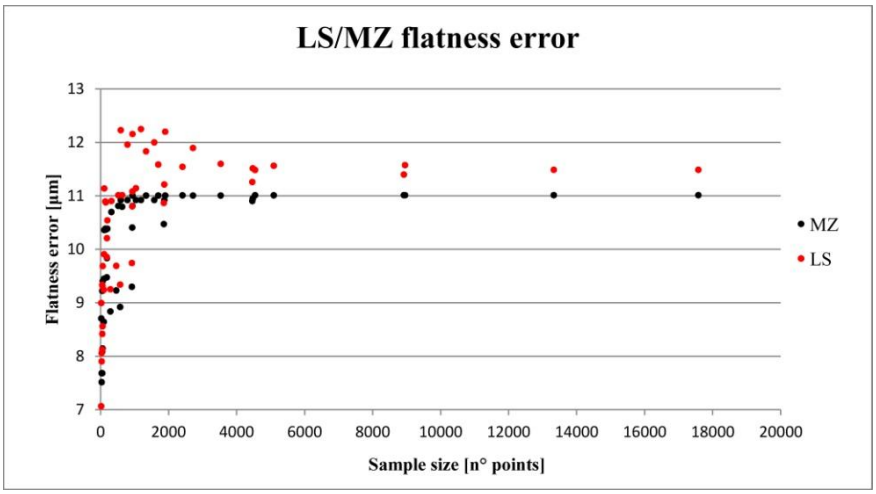

Figure 4.4 - Estimation of flatness error regardless instrument accuracy. LS systematically overestimates.

For the experimental estimation of the flatness evaluation uncertainty (by means of the bootstrap method), Figure 4.5 shows very similar trends for both MZ and LS association criteria, with the only difference in the asymptote values. For LS method it is about 0.1 µm while for MZ it is 0.001 µm. The excellent performance of MZ method is a consequence of the feature shape being particularly smooth: if the actual extreme points are not contained in some bootstrap sample then the extreme point will be some of its neighbours that, because of the very smooth shape, have a very similar height (z coordinate). Hence, the actual variability of MZ estimation over the bootstrap samples (the standard deviation used to estimate uncertainty) is very low. For the LS method the effect is rather different because it is not just a matter of getting the right extreme points; or some very similar to these. Even if from the point of view of MZ criterion a bootstrap sample may seem to be equal to the original dataset (the actual extreme points are contained at least once), from the point of view of LS method it is almost certainly different. Some points of the original dataset may not be present at all while others may be present more than once. This means that the LS reference plane is every time different and a slightly different flatness error is evaluated. The greater uncertainty is then explained by the effect of bootstrapping on the uniformity of sampling, therefore on the coefficients of LS reference plane. This idea can be proved by comparing the results of bootstrap and analytic estimation of LS uncertainty (see Figure 4.6).

The analytic and the experimental (bootstrap) approach for assessing the implementation uncertainty are very different in nature. The former starts from the problem formulation and uses partial derivatives to express the sensitivity of the output with respect to perturbations on each input variable, and then composes their effects: it is a clear-box approach. On the other hand, the latter introduces small perturbations to the inputs to observe the variability of the output: it is a black-box approach. However, despite the different nature, both approaches agree on the assessment of the implementation uncertainty of LS-based verification operators (Figure 4.6) that, in this case, reflects the density of sampling strategy and the position of measurement points only.

Particularly, for an infinite accurate sampling (MPE = 0), the LS implementation uncertainty is represented by the uncertainty related with the estimation of the parameters describing the equation of the LS reference plane only. The first six terms of equation (3.4) equal zero and the implementation uncertainty can be simplified according to equation (4.1) that, in other words, represents the stability of the LS reference plane with respect to the spatial distribution of sampling points.

$$u_{Im}^2 = u_e^2 = \cancel{\left(\frac{\partial\delta}{\partial x_1}u_{x_1}\right)^2} + \cancel{\left(\frac{\partial\delta}{\partial x_2}u_{x_2}\right)^2} + \cancel{\left(\frac{\partial\delta}{\partial y_1}u_{y_1}\right)^2} + \cancel{\left(\frac{\partial\delta}{\partial y_2}u_{y_2}\right)^2} + \cancel{\left(\frac{\partial\delta}{\partial z_1}u_{z_1}\right)^2} + \cancel{\left(\frac{\partial\delta}{\partial z_2}u_{z_2}\right)^2} + \left(\frac{\partial\delta}{\partial a}u_a\right)^2 + \left(\frac{\partial\delta}{\partial b}u_b\right)^2 + 2\frac{\partial\delta}{\partial a}\frac{\partial\delta}{\partial b}\rho_{ab}u_a u_b \quad \textbf{(4.1)}$$

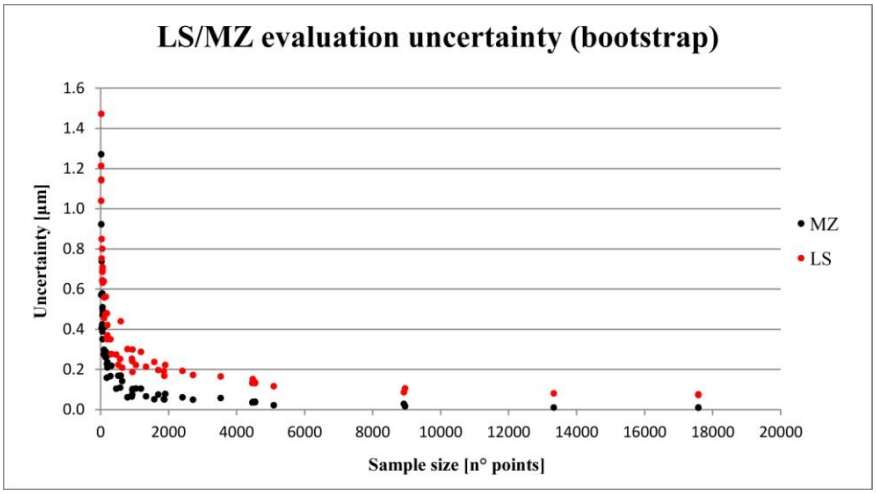

Figure 4.5 - Comparing the experimental estimation of implementation uncertainty we find a slightly higher uncertainty for LS method: 0.1µm against the 0.001µm of MZ.

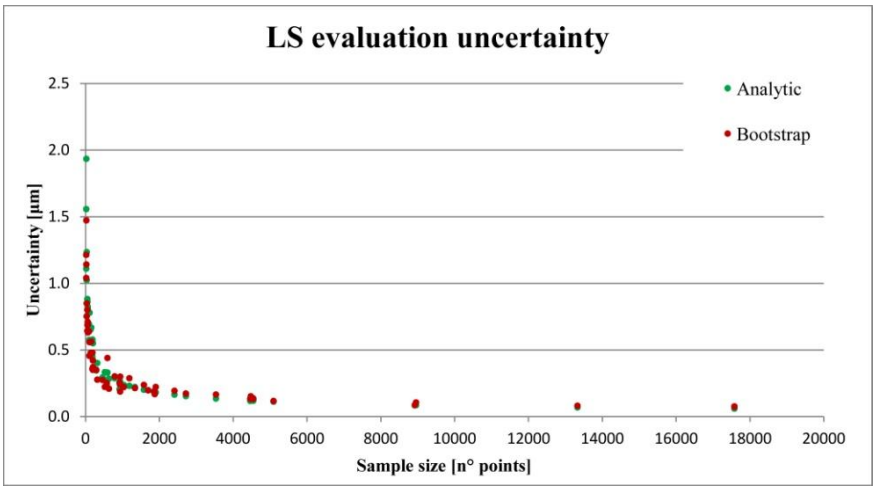

Figure 4.6 - In case of infinite sampling accuracy (MPE=0), experimental and analytic estimation of LS evaluation uncertainty are almost identical. Both are considering the effect of spatial distribution of sampling points on the stability of the LS reference plane; the former with a black-box approach while the latter with a clear-box approach.

According to the initial purpose to understand the capability of sampling grids in detecting form deviation, no remarkable difference can be noticed. In Figure 4.4, for both association criteria, there are continuous trends that are, in the two extreme regions (near the origin and at the asymptote), very similar to those of the case study (Figure 3.8 or Figure 3.17). However, for the simulated measurement, there is no discontinuity in the central area of the graph. Obviously this is a consequence of the very smooth geometry of the virtual surface that has been used to simulate the measurement, and of the absence of form defects with a wavelength shorter than the distance between the straightness profiles that have been used to build the sampling grids. This observation confirms the recommendation of GPS standards to pay particular attention to the selection of the sampling grid whenever particular form errors can be expected along some preferential direction [11].

4.6 Analysis of real (simulated) measurements

The purpose of this experimental campaign is to have the simulation of verification operators based on real measuring instruments: an experiment dual to the one presented in Chapter 3, to be compared with the one presented in §4.5. Such a comparison allows pointing out the effects of instrument accuracy (measurement uncertainty in each sampling point) on the flatness error evaluation. To respect the same construction of the experiment used in §3.4, measurement has been simulated once for the perfect verification operator (according to §4.4) and all the simplified verification operators have then been obtained as subsamples. The results are summarized in Annex D using the same logic used for the case study.

Figure 4.7 shows the results of flatness error assessment for both LS and MZ criteria (Table D.1 and Table D.3). As expected, LS slightly overestimates the flatness error but the trends are very similar to those observed for the ideal-instrument-based verification operators (Figure 4.4). However, in Figure 4.7, both curves are shifted towards larger values of form error and their shape is more resembling of a Gaussian cumulate function.

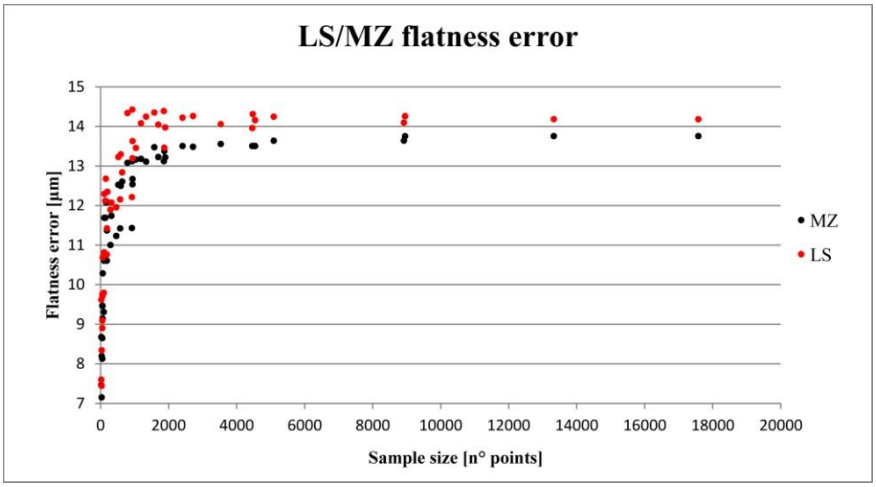

Figure 4.7 - For the simulated measurement dataset LS and MZ association criteria show very similar performances.

According to the uncertainty of the evaluation (implementation uncertainty), reported in Figure 4.8, both the association criteria show the same trend but with LS method being shifted towards higher values of uncertainty. This is a consequence of LS estimation being affected simultaneously by: the presence of the real extreme points (or of neighbours with very similar height) in the bootstrap sample, and the statistics of all the points included in each bootstrap sample (stability of the LS reference plane). The latter being the main difference between statistical and extreme fit association criteria. This aspect has already been explained, more in detail, in §4.5.

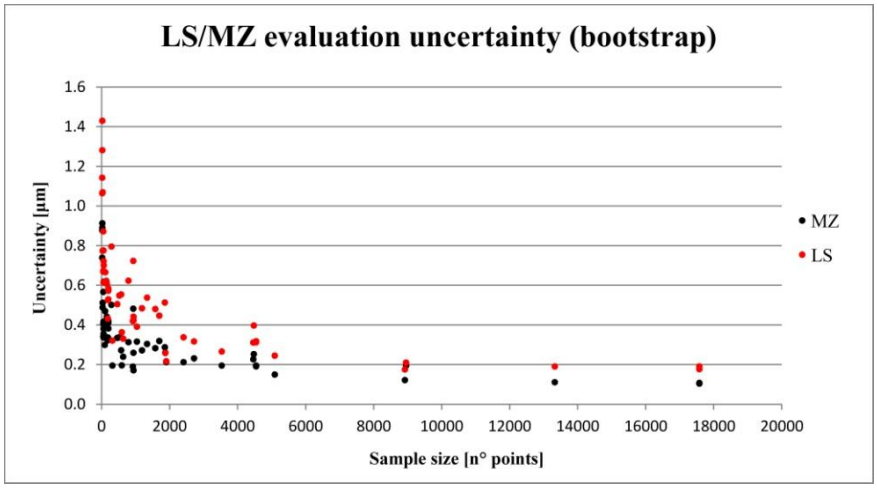

Figure 4.8 - Experimental assessment of the uncertainty of flatness evaluation for LS and MZ criteria. Trends are similar but with LS showing higher uncertainty.

Particularly interesting is the difference between the assessment of LS evaluation uncertainty with the experimental and analytic method (Figure 4.9). The result of the analytic assessment is the same observed for the case study (Figure 3.11) because the measurement uncertainty introduced by the instrument during sampling is the same. However, for the ideal-instrument-based verification operators, the experimental and analytic approaches agree, with respect to the uncertainty associated with the density and distribution of sampling points (Figure 4.6). Therefore, the difference between the two curves plotted in Figure 4.9 can be interpreted only as an effect of the measurement uncertainty associated with sampling points.

Finally, in order to test the hypothesis that the particularly poor performance of the Quadratic Response Surface Regression for implementation uncertainty (§3.10.4) is a consequence of the particular shape of the case study's flatness feature, the same kind of model has been determined also for the experiment at hand. The Quadratic Response Surface Regressions have been determined for the measurement uncertainty (§4.6.1), the method uncertainty (§4.6.2) and the implementation uncertainty (§4.6.3), particularly for the case in which implementation is assessed with an analytic approach.

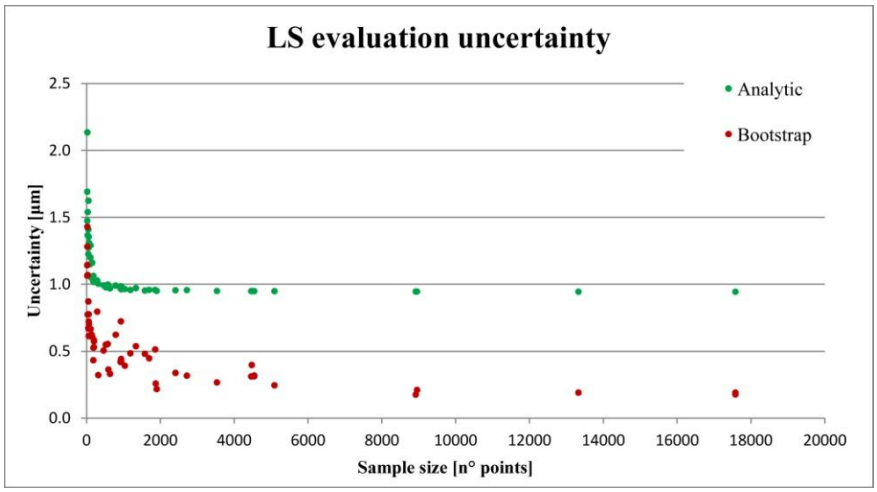

Figure 4.9 - LS analytic uncertainty estimation shows the same trend noticed for the case study's real surface (Figure 3.11): asymptotes are the same because both the real and simulated instrument have the same MPE.

4.6.1 Quadratic Response Surface Regression for measurement uncertainty

The response surface for measurement uncertainty (Table 4.1) shows that only factors *d* and *Grid* are significant for the verification of the virtual surface. There is not a marked form error with a short wavelength, such as the signature of the mill exit point on the case study's surface. Therefore, parameter *D* is no longer significant and sampling density becomes the most important factor. Parameters *d* and sampling *Grid* represent the sample density more than *D*. As a matter of fact, if for a fixed couple *d-D* the extraction *Grid* is changed (for example Union Jack is chosen instead of Py or Px) the number of sampling points is nearly doubled, and vice versa. Therefore, factor *Grid* is more important than *D*. Furthermore, the reliability of the regression model obtained is very remarkable. With an R-sq value of 90% about, it is able to explain almost all the variability contained in the experiment results.

Figure 4.10 shows the residuals analysis for the Quadratic Response Surface Regression of Table 4.1. Residuals satisfy the assumption on the normality of their distribution but, from their plot against the fitted value, it seems that there is some phenomenon not completely explained. The linear trend visible for fitted values minor than 2 (µm in this case) highlights some difficulty for the model in reproducing the asymptotic trend corresponding to very large samples. Some fluctuation can be noticed also in the plot of residuals against the observation order, however this is an effect of the progressive order in factors variation given that the runs were not randomized.

The effects of different factors on measurement uncertainty are graphically illustrated in Figure 4.11. On a wider perspective, all verification operations represented by at least a turquoise colour in Figure 4.11 are good candidates for verifying the compliance of our flatness requirement.

Term	Coef	SE Coef	T	P
Grid	2.20513	0.33472	6.588	0.000***
d*d	0.20198	0.04739	4.262	0.000***
Grid*Grid	-0.42869	0.05287	-8.109	0.000***

S = 0.579135

R-Sq = 90.13% R-Sq(pred) = 87.03% R-Sq(adj) = 88.91%

Table 4.1 - Significant terms in Quadratic Response Surface Regression of measurement uncertainty versus *D*, *d*, *Grid* and *Association* method. P-values less than 0.01 are marked with ***.

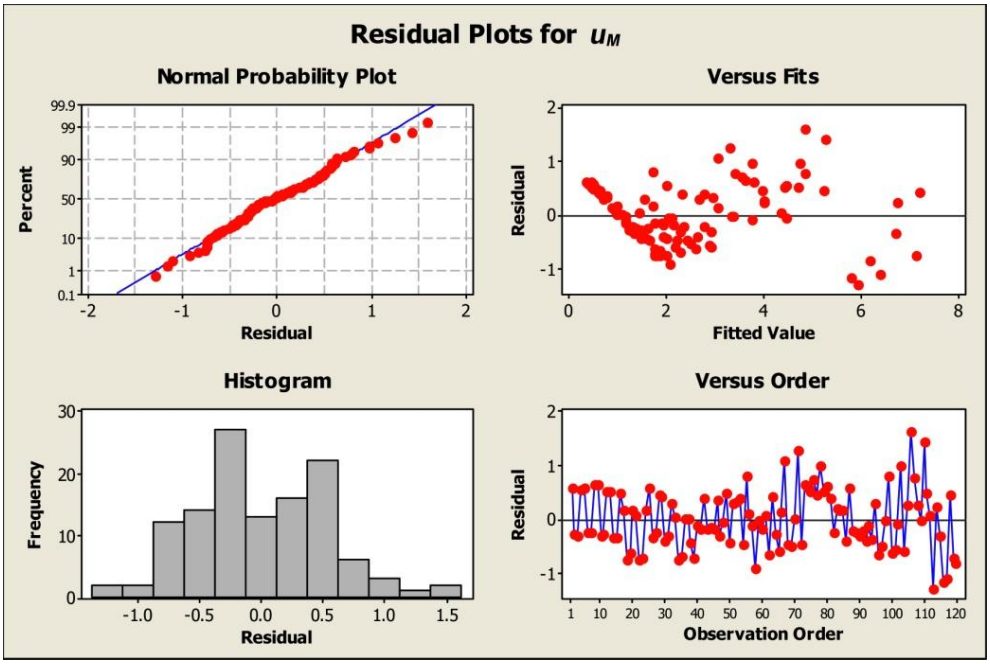

Figure 4.10 - Residuals analysis for the Quadratic Response Surface Regression of measurement uncertainty.

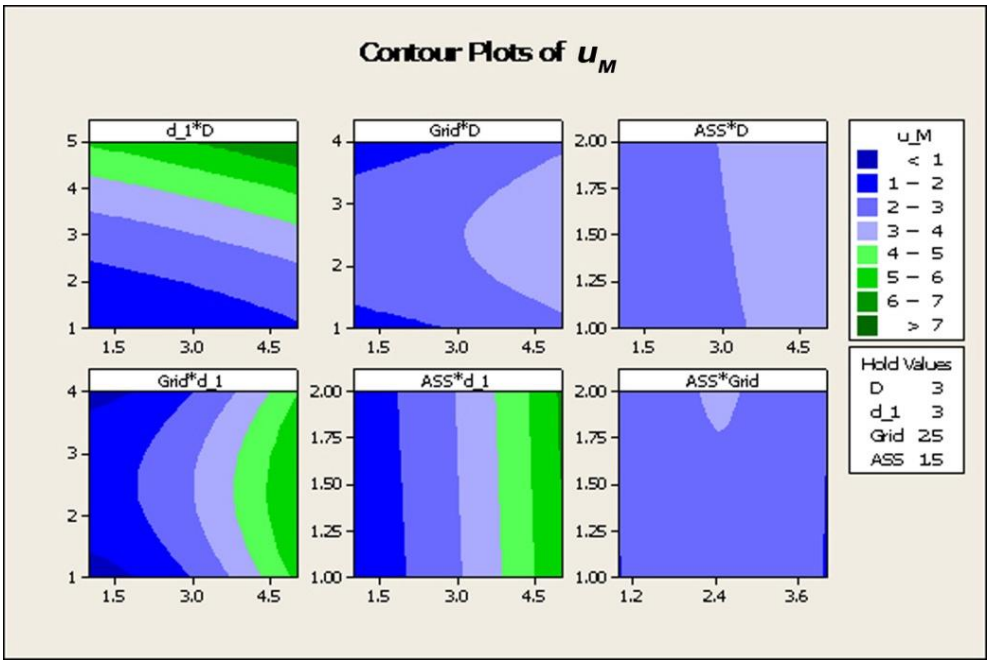

Figure 4.11 - Contour plot with the effect of different factors on measurement uncertainty.

4.6.2 Quadratic Response Surface Regression for method uncertainty

The response surface of method uncertainty, presented in Table 4.2, has the same reliability of the response surface for measurement uncertainty. The *association* criterion becomes significant as it introduces a systematic overestimation if LS is used instead of MZ.

Term	Coef	SE Coef	T	P
Constant	-2.07548	0.95836	-2.166	0.033**
Grid	2.62147	0.37471	6.996	0.000***
d*d	0.18397	0.05305	3.468	0.001***
Grid*Grid	-0.49547	0.05918	-8.372	0.000***
D*ASS	0.19816	0.10959	1.808	0.073*

S = 0.648323
R-Sq = 90.01% R-Sq(pred) = 86.84% R-Sq(adj) = 88.78%

Table 4.2 - Significant terms in Quadratic Response Surface Regression of method uncertainty versus *D, d, Grid* and *Association* method. P-values less than 0.10 are marked with *, less than 0.05 with **, less than 0.01 with ***.

4.6.3 Quadratic Response Surface Regression for implementation uncertainty

The response surface for implementation uncertainty presented in Table 4.3 is much more reliable than the analogous response surface calculated for the case study (Table 3.4). R-sq is now 83% about therefore the model is much more likely to correctly interpolate the experiment results.

Term	Coef	SE Coef	T	P
Constant	0.872616	0.141431	6.170	0.000***
ASS	0.158755	0.067331	2.358	0.020**
d*d	0.045735	0.007829	5.841	0.000***
d*ASS	-0.099240	0.016172	-6.136	0.000***

S = 0.0956770
R-Sq = 83.14% R-Sq(pred) = 75.41% R-Sq(adj) = 81.07%

Table 4.3 - Significant terms in Quadratic Response Surface Regression of implementation uncertainty versus *D, d, Grid* and *Association* method. P-values less than 0.05 are marked with **, less than 0.01 with ***.

4.7 Replication of verification operators

For a virtual surface the form error is perfectly known as it is defined by the equation that defines the surface geometry. Measurement can be simulated according to §4.4, a completely inexpensive operation with respect to a real CMM sampling. Inexpensive simulated measurements can be used to estimate the uncertainty of verification operators through the Monte Carlo method: by simulating verification operators for a number of times large enough for doing statistical inference. Particularly, measurement simulation has been repeated 100 times for each verification operator, and flatness error has been evaluated with both LS and MZ association criteria. Then, the flatness deviation and uncertainty of its evaluation have been defined, starting from the statistics of the 100 repetitions, as the average (4.2) and standard deviation (4.3) respectively.

$$\bar{\delta} = \frac{\sum_{i=1}^{N} \delta_i}{N} \tag{4.2}$$

$$\sigma_\delta = \sqrt{\frac{1}{N} \sum_{i=1}^{N} (\delta_i - \bar{\delta})^2} \tag{4.3}$$

The results of simulations are summarized in Table E.1, and briefly analysed through the aid of some pictures. With respect to MZ association criterion, Figure 4.12 compares the average result of the 100 real-instrument-based verification operators with the real flatness deviation (named true deviation) that would be measured performing the same operators with an ideal instrument. Both for the true and measured flatness deviation there is an asymptotic convergence. The distance between the two asymptotes represents the effect of sampling accuracy. All grids but Py show consistent results due to the fact that the virtual surface has been defined as a regression of the case study's one, thus similar problems, even if with lower magnitude, affect Py grids.

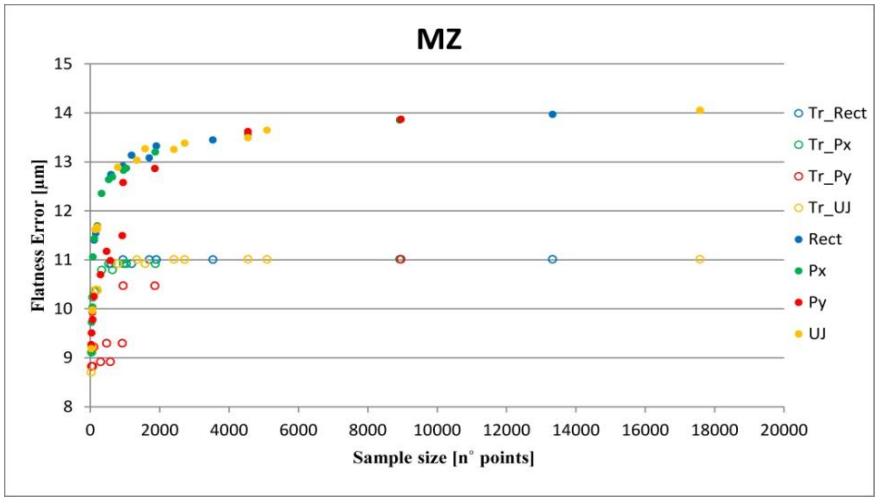

Figure 4.12 - Average of the 100 measurements of MZ flatness error (filled dots) compared with the true form error measured with the ideal instrument (unfilled dots).

Figure 4.13 performs the same comparison just explained above, but for verification operators based on LS association. It is interesting to point out how small samples of nominal points end up with estimations of LS flatness deviation even higher than the asymptote. It is just a consequence of the orientation of the LS reference plane that, with few points, can be very unstable. However, both for the evaluation of true error and the estimation from simulated measurement, LS method leads to an overestimation with respect to MZ (Figure 4.14). The overestimation is the same in both cases because it is a consequence of the evaluation algorithm only, and not of the measurement uncertainty that affects sampling points.

Looking at Figure 4.14 it can be noticed also that the simulated estimations of flatness error (filled dots) plotted against the sample size resemble, for both association criteria, a cumulative Gaussian trend. This trend is absent for the true error detection. It clearly means

that it is an effect induced by sampling errors (which are defined as a Gaussian distributed phenomenon) whose effect is stressed by the number of points on which the average is based (the sample size multiplied by the 100 repetitions). Figure 4.15 provides a further clearer proof.

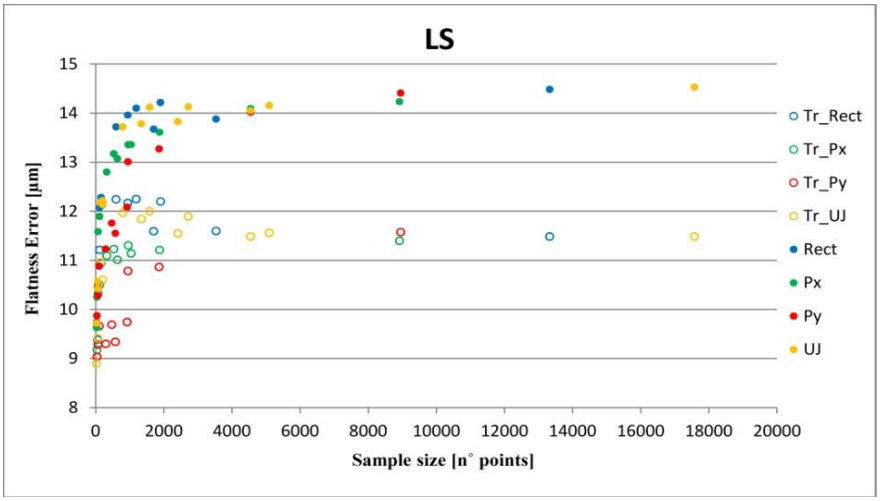

Figure 4.13 - Average of the 100 measurements of LS flatness error (filled dots) compared with the true form error measured with the ideal instrument (unfilled dots).

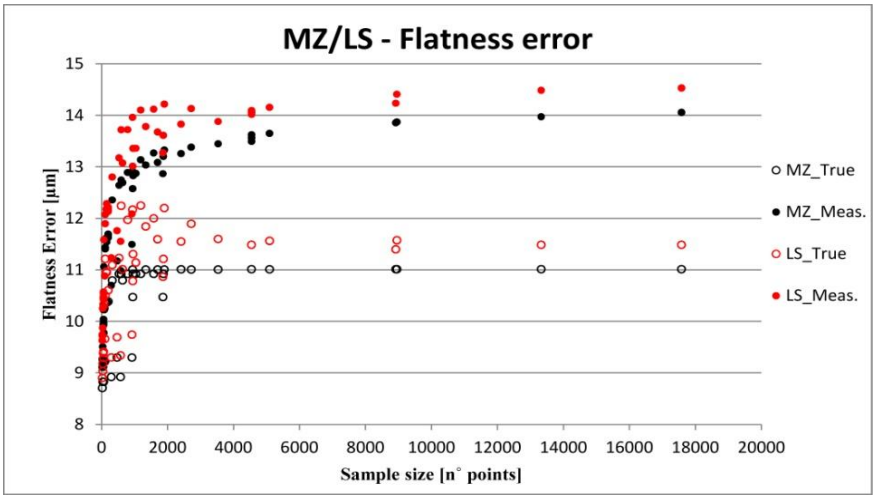

Figure 4.14 - Comparison of MZ and LS flatness deviation on both the nominal measurement points (unfilled dots) and simulated measurement datasets (filled dots). LS systematically overestimates.

The difference between the true form error and the one estimated through simulated measurements has been plotted, in Figure 4.15, after normalizing with respect to the standard deviation of the Gaussian distribution used to simulate the instrument accuracy ($\sigma = MPE/6 = 4/6\mu m$). This normalization is chosen in order to relate the uncertainty introduced by the instrument over the sampling of each measuring point, with the effect perceived (in terms of form error evaluation) after the application of an association criterion. Figure 4.14 already showed that with the increase of sample size, also the understanding of the actual surface geometry improves. However, Figure 4.15 shows that while the measurand knowledge improves, by measuring more points, a broader range of sampling errors is experienced.

These are processed by the association criterion and affect the evaluation result. Looking at the way sampling accuracy affects flatness estimation (Figure 4.15) it can be noticed that, towards the asymptote, the flatness error is overestimated, in average, of a quantity that is slightly minor than the instrument MPE (5/6 of it). The trend is the same for both association criteria, as it is a function of the number of points on which the average is based.

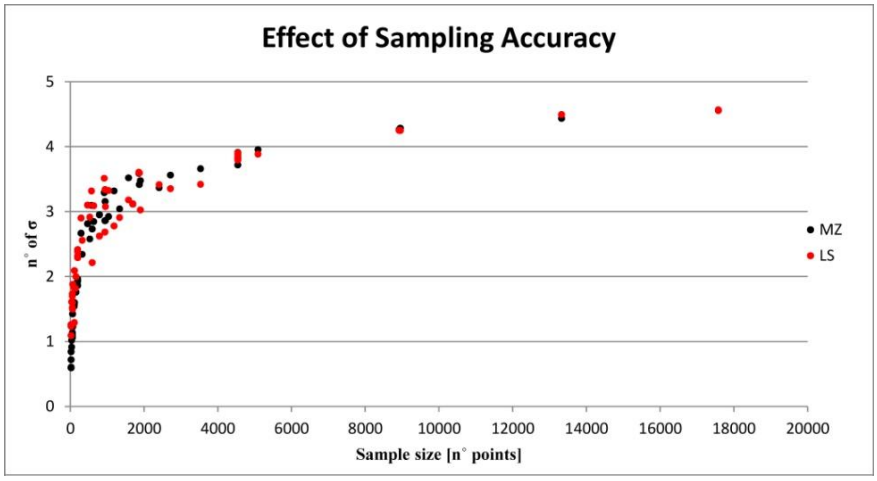

Figure 4.15 - Deviation of estimated flatness error from the true one. Values are normalized with respect to MPE/6, the standard deviation of sampling error.

Reasoning in terms of uncertainty of the whole flatness verification operator, Figure 4.16 shows that it steadily decreases when sample size increases, following an hyperbolical trend: the knowledge of the feature geometry and of sampling errors population both improve. In particular, LS uncertainty is always slightly larger than MZ one because of the form error overestimation introduced by the LS itself.

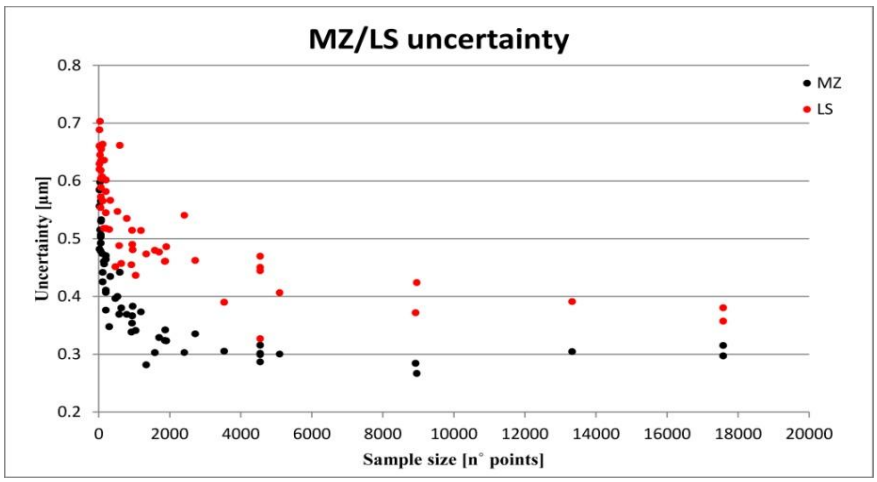

Figure 4.16 - Comparison of implementation uncertainty for MZ and LS based verification operators. MZ method systematically performs slightly better.

According to the results presented in this section, the only difference between MZ and LS association criteria is in the overestimation introduced by LS. This difference apart and not taking into account the computation time, there is no element to distinguish different behaviours with respect to the measurement uncertainty affecting the sampling points.

The possibility to replicate measurements gives the opportunity to point out the uncertainty introduced by the measuring instrument during sampling, disregarding the uncertainty associated with the actual knowledge of the measurand surface (see Figure 4.17). Therefore, the reduction of the uncertainty caused by replications has to be interpreted as a better understanding of the measurement uncertainty affecting the sampling of measurement points. This better understanding is then translated into a higher form error estimation (with a lower standard deviation), as the effect of measurement uncertainty cannot be separated from the actual form error. Replication allows the reduction of the implementation uncertainty of verification operators relying on small samples (see Figure 4.18) however, if these are not compliant with specifications, it does not allow any improvement in the accomplishment of the designer intent. This objective can be reached only reducing method uncertainty: the divergence between the used verification operator and that intended by the designer (the perfect verification operator).

4.8 Comparisons

The main results of the experiments presented in this chapter have been resumed in Table 4.4. Some comparisons have already been done during the analysis of each experiment, in order to fully understand the results, others will be presented in this section for the first time.

	Flatness error [µm]		**Implementation uncertainty [µm]**		
Simulation	**MZ**	**LS**	**MZ**	**LS**	**Method**
Ideal instrument	~11	~11.5	~0.001	~0.1	Bootstrap
			~0.001	~0.1	Analytic
Real instrument	~13.8	~14.2	~0.1	~0.2	Bootstrap
			~1	~1	Analytic
100 replications	~14	~14.5	~0.3	~0.4	σ_δ

Table 4.4 - Resume of the results from simulations of verification operators. The values shown in this table are the asymptotic trends of each experiment.

One of the first considerations that could be done looking at Table 4.4 is that MZ method always outperforms LS, from the point of view of the estimated form error but also from that of the estimation uncertainty (u_{Im}). However, the values reported in Table 4.4 are referred to the asymptotic behaviours of different methods, and considerations valid in the asymptote area do not necessary apply equally near the origin.

Simulations of verification operators based on the ideal instrument show that MZ and LS evaluations have different magnitudes of uncertainty. The effect, as explained in §4.3, is due to the different nature of the two methods. For extreme fit association criteria the uncertainty is associated only with the probability of getting extreme points corresponding, or very similar, to the actual extremes. Thus, if the surface is smooth, and the sampling uniform, uncertainty is very low. On the other hand, for statistical association criteria, the component

of uncertainty associated to the sampling of the actual extreme points, or to some more or less similar to them, is accompanied by a further uncertainty on the estimation of the method statistics (e.g. coefficients of the LS reference plane). The results obtained for the bootstrap estimation are confirmed also by the analytic estimation (see Table 4.4 and the detailed analysis in §4.3), suggesting that both methods deal in the same way with the uncertainty associated with the sampling density and the distribution of points over the measurand surface.

The congruence between analytic evaluation and bootstrap method, which is valid for the ideal instrument, is lost if we suppose the verification process to be affected by some measurement uncertainty. With reference to the bootstrap assessment of LS implementation uncertainty, for the particular surface taken into account, there is a difference of 0.1 μm between the two measurements. Comparing the results with those obtained for the ideal instrument, it is possible to notice that measurement uncertainty (intended as the standard deviation of the measurement error affecting each sampling point: σ = MPE/6) has been largely propagated into the uncertainty of the evaluation result (u_{Im}). Moreover, a form error much larger than the actual one has been measured. For very large samples, the effect of sampling errors results in an overestimation of the flatness error of 3 μm about. This is a consequence of the sample size only and of the phenomenon clearly explained in §4.6.2 and by Figure 4.15: an increase in sample size improves also the knowledge of the population of measurement errors. Therefore, increasing the number of points considered by the statistics, we expect to find out all the range of possible measurement errors: the instrument MPE. An asymptotic situation in this sense can be represented by the 100 replications of the verification operator. As a matter of fact, the central row of Table 4.4 (the results of the single simulation of verification operators based on a real instrument) is included between the two utopian verification processes: the one based on an ideal instrument and the other inexpensive that can be replicated a number of times large enough to allow a good statistical inference. In order to prove this last statement, the uncertainties of some more simulations of the verification operator have been plotted, for the LS method, together with the boundaries represented by the two utopian conditions (see Figure 4.17). The dispersion of results narrows with the increase of sample size, because the robustness of the estimation of standard deviation increases with sample size. On the other hand, a higher uncertainty can be observed for smaller samples (Figure 4.18) where the trend of uncertainty assessment on 100 replications becomes no longer representative of the implementation uncertainty associated with the single verification operator.

Replication can be a useful tool to reduce implementation uncertainty, but it does not allow the reduction of method uncertainty that takes into account the divergence of the actual verification operator from the perfect one. Method uncertainty accounts for the effects of simplified sampling strategies (fewer points) or the use of association criteria different from requirements.

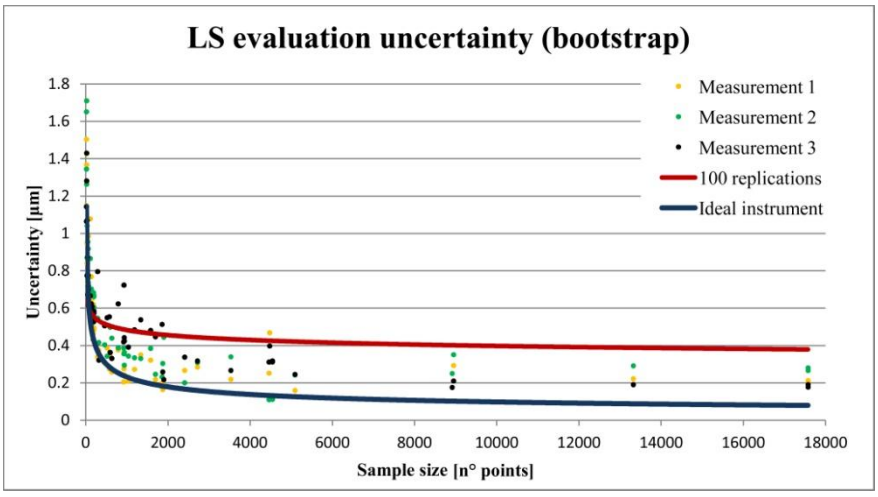

Figure 4.17 - The uncertainty of some verification operators based on a real instrument is compared against the two extreme conditions represented by an ideal instrument and the possibility to obtain 100 replications.

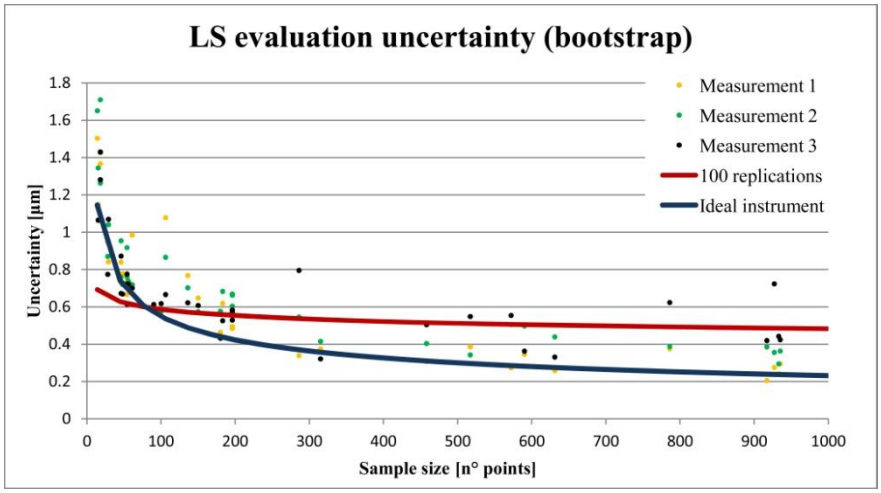

Figure 4.18 - Zoom on Figure 4.17 to highlight that the possibility to replicate verification operators allows the reduction of uncertainty when the sample size is small (minor than 100 points).

Things are a little different if the analytic approach is used in order to assess the uncertainty of statistical methods (LS in this case). The analytic assessment agrees with the bootstrap method only for verification processes based on the ideal instrument (§4.3). When some error (uncertainty) is supposed for the sampling of measurement points, the analytic approach rapidly overestimates the actual uncertainty of the LS method (that assessed through the 100 replications). According to this study, the value estimated with 100 replications of the verification operator can be considered as the best estimation of the actual uncertainty of the LS method. At the same time, mainly for large sample sizes, this value is quite lower than the one obtained through the analytic computation. It seems clear that the analytical assessment is introducing some overestimation of the effect of the measurement errors occurring during sampling, over the stability of the LS reference plane. However, this approach, staying on the side of safety, is really likely to be preferred by most of practitioners.

4.9 Conclusions

The set of experiments presented in this chapter allowed understanding the different results generated by the approaches available for the assessment of measurement uncertainty (analytical VS experimental) in cases where the measurement consists of a complex set of operations. One of the main results of this research regards the analytic assessment of the uncertainty of LS based verification operators; the most consolidated approach in literature and the only one to be justified by a theoretical formulation. This approach overestimates the propagation effect of the uncertainty affecting the sampling of measurement points. The terms of equation (4.1) dealing with the stability of the LS reference plane are proved to be effective by experimental analysis (§4.3) while the remaining terms, those entrusted to deal with the uncertainty associated with the selection of particular extreme points and with their measurement uncertainty, are proved to return a systematic overestimation (§4.6). The result is a function that usually reflects only the sample size and shows a lower sill determined by the uncertainty on measurement points only (a function of the instruments MPE); see Figure 3.11 or Figure 4.9 for a graphical evidence and Appendix B for a thorough examination.

On the other hand, experimental approaches are more representative of the whole measurement process but, mainly if based on bootstrap methodology and relying on a single measurement, are limited by the information collected with the verification operator at hand. If, as it happened for the case study (see Figure 3.21), the sampling strategy is not adequate to detect all the form error, the result can be an implementation uncertainty lower than expected and the illusion that the verification operator is very good. However, if this verification operator is different from the perfect verification operator, a very high method uncertainty will be associated. For this reason, if an analogous analytical method is available, it should be used in parallel to the experimental one and the results of the latter should be used only if more conservative. This could be a gold rule mainly for small samples: those with a size lower than the one corresponding to the knee in the trend of analytical estimation (few hundreds of points for the analyzed examples).

4.10 References

[1] ISO/IEC (2007) *International vocabulary of metrology - Basic and general concepts and associated terms (VIM)*.

[2] Hoppe H., DeRose T., Duchampy T., McDonaldz J. and Stuetzlez W. (1992) *Surface Reconstruction from Unorganized Points.* In Computer Graphics (SIGGRAPH '92 Proceedings), **26** 71-78.

[3] Vemuri B.C., Mitiche A. and Aggarwal J.K. (1986) *Curvature-based representation of objects from range data.* Image and Vision Computing, **4** (2) 107-114.

[4] Vemuri B. and Aggarwal J. (1987) *Representation and recognition of objects from dense range maps* Circuits and Systems, IEEE Transactions on, **34** (11) 1351-1363.

[5] Carr J.C., et al. (2001) *Reconstruction and representation of 3D objects with radial basis functions*. in proc. of ACM SIGGRAPF '01, New York, NY, USA.

[6] Bloomenthal J. (1997) *Introduction to implicit surfaces*, San Francisco, California.

[7] Turk G. and O'Brien J.F., *Variational implicit surfaces*, in *Technical Report GIT-GVU-99-15*1999, Georgia Institute of Technology.
[8] Turk G. and O'Brien J.F. (1999) *Shape transformation using variational implicit functions.* In proc. of ACM SIGGRAPH 2005 Courses, Los Angeles, California.
[9] Carr J.C., Fright W.R. and Beatson R.K. (1997) *Surface interpolation with radial basis functions for medical imaging.* IEEE Transactions on Medical Imaging, **16** (1) 96-107.
[10] Montgomery D.C. (2005) *Introduction to Statistical Quality Control,* 5th ed.
[11] ISO/TS 12781-2 (2011) *Geometrical product specifications (GPS) - Flatness - Part 2: Specification operators*. ISO, Geneve.

5 Encapsulating GPS for effective design and verification

5.1 Introduction

The aim of the GPS standards framework is to grant coherence to all the data generated in a product's lifecycle in order to enable the information age industry to be more cost effective [1]. This aim is pursued through the definition of a new rigorous language, based on mathematics, that, relying on the concepts of operations, operators and uncertainties [2], enables the harmonization of information throughout a global scale manufacturing industry [3]. Such a language, completely based on mathematics, enables the information consistency but still needs to be encapsulated into an integrated information system to spread into industrial practice, as it often turns out to be too complicated to be used directly [4].

Among the different modelling techniques available at the state of the art, category-based design (named also categorical design) has been identified as the most promising [5]. It relies on Category Theory (CT), a branch of pure mathematics, stemming from algebraic topology, which has strongly influenced computer science enabling the modelling and study of relationships of complex systems in a compact and effective manner [6]. Some categorical data models have been proposed to manage surface roughness [5] and cylindricity specifications [7] but, until now, there has been no research offering a model able to cope with uncertainty and cost evaluations.

This chapter presents a novel categorical model able to manage the processes of specification and verification of a flatness tolerance and able to evaluate the uncertainty and cost of the whole verification process. Two different scenarios have been identified for dealing with uncertainty estimation: one based on an experimental model, which can be built ad hoc or based on information available from the literature, and another based on the definition of a "verification master" to be used as benchmark for simplified verification operations. The details are discussed in §5.3.

A software demonstrator has then been developed (§5.6) translating the categorical data model for flatness verification into an object-oriented programming language [8]. This software is able to translate specification requirements into verification instructions, estimate the uncertainty introduced by simplified verification operations and evaluate costs and risks of verification operations. It provides an important tool for designers, as it allows a responsible definition of specifications (designer can simulate the interpretation of specifications and have an idea of the costs related with their verification), and for metrologists, as it can be a guide for designing GPS compliant verification missions or handling the usual verification procedures according to the GPS standards.

5.2 Category theory

CT is a basic conceptual and notational framework, as is set theory or graph theory, though it results in more abstract constructions. It is an abstract way to handle mathematical structures and the relationships between them, a high-level language focusing on how things behave rather than on their internal details [6], thus it is particularly suitable to model real-world objects and to grasp their internal links at any level of complexity. Since its first introduction in 1945 CT has been in continuous development and in the last decades, thanks to its sound mathematical bases, has provided important applications for algebra, computer sciences, and database design and management [9].

As a mathematical formalism, CT is essentially graphical in nature: its two fundamental concepts are arrows and internal objects. The classical example is that of Figure 5.1, where category P consists of three internal objects A, B and C together with arrows *f*, *g*, the associated arrow $h = g \circ f$ and the identity arrows I_A, I_B and I_C. Composition operator on arrows *f* and *g* satisfies *cod*(f) = *dom*(g) and so the associated arrow $h = g \circ f : dom(f) \rightarrow cod(g)$.

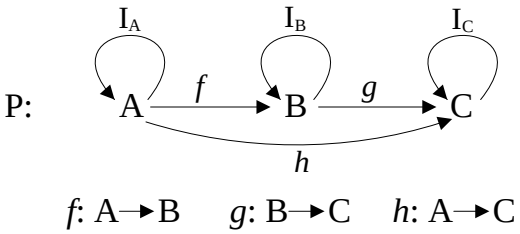

Figure 5.1 - Example of a category P.

Thanks to various constructs (functors, pullbacks, natural transforms etc.) CT can easily describe complex structures, including also modelling hierarchies of categories of categories. Among these constructs, pullbacks will be briefly introduced, which will be used in this work mainly to model relationships [5]. A pullback of the pair of arrows $f : A \rightarrow C$ and $g : B \rightarrow C$ is a triple P, g', f', where P is an object and $g' : P \rightarrow A$ and $f' : P \rightarrow B$ are two arrows such that $f \circ g' = g \circ f'$ (see Figure 5.2). If $i : X \rightarrow A$ and $j : X \rightarrow B$ are such that $f \circ i = g \circ j$ then there is a unique $k : X \rightarrow A$ such that $i = g' \circ k$ and $j = f' \circ k$. In this situation f' is said to be a pullback of *f* along *g* and that g' is a pullback of *g* along *f* [6].

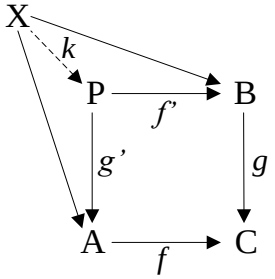

Figure 5.2 - Pullback scheme [6].

5.3 Scenarios of verification

One of the main aims of this work is to introduce an approach for estimating the uncertainty of the verification processes with respect to the design specification. The approach is presented and detailed for a flatness requirement; nevertheless it has general validity and can be applied to the assessment of any geometrical tolerance.

For several reasons, in practice, verification operations are often performed with important deviations from the perfect verification operator. The equipment available in metrology laboratories and the sampling strategies adopted are often the result of a compromise between the company needs for flexibility and the actual verification requirements. The instrument accuracy can be inadequate or the time required for a sampling compliant with the perfect verification operator can be too long if performed with the instruments available. Hence, simplified sampling strategies are adopted.

Anyway, despite the nature of the used verification operator, the acceptance rule introduced by ISO 14253-1 requires the estimation of the uncertainty related with the form error assessment, in order to compare the verification result with the specification limits. The uncertainty to be used when dealing with form error evaluations is the *compliance uncertainty*, which contains the effects of the actual verification operator, the measurement instrument accuracy, the deviations from the perfect specification operator and the eventual ambiguities caused by a non-clear specification. If the specification is fully adequate to guarantee the workpiece functional requirements, then the correlation uncertainty is null and the compliance uncertainty becomes synonymous with the total uncertainty.

Two different approaches have been formalized to estimate the uncertainty of form error evaluation in each of the two main scenarios occurring in metrology laboratories. The two scenarios correspond to the *serial inspection of mass productions* and the work of *small flexible metrology laboratories*. Both will be detailed in §5.3.1 and §5.3.2 respectively.

5.3.1 Scenario 1: *serial inspection of mass productions*

This scenario usually corresponds to the manufacturing of high precision components that, it is particularly common in the aerospace field, demand for the verification of every workpiece. This scenario can justify the use of the perfect verification operator on a few workpieces, to make sure that the manufacturing process (and obviously also the verification process used for checking the compliance with specifications) is under control, but not on all production workpieces.

If the perfect verification operators (over a set of workpieces randomly sampled from the whole of production) show a stable average value together with a contained variability and uncertainty, then verification processes with a higher degree of uncertainty can be used while being confident to be able to assess the correct workpiece compliance. The grey zone of the acceptance test can be enlarged [10] until there is still confidence that compliant workpieces are not discarded.

In this case, a reference error value $\tilde{\delta}$ can be defined as the average of all the estimations performed with the perfect operator and the stability of both the manufacturing and verification process is well represented by the standard deviation $\sigma_{\tilde{\delta}}$ of these estimations. The majority of production can then be inspected with a simplified verification operator (based on a small number of sampling points) and the method uncertainty 'u_{Mt}' can be defined, according to (5.1); where δ_j is the error estimated with the actual verification operator [11].

$$u_{Mt} = \tilde{\delta} - \delta_j \quad \textbf{(5.1)}$$

Compliance uncertainty (that in case of complete specifications is equal to the measurement uncertainty 'u_M') can then be estimated, adding (in the sense of the word according to GUM [12]) the implementation uncertainty for the verification operator at hand 'u_I' to the method uncertainty:

$$u_C = u_M = \sqrt{u_{Mt}^2 + u_I^2} \quad \textbf{(5.2)}$$

The different methods available for the evaluation of implementation uncertainty, according to the association criterion selected, are those presented and analysed in §3.5 and §3.6. Note that this kind of approach will never generate a rejection, according to ISO 14253-1, because, at the first instance, a deviation from the expected form error is attributed to the uncertainty of the verification process (it is accounted as method uncertainty) enlarging the grey zone of acceptance test (Figure 5.3). In the worst case, the error evaluation result will fall in the grey zone and it will not be possible to complete the acceptance test with the actual verification operator. Metrologists should improve the verification process until u_I is small enough or until, after the implementation of the perfect verification operator, the workpiece is proved to be not acceptable.

Particularly, Figure 5.3-b shows the case of a workpiece whose flatness deviation δ_j is within the specification limits but is far enough from the reference error to generate a grey zone that prevents a reliable decision (the grey zone includes the specification limit). In this case, the rejection is caused by method uncertainty mainly and the only way to decide if the workpiece is actually compliant is to use a perfect verification operator. By doing so, the method uncertainty is eliminated by definition, the workpiece can be considered regardless the verification master, and any difference between δ_j and $\tilde{\delta}$ is interpreted as an actual difference of the feature shape. A similar circumstance occurs in Figure 5.3-c where the measurement result δ_j is outside the specification limits. However at a first instance the responsibility of this result is attributed to the actual verification operator (therefore accounted as method uncertainty) because, by hypothesis, the manufacturing process is under control.

This kind of situation is an alarm signal about the stability of the verification or manufacturing process. However, neither the former nor the latter can be blamed without a

wise investigation. The responsible for quality insurance shall consider the actual manufacturing and verification process and address investigation towards a perfect verification operator (combined with a recalibration of the instrument) or towards a control of the process parameters. The former avoids any doubt that the problem may be related with the verification phase while the latter verifies if the manufacturing process is actually under control.

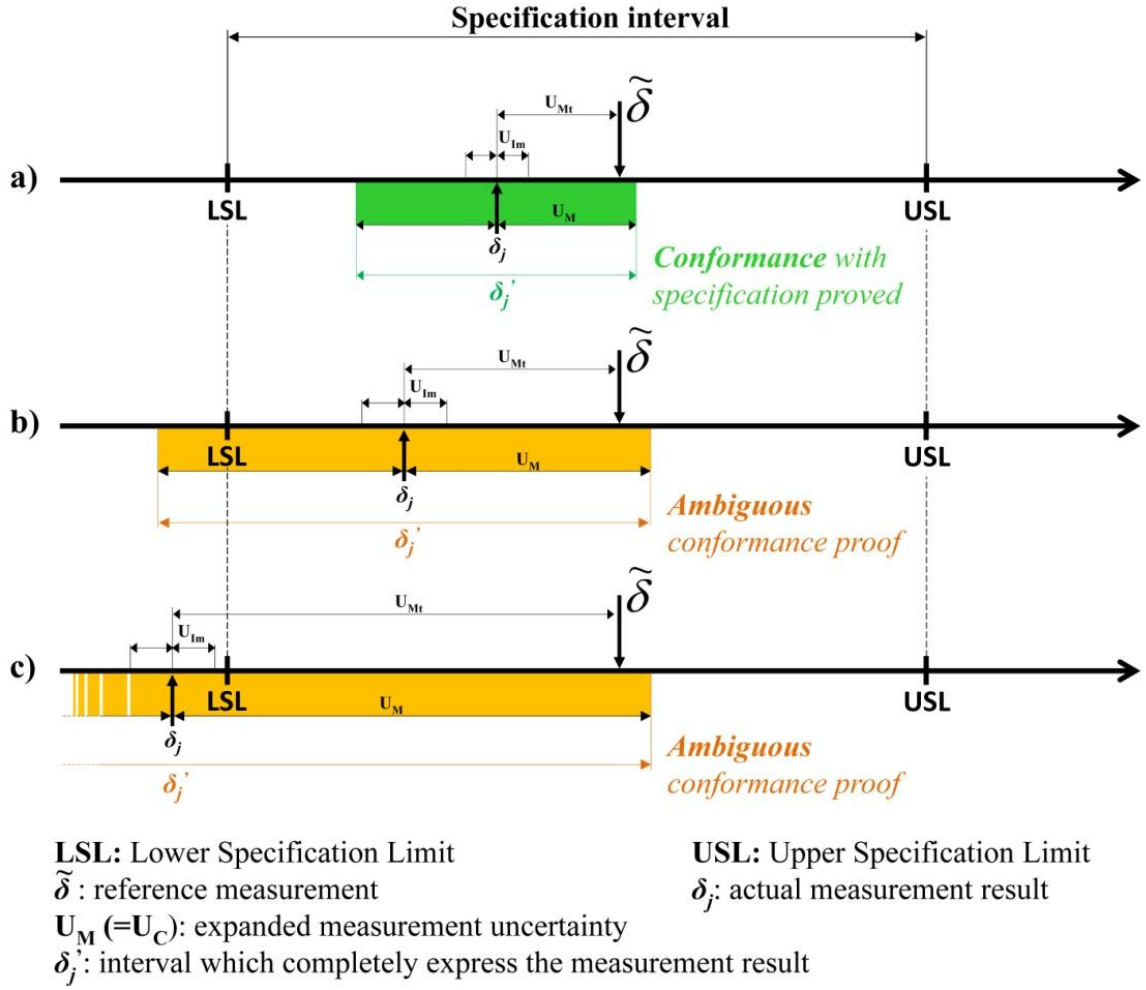

Figure 5.3 – In the "serial inspection of mass productions" scenario, non-compliance cannot be assessed unless a perfect verification operator is used (u_{Mt} = 0). Otherwise, any deviation from the reference value is interpreted, at a first instance, as a bias of the simplified verification operator (as method uncertainty).

5.3.2 Scenario 2: *small flexible verification laboratories*

The second scenario occurs frequently in metrology laboratories where CMMs are usually deployed in order to guarantee the necessary level of flexibility and accuracy. In these circumstances, the GPS perfect verification would result in a sampling strategy that is too expensive and there is no way to estimate the uncertainty introduced by the eventual simplification in a direct way.

In this case, the idea is to use a Design of Experiment (DoE) based approach to extrapolate the mathematical model behind the uncertainties associated with a certain

verification operator (sampling grid, sampling distance, profiles spacing, association criterion) applied to a certain type of feature (e.g. flatness feature of a workpiece of a given material obtained with a given manufacturing process). Namely the Surface Response Regressions obtained in §3.10, if we want to contextualize to this thesis.

The validity of this model is limited to the range of verification variables actually explored by the experiments but extends to any feature belonging to the same class in terms of material, size and manufacturing process [13]. For each class the inspection of several workpieces is required, in order to calibrate the model. These inspections should be performed with a perfect verification operator and possibly with an instrument whose maximum permissible error (MPE) is negligible with respect to the error to be detected. In this way all the simplified verification operators can be simulated from the complete measurement dataset decimating measurement points as would happen with simplified verifications (the same approach used in §3.4). The final aim is to allow a reasonable estimation of measurement uncertainty (therefore of compliance uncertainty if the specification is complete) even in the preliminary phases of the verification design.

The uncertainty introduced by the extraction operation and association criterion, regardless of the accuracy of the instrument actually used, is the combination of method uncertainty (the effect of the extraction grid) together with the component of implementation uncertainty due to the association criterion. Therefore, this term of uncertainty is named method and implementation uncertainty '$u_{Mt\&I}$' and is defined according to (5.3), where f represents the regression function of the experimental model.

$$u_{Mt\&I} = f\left(Spec_{para}, Verif_{para}\right) \tag{5.3}$$

To obtain the compliance uncertainty (in case of complete specification it is equal to the measurement uncertainty) the accuracy of the measuring equipment has still to be taken into account. Under the hypothesis of Gaussian distribution of errors, it can be roughly considered as the sixth part of the instrument MPE; see (5.4).

$$u_C = u_M = \sqrt{u_{Mt\&I}^2 + \left(MPE/6\right)^2} \tag{5.4}$$

5.4 Model for cost management

A cost model is built to assess the effect of verification parameters on budgeting. Verification cost 'C_V' obviously depends on the time taken by probing or scanning a surface '$g_1(Pt_{Nr})$' (thus on the inspection instrument in use and on its depreciation) and on time required for data elaboration '$g_2(Elab_{Time})$'. The latter is often directly related to the amount of measurement data to be treated, thus to the number of points.

$$C_V = g_1\left(Pt_{Nr}\right) + g_2\left(Elab_{Time}\right) \tag{5.5}$$

Further, the total cost related to the complete inspection plan of a workpiece 'C_{TOT}' should take into account also the cost related to the possibility of accepting a non-compliant workpiece (and vice versa):

$$C_{TOT} = C_V + \mathrm{h}\ u \tag{5.6}$$

The cost function 'h(u)' calculates the Expected Cost of an Error (ECE) [14] simply relating the uncertainty of the verification process to the cost, to the company, of having workpieces discarded or undergoing disputes if they deliver a non compliant one. The coefficients of functions g_1, g_2 and h, in equations (5.5) and (5.6), have to be properly defined by each company according to the instruments available, the value added on the workpiece through manufacturing operations and the general internal economic policies.

5.5 The categorical data model to manage flatness verification

Traditionally specification and verification environments communicate by means of official technical documents (drawings) in which the information necessary for the correct manufacture and verification of every feature are reported in a standard language. The drawing callout is entrusted to carry this information through manufacturing facilities operating on a global scale, thus it will be the bridge between specification and verification environments also in the categorical data model proposed in this work (Figure 5.4). In particular, the specification category model produces a flatness callout that becomes the input for the verification category model. Without taking into account the interfaces for specification or verification design, according to the duality principle [15, 16], the data model defining both flatness operators is the same.

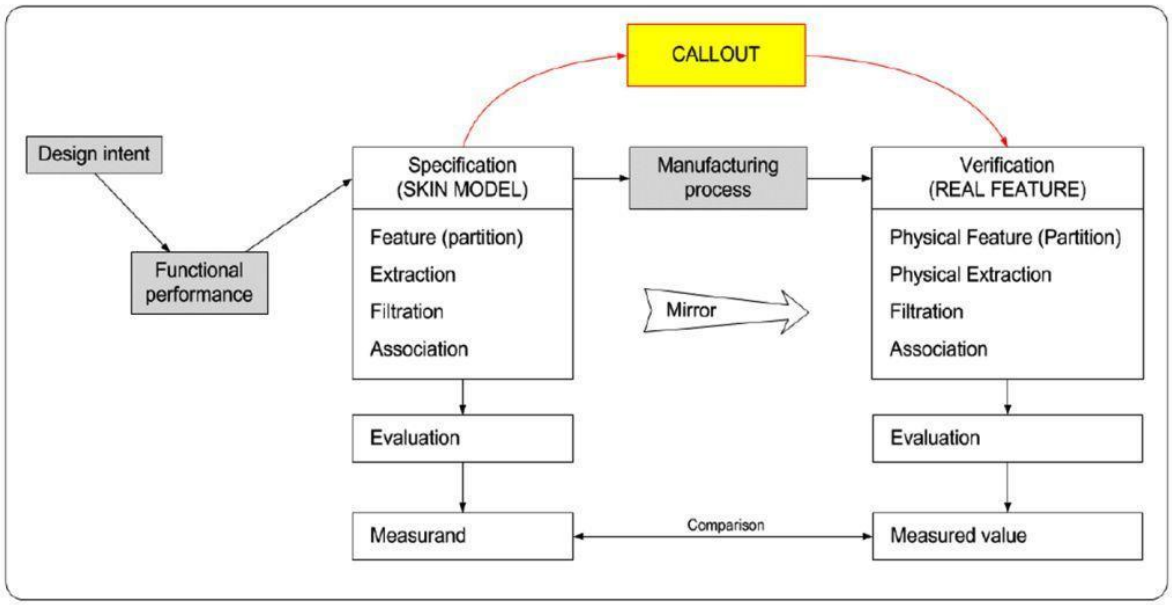

Figure 5.4 - High level scheme of the categorical data model: specification and verification operators share the same data structure but communicate only by means of the drawing callout.

Only the data model for the verification operator is presented in this work, as it carries the novelty of an engine enabling the management of uncertainty and verification costs. Every operation in the verification operator (partition, extraction, filtration, association and evaluation) corresponds to a class in the categorical model. Further classes are added to deal with the operations of uncertainty estimation and cost evaluation, in order to manage the input/output interfaces, define databases and characterize particular pieces of information (e.g. set of measurement points, filtered points, verification master, etc.). Each class is represented by a rectangular box and is named after the operation it represents.

5.5.1 Classification of flatness features

For the purpose of this work flatness characteristics have been classified in two different families according to the presence or absence of revolute symmetry. As a matter of fact, in many cases the presence of revolute symmetry endorses manufacturing processes with circular tool paths. On the other hand, the flatness feature should be measured with a sampling grid suitable to detect the signature eventually left by the manufacturing process. Therefore, it is clear that polar grids is more likely to be suitable for inspecting flatness features with revolute symmetry rather than features that do not present this symmetry. However, if the metrologist is aware of the manufacturing process undergone by the workpiece, the choice of the sampling grid should be tailored on that, rather than on a mere consideration of symmetry [17].

In this work, in order to deal with flatness features that do not have any particular symmetry, the smallest circumscribed rectangle is taken into account (Figure 5.5). In this way we are able to identify two characteristic dimensions: a **Long** and a **Short** one.

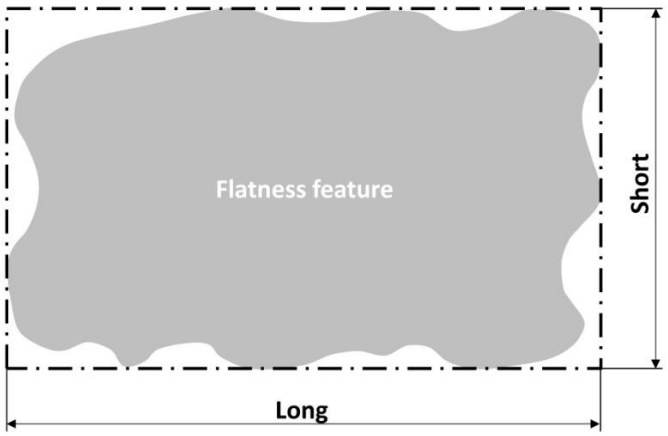

Figure 5.5 - Approximation and characteristic dimensions of a flatness surface that does not present rotational symmetry.

On the other hand, if the flatness feature presents revolute symmetry, it can be easily approximated by means of inscribed and circumscribed circles (Figure 5.6). In this way the characteristic dimensions are the radii "**r**" and "**R**" of the inscribed and circumscribed circle respectively.

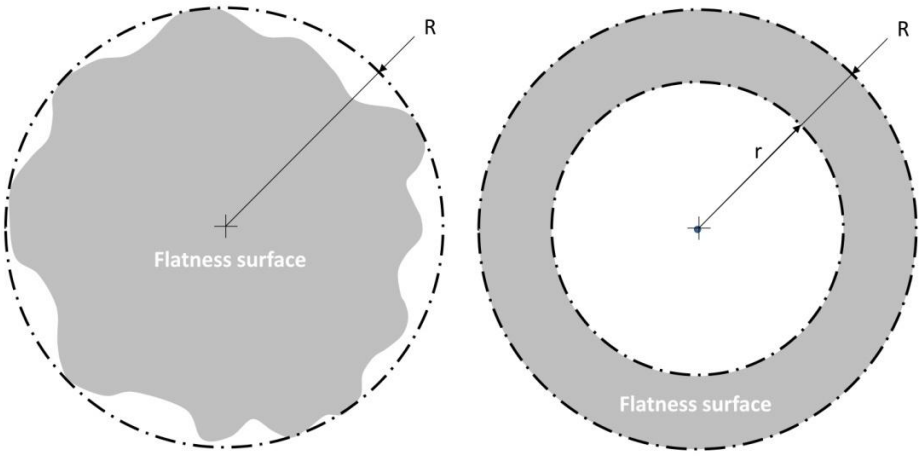

Figure 5.6 - Approximation and characteristic dimensions of flatness features presenting revolute symmetry.

5.5.2 Input collection and partition operation

With reference to Figure 5.7, an input class (VI) whose elements represent the main interfaces of the developed software activates the categorical model. In particular the element '*Tolerance_callout*' is defined as a category itself, to keep the consistency of the information it carries, and its element '*Feature*' is defined as a further category which substitutes the partition operator, that has not been completely defined by GPS standards yet. All the elements in categories VI, TC and Fe correspond to data to be provided by the software user through an interface (§5.6). However, with a further integration into PLM packages, user's inputs could be easily substituted by internal interfaces among CAD and metrology software.

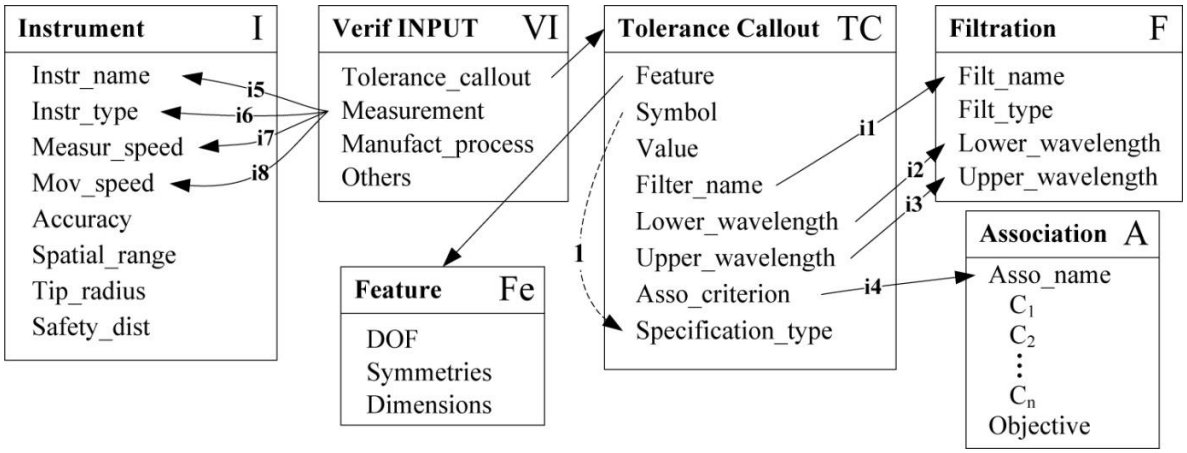

Figure 5.7 - The categorical data model for flatness verification: input collection and partition operation.

The information collected by the input categories is reallocated through inheritance relationships, when possible (see arrows named **i1** to **i8**), or directly used in pullbacks. Such a structure of input categories is suitable for any type of geometrical feature, not only flatness, therefore **pullback 1** (the dashed arrow in Figure 5.7) has the function to start the right verification management model according to the tolerance symbol reported in the drawing callout. The system associates to each symbol the right specification type, according to the

main international standards [14, 18, 19]; the corresponding categorical model (in our case the flatness data model) is then activated.

5.5.3 Extraction

Extraction is the operation used to identify the coordinates of a finite number of points of the real workpiece surface in order to evaluate its compliance with specifications [15]. This operation is characterized both by the instrument and by the sampling strategy adopted, thus two different categories are identified to represent it (see Figure 5.8): category '*Instrument*' contains all the information regarding the instrument at hand, while category '*Sampling*' manages all the details about the implemented sampling strategy.

In particular category '*Instrument*' is strongly characterized by its element '*Instr_type*', which classifies measuring instruments in 5 different families and conditions the choices of sampling strategies; see Table 5.1 for a schematic representation of the sampling parameters required by each instrument type ('*Instr_type*'). With respect to category '*Sampling*' the key parameters used to define the sampling strategy are the same used to define the Design of Experiment in §3.4 (see Table 3.2). Particularly parameter ***D*** is represented by the element '*D_profiles_spacing*', ***d*** by '*d_profile_spacing*' and ***Grid*** by '*Sampling_strategy*'.

The different pullbacks of the extraction operator (Figure 5.8 and Figure 5.9) are briefly explained in cases where the flatness feature does not show rotational symmetry. The actual feature is approximated with the smallest circumscribed rectangle in order to simplify the calculations and to define a simple reference system consisting of the directions of two adjacent edges named, after their length, as *long edge* and *short edge* (see Figure 3.5).

- **Pullback 2 -** A first selection among the sampling grids offered by standards [17] can be performed according to the feature invariance class 'DOF' and to the presence of particular 'Symmetries'; e.g. a flatness feature with rotational symmetry endorses the use of a polar grid.
- **Pullback 3 -** In case where there is no rotational symmetry, several grids are available (rectangular, parallel profiles, Union Jack) and if some particular form deviation is expected, due to manufacturing processes or other information, the most adequate grid to detect this form deviation has to be selected [17].
- **Pullback 4 -** According to ISO/TS 12780-2 [20] the maximum sampling space '*Samp_space*' can be calculated by dividing the lower cut-off wavelength '*Lower_wavelength*' (λ_c) by the number of cut-offs '*Num_cutoff*'. In particular $Num\_cutoff \geq 7$ to avoid aliasing [20].
- **Pullback 5 -** If the type of instrument chosen for measurement requires a stylus to probe the surface, the stylus tip radius has to be selected according to λ_c. Table 1 in [20] provides the maximum values of stylus tip radii with respect to the λ_c of specification. If radii larger than recommended are used, the measurement is biased by an undesired morphological filtration.

Instrument type	***D***	***d***	***Grid***
Optical surface acquisition	✗	✗	✗
Continuous contact profile scanning	✓	✗	✓
Contact trigger inspection	✓	✓	✓
Continuous non-contact profile scanning	✓	✗	✓
Non-contact trigger inspection	✓	✓	✓

Table 5.1 - Sampling parameters required by each instrument type. Required parameters are checked with a ✓, non required ones with a ✗.

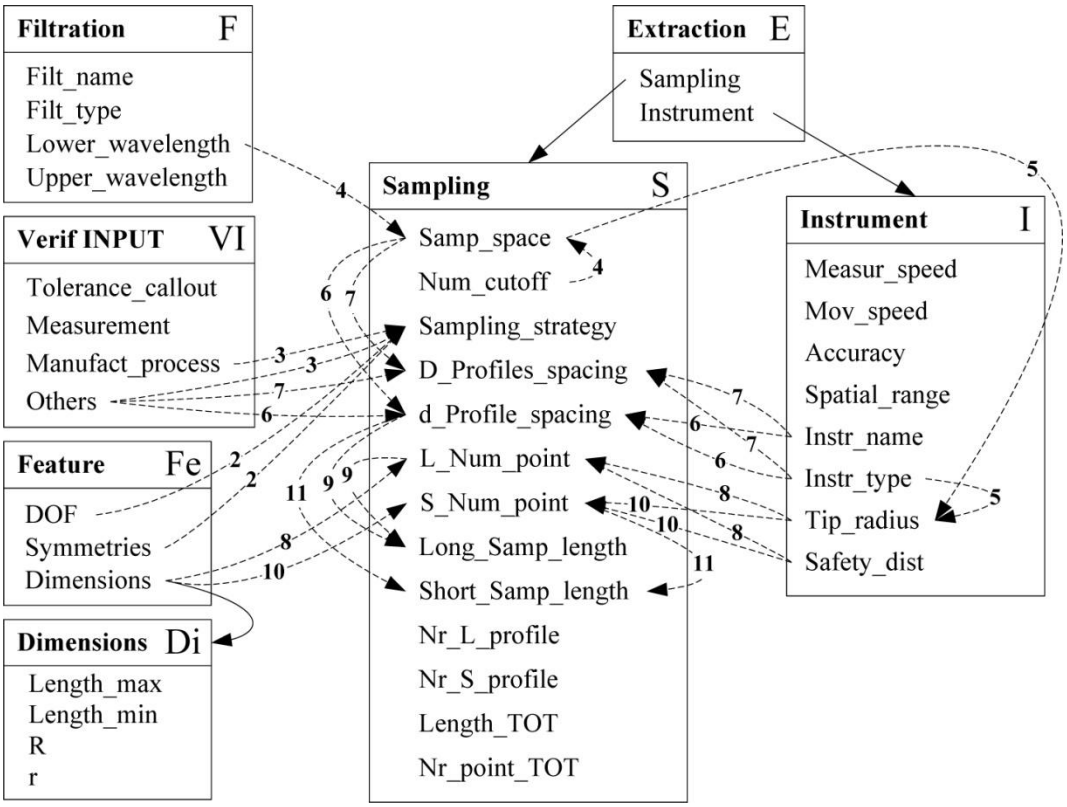

Figure 5.8 - The categorical data model for extraction operations.

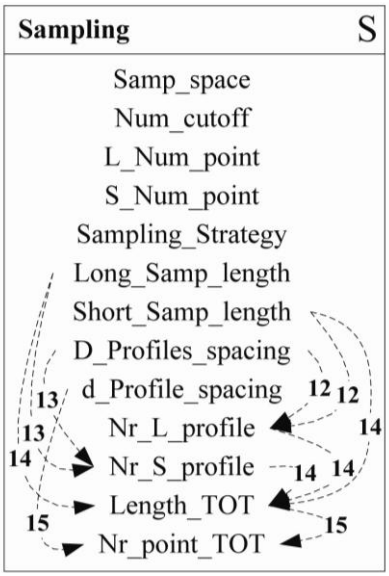

Figure 5.9 - The categorical data model for characterizing the sampling effort.

- **Pullback 6 -** According to the inspection instrument at hand ('*Instr_name*' and '*Instr_type*') and to cost considerations (*'Others'* in category *'Verif INPUT'*) it is possible to define a sampling distance along the straightness profiles '*d_Profiles_spacing*' different from that required by the cut-off wavelength. Sampling can be denser, in order to have the oversampling required to perform a good filtration, or coarser if cost is too sensitive to the sampling operations.
- **Pullback 7 -** User can set a distance between straightness profiles '*D_Profiles_spacing*' larger than the one compliant with standards, according to the same cost considerations driving pullback 6.
- **Pullback 8 -** The number of points '*L_Num_point*' used to sample straightness profiles parallel to the long edge must be an integer value. It can be calculated taking into account the length of the long edge '*Length_max*', the probe tip radius '*Tip_radius*', a safety distance from feature edges '*Safety_dist*' (where the stylus could collide with other adjacent surfaces), and the sampling space '*Samp_space*' according to the following equation:

$$L\_Num\_point = \text{floor}\left(\frac{Length\_max - 2\ Tip\_radius + Safety\_dist}{d\_Profile\_spacing} \right) \quad \textbf{(5.7)}$$

- **Pullback 9 -** The length of the straightness profile sampled along the long edge direction is slightly shorter than the feature actual length ('*Length_max*') due to pullbacks 6 and 8. Thus the actually sampled length '*Long_Samp_length*' is:

$$Long\_Samp\_length = L\_num\_point * d\_Profile\_Spacing \quad \textbf{(5.8)}$$

- **Pullback 10 -** The same considerations of pullback 8 apply also along the short edge direction and a similar equation can be used to calculate the number of points '*S_Num_point*' used to sample these straightness profiles:

$$S\_Num\_point = \text{floor}\left(\frac{Length\_min - 2\ Tip\_radius + Safety\_dist}{d\_Profile\_spacing} \right) \quad \textbf{(5.9)}$$

- **Pullback 11 -** Similarly to pullback 9, the length actually sampled along the short edge direction '*Short_Samp_length*' can be calculated as:

$$Short\_Samp\_length = S\_num\_point * d\_Profile\_Spacing \quad \textbf{(5.10)}$$

- **Pullback 12 -** The number of profiles parallel to the long edge '*Nr_L_profile*' is calculated, starting from the profile spacing '*D_Profiles_spacing*' and the length of the orthogonal profile '*Short_Samp_Length*', according to the following equation:

$$Nr\_L\_profile = \frac{Short\_Samp\_length}{D\_Profiles\_spacing} \quad \textbf{(5.11)}$$

- **Pullback 13 -** The number of profiles parallel to the short edge '*Nr_S_profile*' can be calculated with an equation similar to (5.11), namely:

$$Nr\_S\_profile = \frac{Long\_Samp\_length}{D\_Profiles\_spacing} \quad \textbf{(5.12)}$$

- **Pullback 14 -** The total length of straightness profiles extracted from the flatness surface '*Length_TOT*' can be calculated according to the following equation:

$$Lenght\_ToT = Nr\_L\_profile * Long\_Samp\_length + Nr\_S\_profile * Short\_Samp\_length \quad \textbf{(5.13)}$$

- **Pullback 15 -** The total number of points to be inspected by instruments in trigger inspection mode '*Nr_point_TOT*' can be determined, considering the total length of inspected profiles '*Length_TOT*' and the sampling distance along profiles '*d_Profile_spacing*', as:

$$Nr\_point\_TOT = \frac{Length\_TOT}{d\_Profile\_spacing} \quad \textbf{(5.14)}$$

5.5.4 Filtration, association and evaluation

Association is the operation used to fit ideal features to real measurement data by means of different criteria [15]. The ideal feature obtained is then used as a reference for the evaluation of the real feature deviations. Different association criteria are available for each type of geometrical feature, allowing the definition of different reference planes and the estimation of slightly different geometrical errors. The categorical data model to manage these operations is presented in Figure 5.10 and its pullbacks are briefly explained below.

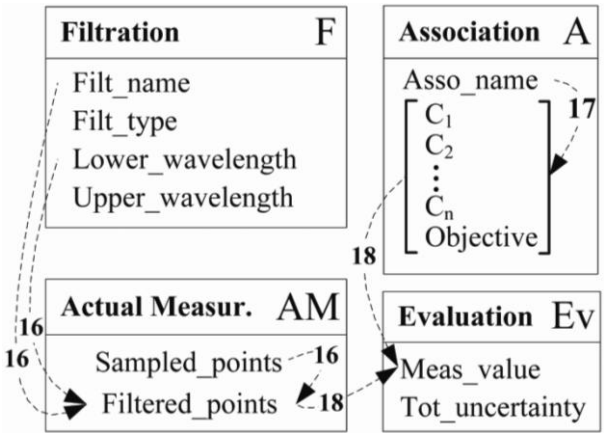

Figure 5.10 - The categorical data model for filtration, association and evaluation operations.

- **Pullback 16 -** According to the selected filter '*Filt_name*' and lower cut-off wavelength '*Lower_wavelength*' the set of measurement points '*Sampled_points*' is filtered and the resulting dataset stored in the variable '*Filtered_points*'.
- **Pullback 17 -** The association criterion equation (represented by a set of parameters and an objective function) is selected from a database according to the association criterion specified in the flatness callout or alternatively as required by the user. According to ISO/TS 12781-1, different flatness parameters can be calculated if LS association criterion is selected. Therefore, according to the scheme of Table 5.2, a total of 5 different form error estimations could be performed.

ASSOCIATION	PARAMETERS			
	FLTt Peak to valley	**FLTp** Peak to reference	**FLTv** Valley to reference	**FLTq** Root mean square
MZPL (Minimum Zone reference planes)	✓			
LSPL (Least Square reference plane)	✓	✓	✓	✓

Table 5.2 - Parameters for flatness assessment according to different association criteria.

- **Pullback 18 -** The equation implementing the selected association criterion is then applied to the set of filtered measurement points returning the form error estimation.

5.5.5 Uncertainty management

The categorical data model implementing the two approaches for uncertainty management, presented in §5.3, is shown in Figure 5.11. Pullbacks 19, 20 and 21 deal with the scenario of serial verification of mass productions by implementing the uncertainty estimation approach based on the availability of a verification master (§5.3.1). On the other hand, pullbacks 22, 23 and 24 handle the scenario of small flexible metrology laboratories by estimating the uncertainty with a DoE based approach (§5.3.2).

- **Pullback 19 -** Implementation uncertainty '*u_I*' is estimated for the verification operator at hand, using the dataset of filtered points or the parameters of error evaluation. It depends on whether an analytic or experimental method is chosen for the estimation of uncertainty.
- **Pullback 20 -** Method uncertainty is determined, according to (5.1), as the difference between the flatness error estimated with the simplified verification operator '*Meas_value*' and the reference value '*Average_ref_error*'.
- **Pullback 21 -** In case of complete specification there is no specification uncertainty and compliance uncertainty is equal to measurement uncertainty. Compliance uncertainty can then be estimated as the sum, according to equation (5.2), of method and implementation uncertainties.
- **Pullback 22 -** A regression model is searched into the database ('*Flatness DB*') according to the geometrical characteristics of the flatness feature (data from category Fe) and to other information used to classify regression models and establish their validity domain (manufacturing process, workpiece material and others from category VI).
- **Pullback 23 -** If a suitable regression model is found, the uncertainty of the verification operator at hand '*u_Mt&I*' can be estimated starting from the parameters which describe the verification operator. Obviously, all the regression models stored in the database have to be defined according to a common and consistent representation of the verification parameters. This is particularly important for qualitative parameters, such as association

criteria and sampling grids, which are represented in the regression model by integer numbers: e.g. LS method shall be always identified by 1, MZ by 2, etc..

- **Pullback 24 -** This pullback finally estimates the compliance uncertainty (synonymous of measurement uncertainty when specification is complete) by adding the instrument accuracy '*Accuracy*' (that is the measurement uncertainty introduced for the sampling of each measurement point) to the uncertainty embedded in the sampling strategy and association criterion: '*u_Mt&I*'. The two uncertainty terms are composed according to (5.4).

Given that compliance uncertainty is able to represent all the deviations (intentional and non) of the actual verification operator from the perfect one compliant with specification, it can be used to accompany the estimated form error and to enable the acceptance decision rule: inheritance relationship **i9** in Figure 5.11.

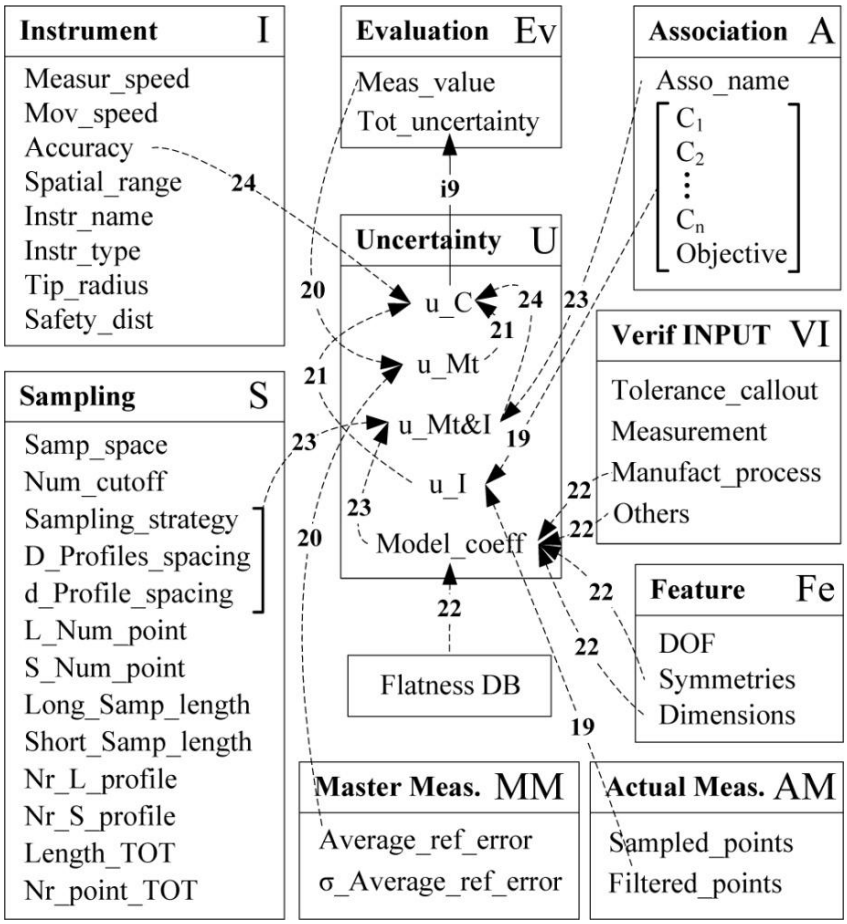

Figure 5.11 - The categorical data model for uncertainty management.

5.5.6 Cost management

The model for cost management presented in §5.4 is now implemented in the categorical data model shown in Figure 5.12 and Figure 5.13. Pullback 25 selects the model for the evaluation of sampling cost corresponding to the instrument in use while pullbacks 26, 27 and 28 prepare the model variables '*SC_f_var*', consisting of times, according to the typology of instrument. The pullbacks modelling the cost management are briefly explained below:

- **Pullback 25 -** An adequate cost function is loaded according to the instrument in use '*Instr_name*' and to the typology of measurement it performs '*Instr_type*'. For each instrument, the cost function is defined as a set of coefficients '*SC_f_coeff*' to be combined with measurement variables to be expressed in the form of times.
- **Pullback 26 -** In cases of optical instruments, the sampling time depends on the number of shots (measurements) required to cover the entire flatness surface, thus it is directly related to the flatness feature extension, as shown in the following equation:

$$SC\_var = \frac{Long\_Samp\_length * Short\_Samp\_length}{Spatial\_range\ [\mathrm{mm}^2]} \quad \textbf{(5.15)}$$

- **Pullback 27 -** In cases of instruments capable of continuous profiles scanning the sampling time is given by the total length to be inspected '*Length_TOT*' divided by the measurement speed '*Measur_speed*':

$$SC\_var = \frac{Length\_TOT}{Measur\_speed\ [\mathrm{mm/s}]} \quad \textbf{(5.16)}$$

- **Pullback 28 -** In cases of instruments performing profiles extractions with a trigger measurement, in a first approximation, the sampling time is given by the time necessary to extract the points plus the time for positioning the probe along the measurement path:

$$SC\_var = \frac{Nr\_point\_TOT}{Measr\_speed\ [\mathrm{points/s}]} + \frac{Length\_TOT}{Mov\_speed\ [\mathrm{mm/s}]} \quad \textbf{(5.17)}$$

- **Pullback 29 -** Once the cost function has been selected and the cost variable has been conveniently prepared it is possible to calculate the cost related to sampling '*Samp_cost*' according to function g_1.
- **Pullback 30 -** Elaboration cost depends on the time spent for data analysis, mainly on computation time for filtration operations and on that required by the algorithm implementing the association criterion ('Other' in category VI); thus it is roughly proportional to the total number of points '*Nr_point_TOT*'.
- **Pullback 31 -** The ECE is calculated according to the probability that an evaluation error occurs ('*Tot_uncertainty*' of verification operator) and function h(*u*). This function has to be tailored on the economic policy of each company and on the actual value of each manufactured workpiece ('*Other*' in category VI).
- **Pullback 32 -** Finally, the overall cost of verification operator is calculated by adding up all cost contributions.

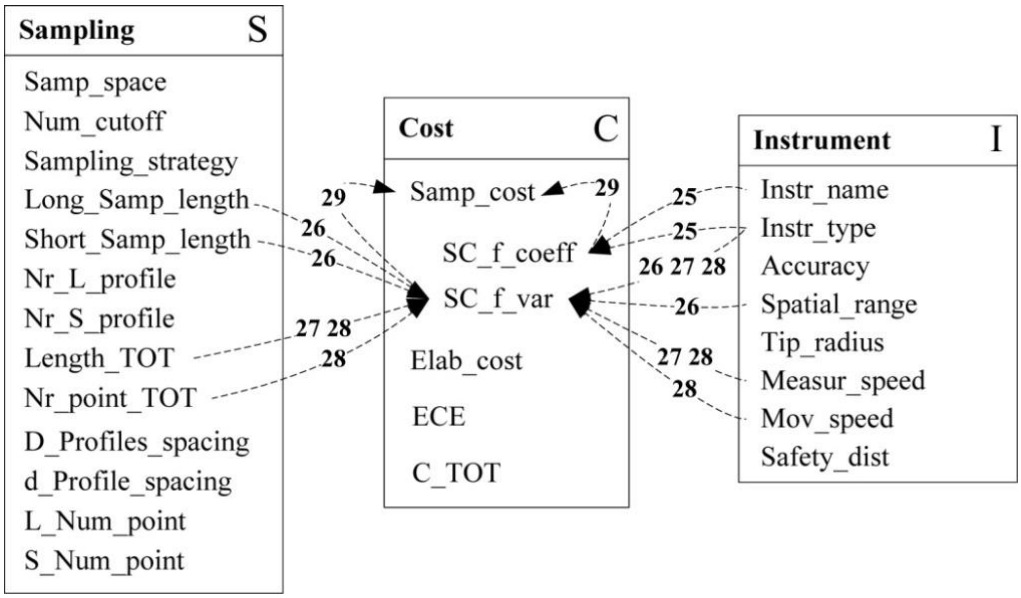

Figure 5.12 - The categorical data model for cost evaluation and comparison, part I.

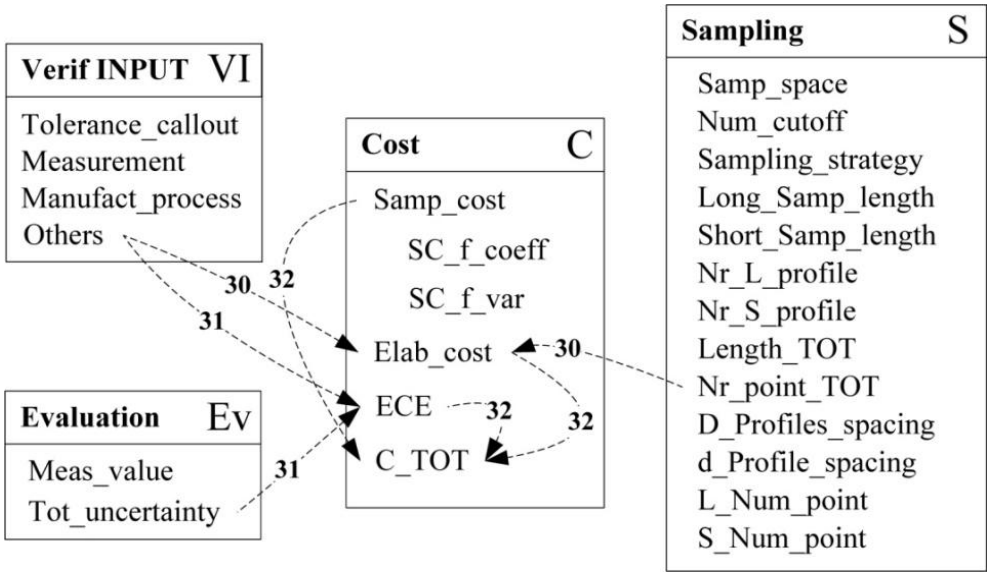

Figure 5.13 - The categorical data model for cost evaluation and comparison, part II.

5.5.7 Comparison

The operation of comparison implements the acceptance rule, provided by GPS standards [10], consisting of a comparison of the geometrical deviation assessed on the workpiece (in terms of estimated form error and related uncertainty) against drawing specifications. The categorical data model for this operation is represented by pullback 33 in Figure 5.14. This is the last operation for the verification operator and the categorical model too; then all the results are stored in the verification output class (VO) through inheritance relationships **i10**, **i11**, **i12** and **i13**. Outputs collected in VO class are then graphically displayed to the user (through the interface shown in Figure 5.18).

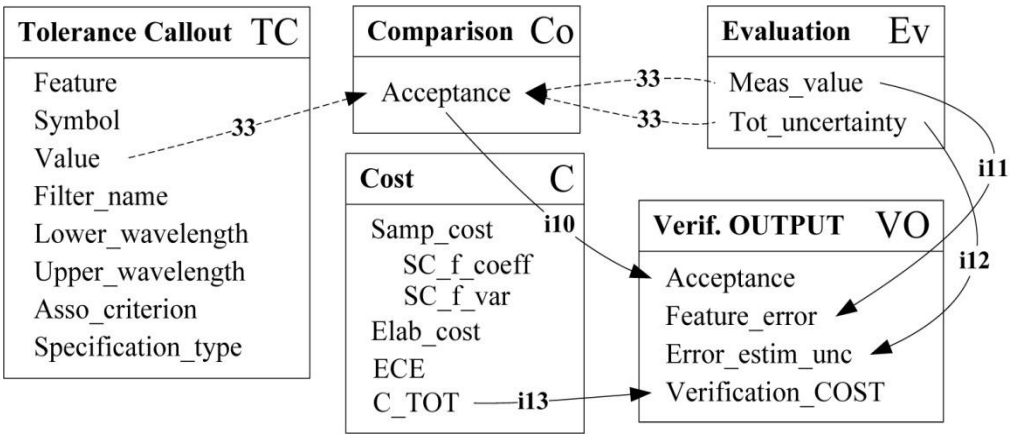

Figure 5.14 - Acceptance test according to ISO/TS 14253-1 and storage of results in output category.

5.6 The categorical software for flatness management

The novel categorical data model presented in §5.5 has its most innovative points in the capability to deal with verification operators providing an estimation of uncertainties and costs at stake. This capability has been used to design a software that enables also the less experienced metrologists to perform the verification of flatness tolerances exploiting, in the most effective way, the new concepts offered by GPS standards. Up to now, the software has been developed for flatness tolerance only because this was the categorical data model available (§5.5). However, both the approach used to define the data model of flatness verification, and that used to derive a software from it, have a general validity and can be developed, similarly, for any geometrical tolerance.

Furthermore, implementing the flatness data model into a software enables a responsible definition of geometrical specifications. Designers could (and should) use the software to simulate the perfect verification operator associated with the specifications they are going to set. They would get a valuable perspective about the uncertainties and costs associated with each specification, being therefore able to combine functional and cost considerations for the choice of the optimal specification.

Categorical data models find a natural software implementation in objected oriented programming languages [8]. As a matter of fact, the concepts of category and arrow, easily match with those of class and method, on which objected oriented languages are founded [8]. The categorical data model has been developed between an input and an output category, in which are concentrated the interactions with metrologists. The former, in particular, has been divided in 3 sequential interfaces that conceptually reproduce the development of a verification process and correspond to: specification operator (Figure 5.15), definition of the actual verification operator (Figure 5.16) and selection of the scenario in which the verification is performed (Figure 5.17) respectively.

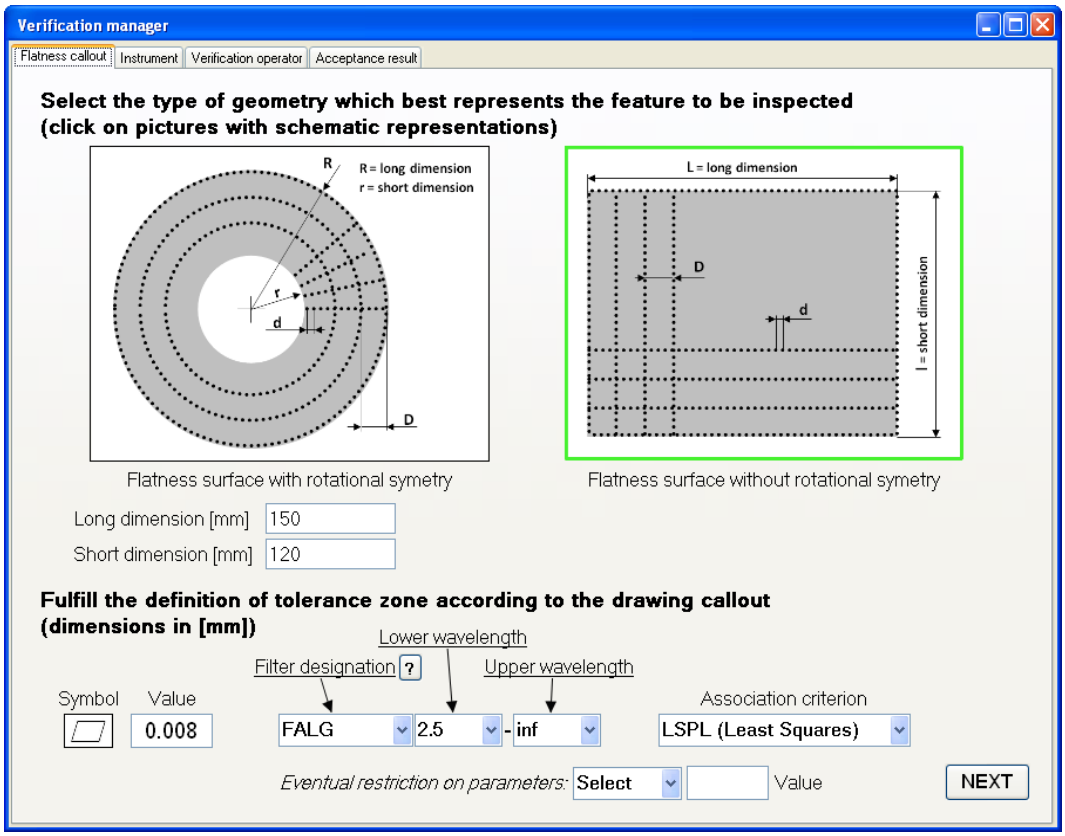

Figure 5.15 - Interface for defining the specification operator. The information required is contained in the part drawing: dimensions and geometrical tolerance callout that define the feature to be measured.

The interface for defining the complete specification operator (Figure 5.15) could be easily eliminated by integrating this software into a broader PLM package. As a matter of fact, the only purpose of this interface is to inform the system about the specification that is under verification. According to GPS standards, all the information necessary to completely define the specification operator must be reported in the drawing callout: thus, it shall be contained into the product CAD model also. Therefore, if this software is integrated aside a CAD system, all the information collected with this interface could be acquired automatically from the feature definition inside the CAD model. For example, a click on the feature to be verified could be enough in order to inform the software about the feature specifications.

The second input interface, Figure 5.16, is devoted to the definition of the actual verification operator. Two different parts can be identified: the first one collects the information about the measuring instrument (type of instrument and its name, probe characteristics) and the operational parameters we are going to set for the measurement (speed during positioning movements and measurement speed); the second one specifies the sampling strategy to be followed. In particular, once a grid has been chosen, the user can select sampling parameters compliant with GPS standards (*D* and *d*), or can customize in order to reduce sampling time and costs. In the first case, the software proposes the maximum sampling distances allowed by standards with respect to the flatness specification (Table 1 in ISO/TS 12780-2).

The third input interface, Figure 5.17, is used to define the scenario in which verification is performed. The definition of scenario passes through the selection of the approach to be used for estimating the uncertainty of the whole verification process: a different method is associated to each scenario. If the "DoE based approach" is selected it means that scenario 2 occurs (§5.3.2) and the software uses the specification operator, the sampling strategy defined for the actual verification operator and some additional inputs about the workpiece material and typology of manufacturing process, in order to search for a suitable regression model in the knowledge database. If a suitable model is found the user can select and use it, otherwise a new section is activated for refinement of search parameters or in order to add a new regression model to the database. If user ticks the option "verification master available", he is specifying a scenario 1 verification (§5.3.1) and will be asked to insert the verification master data (reference flatness error and its standard deviation) together with the output of the actual verification operator: the flatness deviation with the relative implementation uncertainty.

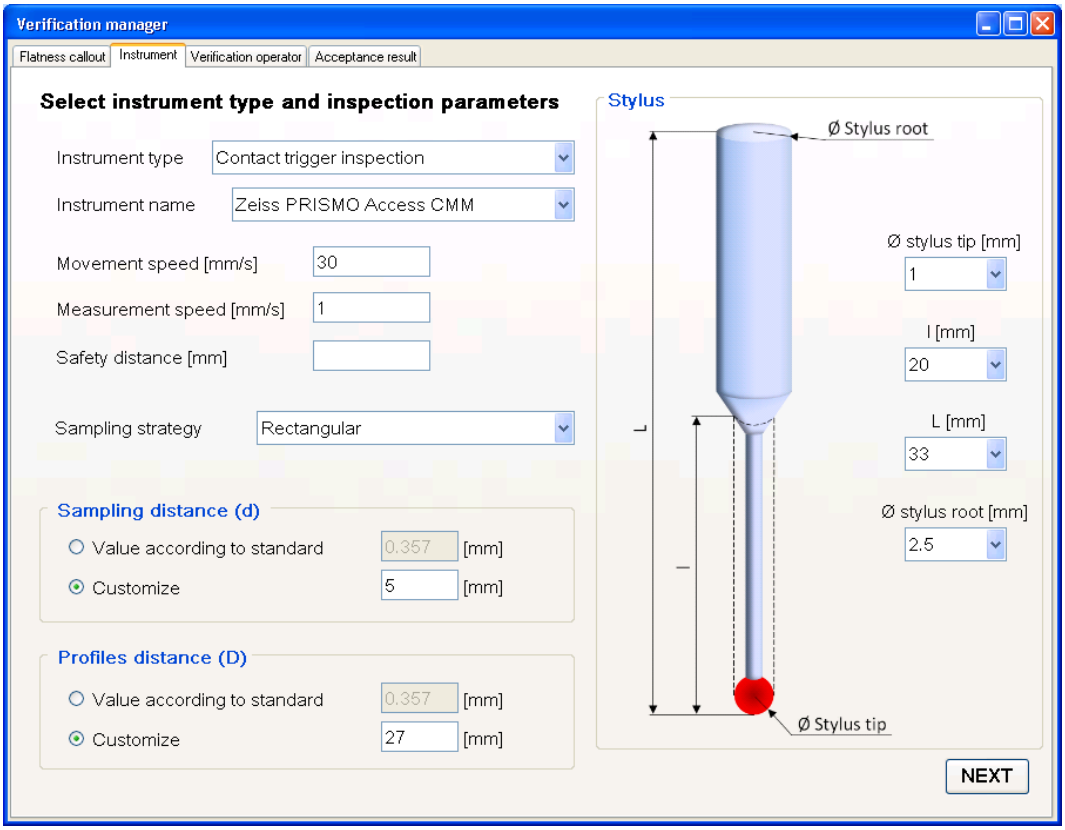

Figure 5.16 - Input interface for defining the actual verification operator: instrument selection, definition of sampling grid and of measuring parameters.

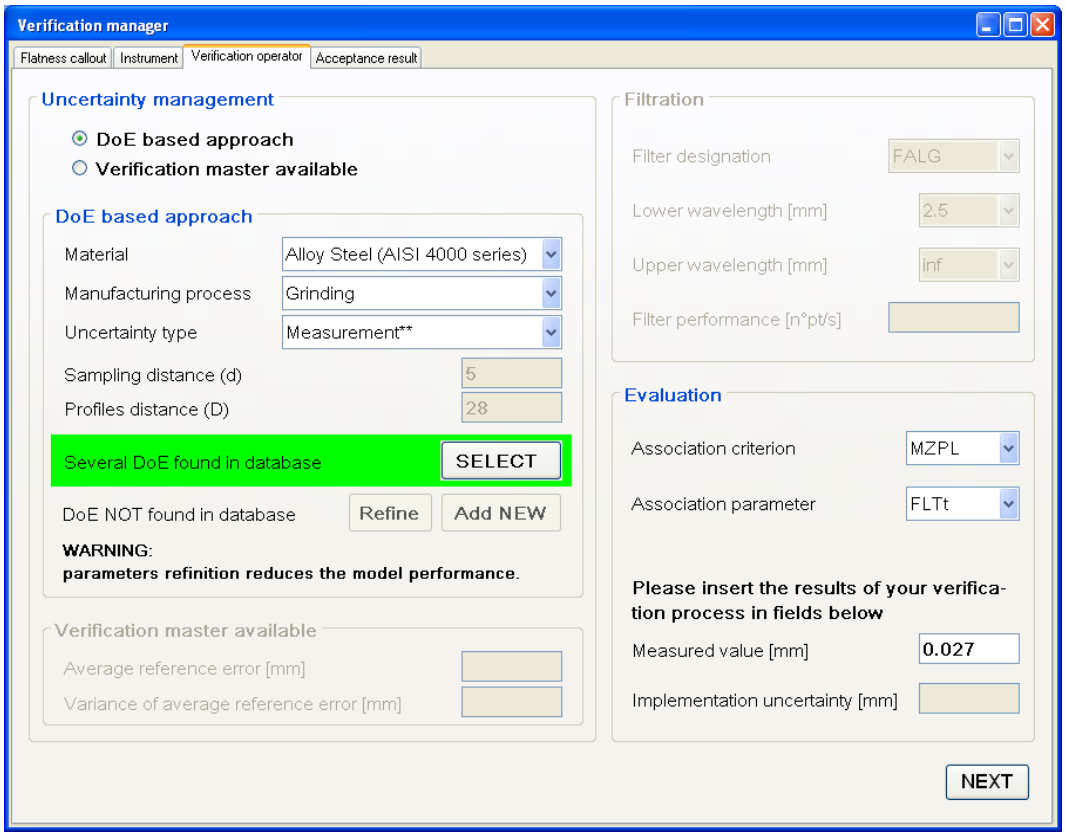

Figure 5.17 - The scenario in which verification is performed is selected through the choice of the approach to be used for uncertainty estimation.

Finally, once the verification operator has been completed and its uncertainty has been evaluated, it is possible to check the conformance of the workpiece geometry against specifications, according to the GPS acceptance rule [10]. The output of the verification process is displayed beside a traffic light which graphically represents the acceptance test result. A green light means that the feature is compliant with specification while a red one that it is not. A yellow light means that neither conformance nor non-conformance can be proved over any doubt (ambiguous result). These kind of situations could be avoided reducing the uncertainty of the measurement process, however if it is not possible, the uncertainty always counts against the part that is providing the proof of conformance [10], thus if you are a customer you cannot reject the part and if you are a supplier you cannot state its compliance.

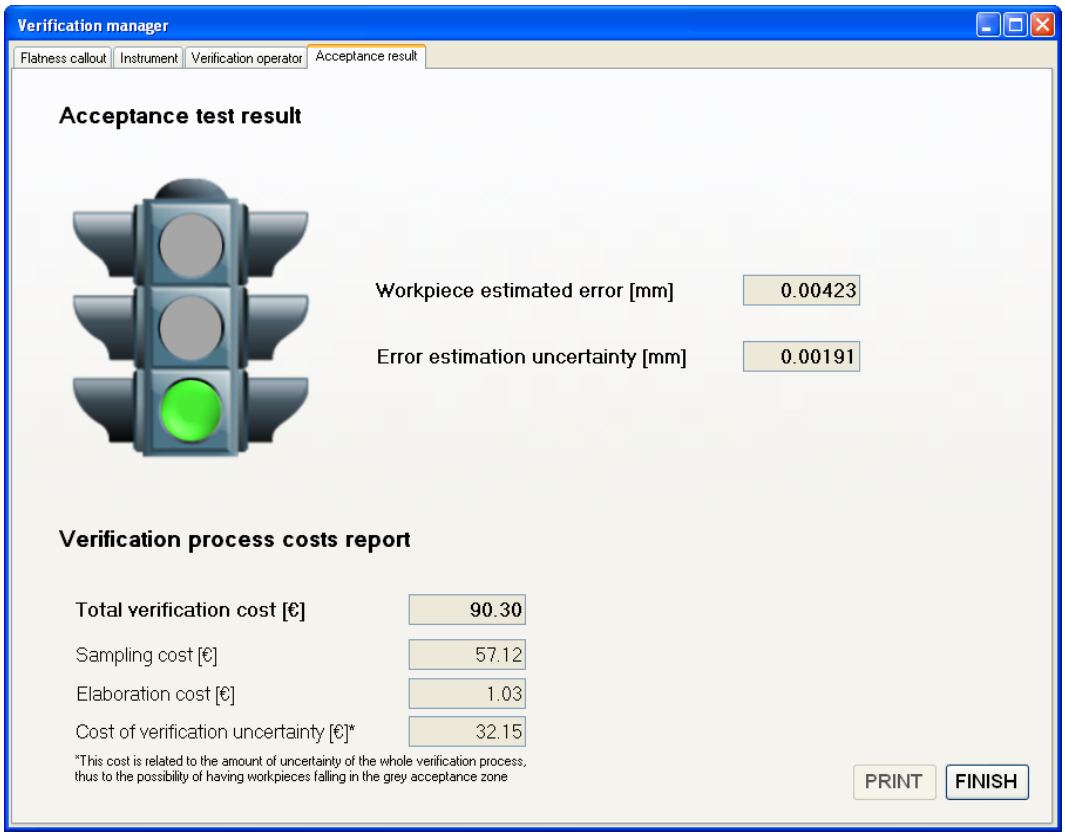

Figure 5.18 - Output interface collecting the results of verification process in term of flatness deviation and uncertainty of the estimation, the assessment of compliance with respect to specification and the evaluation of verification costs.

5.7 Conclusions

This categorical data model and the derived software represent the first application capable to implement the GPS approach for production management that is able to handle uncertainty from an economic point of view.

The software developed on the categorical model presented in this thesis allows an effective management of the verification processes. All process parameters are considered and managed according to GPS standards enabling metrologists to have a quantitative idea of the costs and uncertainties that are related with a certain verification operator.

The power of this software increases if the user invests in constructing a good database of experimental models and exploits the predictive nature of the DoE-based approach. In this case, metrologists would be able to simulate different verification scenarios and choose the best one based on rational considerations; while, on the other hand, designers could use the same scenario simulation to improve their awareness about the effects of a certain specification when the workpiece comes to be verified.

Further work is required to improve the software interfaces. With the integration into a PLM platform, many parameters could be directly imported from other softwares that manage design or verification instruments and procedures.

5.8 References

[1] Srinivasan V. (2008) *Standardizing the specification, verification, and exchange of product geometry: Research, status and trends.* Comput. Aided Des., **40** (7) 738-749.

[2] ISO/TS 17450-2 (2002) *Geometrical product specifications (GPS) - General concepts - Part 2: Basic tenets, specifications, operators and Uncertainties*. ISO, Geneve.

[3] Nielsen H.S. (2006) *New concepts in specifications, operators and uncertainties and their impact on measurement and instrumentation.* Measurement Science and Technology, **17** (3) 541.

[4] Xu Y., Xu Z., Jiang X. and Scott P. (2011) *Developing a knowledge-based system for complex geometrical product specification (GPS) data manipulation.* Knowledge-Based Systems, **24** (1) 10-22.

[5] Wang Y., *A knowledge-based intelligent system for surface texture (virtual surf)*, 2008, University of Huddersfield.

[6] Pierce B.C. (1991) *Basic Category Theory for Computer Scientists*.

[7] Lu W. and et al. (2010) *Modeling the integration between specifications and verification for cylindricity based on category theory.* Measurement Science and Technology, **21** (11) 115107.

[8] Mens T. (2001) *A formal foundation for object-oriented software evolution*. in proc. of Software Maintenance, 2001. Proceedings. IEEE International Conference on, pp 549-552.

[9] Barr M. and Wells C. (1995) *Category theory for computer science*, 2nd ed.

[10] ISO 14253-1 (1999) *Geometrical product specifications (GPS) - Inspection by measurement of workpieces and measuring equipment – Part 1: Decision rules for proving conformance or non-conformance with specifications*. ISO, Geneve.

[11] Lu W.L., Jiang X., Liu X.J. and Xu Z.G. (2008) *Compliance uncertainty of diameter characteristic in the next-generation geometrical product specifications and verification.* Meas. Sci. Technol, **19**.

[12] ISO/IEC (2008) *Guide to the Expression of Uncertainty in Measurement (GUM: 1995)*. BIPM, IEC, IFCC, ISO, IUPAP, IUPAC, OIML.

[13] Chiabert P., De Maddis M., Ricci F. and Ruffa S. (2011) *Uncertainty management in flatness verification operations within the GPS framework*. in proc. of AITeM, Naples.

[14] ISO 14253-4 (2010) *Geometrical product specifications (GPS) - Inspection by measurement of workpieces and measuring equipment – Part 4: Background on functional limits and specification limits in decision rules*. ISO, Geneve.

[15] ISO/TS 17450-1 (2005) *Geometrical product specifications (GPS) - General concepts - Part 1: Model for geometrical specification and verification*. ISO, Geneve.

[16] ISO/DIS 14659.2 (2009) *Geometrical product specification (GPS) – Fundamentals – Concepts, principles and rules* ISO, Geneve.

[17] ISO/TS 12781-2 (2011) *Geometrical product specifications (GPS) - Flatness - Part 2: Specification operators*. ISO, Geneve.

[18] ISO 1101 (2004) *Geometrical product specifications (GPS) - Geometrical tolerancing - Tolerances of form, orientation, location and run-out*. ISO, Geneve.

[19] ASME Y 14.5 (2009) *Dimensioning and Tolerancing – Engineering Drawing and Related Documentation Practices*.

[20] ISO/TS 12780-2 (2003) *Geometrical product specifications (GPS) - Straightness - Part 2: Specification operators*. ISO, Geneve.

6 Adaptive verification strategies

6.1 Introduction

In the previous chapters the main effects of ISO-GPS standards on the use of CMMs for verification of form features have been explored. CMMs introduce a new philosophy in form error assessment, but open a large number of issues still far to be solved. In order to achieve the highest generality, the new ISO standards regard measurement issues as related to the filtration of information from an unknown source, the feature, following an approach inspired by signal processing theory.

With respect to flatness tolerance, the flatness feature is regarded as the composition of several straightness profiles measured in the same reference frame [1]. This interpretation is consistent with the traditional verification approach suggested by ISO and ASME standards for verification by means of dial gauges [2-4]. Particularly, for GPS standards the straightness profiles shall be treated as finite length signals [5] and reconstructed from discrete samplings, if an instrument capable of continuous profile scanning is not available. The will to contain the number of sampling points leads to the definition of the minimum cut-off wavelength; a parameter entrusted to limit the amount of information theoretically needed [6] and that (according to new draft ISO 1101 amendment 2) will be added to the flatness callout in drawing specifications. Cut-off wavelength defines the shortest variation of shape that can be measured, thus defines the maximum distance between sampling points and the probe tip diameter. Different grid arrangements are suggested for the inspection of straightness profiles [5], but none is defined (set) as default and the choice is delegated to the metrologist according to the experience from other pieces of the same batch, or to some information inherited from manufacturing or previous experiences.

However, non-standard approaches based on intelligent algorithms can potentially reach performances better than any blind, a priori, fixed-grid extraction strategy by fully exploiting the potential of CMMs. As a matter of fact, CMMs can measure points only on a sequential base, and with fast enough algorithms, adaptive sampling strategies may be designed which exploit the information contained in the points already measured in order to suggest the best location where to sample the next point. In this chapter, an adaptive algorithm based upon the use of Kriging models, and on sequential probing of the points to be inspected, is suggested and analyzed. In particular, different approaches to the use of Kriging models are examined and compared based on different experiments: different correlation functions selected taking into account the technological signature of the surface analyzed, different criteria for selecting the successive inspection point and different evaluation methods (i.e. least squares and minimum zone methods).

The Kriging modelization and the uncertainty of Kriging predictions for responses of physical experiments is presented in §6.2. Section 6.4 presents the application of an adaptive approach for generating sequential sampling plans, illustrated by a case-study based on real CMM measurements (the same flatness feature used in Chapter 3). A discussion, on the basis of experiments performed (§6.7 and §6.8), compares the operating characteristics of Kriging modelization using different correlation functions, selected taking into account the technological signature, and different criteria for selecting the successive inspection points, based both on least squares or minimum zone methods for tolerance estimation.

6.2 Kriging modelization

Kriging models were extensively used to predict spatial data in geostatistics [7]; recently, their use is strongly suggested to approximate the output of Computer Experiments [8, 9]. Once more, Kriging models have been adopted in industrial metrology to drive the online construction of sequential designs for inspecting industrial parts on CMM [10] because of their recognized ability to provide good predictions [11, 12].

The Kriging model considers the response $y(\mathbf{x})$, for $\mathbf{x} \in \mathcal{X}_d \subset \mathbb{R}^d$, as a realization of a Gaussian random field $Y(\mathbf{x})$:

$$Y(x) = \mathbf{f}'(\mathbf{x})\,\boldsymbol{\beta} + Z(\mathbf{x}) \qquad \textbf{(6.1)}$$

where:

- $\mathbf{f}(\mathbf{x}) = (f_1(\mathbf{x}), f_2(\mathbf{x}), \ldots, f_m(\mathbf{x}))'$ is a set of specified trend functions,
- $\boldsymbol{\beta} = (\beta_1, \beta_2, \ldots, \beta_m)'$ is a set of (usually unknown) parameters,
- $Z(\mathbf{x})$ is Gaussian random field.

Let us consider a Gaussian random field $Y(\mathbf{x})$ with zero mean and stationary covariance over a design space $\mathcal{X}_d \subset \mathbb{R}^d$, i.e. $\mathbb{E}[Y(\mathbf{x})] = 0$ and $\mathrm{Cov}(Y(\mathbf{x}), Y(\mathbf{x}+\mathbf{h})) = \sigma_Y^2 R(\mathbf{h};\boldsymbol{\theta})$, where σ_Y^2 is the field variance and R is the Stationary Correlation Function (SCF) depending only on the displacement vector $\mathbf{h}$ between any pair of points in $\mathcal{X}_d$ and on a vector parameter $\boldsymbol{\theta}$.

The most popular choice for the correlation function among the practitioners of Computer Experiments is within the power exponential family:

$$R(h;\theta) = \prod_{s=1}^{d} \exp\left(-\theta_s |h_s|^p\right) = \exp\left\{-\sum_{s=1}^{d} \theta_s |h_s|^p\right\} \qquad \text{with } 0 < p \le 2 \qquad \textbf{(6.2)}$$

where $\boldsymbol{\theta} = (\theta_1, \theta_2, \ldots, \theta_d, p)'$; p is a common smoothing parameter and θ_s, $s = 1, 2, \ldots, d$, are positive scale parameters representing the rapidity of the correlation decay in direction s when increasing distance h_s. Notice that if $\theta_s = \theta$, $\forall s = 1, 2, \ldots, d$, the correlation depends only on the distance $|\mathbf{h}|$ between any pair of points $\mathbf{x}$ and $\mathbf{x} + \mathbf{h}$, i.e. isotropic SCF. However, the use of

the *variogram* (§6.5) has been favoured, because it is very informative about the random process Z(**x**). This is also what the pioneers of the Kriging models in geostatistics do for predicting noisy spatial responses from a generally small number of observations [13, 14], a situation rather different from a computer experiment.

For the prediction of the response $Y(\mathbf{x}_0)$ at an untried point $\mathbf{x}_0$, most of the practitioners suggest resorting to Bayesian estimators. The prior information on the set $\mathbf{Y}^n = Y(\mathbf{x}_1), Y(\mathbf{x}_2), ..., Y(\mathbf{x}_n)'$ of field variables at $\mathbf{x}^n = (\mathbf{x}_1, \mathbf{x}_2, ..., \mathbf{x}_n)$, also named training data, is used for predicting the unknown output $Y(\mathbf{x}_0)$. For flatness, being $d = 2$, the points are pertaining to a regular rectangular lattice: i.e. $\mathcal{X}_d = \{1, ..., l\}^2$.

The distribution of the joint random variable $(Y(\mathbf{x}_0), Y(\mathbf{x}_1), Y(\mathbf{x}_2), ..., Y(\mathbf{x}_n))$ is assumed to be normal distributed [15]:

$$N\left[\mathbf{f}_0', \mathbf{F}'\boldsymbol{\beta}, \sigma_Z^2\boldsymbol{\Sigma}\right] \qquad \textbf{(6.3)}$$

with:

- $\Sigma = \begin{pmatrix} 1 & \mathbf{r}_0' \\ \mathbf{r}_0 & \mathbf{R} \end{pmatrix}$
- $\mathbf{r}_0$ is the correlation vector $(R(\mathbf{x}_0 - \mathbf{x}_1), ..., R(\mathbf{x}_0 - \mathbf{x}_n))'$
- $\mathbf{R}$ is the $n \times n$ correlation matrix whose (i, j) element is $R(\mathbf{x}_{ij} = \mathbf{x}_i - \mathbf{x}_j)$
- $\mathbf{F}$ is the $n \times m$ matrix $f_j(\mathbf{x}_i)_{\substack{i=1,...n \\ j=1,...m}}$ of the trend functions evaluated in $(\mathbf{x}_1, \mathbf{x}_2, ..., \mathbf{x}_n)$.

Under the assumption that no a-priori knowledge on the trend function $\mathbf{f}'(\boldsymbol{\beta})$ is available to direct the user in its choice (in fact, in §6.5, we assume that no a-priori knowledge on the surface error is available), the *ordinary* Kriging model shall be used (i.e. $\mathbf{f}'(\boldsymbol{\beta}) = \beta$), then:

$$Y(\mathbf{x}) = \beta + Z(\mathbf{x}) \qquad \textbf{(6.4)}$$

Even if the unknown trend function of equation (6.4) is supposed to be constant, the prediction fidelity is not affected [8].

If β is known, the conditional expectation of $Y(\mathbf{x}_0)$ given $Y(\mathbf{x}_1), Y(\mathbf{x}_2), ..., Y(\mathbf{x}_n)'$, $\hat{Y}_0 = \mathbb{E}\left[Y(\mathbf{x}_0) \middle| \mathbf{Y}^n\right]$, is the unique predictor and the Best Linear Unbiased Predictor (BLUP) of $Y(\mathbf{x}_0)$:

$$\hat{Y}_0 = \beta + \mathbf{r}_0'\mathbf{R}^{-1}(\mathbf{Y}^n - \beta\mathbf{1}) \quad \text{with} \quad \mathbf{1} = (1,1,\ldots,1)' \qquad \textbf{(6.5)}$$

because it minimizes the Mean Squared Prediction Error (MSPE):

$$MSPE\left[\hat{Y}_0\right] = \mathrm{E}\ (\hat{Y}_0 - Y(\mathbf{x}_0))^2 = \sigma_z^2\ 1 - \mathbf{r}_0' \mathbf{R}^{-1} \mathbf{r}_0 \qquad \textbf{(6.6)}$$

MSPE, usually called Kriging variance, is a measure of the uncertainty of predictions. It is large when x_0 is away from the experimental points, small when it is close to them and it vanishes at the experimental points, due to the interpolatory property of Kriging.

However, equation (6.6) holds only if β and $R(\mathbf{h};\theta)$ are known, which is hardly the case in experimental setting. If β is to be estimated, the BLUP is given by (6.5) with β replaced by its generalized least squares estimator:

$$\hat{\beta} = \mathbf{1}' \mathbf{R}^{-1} \mathbf{1}^{-1} \mathbf{1}' \mathbf{R}^{-1} \mathbf{Y}^n \qquad \textbf{(6.7)}$$

In such a case the Kriging variance (6.6) is larger because of an additional uncertainty component, and becomes:

$$\mathrm{E}\left[(\hat{Y}_0 - Y(\mathbf{x}_0))^2\right] = \sigma_z^2\ 1 - \mathbf{r}_0' \mathbf{R}^{-1} \mathbf{r}_0 + \mathbf{c}_0'\ \mathbf{1}' \mathbf{R}^{-1} \mathbf{1}^{-1} \mathbf{c}_0 \qquad \textbf{(6.8)}$$

with $\mathbf{c}_0 = 1 - \mathbf{1}' \mathbf{R}^{-1} \mathbf{r}_0$.

The unknown parameter vector θ in $R(\mathbf{h};\theta)$ can be estimated by maximum likelihood, cross-validation, or by the posterior mode (for a thorough reading see [15]). The predictor obtained by plugging the estimates $\hat{\mathbf{r}}_0 = \mathbf{r}_0(\hat{\boldsymbol{\theta}}_{\mathrm{ML}})$ and $\hat{\mathbf{R}} = \mathbf{R}(\hat{\boldsymbol{\theta}}_{\mathrm{ML}})$ into (6.8) is named Empirical Best Linear Unbiased Predictor (EBLUP), even if the predictions are no longer linear in the observations as $\hat{\mathbf{r}}_0$ and $\hat{\mathbf{R}}$ may have a highly non-linear dependence on observations. Another notable consequence of using the EBLUP is that (6.8) underestimates prediction variance as it does not account for the extra variability transmitted to $\hat{\mathbf{r}}_0, \hat{\mathbf{R}}$ and $\hat{\beta}$ by $\hat{\boldsymbol{\theta}}$. A possible way to overcome this problem is to resort to an empirical estimate of the variance. Den Hertog *et al*. [16] use parametric bootstrap while Kleijnen and van Beers [11] use cross validation and jackknife. In this work, the correlation parameters have been estimated by maximum likelihood using the algorithm proposed by Lophaven [17].

Predictions made at the experimental points have zero variance being the kriging predictor interpolatory. This is often unsuitable for modelling data which are affected by random noise, as measurement error is in physical experiments. In order to accommodate for it, the geostatisticians suggest to modify model (6.5) by adding a random error:

$$Y\ \mathbf{x}_i = \beta + Z\ \mathbf{x}_i + \varepsilon_i \qquad i = 1, 2, \ldots, n \qquad \textbf{(6.9)}$$

where ε_i are i.i.d. normal random variables with zero mean and constant variance σ_ε^2. The consequence of the model modification reproduces on SCF with the so called *nugget effect* [8]:

$$R\ \mathbf{h};\boldsymbol{\theta}, nugget = (1 - nugget)\ R\ \mathbf{h};\boldsymbol{\theta} \qquad \textbf{(6.10)}$$

where

$$nugget = \frac{\sigma_\varepsilon^2}{\sigma_z^2 + \sigma_\varepsilon^2} \quad (0 \le nugget < 1)\,. \tag{6.11}$$

This prevents predictions from exactly interpolating experimental data and results in a smoother prediction surface. The nugget can be estimated by maximum likelihood while estimating the unknown parameters of the SCF. As the estimated process variance is much larger, the nugget effect is indeed very small in our application and could be safely not considered (typical values of measurement errors variance in CMM measurements are in the interval $[10^{-8}, 10^{-6}]$ mm^2).

6.3 Adaptive sampling through a case study

The same flatness feature that has been used to delve into the effects of ISO GPS standards on the verification of form errors based on CMMs (§3), has been used also to test the adaptive sampling strategy proposed in this chapter. The flatness surface showed in Figure 6.1 has been measured by means of a CMM (Dea Iota 0101) with a sampling strategy that complies with specification according to the GPS standards: namely with a perfect verification operator. The dataset obtained has then been used as test bench for the adaptive sampling algorithm. This approach has been used in order to avoid direct interfacing with CMM software during the test of sampling strategy. Software integration is a problem that has to be solved for on-line applications, but it does not affect the method itself. On the other hand, the computation time required by the adaptive sampling algorithm has to be small enough to guarantee an effective performance of the whole measurement process. However, at this stage, the computation time has not been taken into account yet and the focus is rather on the real method capabilities.

Figure 6.1 – The case study's flatness feature, on the measurement bench of CMM (model: Dea Iota 0101), for the tolerance verification. Tolerances are reported in Figure 3.1.

6.3.1 The problem of flatness error estimation

According to ISO-GPS standards, two different association criteria can be used to estimate the flatness error: Least Squares or Minimum Zone.

LS method estimates the parameters of the least square plane by fitting a reference model (or ideal feature) to the sampled data set. The distance of each point of the data set from the fitted plane is calculated (it is named residual) and the sum of the highest and lowest value provides the estimation of the flatness error. In the case study at hand, normality of residuals, one of the relevant assumptions in the estimation method, is not complied (Figure 6.2-a). Nevertheless, LS method is still considered because its use may be required by specification (regardless the characteristics of measurement data) and it is widely used and implemented in every CMM software.

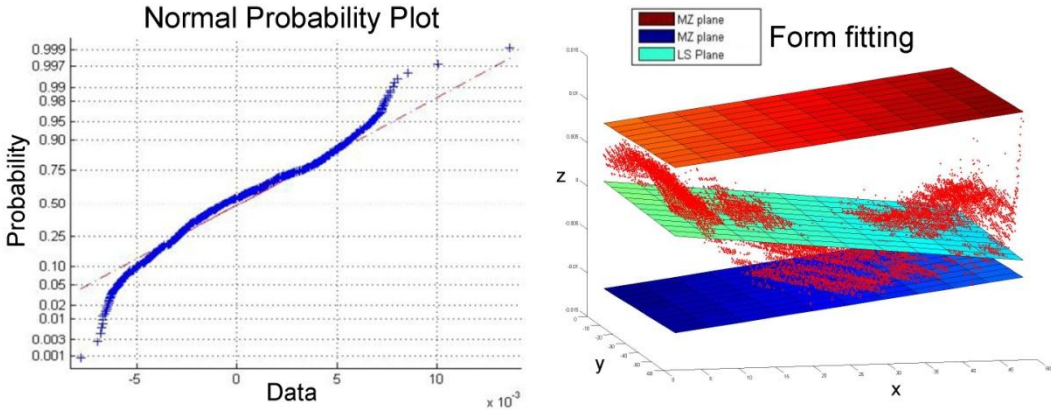

Figure 6.2 - LS residuals probability plot on the left (a), and the comparison of LS and MZ method on the right (b).

On the other hand, MZ method computes the equations of two parallel planes with the constraint of containing all the sampled points among the plane surfaces and of minimizing their distance.

The two methods are of course different and end up in different estimations of the flatness error. Figure 6.2-b shows the difference between the two methods in terms of orientation of the reference plane: the LS reference plane, in the middle, has a completely different orientation with respect to the two MZ planes. The MZ reference plane is not represented for the sake of clearness, but it lays halfway between the two MZ planes, with their same orientation. The main aspects related with the use of LS and MZ association criteria have been investigated in Chapter 3 and Chapter 4. However, a consideration that is always valid is that LS systematically overestimates the form error.

6.4 Sequential selection of sampled points

In the conventional factorial designs, all the sampling points are decided prior to the experiment execution. On the contrary, in a sequential design approach, the points to be sampled are adaptively selected, at each run, relying on the information acquired from the

sampling points up to that time. The choice of sequential designs is motivated by their efficiency, as they are generally considered more efficient than one-stage designs. A sequential design usually starts with a space-filling design such as Latin Hypercube Sampling designs, distance-based designs or uniform designs (see [15] or [18] for a review) in order to start with an optimal coverage of the measurand.

In the case study at hand the starting design has been a 4 Latin Hypercube design plus the 4 points at the vertices (Figure 6.3). Among the possible selections of 4 points Latin Hypercube designs, it has been chosen the one which provides the lowest expected error for the Kriging model [19]. The idea of *minimizing the uncertainty of Kriging predictions* has been used also for the selection of the next sampling point, within more complex decision rules. On the other hand, the 4 points at the vertices have been suggested by experience: most of the form deviation is usually concentrated near the edges where transient states occur in the manufacturing process (e.g. transients of the forces at the interface between the tool and workpiece and related deformations). Moreover, the extreme points of the domain are included in the initial set of design points in order to avoid extrapolation when predicting with the Kriging model. In our case, the $n_0 = 8$ is a reasonably low number of data needed to estimate the parameters β of the ordinary Kriging model, the parameters θ of the correlation function, and σ_z^2.

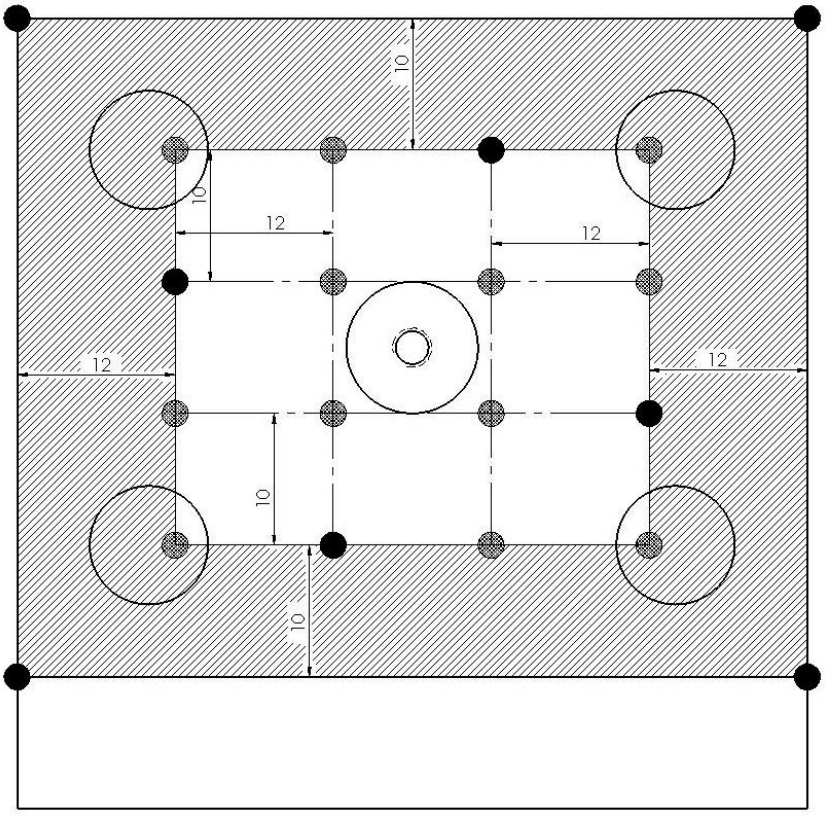

Figure 6.3 - Selection of starting sampling points. The 4 points on the extreme corners of flatness feature have been selected while, in the central area, other 4 points are selected with Latin Hypercube.

Based on the initial set of points, the experimental design is iteratively built up by adding one point at a time. The next measurement point is selected, according to a specific criterion, among a set of candidate points located on a uniformly spaced and *tight* rectangular grid.

The criterion for the selection of next sampling point can be based on the MSPE (6.8) of the Kriging model, estimated by means of the already measured points, or on the basis of an increase in the evaluation of flatness error. Particularly, the latter considers the candidate sampling points one at a time, supposing to add each of them to the current dataset of measured points and analyzing the result of the evaluation. If some points lead to an evaluation of flatness error higher than the dataset of points already measured, then the one generating the largest increase is selected. However, this method could be biased by a particularly high uncertainty of the Kriging prediction. In such a case, a refinement of the Kriging model itself (then the selection of the candidate point whit the maximum MSPE) would be preferable. The two criteria may be used individually, as presented above, or, better, they could be mixed according to different rules. Particularly, two rules are considered which have been named respectively:

- **Δ-MSPE**: if some points are expected to generate an increase in the flatness error evaluation, then the point that generates the maximum increase is selected, otherwise the point having the maximum MSPE is preferred. It means that if the actual model cannot detect points which would lead to an increase in the flatness error evaluation (that would be higher peaks or deeper valleys), a refinement of the model itself is preferred.
- **Δ-MSPE *average***: if there are points expected to generate an increase in the estimated flatness error, the point which would generate the maximum increase is selected given that its MSPE is less than the average MSPE (with respect to the whole set of points). Otherwise, it means that the prediction is not reliable enough and the purpose of next point will be to improve it; then the next point will be sampled where the MSPE is maximum.

After the *winning* candidate point has been selected, the measurement is performed at this new site and the point becomes part of the current dataset. Then, the Kriging correlation function is estimated by Maximum Likelihood, basing on the current dataset, and the new Kriging model is now used to provide new predictions. It is worthwhile to point out that, as the predictions are inexpensive, it is possible to predict over a convenient *tight* grid. Finally, the estimate of flatness error is computed by applying LS or MZ methods to the large points sample made up of both the current experimental points and the new predictions.

6.5 Variogram and correlation function

As stated in §6.2, the most popular choice for the correlation function among the practitioners of Computer Experiments is within the power exponential family (6.2).

However, we favour the use of the *variogram* in its choice because it is very informative about the random process Z(**x**). The variogram is defined as:

$$2\gamma\ \mathbf{x}_1-\mathbf{x}_2\ = \mathrm{Var}\left[\ Z\ \mathbf{x}_1\ - Z\ \mathbf{x}_2\ \right] \qquad \forall\, x_1, x_2 \in \boldsymbol{\chi}_d \tag{6.12}$$

A natural estimator of the variogram based on the method of moments [20], under the assumption that , is:

$$2C\ \mathbf{h}\ = \frac{1}{\#N\ \mathbf{h}} \sum_{N\ \mathbf{h}} \left[\ Z\ \mathbf{x}_i\ - Z\ \mathbf{x}_j\ \right]^2 \tag{6.13}$$

where $N(\mathbf{h}) = \{(\mathbf{x}_i, \mathbf{x}_j) : \mathbf{x}_i - \mathbf{x}_j = \mathbf{h};\ i, j = 1, 2, \ldots, n\}$ and $\#N(\mathbf{h})$ is the number of pairs $N(\mathbf{h})$ that are distinct.

If the value of the variogram depends only on the length of vector **h**, then the stochastic process underlying the variogram is isotropic; opposite the process is anisotropic. Isotropic processes form an inadequate basis in modelling many spatially distributed data, especially when the monitored manufactured part shows technological signature.

In our case, the manufacturing process cannot be considered isotropic as the estimated variogram shows different trends with respect to the considered direction: see Figure 6.4. Particularly, variograms in *x* and *y* directions seem to be very different and, for this reason, exponential functions with different parameters have been chosen as correlation function in the Kriging method, that is:

$$R\ \mathbf{h};\boldsymbol{\theta}\ = \prod_{s=1}^{2} \exp\ -\theta_{1s}\left|h_s\right|^{\theta_{2s}}\ = \exp\left\{-\sum_{s=1}^{2} \theta_{1s}\left|h_s\right|^{\theta_{2s}}\right\} \qquad \text{with } 0 < \theta_{2s} \le 2 \tag{6.14}$$

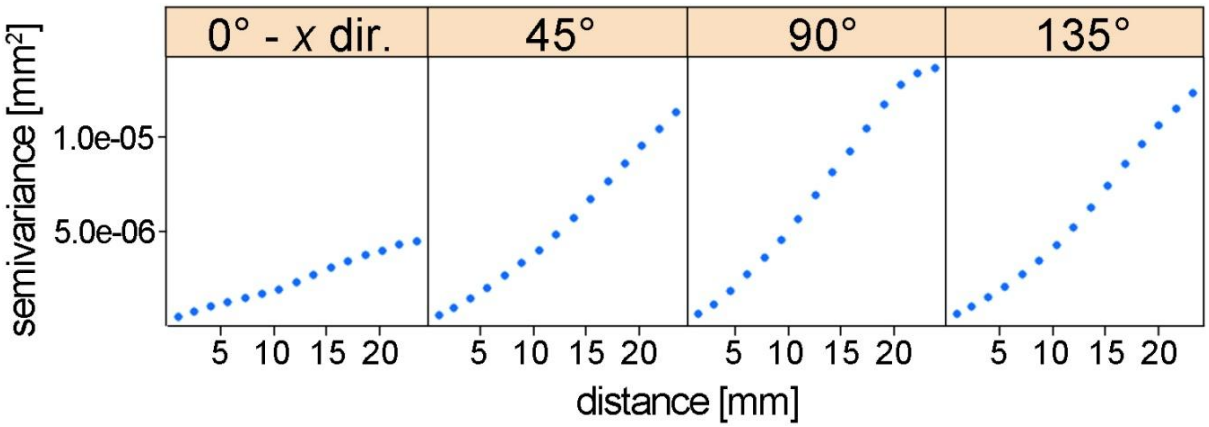

Figure 6.4 - Different variograms in the four angle direction (= 0°, 45°, 90° and 135°).

For the case study at hand the use of variogram is allowed by the knowledge of the surface geometry determined with the preliminary measurement. However, even if the measurand is completely unknown (as it is in normal measurements) some useful information about the spatial correlation function could be derived from the technological signature. Therefore it could be supposed if the manufacturing process is known.

6.6 Algorithm description

The main steps of the adaptive sampling algorithm are summarized in this section. To estimate the Kriging model the algorithm proposed by Lophaven et al. [17] has been used changing only the correlation function as described in §6.5.

N indicates the total number of points on the grid and N_m the number of points which have been actually measured; i.e. the set $\{x_i, y_i, z_i\}_{i=1}^{N_m}$. For each iteration the following steps are repeated:

1. Flatness error t_m is computed on the set of measured points and, according to the Kriging model, the *z* coordinate is predicted for the grid of candidate sampling points in order to obtain the new set of points: $\{x_i, y_i, \hat{z}_i\}_{i=1}^{N-N_m}$.
2. For each predicted sampling point $(x_j, y_j, \hat{z}_j)$ in $\{x_i, y_i, \hat{z}_i\}_{i=1}^{N-N_m}$ the flatness error t_j^* and the ratio $\delta_j = t_j^* / t_m$ is computed (using both LS and MZ) on the set of points $\{x_i, y_i, z_i\}_{i=1}^{N_m} \cup \{x_i, y_i, \hat{z}_i\}$: namely adding the predicted measurement point to the set of points actually measured.
3. The next sampling point is selected by implementing one of the two decision rules presented in §6.4:
   - **Δ-MSPE:**
     3.1. Find j* such that $\delta_{j^*} = \max_{i \in (1 \ldots N-N_m)} (\delta_i)$.
     3.2. Find j** such that $MSPE_{j^{**}} = \max_{i \in (1 \ldots N-N_m)} (MSPE_i)$ where $MSPE_i$ is the Kriging model error in the i[th] point.
     3.3. If $\delta_{j^*} > 1$, then $(x_{j^*}, y_{j^*}, z_{j^*})$ is the next point to be measured: else $(x_{j^{**}}, y_{j^{**}}, z_{j^{**}})$ is the next point.
   - **Δ-MSPE average**
     3.1. Find j* such that $\delta_{j^*} = \max_{i \in (1 \ldots N-N_m)} (\delta_i)$.
     3.2. Find j** such that $MSPE_{j^{**}} = \max_{i \in (1 \ldots N-N_m)} (MSPE_i)$ where $MSPE_i$ is the Kriging model error in the i[th] point.
     3.3. If $\delta_{j^*} > 1$ and $MSPE_{j^*} < \sum_{i=1}^{N-N_m} \frac{MSPE_i}{N - N_m}$, then $(x_{j^*}, y_{j^*}, z_{j^*})$ is the next point; else $(x_{j^{**}}, y_{j^{**}}, z_{j^{**}})$ is the next point.
4. The algorithm has two different outputs:
   - Flatness error computed on the set of measured points $\{x_i, y_i, z_i\}_{i=1}^{N_m}$ referred to as d_m.
   - Flatness error computed on $\{x_i, y_i, z_i\}_{i=1}^{N_m} \cup \{x_i, y_i, \hat{z}_i\}_{i=1}^{N-N_m}$ referred to as d_s.

While testing this model, no stopping rule has been applied either based on the quality of regression model or convergence of flatness estimation results. However, stopping rules could be useful in different experimental contexts and are necessary for effective implementation in industrial practice. The algorithm has been stopped when $N = 40$ thus, if taking into account also the initial 8 points dataset, with a total of 48 measured points. 40 iterations have proved to go further the stopping point that could be established by reasonable rules. This allows to check the algorithm evolution also after the point where it should have stopped, thus to verify the goodness of stopping rules.

6.7 Test of the adaptive sampling algorithm

In the following, the results of the adaptive sampling strategy based on the Kriging modelization are reported according to different association methods (LS or MZ) and different criteria for the selection of the next sampling point: see Figure 6.5.

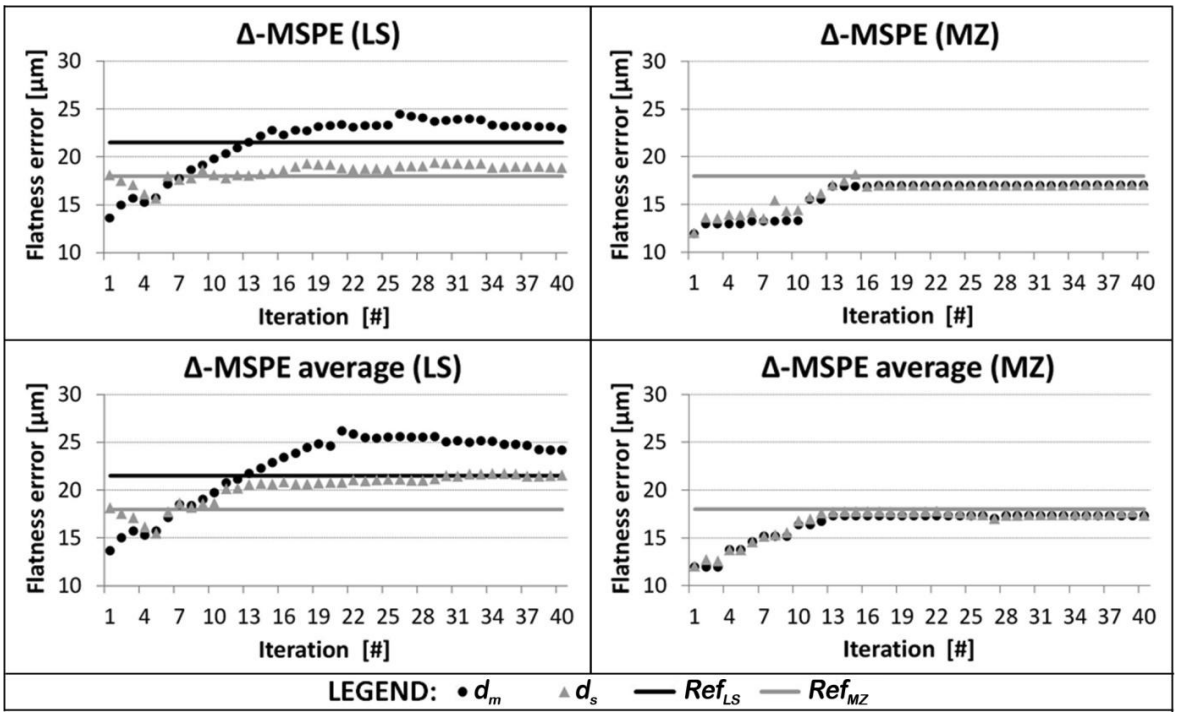

Figure 6.5 - Results for different selection criteria and different association methods.

As it can be noticed from Figure 6.5, in 15 iterations (23 sampled points) the method with MZ association criterion computes the right flatness error both using only the set of measured points (d_m line) and using the measured points together with those estimated with the Kriging model (d_s line).

On the other hand, the LS method overestimates the flatness error if the form error estimation is based only on the actually measured points. On the contrary, if it is computed using the whole set of data (estimated and measured points) then a more precise evaluation can be obtained in few iterations. This behaviour is typical of the LS association criterion, as for small samples the orientation of the LS reference plane is very sensitive to the addition of

new measurement points and can take orientations quite different from the true one. Therefore taking into account the predictions on the grid of candidate sampling points helps to reduce the instability of the LS reference plane even if some error is introduced due to areas of the flatness feature where the Kriging model is not very reliable (high MSPE). However the two aspects combines very well as, for very small samples, the error due to the stability of the LS reference plane is very large but almost disappears as soon as the sample size reaches 50 points about (see the amount of uncertainty associated with the stability of LS reference plane: Figure B.1). Similarly, the reliability of the Kriging prediction improves and the probability that some of the extreme points (the most determinant for the assessment of form deviation) is biased by a large MSPE reduces as the measurand is sampled with a higher density (larger sample size).

According to these results, the adaptive sampling strategy based on the Kriging method seems to be a promising approach to evaluate the flatness error, given that both using LS and MZ it is possible to obtain in few iterations the right tolerance value (obviously if with LS d_s is considered instead of d_m). Nevertheless further analyses should be carried out in order to evaluate the method performances with other kinds of flat surfaces obtained with different manufacturing processes.

6.8 Comparison with random sampling

In this section, the results of a random sampling strategy are presented as a benchmark for the Kriging-based adaptive sampling. Figure 6.6 shows that the random sampling strategy is far from the reference value of flatness deviation even if the maximum number of points is considered (N = 48 points). Particularly, the random sampling strategy presented here, as a benchmark, consists of the random selection of the next measurement point within the set of candidate measurement points. It is a well established practice and is present also within the arrangement for sampling points (sampling grids) suggested by GPS standards for the verification of flatness tolerance [5].

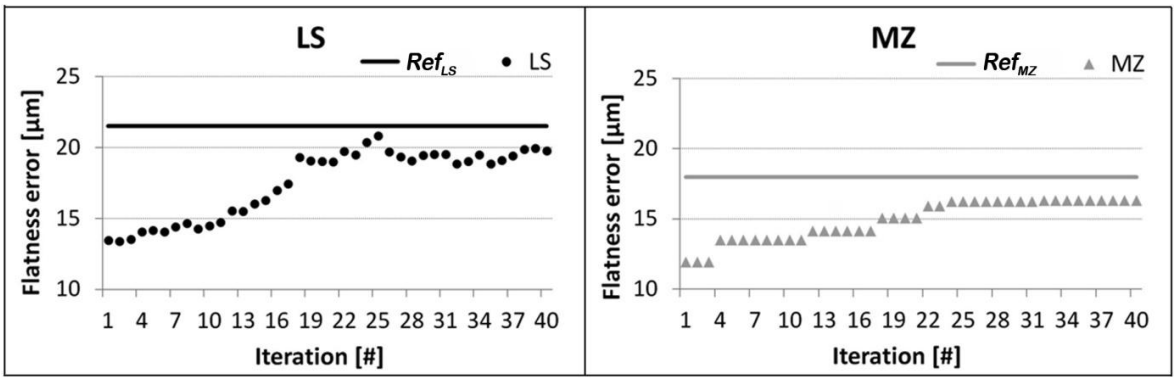

Figure 6.6 - Results for different association criteria if a random point is added at each iteration.

6.9 Conclusion

The Kriging-based adaptive sampling presented in this chapter showed great potential for the improvement of CMM based verification processes; particularly when the CMM is capable of touch trigger inspection only. After 15 iterations about, it has been able to detect almost all the workpiece form deviation (see Figure 6.5), much more effectively than a classical random sampling (Figure 6.6).

However, in this study the issues related with the online implementation have not been considered. One of the main aspects, in this sense, is indeed represented by the computation time required for the construction of the Kriging interpolatory model. At the moment, this aspect has not been afforded jet, as the main concern was the investigation of the effectiveness of the method itself. Now that the effectiveness has been proved, further work is required for a deeper testing on other technological signatures, for addressing the verification of other tolerances and for optimizing the algorithms for a faster computation.

Another aspect deserving further investigation is the relationship between variogram (thus the spatial correlation function) and the technological signature left on the workpiece by manufacturing processes. In this context variogram can be used to classify and characterize manufacturing processes, particularly those generating anisotropic signatures.

6.10 References

[1] ISO/TS 12781-1 (2003) *Geometrical product specifications (GPS) - Flatness - Part 1: Vocabulary and parameters of flatness*. ISO, Geneve.

[2] ASME Y 14.5 (2009) *Dimensioning and Tolerancing – Engineering Drawing and Related Documentation Practices*.

[3] ISO 1101 (2004) *Geometrical product specifications (GPS) - Geometrical tolerancing - Tolerances of form, orientation, location and run-out*. ISO, Geneve.

[4] ASME Y 14.5.1.M (1994) *Mathematical Definition of Dimensioning and Tolerancing Principles*.

[5] ISO/TS 12781-2 (2011) *Geometrical product specifications (GPS) - Flatness - Part 2: Specification operators*. ISO, Geneve.

[6] ISO/TS 12780-2 (2003) *Geometrical product specifications (GPS) - Straightness - Part 2: Specification operators*. ISO, Geneve.

[7] Krige D.G., *A statistical approach to some mine valuations and allied problems at the Witwatersrand*, 1951, University of Witwatersrand.

[8] Sacks J., Schiller S.B. and Welch W.J. (1989) *Designs for Computer Experiments.* Technometrics, **31** (1) 41-47.

[9] Sacks J., Welch W.J., Mitchell T.J. and Wynn H.P. (1989) *Design and Analysis of Computer Experiments.* Statistical Science, **4** (4) 409-423.

[10] Pedone P., Vicario G. and Romano D. (2009) *Kriging-based sequential inspection plans for coordinate measuring machines.* Applied Stochastic Models in Business and Industry, **25** (2) 133-149.

[11] Kleijnen J.P.C. and Beers W.C.M. (2004) *Application-driven sequential designs for simulation experiments: Kriging metamodelling.* Journal of the Operational Research Society, **55** 876-883.

[12] Simpson T.W., Poplinski J.D., Koch P.N. and Allen J.K. (2001) *Metamodels for Computer-based Engineering Design: Survey and recommendations.* Engineering with Computers, **17** (2) 129-150.
[13] Cressie N.A. (1993) *Statistics for Spatial Data*, New York.
[14] Matheron G. (1971) *The theory of regionalized variables and its applications*, Les Cahiers du Centre de Morphologie Mathématique, Paris.
[15] Santner T.J., Williams B.J. and Notz W.I. (2003) *The Design and Analysis of Computer Experiments,* New York.
[16] Hertog D.d., Kleijnen J.P.C. and Siem A.Y.D. (2006) *The correct Kriging variance estimated by bootstrapping.* Journal of the Operational Research Society, **57** 400-409.
[17] Lophaven S., Nielsen H. and Sondergaard J., *DACE — A Matlab kriging toolbox, version 2.0*, in *Informatics and Mathematical Modelling*2002, Technical University of Denmark.
[18] Fang K.-T., Li R.-z. and Sudjianto A. (2006) *Design and Modeling for Computer Experiments*, Boca Raton.
[19] Pistone G. and Vicario G. (2010) *Comparing and generating Latin Hypercube designs in Kriging models.* AStA Advances in Statistical Analysis, **94** (4) 353-366.
[20] Matheron G. (1962) *Traité de géostatistique appliquée, Tome I: Mémoires du Bureau de Recherches Géologiques et Minières*, n° 14, Editions Technip: Paris, p. 333.

Annex A - **Case study: results**

SAMPLING				(LS) *FLT*t					
				Error evaluation		u_{lm} ANALYTIC		u_{lm} EXPERIMENTAL	
D [mm]	d [mm]	Grid	points [n°]	*FLT*t [µm]	t_{FLTt} [s]	u_{lm} [µm]	t_u [s]	u_{lm} [µm]	t_u [s]
0.35	0.35	Rect	17575	24.100	0.0407	0.946	2.543	0.281	1.177
0.35	0.35	Px	17575	24.100	0.0407	0.946	2.543	0.281	1.177
0.35	0.35	Py	17575	24.100	0.0407	0.946	2.543	0.281	1.177
0.35	0.35	UJ	17575	24.100	0.0407	0.946	2.543	0.281	1.177
0.7	0.35	Rect	13323	24.160	0.0088	0.947	2.527	0.343	0.822
0.7	0.35	Px	8915	24.028	0.0371	0.949	0.307	0.766	0.770
0.7	0.35	Py	8949	24.360	0.0083	0.950	0.735	0.221	0.786
0.7	0.35	UJ	17575	24.100	0.0144	0.946	0.722	0.248	1.585
0.7	0.7	Rect	4540	24.282	0.0034	0.956	0.690	0.869	0.426
0.7	0.7	Px	4459	24.073	0.0034	0.956	0.728	0.695	0.439
0.7	0.7	Py	4473	24.509	0.0034	0.956	0.733	0.727	0.439
0.7	0.7	UJ	4540	24.282	0.0034	0.956	0.727	0.631	0.437
3.5	0.35	Rect	3529	24.372	0.0032	0.959	0.765	2.346	0.218
3.5	0.35	Px	1870	23.734	0.0018	0.953	0.744	2.285	0.150
3.5	0.35	Py	1856	13.404	0.0018	0.956	0.724	0.185	0.151
3.5	0.35	UJ	5089	24.328	0.0039	0.954	0.735	2.159	0.395
3.5	0.7	Rect	1693	24.293	0.0017	0.977	0.725	3.506	0.146
3.5	0.7	Px	933	23.630	0.0014	1.002	0.706	3.125	0.096
3.5	0.7	Py	927	13.391	0.0012	0.971	0.734	0.302	0.102
3.5	0.7	UJ	2405	24.390	0.0026	0.967	0.721	2.839	0.214
3.5	3.5	Rect	196	12.567	0.0009	1.146	1.310	0.731	0.049
3.5	3.5	Px	180	12.641	0.0008	1.067	1.886	0.773	0.051
3.5	3.5	Py	183	12.474	0.0008	1.159	0.520	0.724	0.051
3.5	3.5	UJ	196	12.567	0.0008	1.146	0.473	0.729	0.051
7	0.35	Rect	1897	24.756	0.0041	0.952	4.978	2.924	0.155
7	0.35	Px	1035	23.601	0.0014	0.960	0.430	2.548	0.094
7	0.35	Py	917	12.123	0.0013	0.972	0.432	0.388	0.087
7	0.35	UJ	2714	24.648	0.0028	0.962	0.439	2.958	0.227
7	0.7	Rect	935	24.707	0.0014	1.003	0.440	3.020	0.095
7	0.7	Px	517	23.440	0.0010	1.038	0.443	3.214	0.065
7	0.7	Py	458	12.244	0.0010	1.001	0.434	0.461	0.062
7	0.7	UJ	1334	24.673	0.0017	0.985	0.455	4.163	0.111
7	3.5	Rect	150	12.246	0.0008	1.165	0.435	0.702	0.047
7	3.5	Px	100	11.814	0.0008	1.079	0.429	0.726	0.046
7	3.5	Py	90	11.971	0.0008	1.190	0.436	1.108	0.045
7	3.5	UJ	196	12.567	0.0008	1.146	0.434	0.756	0.050
7	7	Rect	54	10.417	0.0007	1.339	0.445	0.812	0.043
7	7	Px	46	8.390	0.0007	1.185	0.431	0.805	0.043
7	7	Py	48	8.936	0.0007	1.298	0.421	0.761	0.043
7	7	UJ	54	10.417	0.0007	1.339	0.431	0.619	0.043
14	0.35	Rect	1184	25.038	0.0018	0.959	0.439	3.461	0.097
14	0.35	Px	631	23.542	0.0011	0.974	0.433	3.242	0.067
14	0.35	Py	572	11.526	0.0011	0.984	0.441	0.321	0.065
14	0.35	UJ	1576	24.712	0.0017	0.955	0.464	3.785	0.113
14	0.7	Rect	590	24.829	0.0017	1.038	0.436	4.682	0.064
14	0.7	Px	315	23.234	0.0009	1.085	0.428	4.436	0.056
14	0.7	Py	286	11.618	0.0009	1.024	0.435	0.474	0.052
14	0.7	UJ	786	24.608	0.0013	1.013	0.429	4.954	0.076
14	3.5	Rect	106	12.529	0.0008	1.244	0.425	0.798	0.044
14	3.5	Px	61	11.299	0.0007	1.133	0.436	0.757	0.045
14	3.5	Py	56	11.221	0.0007	1.276	0.458	1.082	0.043
14	3.5	UJ	136	12.879	0.0010	1.215	0.470	0.836	0.048
14	7	Rect	46	10.423	0.0007	1.420	0.494	0.822	0.040
14	7	Px	28	7.612	0.0007	1.408	0.449	0.766	0.041
14	7	Py	29	9.171	0.0007	1.560	0.461	0.911	0.043
14	7	UJ	54	10.417	0.0007	1.339	0.453	0.830	0.043
14	14	Rect	18	9.157	0.0007	2.181	0.441	1.144	0.039
14	14	Px	14	7.436	0.0007	1.489	0.442	1.123	0.040
14	14	Py	15	8.238	0.0007	1.838	0.447	1.168	0.041
14	14	UJ	18	9.157	0.0007	2.181	0.448	1.380	0.041

Table A.1 - Evaluation of *FLT*t error with LS method for all the possible simplified grids.

SAMPLING				(MZ) *FLT*t					
				Error evaluation		u_{lm} ANALYTIC		u_{lm} EXPERIMENTAL	
D [mm]	d [mm]	Grid	points [n°]	*FLT*t [µm]	t_{FLTt} [s]	u_{lm} [µm]	t_u [s]	u_{lm} [µm]	t_u [s]
0.35	0.35	Rect	17575	18.967	3.63	0.967	200.07	0.219	202.49
0.35	0.35	Px	17575	18.967	3.63	0.967	200.07	0.219	202.49
0.35	0.35	Py	17575	18.967	3.63	0.967	200.07	0.219	202.49
0.35	0.35	UJ	17575	18.967	3.63	0.967	200.07	0.219	202.49
0.7	0.35	Rect	13323	18.967	2.04	0.980	184.94	0.174	189.07
0.7	0.35	Px	8915	18.964	1.46	0.955	138.73	0.668	138.03
0.7	0.35	Py	8949	18.602	1.76	0.970	162.93	0.174	162.55
0.7	0.35	UJ	17575	18.967	2.08	0.967	197.68	0.203	196.86
0.7	0.7	Rect	4540	18.508	1.18	1.005	115.29	0.381	111.53
0.7	0.7	Px	4459	18.448	1.13	1.004	105.20	0.382	105.08
0.7	0.7	Py	4473	18.508	1.06	1.019	100.62	0.426	99.11
0.7	0.7	UJ	4540	18.508	1.18	0.992	114.29	0.387	111.63
3.5	0.35	Rect	3529	18.807	1.15	1.838	98.82	1.521	100.05
3.5	0.35	Px	1870	18.743	0.75	1.710	65.32	1.334	62.70
3.5	0.35	Py	1856	12.518	1.29	0.950	100.66	0.111	99.70
3.5	0.35	UJ	5089	18.872	1.50	1.556	125.59	1.219	125.27
3.5	0.7	Rect	1693	18.125	0.85	2.167	75.98	1.932	74.60
3.5	0.7	Px	933	17.977	0.59	1.718	53.16	1.780	52.26
3.5	0.7	Py	927	12.433	0.63	0.968	57.77	0.166	55.35
3.5	0.7	UJ	2405	18.240	1.07	1.796	90.08	1.223	88.50
3.5	3.5	Rect	196	11.217	0.42	0.982	31.87	0.262	31.66
3.5	3.5	Px	180	10.905	0.34	0.953	25.78	0.214	25.14
3.5	3.5	Py	183	10.874	0.40	1.004	29.01	0.209	28.35
3.5	3.5	UJ	196	11.217	0.42	0.991	32.24	0.259	31.48
7	0.35	Rect	1897	18.807	0.94	2.421	81.02	1.380	79.10
7	0.35	Px	1035	18.659	0.59	1.909	50.21	1.753	49.06
7	0.35	Py	917	10.975	0.81	0.954	64.30	0.168	62.63
7	0.35	UJ	2714	18.872	1.23	1.590	100.30	1.333	99.31
7	0.7	Rect	935	18.094	0.68	2.036	54.51	1.758	54.14
7	0.7	Px	517	17.370	0.47	2.097	40.65	1.764	39.26
7	0.7	Py	458	10.975	0.43	0.962	39.24	0.232	38.56
7	0.7	UJ	1334	18.240	0.92	1.926	69.92	1.888	68.14
7	3.5	Rect	150	10.899	0.33	1.015	24.78	0.308	24.02
7	3.5	Px	100	10.216	0.25	1.047	15.60	0.460	14.94
7	3.5	Py	90	9.914	0.21	1.306	15.17	0.452	14.02
7	3.5	UJ	196	11.217	0.42	0.985	31.94	0.253	30.99
7	7	Rect	54	9.718	0.13	1.085	8.85	0.402	8.08
7	7	Px	46	7.222	0.13	1.081	7.82	0.342	7.55
7	7	Py	48	8.021	0.15	1.016	10.90	0.327	9.82
7	7	UJ	54	9.718	0.13	1.096	9.16	0.543	8.68
14	0.35	Rect	1184	18.807	0.80	3.461	67.79	1.863	66.88
14	0.35	Px	631	18.659	0.46	3.271	41.15	1.930	40.13
14	0.35	Py	572	10.452	0.53	0.947	45.24	0.094	44.79
14	0.35	UJ	1576	18.872	0.95	1.921	82.45	1.860	80.12
14	0.7	Rect	590	18.094	0.54	3.078	45.11	2.688	44.55
14	0.7	Px	315	17.370	0.37	2.595	32.11	2.393	29.40
14	0.7	Py	286	10.450	0.31	0.953	27.88	0.137	26.78
14	0.7	UJ	786	18.240	0.66	2.302	52.14	2.651	51.19
14	3.5	Rect	106	10.899	0.29	1.037	21.37	0.424	20.48
14	3.5	Px	61	10.151	0.20	1.095	12.47	0.559	11.63
14	3.5	Py	56	9.575	0.15	1.439	10.43	0.546	9.86
14	3.5	UJ	136	11.191	0.32	1.038	25.69	0.353	24.99
14	7	Rect	46	9.718	0.13	1.050	9.21	0.449	8.57
14	7	Px	28	6.682	0.11	0.985	6.38	0.415	5.77
14	7	Py	29	7.839	0.09	1.009	6.26	0.436	5.61
14	7	UJ	54	9.718	0.14	1.069	9.24	0.483	8.61
14	14	Rect	18	9.024	0.06	1.819	3.71	0.753	3.21
14	14	Px	14	6.152	0.05	1.450	3.25	0.845	2.64
14	14	Py	15	7.280	0.06	1.539	3.64	0.732	3.01
14	14	UJ	18	9.024	0.06	1.448	3.83	0.884	3.30

Table A.2 - Evaluation of *FLT*t error with MZ method for all the possible simplified grids.

SAMPLING			MZ		u_{Im} An.	u_{Im} Exp.	LS		u_{Im} An.	u_{Im} Exp.
D [mm]	d [mm]	Grid	*FLT*t [µm]	u_{Mt}[µm]	u_M [µm]	u_M [µm]	*FLT*t [µm]	u_{Mt}[µm]	u_M [µm]	u_M [µm]
0.35	0.35	Rect	18.967	0.000	0.967	0.219	24.100	5.132	5.219	5.140
0.35	0.35	Px	18.967	0.000	0.967	0.219	24.100	5.132	5.219	5.140
0.35	0.35	Py	18.967	0.000	0.967	0.219	24.100	5.132	5.219	5.140
0.35	0.35	UJ	18.967	0.000	0.967	0.219	24.100	5.132	5.219	5.140
0.7	0.35	Rect	18.967	0.000	0.980	0.174	24.160	5.192	5.278	5.204
0.7	0.35	Px	18.964	0.003	0.955	0.668	24.028	5.061	5.149	5.118
0.7	0.35	Py	18.602	0.366	1.037	0.405	24.360	5.393	5.476	5.397
0.7	0.35	UJ	18.967	0.000	0.967	0.203	24.100	5.132	5.219	5.138
0.7	0.7	Rect	18.508	0.459	1.105	0.597	24.282	5.315	5.400	5.386
0.7	0.7	Px	18.448	0.519	1.130	0.644	24.073	5.106	5.195	5.153
0.7	0.7	Py	18.508	0.459	1.118	0.627	24.509	5.542	5.623	5.589
0.7	0.7	UJ	18.508	0.459	1.093	0.601	24.282	5.315	5.400	5.353
3.5	0.35	Rect	18.807	0.160	1.845	1.530	24.372	5.405	5.489	5.892
3.5	0.35	Px	18.743	0.224	1.725	1.353	23.734	4.767	4.861	5.286
3.5	0.35	Py	12.518	6.450	6.519	6.451	13.404	5.563	5.645	5.566
3.5	0.35	UJ	18.872	0.096	1.559	1.223	24.328	5.361	5.445	5.780
3.5	0.7	Rect	18.125	0.842	2.325	2.108	24.293	5.326	5.415	6.376
3.5	0.7	Px	17.977	0.990	1.983	2.037	23.630	4.663	4.769	5.614
3.5	0.7	Py	12.433	6.534	6.605	6.536	13.391	5.576	5.660	5.584
3.5	0.7	UJ	18.240	0.727	1.937	1.422	24.390	5.423	5.508	6.121
3.5	3.5	Rect	11.217	7.750	7.812	7.754	12.567	6.400	6.502	6.442
3.5	3.5	Px	10.905	8.062	8.118	8.065	12.641	6.326	6.416	6.373
3.5	3.5	Py	10.874	8.093	8.155	8.096	12.474	6.493	6.595	6.533
3.5	3.5	UJ	11.217	7.750	7.813	7.754	12.567	6.400	6.502	6.442
7	0.35	Rect	18.807	0.160	2.426	1.389	24.756	5.789	5.867	6.486
7	0.35	Px	18.659	0.309	1.934	1.780	23.601	4.633	4.732	5.288
7	0.35	Py	10.975	7.992	8.049	7.994	12.123	6.845	6.913	6.856
7	0.35	UJ	18.872	0.096	1.593	1.337	24.648	5.681	5.762	6.405
7	0.7	Rect	18.094	0.873	2.215	1.963	24.707	5.740	5.827	6.486
7	0.7	Px	17.370	1.597	2.636	2.380	23.440	4.473	4.591	5.507
7	0.7	Py	10.975	7.992	8.050	7.996	12.244	6.724	6.798	6.739
7	0.7	UJ	18.240	0.727	2.059	2.023	24.673	5.706	5.790	7.063
7	3.5	Rect	10.899	8.068	8.132	8.074	12.246	6.721	6.821	6.758
7	3.5	Px	10.216	8.751	8.813	8.763	11.814	7.153	7.234	7.190
7	3.5	Py	9.914	9.053	9.147	9.064	11.971	6.996	7.096	7.083
7	3.5	UJ	11.217	7.750	7.812	7.754	12.567	6.400	6.502	6.445
7	7	Rect	9.718	9.250	9.313	9.258	10.417	8.550	8.655	8.589
7	7	Px	7.222	11.745	11.795	11.750	8.390	10.577	10.643	10.608
7	7	Py	8.021	10.946	10.993	10.951	8.936	10.031	10.115	10.060
7	7	UJ	9.718	9.250	9.314	9.265	10.417	8.550	8.655	8.573
14	0.35	Rect	18.807	0.160	3.464	1.870	25.038	6.070	6.146	6.988
14	0.35	Px	18.659	0.309	3.285	1.954	23.542	4.575	4.678	5.607
14	0.35	Py	10.452	8.516	8.568	8.516	11.526	7.441	7.506	7.448
14	0.35	UJ	18.872	0.096	1.923	1.863	24.712	5.745	5.823	6.879
14	0.7	Rect	18.094	0.873	3.199	2.826	24.829	5.862	5.953	7.502
14	0.7	Px	17.370	1.597	3.047	2.877	23.234	4.267	4.403	6.155
14	0.7	Py	10.450	8.517	8.570	8.518	11.618	7.349	7.420	7.365
14	0.7	UJ	18.240	0.727	2.414	2.748	24.608	5.641	5.731	7.507
14	3.5	Rect	10.899	8.068	8.135	8.079	12.529	6.439	6.558	6.488
14	3.5	Px	10.151	8.816	8.884	8.834	11.299	7.669	7.752	7.706
14	3.5	Py	9.575	9.393	9.502	9.408	11.221	7.746	7.851	7.821
14	3.5	UJ	11.191	7.777	7.846	7.785	12.879	6.088	6.208	6.145
14	7	Rect	9.718	9.250	9.309	9.260	10.423	8.545	8.662	8.584
14	7	Px	6.682	12.285	12.325	12.292	7.612	11.355	11.442	11.381
14	7	Py	7.839	11.129	11.174	11.137	9.171	9.796	9.919	9.838
14	7	UJ	9.718	9.250	9.311	9.262	10.417	8.550	8.655	8.591
14	14	Rect	9.024	9.943	10.108	9.972	9.157	9.810	10.049	9.876
14	14	Px	6.152	12.815	12.897	12.843	7.436	11.531	11.627	11.585
14	14	Py	7.280	11.687	11.788	11.710	8.238	10.729	10.886	10.793
14	14	UJ	9.024	9.943	10.048	9.982	9.157	9.810	10.049	9.906

Table A.3 - Method and measurement uncertainty of all simplified verification operators.

Annex B - **Analysis of the LS uncertainty terms**

Starting from the formulation of the LS reference plane an analytical method has been defined for the assessment of implementation uncertainty in LS based verification processes (§3.5.1). The final equation for the assessment of LS uncertainty (3.4) is reported below in order to insert an identification number for each of its terms:

$$u_{Im}^2 = u_e^2 = \overbrace{\left(\frac{\partial\delta}{\partial x_1}u_{x_1}\right)^2}^{(1)} + \overbrace{\left(\frac{\partial\delta}{\partial x_2}u_{x_2}\right)^2}^{(2)} + \overbrace{\left(\frac{\partial\delta}{\partial y_1}u_{y_1}\right)^2}^{(3)} + \overbrace{\left(\frac{\partial\delta}{\partial y_2}u_{y_2}\right)^2}^{(4)} + \overbrace{\left(\frac{\partial\delta}{\partial z_1}u_{z_1}\right)^2}^{(5)} + \underbrace{\left(\frac{\partial\delta}{\partial z_2}u_{z_2}\right)^2}_{(6)} + \underbrace{\left(\frac{\partial\delta}{\partial a}u_a\right)^2}_{(7)} + \underbrace{\left(\frac{\partial\delta}{\partial b}u_b\right)^2}_{(8)} + \underbrace{2\frac{\partial\delta}{\partial a}\frac{\partial\delta}{\partial b}\rho_{ab}u_a u_b}_{(9)} \tag{B.1}$$

The partial derivatives of equation (B.1) are the sensitivity coefficients that are responsible of weighting the effect of each input uncertainty (the uncertainty affecting the measurement of sampling points, in terms 1 to 6, as well as the robustness of the form fitting algorithm, in terms 7 to 9) on the overall implementation uncertainty. Considering the function which describe the form error δ, equation (3.3), the partial derivatives of equation (B.1) are:

- $$\frac{\partial\delta}{\partial x_1} = -\frac{\partial\delta}{\partial x_2} = \frac{-a}{\sqrt{1+a^2+b^2}} \tag{B.2}$$
- $$\frac{\partial\delta}{\partial y_1} = -\frac{\partial\delta}{\partial y_2} = \frac{-b}{\sqrt{1+a^2+b^2}} \tag{B.3}$$
- $$\frac{\partial\delta}{\partial z_1} = -\frac{\partial\delta}{\partial z_2} = \frac{-1}{\sqrt{1+a^2+b^2}} \tag{B.4}$$
- $$\frac{\partial\delta}{\partial a} = \frac{-x_1+x_2}{\sqrt{1+a^2+b^2}} - \frac{a\left[\,z_1-z_2-a\;\;x_1-x_2\;\;-b\;\;y_1-y_2\,\right]}{1+a^2+b^{2\;\;3/2}} \tag{B.5}$$
- $$\frac{\partial\delta}{\partial b} = \frac{-y_1+y_2}{\sqrt{1+a^2+b^2}} - \frac{b\left[\,z_1-z_2-a\;\;x_1-x_2\;\;-b\;\;y_1-y_2\,\right]}{1+a^2+b^{2\;\;3/2}} \tag{B.6}$$

The values of sensitivity coefficients have been registered, for each of the 60 verification operators, and reported in Table B.1. It is easy to notice how the most important coefficients are those associated with the stability of the reference plane (terms 7 to 9 of equation (B.1)). Soon after these, in order of relevance, we find the sensitivity coefficients associated with the uncertainty on the *z* coordinate of measurement points (terms 5 and 6 of equation (B.1)). These coefficients are, in average, six orders of magnitude larger than those associated with

the uncertainty on the *x* and *y* coordinates of measurement points (terms 1 to 4 of equation (B.1)). This is correct as the reference frame used for measuring the flatness surface is normal to it and flatness deviation, at a first instance, corresponds to the variability of the z coordinate of the points measured on the surface.

Even if sensitivity coefficients are the lowest, the uncertainties associated with the sampling of measurement points (terms u_{xi}, u_{yi} and u_{zi} in equation (B.1)) are the largest uncertainty inputs: MPE/6 on each coordinate of measurement points, independently from the sample size (see variances reported in Table B.2). On the other hand, the uncertainties associated with the stability of the LS reference plane (u_a, u_b and $\rho_{ab}u_a u_b$ in equation (B.1)) are several orders of magnitude lower than the measurement uncertainty on sampling points, but sensitive to the sample size. Looking at Table B.2 it is easy to notice that u_a^2 and u_b^2 grow of three orders of magnitude, going from the largest to the smallest analyzed sample, while $\rho_{ab}u_a u_b$ of six orders of magnitude.

However, in order to understand the effect of input uncertainties on the global assessment of LS implementation uncertainty, these have to be considered together with the relative sensitivity coefficient. Therefore, each term of equation (B.1) has been reported in Table B.3. From this table it is possible to notice that the contribution from the measurement uncertainty on sampling points is nearly constant and defined, almost entirely, by the uncertainty on the *z* coordinate. On the other hand the contribution from the stability of the LS reference plane decreases hyperbolically with the increase of sample size. In order to better understand the effect of these different sources of uncertainty, the contribution from measurement uncertainty in sampling operations (sum of terms from 1 to 6 in equation (B.1)) has been plotted against that from the stability of the LS reference plane (sum of terms from 7 to 9 in equation (B.1)); see Figure B.1. This figure clearly shows how the former overcomes the latter when sample size is larger than 50 points about, and explain the behaviour observed in Figure 3.11.

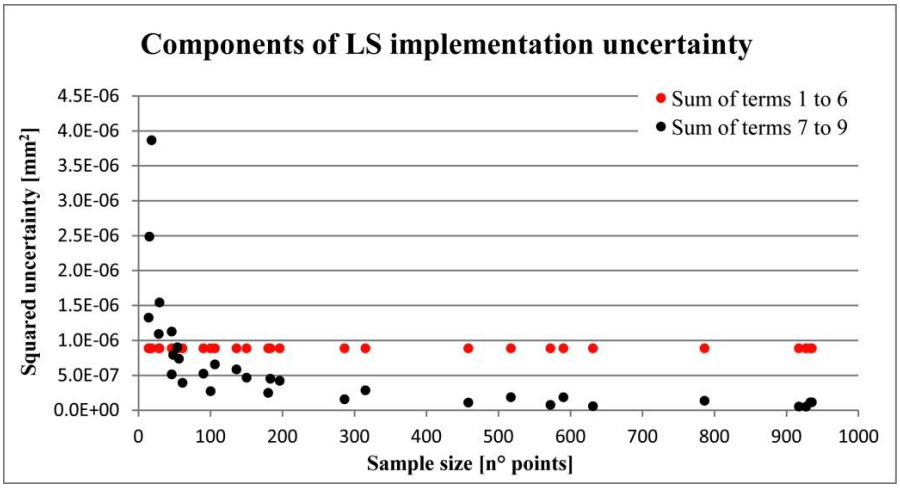

Figure B.1 - Comparison of the sources of uncertainty involved in equation (B.1). The effect of measurement uncertainty in sampling operations (red series) overcomes the effect of LS reference plane stability (black series) for samples larger than 50 points about.

SAMPLING			PARTIAL DERIVATIVES (sensitivity coefficients)								
D [mm]	d [mm]	Grid	$d\delta/dx_1$	$d\delta/dx_2$	$d\delta/dy_1$	$d\delta/dy_2$	$d\delta/dz_1$	$d\delta/dz_2$	$d\delta/da$	$d\delta/db$	$2*d\delta/da*d\delta/db$
0.35	0.35	Rect	8.5E-05	-8.5E-05	-7.8E-06	7.8E-06	0.999999996	-0.999999996	-19.599	55.648	-2181.3208
0.35	0.35	Px	8.5E-05	-8.5E-05	-7.8E-06	7.8E-06	0.999999996	-0.999999996	-19.599	55.648	-2181.3208
0.35	0.35	Py	8.5E-05	-8.5E-05	-7.8E-06	7.8E-06	0.999999996	-0.999999996	-19.599	55.648	-2181.3208
0.35	0.35	UJ	8.5E-05	-8.5E-05	-7.8E-06	7.8E-06	0.999999996	-0.999999996	-19.599	55.648	-2181.3208
0.7	0.35	Rect	8.6E-05	-8.6E-05	-8.4E-06	8.4E-06	0.999999996	-0.999999996	-19.599	55.648	-2181.3208
0.7	0.35	Px	8.4E-05	-8.4E-05	-6.7E-06	6.7E-06	0.999999996	-0.999999996	-19.599	55.298	-2167.6346
0.7	0.35	Py	8.9E-05	-8.9E-05	-1.1E-05	1.1E-05	0.999999996	-0.999999996	-19.599	55.648	-2181.3208
0.7	0.35	UJ	8.5E-05	-8.5E-05	-7.8E-06	7.8E-06	0.999999996	-0.999999996	-19.599	55.648	-2181.3208
0.7	0.7	Rect	8.9E-05	-8.9E-05	-9.7E-06	9.7E-06	0.999999996	-0.999999996	-19.599	55.298	-2167.6346
0.7	0.7	Px	7.9E-05	-7.9E-05	-9.6E-06	9.6E-06	0.999999997	-0.999999997	-19.599	55.298	-2167.6346
0.7	0.7	Py	8.9E-05	-8.9E-05	-1.4E-05	1.4E-05	0.999999996	-0.999999996	-19.599	55.298	-2167.6346
0.7	0.7	UJ	8.9E-05	-8.9E-05	-9.7E-06	9.7E-06	0.999999996	-0.999999996	-19.599	55.298	-2167.6346
3.5	0.35	Rect	9.8E-05	-9.8E-05	-8.9E-06	8.9E-06	0.999999995	-0.999999995	-22.399	52.848	-2367.4844
3.5	0.35	Px	8.2E-05	-8.2E-05	-4.9E-06	4.9E-06	0.999999997	-0.999999997	-28.354	-0.008	0.4650
3.5	0.35	Py	1.1E-04	-1.1E-04	-1.4E-05	1.4E-05	0.999999993	-0.999999993	-20.999	29.750	-1249.4117
3.5	0.35	UJ	9.4E-05	-9.4E-05	-8.8E-06	8.8E-06	0.999999996	-0.999999996	-19.599	55.298	-2167.6346
3.5	0.7	Rect	9.9E-05	-9.9E-05	-9.0E-06	9.0E-06	0.999999995	-0.999999995	-22.399	53.897	-2414.4712
3.5	0.7	Px	7.7E-05	-7.7E-05	-5.8E-06	5.8E-06	0.999999997	-0.999999997	-21.000	55.648	-2337.2338
3.5	0.7	Py	1.1E-04	-1.1E-04	-1.7E-05	1.7E-05	0.999999994	-0.999999994	-20.999	30.799	-1293.4652
3.5	0.7	UJ	9.5E-05	-9.5E-05	-9.7E-06	9.7E-06	0.999999995	-0.999999995	-19.599	55.298	-2167.6346
3.5	3.5	Rect	1.1E-04	-1.1E-04	-8.9E-06	8.9E-06	0.999999994	-0.999999994	-21.000	45.149	-1896.2627
3.5	3.5	Px	6.5E-05	-6.5E-05	-9.5E-06	9.5E-06	0.999999998	-0.999999998	20.999	31.148	1308.1745
3.5	3.5	Py	1.1E-04	-1.1E-04	-3.1E-05	3.1E-05	0.999999993	-0.999999993	-24.499	42.001	-2057.9935
3.5	3.5	UJ	1.1E-04	-1.1E-04	-8.9E-06	8.9E-06	0.999999994	-0.999999994	-21.000	45.149	-1896.2627
7	0.35	Rect	1.2E-04	-1.2E-04	-9.9E-06	9.9E-06	0.999999993	-0.999999993	-28.354	-0.008	0.4650
7	0.35	Px	7.8E-05	-7.8E-05	-4.2E-06	4.2E-06	0.999999997	-0.999999997	-28.354	-0.008	0.4650
7	0.35	Py	1.6E-04	-1.6E-04	-1.8E-05	1.8E-05	0.999999987	-0.999999987	-21.000	33.600	-1411.2023
7	0.35	UJ	1.1E-04	-1.1E-04	-1.0E-05	1.0E-05	0.999999994	-0.999999994	-22.756	52.142	-2373.0492
7	0.7	Rect	1.2E-04	-1.2E-04	-9.8E-06	9.8E-06	0.999999993	-0.999999993	-21.000	55.648	-2337.2337
7	0.7	Px	7.0E-05	-7.0E-05	-4.8E-06	4.8E-06	0.999999998	-0.999999998	-21.000	55.648	-2337.2339
7	0.7	Py	1.6E-04	-1.6E-04	-2.1E-05	2.1E-05	0.999999986	-0.999999986	-21.000	33.600	-1411.2023
7	0.7	UJ	1.1E-04	-1.1E-04	-1.1E-05	1.1E-05	0.999999994	-0.999999994	-19.599	55.298	-2167.6345
7	3.5	Rect	1.3E-04	-1.3E-04	-9.4E-06	9.4E-06	0.999999992	-0.999999992	-21.001	41.649	-1749.3577
7	3.5	Px	5.9E-05	-5.9E-05	-7.3E-06	7.3E-06	0.999999998	-0.999999998	21.000	20.650	867.3165
7	3.5	Py	1.7E-04	-1.7E-04	-3.8E-05	3.8E-05	0.999999986	-0.999999986	-20.999	31.502	-1323.0103
7	3.5	UJ	1.1E-04	-1.1E-04	-8.9E-06	8.9E-06	0.999999994	-0.999999994	-21.000	45.149	-1896.2627
7	7	Rect	1.5E-04	-1.5E-04	-8.3E-06	8.3E-06	0.999999989	-0.999999989	-20.999	34.650	-1455.2333
7	7	Px	4.3E-05	-4.3E-05	-1.1E-05	1.1E-05	0.999999999	-0.999999999	-14.000	34.651	-970.2710
7	7	Py	1.5E-04	-1.5E-04	-5.2E-05	5.2E-05	0.999999987	-0.999999987	-28.000	-20.999	1175.9831
7	7	UJ	1.5E-04	-1.5E-04	-8.3E-06	8.3E-06	0.999999989	-0.999999989	-20.999	34.650	-1455.2333
14	0.35	Rect	1.3E-04	-1.3E-04	-9.5E-06	9.5E-06	0.999999992	-0.999999992	-28.354	-0.008	0.4650
14	0.35	Px	7.6E-05	-7.6E-05	-3.3E-06	3.3E-06	0.999999997	-0.999999997	-28.354	-0.008	0.4650
14	0.35	Py	1.7E-04	-1.7E-04	-2.1E-05	2.1E-05	0.999999986	-0.999999986	-14.001	33.598	-940.8435
14	0.35	UJ	1.2E-04	-1.2E-04	-6.8E-06	6.8E-06	0.999999993	-0.999999993	-28.354	-0.008	0.4650
14	0.7	Rect	1.3E-04	-1.3E-04	-8.2E-06	8.2E-06	0.999999992	-0.999999992	-21.000	55.648	-2337.2337
14	0.7	Px	6.9E-05	-6.9E-05	-1.7E-06	1.7E-06	0.999999998	-0.999999998	-21.000	55.648	-2337.2339
14	0.7	Py	1.7E-04	-1.7E-04	-2.4E-05	2.4E-05	0.999999986	-0.999999986	-14.001	33.598	-940.8435
14	0.7	UJ	1.2E-04	-1.2E-04	-5.7E-06	5.7E-06	0.999999993	-0.999999993	-19.599	55.298	-2167.6345
14	3.5	Rect	1.4E-04	-1.4E-04	-1.1E-05	1.1E-05	0.999999991	-0.999999991	-21.001	41.649	-1749.3576
14	3.5	Px	6.6E-05	-6.6E-05	-6.2E-06	6.2E-06	0.999999998	-0.999999998	21.001	13.650	573.3387
14	3.5	Py	1.7E-04	-1.7E-04	-3.8E-05	3.8E-05	0.999999985	-0.999999985	-14.000	31.500	-882.0313
14	3.5	UJ	1.3E-04	-1.3E-04	-9.8E-06	9.8E-06	0.999999992	-0.999999992	-21.000	45.149	-1896.2626
14	7	Rect	1.5E-04	-1.5E-04	-7.4E-06	7.4E-06	0.999999989	-0.999999989	-20.999	34.650	-1455.2333
14	7	Px	4.7E-05	-4.7E-05	-8.6E-06	8.6E-06	0.999999999	-0.999999999	-14.002	41.652	-1166.4031
14	7	Py	1.6E-04	-1.6E-04	-4.7E-05	4.7E-05	0.999999987	-0.999999987	-28.000	-20.999	1175.9831
14	7	UJ	1.5E-04	-1.5E-04	-8.3E-06	8.3E-06	0.999999989	-0.999999989	-20.999	34.650	-1455.2333
14	14	Rect	1.5E-04	-1.5E-04	-5.6E-06	5.6E-06	0.999999989	-0.999999989	13.656	-41.991	-1146.9055
14	14	Px	-3.1E-05	3.1E-05	-1.1E-05	1.1E-05	0.999999999	-0.999999999	14.000	27.649	774.1997
14	14	Py	1.5E-04	-1.5E-04	-7.3E-05	7.3E-05	0.999999986	-0.999999986	-28.002	-13.999	783.9804
14	14	UJ	1.5E-04	-1.5E-04	-5.6E-06	5.6E-06	0.999999989	-0.999999989	13.656	-41.991	-1146.9055

Table B.1 - Sensitivity coefficients for the analytic assessment of LS implementation uncertainty.

SAMPLING				Measurement variance and variance of the LS model coefficients								
D [mm]	d [mm]	Grid	n°points	u_{x1}^2	u_{x2}^2	u_{y1}^2	u_{y2}^2	u_{z1}^2	u_{z2}^2	u_a^2	u_b^2	$\rho_{ab}u_a u_b$
0.35	0.35	Rect	17575	4.4E-07	4.4E-07	4.4E-07	4.4E-07	4.4E-07	4.4E-07	2.4E-12	1.7E-12	-7.0E-16
0.35	0.35	Px	17575	4.4E-07	4.4E-07	4.4E-07	4.4E-07	4.4E-07	4.4E-07	2.4E-12	1.7E-12	-7.0E-16
0.35	0.35	Py	17575	4.4E-07	4.4E-07	4.4E-07	4.4E-07	4.4E-07	4.4E-07	2.4E-12	1.7E-12	-7.0E-16
0.35	0.35	UJ	17575	4.4E-07	4.4E-07	4.4E-07	4.4E-07	4.4E-07	4.4E-07	2.4E-12	1.7E-12	-7.0E-16
0.7	0.35	Rect	13323	4.4E-07	4.4E-07	4.4E-07	4.4E-07	4.4E-07	4.4E-07	3.2E-12	2.3E-12	-2.9E-16
0.7	0.35	Px	8915	4.4E-07	4.4E-07	4.4E-07	4.4E-07	4.4E-07	4.4E-07	4.8E-12	3.3E-12	-1.7E-15
0.7	0.35	Py	8949	4.4E-07	4.4E-07	4.4E-07	4.4E-07	4.4E-07	4.4E-07	4.8E-12	3.5E-12	-4.6E-16
0.7	0.35	UJ	17575	4.4E-07	4.4E-07	4.4E-07	4.4E-07	4.4E-07	4.4E-07	2.4E-12	1.7E-12	-7.0E-16
0.7	0.7	Rect	4540	4.4E-07	4.4E-07	4.4E-07	4.4E-07	4.4E-07	4.4E-07	9.6E-12	6.8E-12	-1.3E-14
0.7	0.7	Px	4459	4.4E-07	4.4E-07	4.4E-07	4.4E-07	4.4E-07	4.4E-07	9.8E-12	6.7E-12	-7.1E-15
0.7	0.7	Py	4473	4.4E-07	4.4E-07	4.4E-07	4.4E-07	4.4E-07	4.4E-07	9.6E-12	7.1E-12	-8.0E-15
0.7	0.7	UJ	4540	4.4E-07	4.4E-07	4.4E-07	4.4E-07	4.4E-07	4.4E-07	9.6E-12	6.8E-12	-1.3E-14
3.5	0.35	Rect	3529	4.4E-07	4.4E-07	4.4E-07	4.4E-07	4.4E-07	4.4E-07	1.2E-11	8.7E-12	-7.3E-15
3.5	0.35	Px	1870	4.4E-07	4.4E-07	4.4E-07	4.4E-07	4.4E-07	4.4E-07	2.3E-11	1.5E-11	-1.9E-14
3.5	0.35	Py	1856	4.4E-07	4.4E-07	4.4E-07	4.4E-07	4.4E-07	4.4E-07	2.3E-11	1.8E-11	9.0E-15
3.5	0.35	UJ	5089	4.4E-07	4.4E-07	4.4E-07	4.4E-07	4.4E-07	4.4E-07	8.4E-12	6.0E-12	-1.9E-14
3.5	0.7	Rect	1693	4.4E-07	4.4E-07	4.4E-07	4.4E-07	4.4E-07	4.4E-07	2.6E-11	1.8E-11	-4.3E-14
3.5	0.7	Px	933	4.4E-07	4.4E-07	4.4E-07	4.4E-07	4.4E-07	4.4E-07	4.7E-11	3.0E-11	-5.2E-17
3.5	0.7	Py	927	4.4E-07	4.4E-07	4.4E-07	4.4E-07	4.4E-07	4.4E-07	4.6E-11	3.5E-11	-3.8E-14
3.5	0.7	UJ	2405	4.4E-07	4.4E-07	4.4E-07	4.4E-07	4.4E-07	4.4E-07	1.8E-11	1.3E-11	-8.5E-14
3.5	3.5	Rect	196	4.4E-07	4.4E-07	4.4E-07	4.4E-07	4.4E-07	4.4E-07	2.2E-10	1.6E-10	-4.3E-12
3.5	3.5	Px	180	4.4E-07	4.4E-07	4.4E-07	4.4E-07	4.4E-07	4.4E-07	2.5E-10	1.5E-10	-1.5E-12
3.5	3.5	Py	183	4.4E-07	4.4E-07	4.4E-07	4.4E-07	4.4E-07	4.4E-07	2.2E-10	1.8E-10	-1.7E-12
3.5	3.5	UJ	196	4.4E-07	4.4E-07	4.4E-07	4.4E-07	4.4E-07	4.4E-07	2.2E-10	1.6E-10	-4.3E-12
7	0.35	Rect	1897	4.4E-07	4.4E-07	4.4E-07	4.4E-07	4.4E-07	4.4E-07	2.3E-11	1.5E-11	-5.4E-14
7	0.35	Px	1035	4.4E-07	4.4E-07	4.4E-07	4.4E-07	4.4E-07	4.4E-07	4.2E-11	2.4E-11	-5.0E-14
7	0.35	Py	917	4.4E-07	4.4E-07	4.4E-07	4.4E-07	4.4E-07	4.4E-07	4.3E-11	3.2E-11	3.1E-14
7	0.35	UJ	2714	4.4E-07	4.4E-07	4.4E-07	4.4E-07	4.4E-07	4.4E-07	1.6E-11	1.1E-11	6.4E-15
7	0.7	Rect	935	4.4E-07	4.4E-07	4.4E-07	4.4E-07	4.4E-07	4.4E-07	4.7E-11	3.1E-11	-3.0E-13
7	0.7	Px	517	4.4E-07	4.4E-07	4.4E-07	4.4E-07	4.4E-07	4.4E-07	8.6E-11	4.9E-11	8.6E-15
7	0.7	Py	458	4.4E-07	4.4E-07	4.4E-07	4.4E-07	4.4E-07	4.4E-07	8.8E-11	6.4E-11	-5.4E-13
7	0.7	UJ	1334	4.4E-07	4.4E-07	4.4E-07	4.4E-07	4.4E-07	4.4E-07	3.2E-11	2.2E-11	-1.5E-13
7	3.5	Rect	150	4.4E-07	4.4E-07	4.4E-07	4.4E-07	4.4E-07	4.4E-07	2.9E-10	1.9E-10	-9.1E-12
7	3.5	Px	100	4.4E-07	4.4E-07	4.4E-07	4.4E-07	4.4E-07	4.4E-07	4.2E-10	2.1E-10	9.2E-15
7	3.5	Py	90	4.4E-07	4.4E-07	4.4E-07	4.4E-07	4.4E-07	4.4E-07	4.2E-10	3.2E-10	-1.3E-11
7	3.5	UJ	196	4.4E-07	4.4E-07	4.4E-07	4.4E-07	4.4E-07	4.4E-07	2.2E-10	1.6E-10	-4.3E-12
7	7	Rect	54	4.4E-07	4.4E-07	4.4E-07	4.4E-07	4.4E-07	4.4E-07	7.5E-10	4.5E-10	-2.5E-11
7	7	Px	46	4.4E-07	4.4E-07	4.4E-07	4.4E-07	4.4E-07	4.4E-07	7.4E-10	3.1E-10	4.5E-14
7	7	Py	48	4.4E-07	4.4E-07	4.4E-07	4.4E-07	4.4E-07	4.4E-07	6.9E-10	5.4E-10	1.2E-11
7	7	UJ	54	4.4E-07	4.4E-07	4.4E-07	4.4E-07	4.4E-07	4.4E-07	7.5E-10	4.5E-10	-2.5E-11
14	0.35	Rect	1184	4.4E-07	4.4E-07	4.4E-07	4.4E-07	4.4E-07	4.4E-07	3.9E-11	2.4E-11	-6.2E-14
14	0.35	Px	631	4.4E-07	4.4E-07	4.4E-07	4.4E-07	4.4E-07	4.4E-07	7.5E-11	3.5E-11	-3.1E-15
14	0.35	Py	572	4.4E-07	4.4E-07	4.4E-07	4.4E-07	4.4E-07	4.4E-07	6.8E-11	5.8E-11	-9.8E-15
14	0.35	UJ	1576	4.4E-07	4.4E-07	4.4E-07	4.4E-07	4.4E-07	4.4E-07	2.8E-11	1.9E-11	-2.9E-15
14	0.7	Rect	590	4.4E-07	4.4E-07	4.4E-07	4.4E-07	4.4E-07	4.4E-07	7.8E-11	4.9E-11	-5.0E-13
14	0.7	Px	315	4.4E-07	4.4E-07	4.4E-07	4.4E-07	4.4E-07	4.4E-07	1.5E-10	7.1E-11	-2.2E-16
14	0.7	Py	286	4.4E-07	4.4E-07	4.4E-07	4.4E-07	4.4E-07	4.4E-07	1.4E-10	1.2E-10	-6.7E-13
14	0.7	UJ	786	4.4E-07	4.4E-07	4.4E-07	4.4E-07	4.4E-07	4.4E-07	5.7E-11	3.8E-11	-4.0E-13
14	3.5	Rect	106	4.4E-07	4.4E-07	4.4E-07	4.4E-07	4.4E-07	4.4E-07	4.2E-10	2.6E-10	-1.2E-11
14	3.5	Px	61	4.4E-07	4.4E-07	4.4E-07	4.4E-07	4.4E-07	4.4E-07	7.6E-10	3.3E-10	-1.6E-14
14	3.5	Py	56	4.4E-07	4.4E-07	4.4E-07	4.4E-07	4.4E-07	4.4E-07	6.8E-10	6.0E-10	-1.5E-11
14	3.5	UJ	136	4.4E-07	4.4E-07	4.4E-07	4.4E-07	4.4E-07	4.4E-07	3.2E-10	2.1E-10	-8.0E-12
14	7	Rect	46	4.4E-07	4.4E-07	4.4E-07	4.4E-07	4.4E-07	4.4E-07	9.4E-10	5.5E-10	-3.3E-11
14	7	Px	28	4.4E-07	4.4E-07	4.4E-07	4.4E-07	4.4E-07	4.4E-07	1.3E-09	4.8E-10	-6.0E-15
14	7	Py	29	4.4E-07	4.4E-07	4.4E-07	4.4E-07	4.4E-07	4.4E-07	1.3E-09	1.2E-09	3.2E-11
14	7	UJ	54	4.4E-07	4.4E-07	4.4E-07	4.4E-07	4.4E-07	4.4E-07	7.5E-10	4.5E-10	-2.5E-11
14	14	Rect	18	4.4E-07	4.4E-07	4.4E-07	4.4E-07	4.4E-07	4.4E-07	2.8E-09	1.7E-09	-2.4E-10
14	14	Px	14	4.4E-07	4.4E-07	4.4E-07	4.4E-07	4.4E-07	4.4E-07	2.9E-09	9.9E-10	7.0E-15
14	14	Py	15	4.4E-07	4.4E-07	4.4E-07	4.4E-07	4.4E-07	4.4E-07	2.5E-09	2.5E-09	3.3E-11
14	14	UJ	18	4.4E-07	4.4E-07	4.4E-07	4.4E-07	4.4E-07	4.4E-07	2.8E-09	1.7E-09	-2.4E-10

Table B.2 - Terms of uncertainty (variances) concurring to the LS implementation uncertainty.

SAMPLING				Uncertainty terms from equation (B.1)								
D [mm]	d [mm]	Grid	n°punti	(1)	(2)	(3)	(4)	(5)	(6)	(7)	(8)	(9)
0.35	0.35	Rect	17575	3.2E-15	3.2E-15	2.7E-17	2.7E-17	4.4E-07	4.4E-07	9.3E-10	5.3E-09	1.5E-12
0.35	0.35	Px	17575	3.2E-15	3.2E-15	2.7E-17	2.7E-17	4.4E-07	4.4E-07	9.3E-10	5.3E-09	1.5E-12
0.35	0.35	Py	17575	3.2E-15	3.2E-15	2.7E-17	2.7E-17	4.4E-07	4.4E-07	9.3E-10	5.3E-09	1.5E-12
0.35	0.35	UJ	17575	3.2E-15	3.2E-15	2.7E-17	2.7E-17	4.4E-07	4.4E-07	9.3E-10	5.3E-09	1.5E-12
0.7	0.35	Rect	13323	3.3E-15	3.3E-15	3.1E-17	3.1E-17	4.4E-07	4.4E-07	1.2E-09	7.1E-09	6.3E-13
0.7	0.35	Px	8915	3.2E-15	3.2E-15	2.0E-17	2.0E-17	4.4E-07	4.4E-07	1.9E-09	1.0E-08	3.6E-12
0.7	0.35	Py	8949	3.6E-15	3.6E-15	5.3E-17	5.3E-17	4.4E-07	4.4E-07	1.8E-09	1.1E-08	1.0E-12
0.7	0.35	UJ	17575	3.2E-15	3.2E-15	2.7E-17	2.7E-17	4.4E-07	4.4E-07	9.3E-10	5.3E-09	1.5E-12
0.7	0.7	Rect	4540	3.5E-15	3.5E-15	4.2E-17	4.2E-17	4.4E-07	4.4E-07	3.7E-09	2.1E-08	2.8E-11
0.7	0.7	Px	4459	2.8E-15	2.8E-15	4.1E-17	4.1E-17	4.4E-07	4.4E-07	3.8E-09	2.1E-08	1.5E-11
0.7	0.7	Py	4473	3.5E-15	3.5E-15	8.3E-17	8.3E-17	4.4E-07	4.4E-07	3.7E-09	2.2E-08	1.7E-11
0.7	0.7	UJ	4540	3.5E-15	3.5E-15	4.2E-17	4.2E-17	4.4E-07	4.4E-07	3.7E-09	2.1E-08	2.8E-11
3.5	0.35	Rect	3529	4.3E-15	4.3E-15	3.5E-17	3.5E-17	4.4E-07	4.4E-07	6.2E-09	2.4E-08	1.7E-11
3.5	0.35	Px	1870	3.0E-15	3.0E-15	1.1E-17	1.1E-17	4.4E-07	4.4E-07	1.9E-08	1.0E-15	-8.6E-15
3.5	0.35	Py	1856	5.7E-15	5.7E-15	8.8E-17	8.8E-17	4.4E-07	4.4E-07	1.0E-08	1.6E-08	-1.1E-11
3.5	0.35	UJ	5089	3.9E-15	3.9E-15	3.5E-17	3.5E-17	4.4E-07	4.4E-07	3.2E-09	1.8E-08	4.2E-11
3.5	0.7	Rect	1693	4.3E-15	4.3E-15	3.6E-17	3.6E-17	4.4E-07	4.4E-07	1.3E-08	5.3E-08	1.0E-10
3.5	0.7	Px	933	2.6E-15	2.6E-15	1.5E-17	1.5E-17	4.4E-07	4.4E-07	2.1E-08	9.4E-08	1.2E-13
3.5	0.7	Py	927	5.6E-15	5.6E-15	1.3E-16	1.3E-16	4.4E-07	4.4E-07	2.0E-08	3.3E-08	4.9E-11
3.5	0.7	UJ	2405	4.0E-15	4.0E-15	4.1E-17	4.1E-17	4.4E-07	4.4E-07	6.9E-09	3.9E-08	1.8E-10
3.5	3.5	Rect	196	5.6E-15	5.6E-15	3.6E-17	3.6E-17	4.4E-07	4.4E-07	9.8E-08	3.2E-07	8.2E-09
3.5	3.5	Px	180	1.9E-15	1.9E-15	4.0E-17	4.0E-17	4.4E-07	4.4E-07	1.1E-07	1.4E-07	-2.0E-09
3.5	3.5	Py	183	5.7E-15	5.7E-15	4.2E-16	4.2E-16	4.4E-07	4.4E-07	1.3E-07	3.2E-07	3.6E-09
3.5	3.5	UJ	196	5.6E-15	5.6E-15	3.6E-17	3.6E-17	4.4E-07	4.4E-07	9.8E-08	3.2E-07	8.2E-09
7	0.35	Rect	1897	6.2E-15	6.2E-15	4.4E-17	4.4E-17	4.4E-07	4.4E-07	1.8E-08	9.9E-16	-2.5E-14
7	0.35	Px	1035	2.7E-15	2.7E-15	7.8E-18	7.8E-18	4.4E-07	4.4E-07	3.4E-08	1.6E-15	-2.3E-14
7	0.35	Py	917	1.2E-14	1.2E-14	1.5E-16	1.5E-16	4.4E-07	4.4E-07	1.9E-08	3.6E-08	-4.3E-11
7	0.35	UJ	2714	5.0E-15	5.0E-15	4.6E-17	4.6E-17	4.4E-07	4.4E-07	8.1E-09	2.9E-08	-1.5E-11
7	0.7	Rect	935	6.1E-15	6.1E-15	4.2E-17	4.2E-17	4.4E-07	4.4E-07	2.1E-08	9.5E-08	7.0E-10
7	0.7	Px	517	2.2E-15	2.2E-15	1.0E-17	1.0E-17	4.4E-07	4.4E-07	3.8E-08	1.5E-07	-2.0E-11
7	0.7	Py	458	1.2E-14	1.2E-14	2.0E-16	2.0E-16	4.4E-07	4.4E-07	3.9E-08	7.3E-08	7.6E-10
7	0.7	UJ	1334	5.0E-15	5.0E-15	5.2E-17	5.2E-17	4.4E-07	4.4E-07	1.2E-08	6.8E-08	3.2E-10
7	3.5	Rect	150	7.1E-15	7.1E-15	3.9E-17	3.9E-17	4.4E-07	4.4E-07	1.3E-07	3.3E-07	1.6E-08
7	3.5	Px	100	1.5E-15	1.5E-15	2.3E-17	2.3E-17	4.4E-07	4.4E-07	1.8E-07	9.2E-08	8.0E-12
7	3.5	Py	90	1.2E-14	1.2E-14	6.4E-16	6.4E-16	4.4E-07	4.4E-07	1.9E-07	3.2E-07	1.7E-08
7	3.5	UJ	196	5.6E-15	5.6E-15	3.6E-17	3.6E-17	4.4E-07	4.4E-07	9.8E-08	3.2E-07	8.2E-09
7	7	Rect	54	9.9E-15	9.9E-15	3.0E-17	3.0E-17	4.4E-07	4.4E-07	3.3E-07	5.4E-07	3.6E-08
7	7	Px	46	8.3E-16	8.3E-16	5.5E-17	5.5E-17	4.4E-07	4.4E-07	1.4E-07	3.7E-07	-4.3E-11
7	7	Py	48	1.0E-14	1.0E-14	1.2E-15	1.2E-15	4.4E-07	4.4E-07	5.4E-07	2.4E-07	1.4E-08
7	7	UJ	54	9.9E-15	9.9E-15	3.0E-17	3.0E-17	4.4E-07	4.4E-07	3.3E-07	5.4E-07	3.6E-08
14	0.35	Rect	1184	7.3E-15	7.3E-15	4.1E-17	4.1E-17	4.4E-07	4.4E-07	3.1E-08	1.6E-15	-2.9E-14
14	0.35	Px	631	2.5E-15	2.5E-15	4.7E-18	4.7E-18	4.4E-07	4.4E-07	6.0E-08	2.4E-15	-1.4E-15
14	0.35	Py	572	1.2E-14	1.2E-14	2.0E-16	2.0E-16	4.4E-07	4.4E-07	1.3E-08	6.6E-08	9.2E-12
14	0.35	UJ	1576	6.1E-15	6.1E-15	2.0E-17	2.0E-17	4.4E-07	4.4E-07	2.3E-08	1.2E-15	-1.4E-15
14	0.7	Rect	590	7.2E-15	7.2E-15	3.0E-17	3.0E-17	4.4E-07	4.4E-07	3.4E-08	1.5E-07	1.2E-09
14	0.7	Px	315	2.1E-15	2.1E-15	1.2E-18	1.2E-18	4.4E-07	4.4E-07	6.7E-08	2.2E-07	5.2E-13
14	0.7	Py	286	1.2E-14	1.2E-14	2.5E-16	2.5E-16	4.4E-07	4.4E-07	2.7E-08	1.3E-07	6.3E-10
14	0.7	UJ	786	6.1E-15	6.1E-15	1.4E-17	1.4E-17	4.4E-07	4.4E-07	2.2E-08	1.2E-07	8.7E-10
14	3.5	Rect	106	8.4E-15	8.4E-15	5.1E-17	5.1E-17	4.4E-07	4.4E-07	1.8E-07	4.5E-07	2.2E-08
14	3.5	Px	61	1.9E-15	1.9E-15	1.7E-17	1.7E-17	4.4E-07	4.4E-07	3.3E-07	6.2E-08	-8.9E-12
14	3.5	Py	56	1.2E-14	1.2E-14	6.3E-16	6.3E-16	4.4E-07	4.4E-07	1.3E-07	5.9E-07	1.3E-08
14	3.5	UJ	136	7.0E-15	7.0E-15	4.3E-17	4.3E-17	4.4E-07	4.4E-07	1.4E-07	4.3E-07	1.5E-08
14	7	Rect	46	1.0E-14	1.0E-14	2.5E-17	2.5E-17	4.4E-07	4.4E-07	4.2E-07	6.6E-07	4.8E-08
14	7	Px	28	9.7E-16	9.7E-16	3.3E-17	3.3E-17	4.4E-07	4.4E-07	2.6E-07	8.4E-07	7.0E-12
14	7	Py	29	1.1E-14	1.1E-14	9.8E-16	9.8E-16	4.4E-07	4.4E-07	9.9E-07	5.1E-07	3.8E-08
14	7	UJ	54	9.9E-15	9.9E-15	3.0E-17	3.0E-17	4.4E-07	4.4E-07	3.3E-07	5.4E-07	3.6E-08
14	14	Rect	18	9.6E-15	9.6E-15	1.4E-17	1.4E-17	4.4E-07	4.4E-07	5.2E-07	3.1E-06	2.7E-07
14	14	Px	14	4.2E-16	4.2E-16	5.5E-17	5.5E-17	4.4E-07	4.4E-07	5.7E-07	7.5E-07	5.4E-12
14	14	Py	15	1.0E-14	1.0E-14	2.4E-15	2.4E-15	4.4E-07	4.4E-07	2.0E-06	4.9E-07	2.6E-08
14	14	UJ	18	9.6E-15	9.6E-15	1.4E-17	1.4E-17	4.4E-07	4.4E-07	5.2E-07	3.1E-06	2.7E-07

Table B.3 - Components of LS implementation uncertainty. Columns named (1) to (9) contains the nine components of equation (B.1) for each verification operator.

Annex C - **Ideal measuring instrument: results**

SAMPLING				(LS) *FLT*t					
				Error evaluation		u_{lm} ANALYTIC		u_{lm} EXPERIMENTAL	
D [mm]	d [mm]	Grid	points [n°]	*FLT*t [µm]	t_{FLTt} [s]	u_{lm} [µm]	t_u [s]	u_{lm} [µm]	t_u [s]
0.35	0.35	Rect	17575	11.489	0.180	0.060	4.034	0.074	1.158
0.35	0.35	Px	17575	11.489	0.180	0.060	4.034	0.074	1.158
0.35	0.35	Py	17575	11.489	0.180	0.060	4.034	0.074	1.158
0.35	0.35	UJ	17575	11.489	0.180	0.060	4.034	0.074	1.158
0.7	0.35	Rect	13323	11.489	0.121	0.069	3.519	0.082	0.938
0.7	0.35	Px	8915	11.401	0.117	0.084	3.467	0.087	0.653
0.7	0.35	Py	8949	11.578	0.037	0.086	0.456	0.106	0.664
0.7	0.35	UJ	17575	11.489	0.125	0.060	3.867	0.077	1.141
0.7	0.7	Rect	4540	11.486	0.117	0.120	3.216	0.133	0.331
0.7	0.7	Px	4459	11.262	0.034	0.118	0.458	0.133	0.356
0.7	0.7	Py	4473	11.517	0.004	0.120	0.359	0.153	0.458
0.7	0.7	UJ	4540	11.486	0.004	0.120	0.354	0.136	0.354
3.5	0.35	Rect	3529	11.602	0.177	0.136	3.928	0.166	0.278
3.5	0.35	Px	1870	11.215	0.031	0.182	0.484	0.169	0.160
3.5	0.35	Py	1856	10.869	0.003	0.182	0.393	0.191	0.161
3.5	0.35	UJ	5089	11.566	0.005	0.113	0.399	0.117	0.391
3.5	0.7	Rect	1693	11.588	0.002	0.197	0.402	0.198	0.148
3.5	0.7	Px	933	11.085	0.001	0.256	0.406	0.188	0.101
3.5	0.7	Py	927	10.805	0.001	0.256	0.392	0.243	0.103
3.5	0.7	UJ	2405	11.546	0.002	0.165	0.396	0.194	0.228
3.5	3.5	Rect	196	10.544	0.001	0.551	0.404	0.351	0.060
3.5	3.5	Px	180	9.857	0.001	0.450	0.399	0.358	0.048
3.5	3.5	Py	183	10.211	0.001	0.579	0.393	0.480	0.057
3.5	3.5	UJ	196	10.544	0.001	0.551	0.402	0.371	0.049
7	0.35	Rect	1897	12.202	0.002	0.182	0.404	0.223	0.162
7	0.35	Px	1035	11.145	0.001	0.237	0.396	0.223	0.112
7	0.35	Py	917	9.746	0.001	0.207	0.399	0.254	0.101
7	0.35	UJ	2714	11.897	0.003	0.154	0.396	0.173	0.239
7	0.7	Rect	935	12.159	0.001	0.262	0.399	0.300	0.090
7	0.7	Px	517	11.014	0.001	0.334	0.402	0.223	0.068
7	0.7	Py	458	9.693	0.002	0.295	0.398	0.275	0.062
7	0.7	UJ	1334	11.835	0.002	0.222	0.392	0.214	0.123
7	3.5	Rect	150	10.879	0.001	0.668	0.397	0.563	0.046
7	3.5	Px	100	9.910	0.001	0.576	0.399	0.456	0.044
7	3.5	Py	90	9.244	0.001	0.695	0.400	0.640	0.043
7	3.5	UJ	196	10.544	0.001	0.551	0.398	0.422	0.050
7	7	Rect	54	9.317	0.001	0.812	0.404	0.697	0.043
7	7	Px	46	8.126	0.001	0.803	0.407	0.644	0.040
7	7	Py	48	8.420	0.001	0.862	0.406	0.687	0.041
7	7	UJ	54	9.317	0.001	0.812	0.405	0.645	0.041
14	0.35	Rect	1184	12.251	0.001	0.231	0.396	0.288	0.115
14	0.35	Px	631	11.016	0.001	0.285	0.390	0.210	0.070
14	0.35	Py	572	9.342	0.002	0.244	0.395	0.253	0.067
14	0.35	UJ	1576	12.002	0.002	0.202	0.399	0.238	0.145
14	0.7	Rect	590	12.231	0.001	0.331	0.398	0.441	0.070
14	0.7	Px	315	10.906	0.001	0.402	0.399	0.277	0.054
14	0.7	Py	286	9.256	0.001	0.346	0.398	0.351	0.061
14	0.7	UJ	786	11.961	0.001	0.288	0.411	0.302	0.090
14	3.5	Rect	106	11.141	0.001	0.780	0.397	0.559	0.044
14	3.5	Px	61	9.689	0.001	0.795	0.390	0.632	0.041
14	3.5	Py	56	8.563	0.001	0.825	0.408	0.711	0.041
14	3.5	UJ	136	10.897	0.001	0.655	0.394	0.477	0.048
14	7	Rect	46	9.338	0.001	0.882	0.414	0.801	0.040
14	7	Px	28	8.062	0.001	1.025	0.397	0.753	0.039
14	7	Py	29	7.906	0.001	1.235	0.403	0.850	0.039
14	7	UJ	54	9.317	0.001	0.812	0.403	0.688	0.041
14	14	Rect	18	8.998	0.001	1.935	0.415	1.142	0.040
14	14	Px	14	6.980	0.001	1.110	0.399	1.214	0.038
14	14	Py	15	7.068	0.001	1.558	0.400	1.040	0.039
14	14	UJ	18	8.998	0.001	1.935	0.403	1.473	0.038

Table C.1 - Evaluation of *FLT*t error, with LS method, using an ideal measuring instrument.

SAMPLING				(MZ) *FLT*t					
				Error evaluation		u_{Im} ANALYTIC		u_{Im} EXPERIMENTAL	
D [mm]	d [mm]	Grid	points [n°]	*FLT*t [µm]	t_{FLTt} [s]	u_{Im} [µm]	t_u [min]	u_{Im} [µm]	t_u [min]
0.35	0.35	Rect	17575	11.015	267.223	0.002	153.207	0.002	157.424
0.35	0.35	Px	17575	11.015	267.223	0.002	153.207	0.002	157.424
0.35	0.35	Py	17575	11.015	267.223	0.002	153.207	0.002	157.424
0.35	0.35	UJ	17575	11.015	267.223	0.002	153.207	0.002	157.424
0.7	0.35	Rect	13323	11.015	266.684	0.001	155.765	0.001	160.208
0.7	0.35	Px	8915	11.015	165.669	0.003	90.416	0.002	89.307
0.7	0.35	Py	8949	11.015	109.512	0.007	61.830	0.007	62.286
0.7	0.35	UJ	17575	11.015	266.491	0.002	156.272	0.002	158.982
0.7	0.7	Rect	4540	11.015	53.866	0.007	28.645	0.008	29.068
0.7	0.7	Px	4459	10.906	54.667	0.006	29.306	0.005	29.811
0.7	0.7	Py	4473	10.952	53.581	0.006	28.652	0.006	28.556
0.7	0.7	UJ	4540	11.015	53.839	0.006	28.874	0.009	28.684
3.5	0.35	Rect	3529	11.009	65.395	0.036	43.585	0.047	45.981
3.5	0.35	Px	1870	10.924	71.899	0.031	40.338	0.041	39.929
3.5	0.35	Py	1856	10.475	27.905	0.046	19.362	0.051	19.321
3.5	0.35	UJ	5089	11.013	80.699	0.015	50.538	0.011	50.007
3.5	0.7	Rect	1693	11.009	16.369	0.048	11.344	0.042	12.107
3.5	0.7	Px	933	10.814	15.627	0.043	8.362	0.043	8.544
3.5	0.7	Py	927	10.410	8.783	0.062	5.889	0.078	5.855
3.5	0.7	UJ	2405	11.013	22.940	0.014	13.816	0.018	14.034
3.5	3.5	Rect	196	10.388	0.868	0.142	0.697	0.138	0.693
3.5	3.5	Px	180	9.478	0.927	0.154	0.716	0.154	0.652
3.5	3.5	Py	183	9.838	0.856	0.108	0.653	0.142	0.624
3.5	3.5	UJ	196	10.388	0.873	0.157	0.713	0.144	0.636
7	0.35	Rect	1897	11.009	73.843	0.060	53.336	0.059	55.266
7	0.35	Px	1035	10.924	62.808	0.090	36.282	0.081	36.952
7	0.35	Py	917	9.301	27.146	0.058	19.009	0.056	18.226
7	0.35	UJ	2714	11.009	76.601	0.040	51.790	0.043	52.495
7	0.7	Rect	935	11.009	17.677	0.086	13.408	0.101	12.974
7	0.7	Px	517	10.814	12.005	0.080	6.980	0.107	6.656
7	0.7	Py	458	9.233	7.485	0.120	4.802	0.108	4.707
7	0.7	UJ	1334	11.009	19.454	0.042	13.100	0.058	12.693
7	3.5	Rect	150	10.371	0.625	0.150	0.541	0.167	0.502
7	3.5	Px	100	9.453	0.426	0.182	0.365	0.211	0.325
7	3.5	Py	90	8.646	0.347	0.235	0.329	0.264	0.289
7	3.5	UJ	196	10.388	0.875	0.118	0.673	0.144	0.660
7	7	Rect	54	9.226	0.185	0.423	0.198	0.332	0.149
7	7	Px	46	7.685	0.170	0.439	0.178	0.341	0.134
7	7	Py	48	8.089	0.147	0.412	0.173	0.300	0.132
7	7	UJ	54	9.226	0.184	0.531	0.192	0.400	0.160
14	0.35	Rect	1184	10.925	101.749	0.107	67.069	0.106	69.580
14	0.35	Px	631	10.799	58.200	0.120	32.140	0.127	33.085
14	0.35	Py	572	8.923	23.798	0.085	15.703	0.084	15.802
14	0.35	UJ	1576	10.925	101.773	0.043	67.053	0.059	66.836
14	0.7	Rect	590	10.924	22.337	0.182	14.397	0.153	14.675
14	0.7	Px	315	10.701	10.221	0.184	5.901	0.193	5.774
14	0.7	Py	286	8.841	6.064	0.167	3.838	0.149	3.645
14	0.7	UJ	786	10.924	23.175	0.051	14.374	0.065	14.610
14	3.5	Rect	106	10.363	0.555	0.248	0.494	0.290	0.448
14	3.5	Px	61	9.409	0.310	0.390	0.289	0.337	0.242
14	3.5	Py	56	8.147	0.223	0.311	0.244	0.278	0.210
14	3.5	UJ	136	10.388	0.665	0.163	0.564	0.138	0.517
14	7	Rect	46	9.226	0.184	0.488	0.197	0.378	0.153
14	7	Px	28	7.685	0.112	0.653	0.134	0.544	0.089
14	7	Py	29	7.518	0.090	0.482	0.137	0.386	0.092
14	7	UJ	54	9.226	0.183	0.406	0.197	0.460	0.152
14	14	Rect	18	8.709	0.052	1.417	0.094	0.778	0.053
14	14	Px	14	6.279	0.051	1.242	0.085	0.993	0.044
14	14	Py	15	6.641	0.045	0.839	0.090	0.625	0.046
14	14	UJ	18	8.709	0.052	1.772	0.096	0.914	0.053

Table C.2 - Evaluation of *FLT*t error, with MZ method, for verification operators based on the use of an ideal measuring instrument.

SAMPLING			MZ		u_{Im} An.	u_{Im} Exp.	LS		u_{Im} An.	u_{Im} Exp.
D [mm]	d [mm]	Grid	*FLT*t [µm]	u_{Mt}[µm]	u_M [µm]	u_M [µm]	*FLT*t [µm]	u_{Mt}[µm]	u_M [µm]	u_M [µm]
0.35	0.35	Rect	11.015	0.000	0.002	0.002	11.489	0.474	0.477	0.479
0.35	0.35	Px	11.015	0.000	0.002	0.002	11.489	0.474	0.477	0.479
0.35	0.35	Py	11.015	0.000	0.002	0.002	11.489	0.474	0.477	0.479
0.35	0.35	UJ	11.015	0.000	0.002	0.002	11.489	0.474	0.477	0.479
0.7	0.35	Rect	11.015	0.000	0.001	0.001	11.489	0.473	0.478	0.480
0.7	0.35	Px	11.015	0.000	0.003	0.002	11.401	0.386	0.395	0.395
0.7	0.35	Py	11.015	0.000	0.007	0.007	11.578	0.562	0.569	0.572
0.7	0.35	UJ	11.015	0.000	0.002	0.002	11.489	0.474	0.477	0.480
0.7	0.7	Rect	11.015	0.001	0.007	0.008	11.486	0.471	0.486	0.489
0.7	0.7	Px	10.906	0.109	0.109	0.109	11.262	0.247	0.273	0.280
0.7	0.7	Py	10.952	0.064	0.064	0.064	11.517	0.501	0.516	0.524
0.7	0.7	UJ	11.015	0.001	0.006	0.009	11.486	0.471	0.486	0.490
3.5	0.35	Rect	11.009	0.006	0.036	0.047	11.602	0.586	0.602	0.609
3.5	0.35	Px	10.924	0.091	0.096	0.100	11.215	0.200	0.270	0.262
3.5	0.35	Py	10.475	0.540	0.542	0.543	10.869	0.147	0.234	0.241
3.5	0.35	UJ	11.013	0.002	0.015	0.011	11.566	0.550	0.562	0.563
3.5	0.7	Rect	11.009	0.007	0.048	0.042	11.588	0.573	0.606	0.606
3.5	0.7	Px	10.814	0.201	0.206	0.206	11.085	0.070	0.265	0.201
3.5	0.7	Py	10.410	0.606	0.609	0.611	10.805	0.210	0.331	0.321
3.5	0.7	UJ	11.013	0.003	0.015	0.018	11.546	0.531	0.556	0.565
3.5	3.5	Rect	10.388	0.627	0.643	0.642	10.544	0.471	0.725	0.587
3.5	3.5	Px	9.478	1.537	1.545	1.545	9.857	1.158	1.242	1.212
3.5	3.5	Py	9.838	1.178	1.183	1.186	10.211	0.804	0.991	0.936
3.5	3.5	UJ	10.388	0.627	0.647	0.644	10.544	0.471	0.725	0.600
7	0.35	Rect	11.009	0.006	0.061	0.059	12.202	1.187	1.201	1.208
7	0.35	Px	10.924	0.091	0.128	0.122	11.145	0.130	0.270	0.258
7	0.35	Py	9.301	1.714	1.715	1.715	9.746	1.270	1.287	1.295
7	0.35	UJ	11.009	0.006	0.040	0.044	11.897	0.882	0.895	0.899
7	0.7	Rect	11.009	0.007	0.086	0.101	12.159	1.144	1.173	1.182
7	0.7	Px	10.814	0.201	0.217	0.228	11.014	0.001	0.334	0.223
7	0.7	Py	9.233	1.782	1.786	1.785	9.693	1.322	1.355	1.350
7	0.7	UJ	11.009	0.007	0.043	0.058	11.835	0.820	0.850	0.848
7	3.5	Rect	10.371	0.645	0.662	0.666	10.879	0.136	0.682	0.579
7	3.5	Px	9.453	1.562	1.573	1.577	9.910	1.105	1.246	1.196
7	3.5	Py	8.646	2.369	2.381	2.384	9.244	1.772	1.903	1.884
7	3.5	UJ	10.388	0.627	0.638	0.643	10.544	0.471	0.725	0.632
7	7	Rect	9.226	1.789	1.839	1.820	9.317	1.698	1.882	1.836
7	7	Px	7.685	3.330	3.359	3.348	8.126	2.889	2.999	2.960
7	7	Py	8.089	2.926	2.955	2.942	8.420	2.595	2.735	2.685
7	7	UJ	9.226	1.789	1.867	1.834	9.317	1.698	1.882	1.816
14	0.35	Rect	10.925	0.091	0.140	0.140	12.251	1.236	1.257	1.269
14	0.35	Px	10.799	0.217	0.248	0.251	11.016	0.000	0.285	0.210
14	0.35	Py	8.923	2.092	2.094	2.094	9.342	1.673	1.691	1.692
14	0.35	UJ	10.925	0.091	0.100	0.108	12.002	0.987	1.007	1.015
14	0.7	Rect	10.924	0.092	0.204	0.178	12.231	1.216	1.260	1.293
14	0.7	Px	10.701	0.315	0.365	0.369	10.906	0.109	0.417	0.298
14	0.7	Py	8.841	2.175	2.181	2.180	9.256	1.760	1.794	1.795
14	0.7	UJ	10.924	0.092	0.105	0.113	11.961	0.945	0.988	0.993
14	3.5	Rect	10.363	0.652	0.698	0.713	11.141	0.126	0.790	0.573
14	3.5	Px	9.409	1.607	1.653	1.642	9.689	1.327	1.547	1.470
14	3.5	Py	8.147	2.869	2.886	2.882	8.563	2.452	2.587	2.553
14	3.5	UJ	10.388	0.627	0.648	0.642	10.897	0.118	0.665	0.492
14	7	Rect	9.226	1.789	1.855	1.829	9.338	1.677	1.895	1.859
14	7	Px	7.685	3.330	3.394	3.375	8.062	2.953	3.126	3.047
14	7	Py	7.518	3.498	3.531	3.519	7.906	3.110	3.346	3.224
14	7	UJ	9.226	1.789	1.835	1.848	9.317	1.698	1.882	1.832
14	14	Rect	8.709	2.306	2.706	2.434	8.998	2.017	2.795	2.318
14	14	Px	6.279	4.736	4.896	4.839	6.980	4.036	4.186	4.214
14	14	Py	6.641	4.374	4.454	4.419	7.068	3.947	4.243	4.082
14	14	UJ	8.709	2.306	2.908	2.480	8.998	2.017	2.795	2.498

Table C.3 - Method and measurement uncertainty for verification operators based on the use of an ideal measuring instrument.

An attentive reader could notice that for this experiment the time required for the assessment of the MZ flatness deviation is much higher than the time required by the same verification operators implemented with a real measuring instrument (MPE ≠ 0). Reader compares the results reported in Table C.2 and Table D.2. The time required for evaluating the MZ flatness error detected by the perfect verification operators is 267 seconds if the measurement relies on an ideal instrument (Table C.2) and 3.6 seconds if it is based on a real instrument (Table D.2). The difference affects also the implementation uncertainty, for both the analytical and the experimental assessment, and is magnified because of the bootstrap method embedded in both approaches.

In order to understand the different computation times, which indeed are related with the convex-hull calculation and the solution of the MZ problem, it is necessary to compare the convex-hulls of the two measurement datasets. Convex-hulls are not plotted directly, as they are solid entities, but only their vertices are highlighted among the set of measurement points. Particularly, the convex-hull vertices of the two experiments are visible in Figure C.1 and Figure C.2. These figures refer to the perfect verification operator. It is easy to notice that the measurement based on a real instrument generates a convex-hull with fewer vertices (111 vertices) than the measurement based on the ideal instrument (434 vertices). The latter is characterized also by the concentration of vertices on the feature edges, phenomenon that leads to narrow facets of the convex-hull and can compromise the accuracy of the MZ algorithm because of numerical errors. However, this effect is also a consequence of the particular shape of the virtual surface at hand, which indeed is very smooth and characterized by a wavelength of the form deviation much larger than the distance between sampling points.

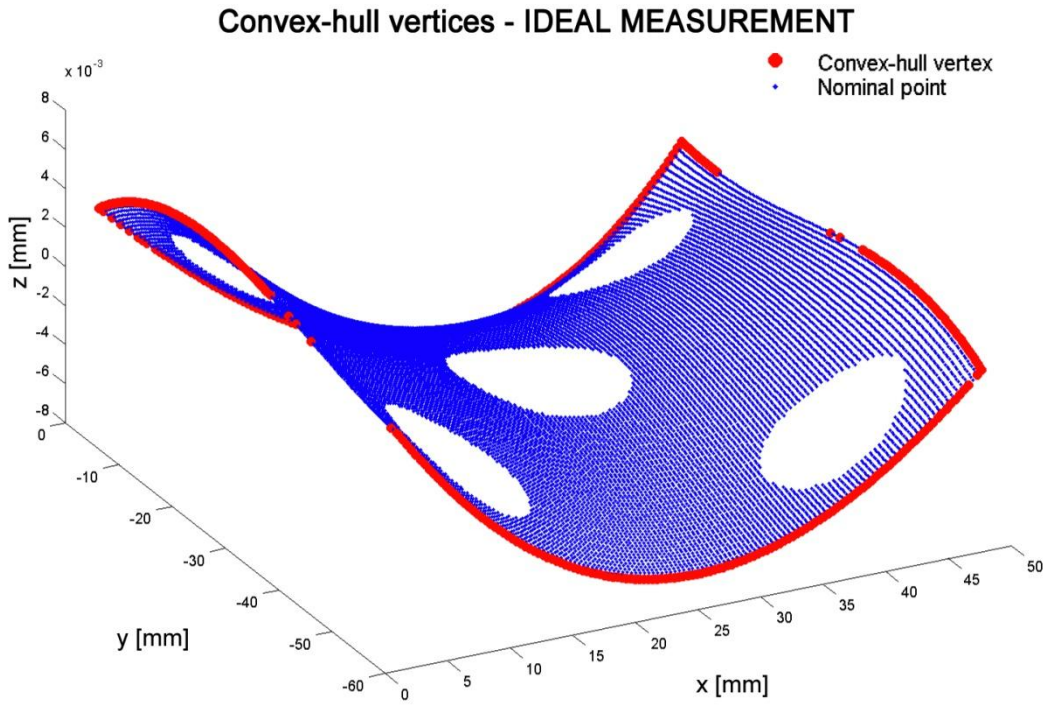

Figure C.1 - Perfect verification operator based on an ideal measuring instrument. Vertices of the convex-hull are concentrated on the feature external edges for a total of 434 points.

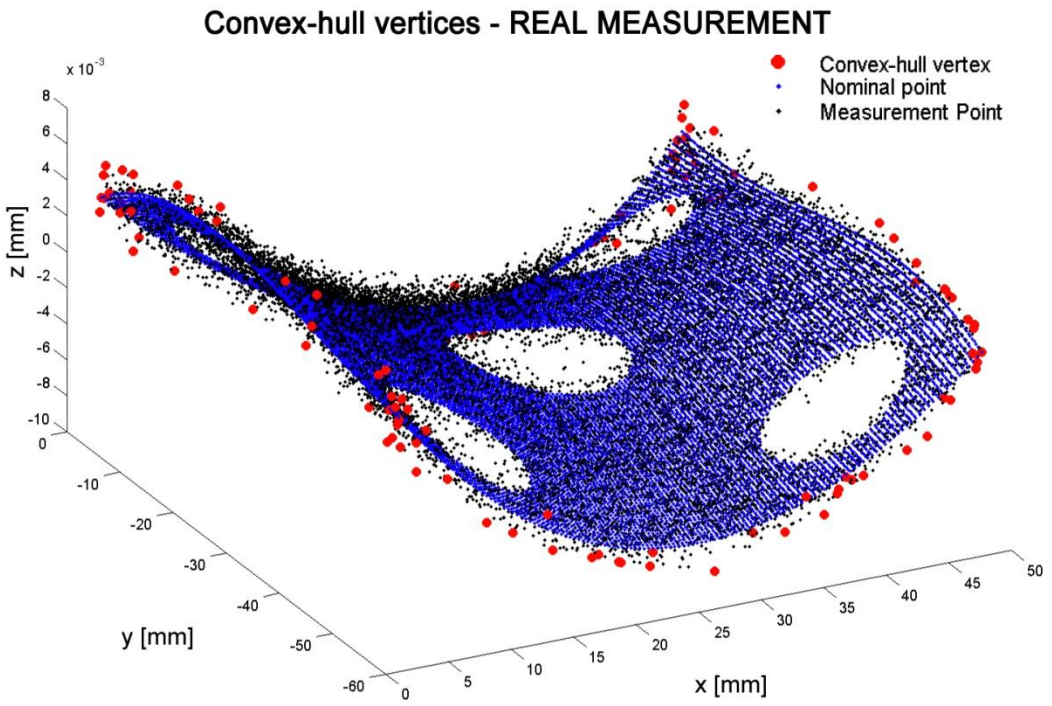

Figure C.2 - Perfect verification operator based on a real (simulated) measuring instrument. Convex-hull has 111 vertices not strictly concentrated along the feature external edges as in Figure C.1.

Annex D - **Real (simulated) measuring instrument: results**

SAMPLING				(LS) *FLT*t					
				Error evaluation		u_{lm} ANALYTIC		u_{lm} EXPERIMENTAL	
D [mm]	d [mm]	Grid	points [n°]	*FLT*t [µm]	t_{FLTt} [s]	u_{lm} [µm]	t_u [s]	u_{lm} [µm]	t_u [s]
0.35	0.35	Rect	17575	14.186	0.2798	0.945	2.8136	0.191	1.6883
0.35	0.35	Px	17575	14.186	0.2798	0.945	2.8136	0.191	1.6883
0.35	0.35	Py	17575	14.186	0.2798	0.945	2.8136	0.191	1.6883
0.35	0.35	UJ	17575	14.186	0.2798	0.945	2.8136	0.191	1.6883
0.7	0.35	Rect	13323	14.188	0.0109	0.945	2.7601	0.191	1.3195
0.7	0.35	Px	8915	14.100	0.0112	0.946	2.2639	0.176	0.9106
0.7	0.35	Py	8949	14.263	0.0070	0.946	2.7421	0.211	0.8512
0.7	0.35	UJ	17575	14.186	0.0186	0.945	2.3234	0.178	1.8398
0.7	0.7	Rect	4540	14.160	0.0032	0.950	2.4242	0.319	0.4346
0.7	0.7	Px	4459	13.960	0.0032	0.950	2.3986	0.312	0.3985
0.7	0.7	Py	4473	14.315	0.0034	0.950	2.7424	0.398	0.4768
0.7	0.7	UJ	4540	14.160	0.0043	0.950	2.5392	0.313	0.4581
3.5	0.35	Rect	3529	14.060	0.0028	0.951	2.3293	0.267	0.3591
3.5	0.35	Px	1870	13.465	0.0018	0.955	2.4784	0.259	0.1922
3.5	0.35	Py	1856	14.392	0.0024	0.958	2.0266	0.514	0.2057
3.5	0.35	UJ	5089	14.250	0.0037	0.949	2.5071	0.246	0.4665
3.5	0.7	Rect	1693	14.048	0.0016	0.959	2.4671	0.447	0.1744
3.5	0.7	Px	933	13.197	0.0012	0.963	2.7270	0.443	0.1159
3.5	0.7	Py	927	14.429	0.0012	0.974	2.9791	0.724	0.1157
3.5	0.7	UJ	2405	14.224	0.0021	0.956	2.4161	0.338	0.2449
3.5	3.5	Rect	196	12.351	0.0188	1.018	2.5272	0.584	0.0486
3.5	3.5	Px	180	10.767	0.0144	1.023	2.6511	0.433	0.0471
3.5	3.5	Py	183	11.427	0.0209	1.063	2.5894	0.526	0.0567
3.5	3.5	UJ	196	12.351	0.0007	1.018	2.4646	0.530	0.0478
7	0.35	Rect	1897	13.977	0.0021	0.951	2.4925	0.218	0.1986
7	0.35	Px	1035	13.460	0.0400	0.965	2.6044	0.392	0.1248
7	0.35	Py	917	12.218	0.0287	0.974	2.4486	0.420	0.1183
7	0.35	UJ	2714	14.267	0.0024	0.957	2.6815	0.318	0.3769
7	0.7	Rect	935	13.633	0.0012	0.986	2.7216	0.425	0.1171
7	0.7	Px	517	13.230	0.0192	0.978	2.9173	0.549	0.1075
7	0.7	Py	458	11.959	0.0320	0.992	2.0425	0.506	0.0792
7	0.7	UJ	1334	14.251	0.0267	0.972	2.6663	0.538	0.1562
7	3.5	Rect	150	12.682	0.0233	1.162	2.6318	0.608	0.0518
7	3.5	Px	100	10.821	0.0215	1.201	2.5424	0.618	0.0428
7	3.5	Py	90	9.798	0.0404	1.150	2.4177	0.613	0.0406
7	3.5	UJ	196	12.351	0.0007	1.018	2.4806	0.574	0.0572
7	7	Rect	54	9.722	0.0006	1.356	2.3702	0.776	0.0667
7	7	Px	46	8.905	0.0083	1.227	2.7611	0.872	0.0419
7	7	Py	48	9.097	0.0110	1.626	2.4183	0.669	0.0569
7	7	UJ	54	9.722	0.0006	1.356	2.4016	0.615	0.0396
14	0.35	Rect	1184	14.082	0.0242	0.958	2.5336	0.485	0.1475
14	0.35	Px	631	12.841	0.0264	0.970	2.3860	0.331	0.0909
14	0.35	Py	572	12.159	0.0178	0.999	2.8704	0.555	0.0765
14	0.35	UJ	1576	14.354	0.0016	0.954	2.6347	0.481	0.1603
14	0.7	Rect	590	13.298	0.0009	0.994	2.4633	0.364	0.0741
14	0.7	Px	315	12.078	0.0286	1.005	2.5106	0.322	0.0577
14	0.7	Py	286	11.899	0.0238	1.029	2.9641	0.796	0.0744
14	0.7	UJ	786	14.341	0.0305	0.991	2.9548	0.624	0.0974
14	3.5	Rect	106	12.298	0.0007	1.291	2.5096	0.667	0.0436
14	3.5	Px	61	10.690	0.0275	1.311	2.1991	0.701	0.0407
14	3.5	Py	56	9.762	0.0007	1.276	1.9804	0.723	0.0415
14	3.5	UJ	136	12.124	0.0240	1.047	2.4600	0.623	0.0534
14	7	Rect	46	9.762	0.0006	1.411	2.2696	0.673	0.0403
14	7	Px	28	7.447	0.0006	1.367	2.2462	0.775	0.0394
14	7	Py	29	8.346	0.0006	1.541	2.5425	1.070	0.0398
14	7	UJ	54	9.722	0.0006	1.356	2.4955	0.722	0.0427
14	14	Rect	18	9.624	0.0103	2.136	2.4105	1.430	0.0381
14	14	Px	14	6.929	0.0007	1.475	2.8224	1.143	0.0402
14	14	Py	15	7.602	0.0006	1.693	2.7791	1.065	0.0629
14	14	UJ	18	9.624	0.0006	2.136	1.1190	1.282	0.0380

Table D.1 - Evaluation of *FLT*t error, with LS method, for a real measuring instrument.

SAMPLING				(MZ) *FLT*t					
				Error evaluation		u_{Im} ANALYTIC		u_{Im} EXPERIMENTAL	
D [mm]	d [mm]	Grid	points [n°]	*FLT*t [µm]	t_{FLTt} [s]	u_{Im} [µm]	t_u [s]	u_{Im} [µm]	t_u [s]
0.35	0.35	Rect	17575	13.758	3.629	0.950	276.040	0.108	4.270
0.35	0.35	Px	17575	13.758	3.629	0.950	276.040	0.108	4.270
0.35	0.35	Py	17575	13.758	3.629	0.950	276.040	0.108	4.270
0.35	0.35	UJ	17575	13.758	3.629	0.950	276.040	0.108	4.270
0.7	0.35	Rect	13323	13.758	2.951	0.952	240.129	0.112	4.038
0.7	0.35	Px	8915	13.643	2.434	0.949	212.586	0.122	3.364
0.7	0.35	Py	8949	13.756	1.934	0.966	184.410	0.195	2.998
0.7	0.35	UJ	17575	13.758	3.166	0.950	268.840	0.105	4.340
0.7	0.7	Rect	4540	13.508	1.340	0.972	129.785	0.192	2.214
0.7	0.7	Px	4459	13.508	1.391	0.979	123.036	0.227	2.156
0.7	0.7	Py	4473	13.508	1.315	0.975	122.023	0.253	2.132
0.7	0.7	UJ	4540	13.508	1.347	0.966	128.569	0.196	2.174
3.5	0.35	Rect	3529	13.558	1.687	0.961	132.854	0.196	2.206
3.5	0.35	Px	1870	13.380	1.263	0.982	98.642	0.261	1.672
3.5	0.35	Py	1856	13.125	1.244	0.982	90.349	0.288	1.534
3.5	0.35	UJ	5089	13.642	1.936	0.950	146.770	0.150	2.529
3.5	0.7	Rect	1693	13.229	0.987	0.996	84.268	0.320	1.500
3.5	0.7	Px	933	12.540	0.730	0.976	58.891	0.260	0.992
3.5	0.7	Py	927	13.125	0.539	1.077	54.629	0.483	0.937
3.5	0.7	UJ	2405	13.508	1.150	0.972	98.033	0.213	1.703
3.5	3.5	Rect	196	12.089	0.377	1.005	25.207	0.413	0.441
3.5	3.5	Px	180	10.610	0.327	0.967	21.743	0.324	0.375
3.5	3.5	Py	183	11.372	0.294	0.986	22.707	0.337	0.388
3.5	3.5	UJ	196	12.089	0.370	1.011	24.913	0.383	0.447
7	0.35	Rect	1897	13.220	1.302	0.960	102.558	0.213	1.759
7	0.35	Px	1035	13.165	0.995	1.011	78.759	0.317	1.318
7	0.35	Py	917	11.436	0.701	0.965	60.341	0.190	1.005
7	0.35	UJ	2714	13.488	1.443	0.980	114.820	0.232	1.926
7	0.7	Rect	935	12.673	0.741	0.967	68.419	0.172	1.224
7	0.7	Px	517	12.527	0.641	1.028	44.714	0.338	0.775
7	0.7	Py	458	11.235	0.478	0.979	41.904	0.335	0.705
7	0.7	UJ	1334	13.113	0.959	0.993	79.913	0.305	1.446
7	3.5	Rect	150	12.089	0.290	1.035	20.353	0.442	0.394
7	3.5	Px	100	10.610	0.208	1.039	14.044	0.470	0.242
7	3.5	Py	90	9.313	0.320	0.995	14.961	0.300	0.308
7	3.5	UJ	196	12.089	0.376	1.018	24.679	0.421	0.452
7	7	Rect	54	9.469	0.189	1.005	9.942	0.418	0.162
7	7	Px	46	8.133	0.124	1.128	7.845	0.567	0.118
7	7	Py	48	8.653	0.146	1.086	9.012	0.342	0.149
7	7	UJ	54	9.469	0.184	0.997	10.299	0.337	0.160
14	0.35	Rect	1184	13.184	1.052	0.979	81.241	0.273	1.377
14	0.35	Px	631	12.609	0.856	0.973	62.988	0.240	1.068
14	0.35	Py	572	11.426	0.430	1.056	37.126	0.273	0.622
14	0.35	UJ	1576	13.478	1.015	0.968	85.507	0.283	1.452
14	0.7	Rect	590	12.501	0.643	0.963	56.209	0.197	0.913
14	0.7	Px	315	11.744	0.559	0.962	37.358	0.195	0.638
14	0.7	Py	286	11.005	0.267	1.114	26.691	0.502	0.451
14	0.7	UJ	786	13.083	0.615	0.999	60.150	0.314	1.020
14	3.5	Rect	106	11.694	0.233	1.043	18.465	0.412	0.303
14	3.5	Px	61	10.289	0.164	1.172	11.102	0.618	0.179
14	3.5	Py	56	9.148	0.155	1.060	10.926	0.357	0.177
14	3.5	UJ	136	11.694	0.285	1.008	22.110	0.332	0.363
14	7	Rect	46	9.469	0.184	1.024	9.669	0.405	0.158
14	7	Px	28	7.156	0.101	1.193	6.075	0.489	0.091
14	7	Py	29	8.200	0.091	1.279	6.214	0.512	0.092
14	7	UJ	54	9.469	0.184	1.018	10.627	0.382	0.159
14	14	Rect	18	8.680	0.063	1.533	3.723	0.914	0.058
14	14	Px	14	6.265	0.051	1.482	3.322	0.878	0.046
14	14	Py	15	7.466	0.054	1.162	3.320	0.739	0.048
14	14	UJ	18	8.680	0.063	1.750	3.841	0.891	0.057

Table D.2 - Evaluation of *FLT*t error, with MZ method, for verification operators based on the use of a real (simulated) measuring instrument: MPE ≠ 0.

SAMPLING			MZ		u_{Im} An.	u_{Im} Exp.	LS		u_{Im} An.	u_{Im} Exp.
D [mm]	d [mm]	Grid	*FLT*t [µm]	u_{Mt}[µm]	u_M [µm]	u_M [µm]	*FLT*t [µm]	u_{Mt}[µm]	u_M [µm]	u_M [µm]
0.35	0.35	Rect	13.758	0.000	0.950	0.108	14.186	0.427	1.037	0.468
0.35	0.35	Px	13.758	0.000	0.950	0.108	14.186	0.427	1.037	0.468
0.35	0.35	Py	13.758	0.000	0.950	0.108	14.186	0.427	1.037	0.468
0.35	0.35	UJ	13.758	0.000	0.950	0.108	14.186	0.427	1.037	0.468
0.7	0.35	Rect	13.758	0.000	0.952	0.112	14.188	0.429	1.038	0.470
0.7	0.35	Px	13.643	0.115	0.956	0.168	14.100	0.342	1.006	0.384
0.7	0.35	Py	13.756	0.002	0.966	0.195	14.263	0.505	1.073	0.547
0.7	0.35	UJ	13.758	0.000	0.950	0.105	14.186	0.427	1.037	0.463
0.7	0.7	Rect	13.508	0.251	1.004	0.316	14.160	0.401	1.031	0.513
0.7	0.7	Px	13.508	0.251	1.011	0.338	13.960	0.202	0.971	0.371
0.7	0.7	Py	13.508	0.251	1.007	0.356	14.315	0.557	1.101	0.684
0.7	0.7	UJ	13.508	0.251	0.998	0.318	14.160	0.401	1.031	0.509
3.5	0.35	Rect	13.558	0.200	0.982	0.280	14.060	0.302	0.997	0.403
3.5	0.35	Px	13.380	0.378	1.052	0.460	13.465	0.293	0.999	0.391
3.5	0.35	Py	13.125	0.634	1.169	0.696	14.392	0.634	1.149	0.816
3.5	0.35	UJ	13.642	0.117	0.957	0.190	14.250	0.491	1.069	0.549
3.5	0.7	Rect	13.229	0.529	1.128	0.618	14.048	0.290	1.002	0.533
3.5	0.7	Px	12.540	1.218	1.561	1.245	13.197	0.561	1.114	0.715
3.5	0.7	Py	13.125	0.634	1.250	0.797	14.429	0.670	1.182	0.986
3.5	0.7	UJ	13.508	0.251	1.004	0.329	14.224	0.466	1.063	0.576
3.5	3.5	Rect	12.089	1.669	1.948	1.720	12.351	1.407	1.737	1.523
3.5	3.5	Px	10.610	3.148	3.294	3.165	10.767	2.992	3.162	3.023
3.5	3.5	Py	11.372	2.386	2.582	2.410	11.427	2.332	2.563	2.390
3.5	3.5	UJ	12.089	1.669	1.951	1.713	12.351	1.407	1.737	1.504
7	0.35	Rect	13.220	0.538	1.101	0.579	13.977	0.219	0.976	0.309
7	0.35	Px	13.165	0.594	1.172	0.673	13.460	0.299	1.010	0.493
7	0.35	Py	11.436	2.323	2.515	2.331	12.218	1.540	1.823	1.597
7	0.35	UJ	13.488	0.271	1.017	0.357	14.267	0.508	1.084	0.599
7	0.7	Rect	12.673	1.085	1.453	1.098	13.633	0.125	0.994	0.443
7	0.7	Px	12.527	1.231	1.604	1.277	13.230	0.528	1.112	0.762
7	0.7	Py	11.235	2.523	2.706	2.545	11.959	1.799	2.055	1.869
7	0.7	UJ	13.113	0.646	1.184	0.714	14.251	0.492	1.090	0.729
7	3.5	Rect	12.089	1.669	1.964	1.727	12.682	1.076	1.584	1.236
7	3.5	Px	10.610	3.148	3.316	3.183	10.821	2.937	3.173	3.002
7	3.5	Py	9.313	4.445	4.555	4.455	9.798	3.960	4.124	4.007
7	3.5	UJ	12.089	1.669	1.955	1.721	12.351	1.407	1.737	1.520
7	7	Rect	9.469	4.289	4.405	4.309	9.722	4.037	4.258	4.111
7	7	Px	8.133	5.625	5.737	5.654	8.905	4.853	5.006	4.931
7	7	Py	8.653	5.105	5.220	5.117	9.097	4.662	4.937	4.710
7	7	UJ	9.469	4.289	4.404	4.302	9.722	4.037	4.258	4.083
14	0.35	Rect	13.184	0.574	1.135	0.636	14.082	0.324	1.011	0.583
14	0.35	Px	12.609	1.149	1.506	1.174	12.841	0.917	1.335	0.975
14	0.35	Py	11.426	2.332	2.560	2.348	12.159	1.599	1.885	1.692
14	0.35	UJ	13.478	0.281	1.008	0.399	14.354	0.595	1.124	0.765
14	0.7	Rect	12.501	1.258	1.584	1.273	13.298	0.460	1.095	0.586
14	0.7	Px	11.744	2.014	2.232	2.024	12.078	1.681	1.958	1.711
14	0.7	Py	11.005	2.753	2.970	2.798	11.899	1.860	2.125	2.023
14	0.7	UJ	13.083	0.676	1.206	0.745	14.341	0.583	1.150	0.854
14	3.5	Rect	11.694	2.064	2.313	2.105	12.298	1.461	1.950	1.606
14	3.5	Px	10.289	3.469	3.662	3.524	10.690	3.068	3.336	3.147
14	3.5	Py	9.148	4.611	4.731	4.624	9.762	3.996	4.195	4.061
14	3.5	UJ	11.694	2.064	2.297	2.091	12.124	1.635	1.941	1.749
14	7	Rect	9.469	4.289	4.410	4.308	9.762	3.997	4.238	4.053
14	7	Px	7.156	6.602	6.709	6.620	7.447	6.312	6.458	6.359
14	7	Py	8.200	5.559	5.704	5.582	8.346	5.413	5.628	5.517
14	7	UJ	9.469	4.289	4.408	4.306	9.722	4.037	4.258	4.101
14	14	Rect	8.680	5.078	5.305	5.160	9.624	4.134	4.653	4.375
14	14	Px	6.265	7.493	7.638	7.544	6.929	6.830	6.987	6.925
14	14	Py	7.466	6.292	6.399	6.336	7.602	6.156	6.384	6.247
14	14	UJ	8.680	5.078	5.371	5.156	9.624	4.134	4.653	4.328

Table D.3 - Method and measurement uncertainty for verification operators based on the use of a real (simulated) measuring instrument.

Annex E - **100 replications**

SAMPLING				True *FLT*t [µm]		Estimated *FLT*t [µm]			
				MZ	LS	MZ		LS	
D [mm]	d [mm]	Grid	points [n°]	*FLT*t	*FLT*t	*FLT*t	u_{lm}	*FLT*t	u_{lm}
0.35	0.35	Rect	17575	11.015	11.489	14.055	0.297	14.534	0.357
0.35	0.35	Px	17575	11.015	11.489	14.055	0.297	14.534	0.357
0.35	0.35	Py	17575	11.015	11.489	14.055	0.297	14.534	0.357
0.35	0.35	UJ	17575	11.015	11.489	14.055	0.297	14.534	0.357
0.7	0.35	Rect	13323	11.015	11.489	13.974	0.305	14.487	0.391
0.7	0.35	Px	8915	11.015	11.401	13.859	0.285	14.237	0.372
0.7	0.35	Py	8949	11.015	11.578	13.873	0.267	14.412	0.424
0.7	0.35	UJ	17575	11.015	11.489	14.061	0.315	14.529	0.381
0.7	0.7	Rect	4540	11.015	11.490	13.564	0.300	14.076	0.451
0.7	0.7	Px	4459	11.015	11.490	13.572	0.287	14.096	0.445
0.7	0.7	Py	4473	11.015	11.490	13.624	0.316	14.021	0.327
0.7	0.7	UJ	4540	11.015	11.490	13.495	0.302	14.053	0.470
3.5	0.35	Rect	3529	11.009	11.602	13.451	0.305	13.883	0.390
3.5	0.35	Px	1870	10.924	11.215	13.204	0.342	13.614	0.461
3.5	0.35	Py	1856	10.475	10.869	12.869	0.324	13.275	0.461
3.5	0.35	UJ	5089	11.013	11.566	13.651	0.301	14.158	0.407
3.5	0.7	Rect	1693	11.009	11.597	13.087	0.329	13.678	0.477
3.5	0.7	Px	933	10.923	11.309	12.833	0.383	13.361	0.481
3.5	0.7	Py	927	10.475	10.786	12.580	0.367	13.014	0.490
3.5	0.7	UJ	2405	11.013	11.552	13.260	0.303	13.831	0.541
3.5	3.5	Rect	196	10.388	10.607	11.678	0.411	12.154	0.518
3.5	3.5	Px	180	10.388	10.607	11.698	0.407	12.135	0.602
3.5	3.5	Py	183	10.388	10.607	11.680	0.471	12.197	0.545
3.5	3.5	UJ	196	10.388	10.607	11.675	0.465	12.145	0.582
7	0.35	Rect	1897	11.009	12.202	13.329	0.323	14.221	0.486
7	0.35	Px	1035	10.924	11.145	12.875	0.341	13.363	0.437
7	0.35	Py	917	9.301	9.746	11.497	0.339	12.089	0.455
7	0.35	UJ	2714	11.009	11.897	13.385	0.335	14.134	0.463
7	0.7	Rect	935	11.009	12.171	12.917	0.354	13.963	0.515
7	0.7	Px	517	10.923	11.232	12.644	0.400	13.177	0.547
7	0.7	Py	458	9.301	9.695	11.178	0.397	11.763	0.452
7	0.7	UJ	1334	11.009	11.845	13.039	0.282	13.786	0.474
7	3.5	Rect	150	10.371	10.953	11.545	0.456	12.287	0.636
7	3.5	Px	100	10.371	10.504	11.438	0.442	11.900	0.566
7	3.5	Py	90	9.226	9.664	10.255	0.474	10.886	0.607
7	3.5	UJ	196	10.388	10.607	11.631	0.377	12.220	0.602
7	7	Rect	54	9.226	9.415	9.947	0.493	10.570	0.604
7	7	Px	46	9.226	9.415	10.041	0.565	10.483	0.573
7	7	Py	48	9.226	9.415	9.933	0.507	10.549	0.589
7	7	UJ	54	9.226	9.415	9.983	0.503	10.430	0.619
14	0.35	Rect	1184	10.925	12.251	13.138	0.373	14.105	0.514
14	0.35	Px	631	10.799	11.016	12.698	0.380	13.077	0.457
14	0.35	Py	572	8.923	9.342	10.989	0.369	11.556	0.488
14	0.35	UJ	1576	10.925	12.002	13.272	0.303	14.124	0.480
14	0.7	Rect	590	10.924	12.246	12.746	0.442	13.724	0.662
14	0.7	Px	315	10.797	11.098	12.360	0.435	12.805	0.567
14	0.7	Py	286	8.923	9.302	10.702	0.348	11.237	0.516
14	0.7	UJ	786	10.924	11.974	12.892	0.369	13.724	0.535
14	3.5	Rect	106	10.363	11.216	11.409	0.426	12.079	0.664
14	3.5	Px	61	10.240	10.333	11.063	0.533	11.587	0.655
14	3.5	Py	56	8.831	9.291	9.782	0.531	10.291	0.635
14	3.5	UJ	136	10.388	10.967	11.622	0.461	12.181	0.518
14	7	Rect	46	9.226	9.386	9.940	0.479	10.456	0.554
14	7	Px	28	9.119	9.181	9.729	0.516	10.255	0.645
14	7	Py	29	8.831	9.037	9.511	0.598	9.876	0.703
14	7	UJ	54	9.226	9.415	9.964	0.507	10.573	0.634
14	14	Rect	18	8.709	8.904	9.113	0.556	9.746	0.661
14	14	Px	14	8.709	8.904	9.106	0.482	9.633	0.620
14	14	Py	15	8.709	8.904	9.272	0.585	9.726	0.630
14	14	UJ	18	8.709	8.904	9.190	0.585	9.726	0.689

Table E.1 - Implementation uncertainty estimated over 100 measurement replications.